HAL open science

Topological Constraints and Defects in Spin Ice

Ludovic D.C. Jaubert

To cite this version:

Ludovic D.C. Jaubert. Topological Constraints and Defects in Spin Ice. Condensed Matter [cond-mat]. Ecole normale supérieure de lyon - ENS LYON, 2009. English. NNT : . tel-00462970

HAL Id: tel-00462970

https://theses.hal.science/tel-00462970v1

Submitted on 10 Mar 2010

HAL is a multi-disciplinary open access archive for the deposit and dissemination of scientific research documents, whether they are published or not. The documents may come from teaching and research institutions in France or abroad, or from public or private research centers.

L'archive ouverte pluridisciplinaire **HAL**, est destinée au dépôt et à la diffusion de documents scientifiques de niveau recherche, publiés ou non, émanant des établissements d'enseignement et de recherche français ou étrangers, des laboratoires publics ou privés.

Distributed under a Creative Commons Attribution 4.0 International License

N° d'ordre : 528
N° attribué par la bibliothèque : _ENSL528

Thèse en vue d'obtenir le grade de

Docteur de l'Université de Lyon - Ecole Normale Supérieure de Lyon

Laboratoire de Physique, ENS Lyon
Ecole Doctorale de Physique et d'Astrophysique de Lyon

présentée et soutenue publiquement le 23 / IX / 2009 par

Ludovic D. C. Jaubert

Topological Constraints and Defects in Spin Ice

---

réalisée sous la direction de

Peter C. W. Holdsworth

Devant la commission d'examen formée de :

M. Fabien Alet	Membre/Rapporteur
M. Leon Balents	Membre
M. Benjamin Canals	Membre/Rapporteur
M. Peter Holdsworth	Directeur de thèse
M. Philippe Mendels	Président
M. Frédéric Mila	Membre

Table of Contents

Acknowledgements **1**

I Introduction **5**
I.1 Magnetic Materials . . . 5
I.1.a Origin of magnetism in condensed matter . . . 6
I.1.b Phase transitions . . . 11
I.1.c 2-dimensional XY-model . . . 15
I.2 Frustration in Physics . . . 18
I.2.a Randomness . . . 19
I.2.b Geometrical frustration . . . 19
I.3 Spin Ice . . . 23
I.3.a Origin . . . 23
I.3.b Dipolar Interactions . . . 28
I.3.c Magnetic Monopoles in Spin ice . . . 33
I.3.d Magnetic field . . . 39
I.3.e Dynamics . . . 46
I.3.f Spin ice candidates . . . 48
I.4 Plan . . . 49

II Methods **51**
II.1 Presentation of the model . . . 51
II.2 Monte Carlo . . . 53
II.3 Worm algorithm . . . 57
II.4 Ewald Method . . . 62
II.4.a General presentation . . . 62
II.4.b Analytical calculation of the series . . . 64
II.4.c Numerical application to spin ice . . . 67
II.5 Transfer matrix . . . 69
II.5.a One dimensional Ising model . . . 69
II.5.b 6-vertex model . . . 71
II.6 Husimi tree . . . 74
II.6.a Bethe approximation . . . 74
II.6.b Bethe lattice . . . 75
II.6.c Husimi tree . . . 77

II.6.d Recursion on the Husimi tree for spin ice . . . 78

III Topological phase transitions **81**
III.1 Constrained Manifold . . . 81
III.1.a Nature of the transitions . . . 81
III.1.b Topological constraints . . . 84
III.2 Kasteleyn transition: $\delta = 0$ . . . 88
III.2.a Husimi Tree . . . 89
III.2.b Worm algorithm . . . 92
III.2.c Upper-critical dimension . . . 94
III.2.d World lines for bosons . . . 95
III.2.e Experiments . . . 96
III.3 A tuneable Kasteleyn transition: $h > 0,\ \delta > 0$ . . . 98
III.4 KDP transition: $h = 0$ . . . 101
III.4.a Apparent 1st order transition . . . 101
III.4.b Multicritical Point of ∞-order . . . 106
III.4.c Rigourous proof: Transfer Matrix method . . . 114
III.4.d Mapping onto a quantum phase transition . . . 122
III.4.e Correlations . . . 125
III.4.f Experiments . . . 126

IV Constrained Monopoles Dynamics **133**
IV.1 Presentation of the problem . . . 133
IV.1.a Magnetic monopoles . . . 133
IV.1.b Dynamics in spin ice . . . 136
IV.2 Deconfined quasi-particles . . . 137
IV.2.a Quantum tunnelling . . . 138
IV.2.b Arrhenius argument . . . 139
IV.3 Spin freezing . . . 142
IV.3.a Dipolar spin ice . . . 142
IV.3.b Magnetic monopoles and Dirac strings . . . 143
IV.3.c Comparison to experiments . . . 148
IV.4 Monopoles in a field . . . 153

V Zero Field Susceptibility in $Ho_2Ti_2O_7$ **155**
V.1 An appealing experimental result . . . 155
V.2 Husimi tree . . . 156
V.3 **Q**-dependance of the susceptibility . . . 160

VI Conclusion **165**

A Generalisation of Pauling's argument **169**

B Demagnetisation Effect **171**

C Neutron Scattering & Pinch Points **173**

List of Figures

I.1 Hydrogen molecule . . . 8
I.2 Gibbs energy for Landau theory . . . 13
I.3 Signature of phase transitions in the susceptibility . . . 16
I.4 Excitations out of the XY ground state . . . 17
I.5 Frustration . . . 18
I.6 Frustrated lattices . . . 20
I.7 Signature of frustration in the susceptibility . . . 21
I.8 Pyrochlore lattice . . . 24
I.9 Models equivalent to spin ice . . . 26
I.10 Degeneracy in spin ice . . . 27
I.11 Zero-point entropy in $Dy_2Ti_2O_7$ . . . 29
I.12 Hyperfine coupling in $Ho_2Ti_2O_7$ . . . 30
I.13 Scattering function in spin ice . . . 31
I.14 Phase transition in dipolar spin ice . . . 33
I.15 Ground state of the dipolar spin ice model . . . 34
I.16 Coulomb potential . . . 38
I.17 Dumbbell model . . . 38
I.18 Ground state in a 110 field . . . 41
I.19 Phase diagram of dipolar spin ice in a 110 field . . . 42
I.20 Ground state of Kagome Ice . . . 43
I.21 Phase Diagram and Kagome Ice plateau in a 111 field . . . 44
I.22 Decoupled spin in a 112-tilted field . . . 45
I.23 Spin ice dynamics . . . 46

II.1 Presentation of the model . . . 52
II.2 Degeneracy lift of the 2 *in* - 2 *out* tetrahedra in a 001 magnetic field . . . 52
II.3 Degeneracy lift of the 2 *in* - 2 *out* tetrahedra with bond distortion. . . . 53
II.4 Loops from the Worm algorithm . . . 58
II.5 Mapping from a spin configuration to an ensemble of strings . . . 59
II.6 Illustration of the Ewald sum . . . 63
II.7 Periodic boundary conditions in the Ewald method . . . 69
II.8 Ising chain . . . 70
II.9 6-vertex model . . . 72
II.10 Configurations of the 6-vertex model . . . 73

II.11 Bethe approximation . . . 75
II.12 Bethe lattice . . . 76
II.13 Husimi tree . . . 78

III.1 Construction of a string . . . 83
III.2 Gibbs potential . . . 85
III.3 Small closed loop . . . 86
III.4 Kasteleyn transition for biomembranes . . . 89
III.5 $3d$ Kasteleyn transition in spin ice . . . 92
III.6 Finite size effects . . . 94
III.7 Logarithmic corrections at the upper-critical dimension . . . 95
III.8 Correlations in a 001 field . . . 96
III.9 Magnetisation in a 001 field for $Dy_2Ti_2O_7$ and $Ho_2Ti_2O_7$ . . . 98
III.10 Tuneable Kasteleyn transition . . . 99
III.11 Logarithmic corrections at the upper-critical dimension . . . 100
III.12 Entropy on the constrained manifold . . . 105
III.13 KDP transition with defects . . . 106
III.14 Gibbs energy for Landau theory (multi-critical point) . . . 107
III.15 Equiprobability of the sectors . . . 112
III.16 Energy E vs magnetisation M . . . 113
III.17 Probability distribution of the energy . . . 114
III.18 Density of tetrahedra . . . 115
III.19 $3d$ Transfer Matrix . . . 116
III.20 $2d$ projection of the pyrochlore lattice . . . 118
III.21 Mean Field critical correlations . . . 126
III.22 Anisotropic correlations . . . 127
III.23 Finite size effects in the correlation . . . 128
III.24 Uniaxial pressure . . . 130
III.25 $Dy_2Ti_2O_7$ under uniaxial pressure . . . 131

IV.1 Coulomb potential . . . 135
IV.2 Emergence of monopoles . . . 136
IV.3 Experimental relaxation time . . . 137
IV.4 Deconfined monopoles . . . 140
IV.5 Density of monopoles . . . 144
IV.6 Creation/annihilation of a pair of quasi-particles . . . 146
IV.7 Spin freezing in $Dy_2Ti_2O_7$ . . . 150
IV.8 Influence of a magnetic field on the dynamics . . . 151
IV.9 Influence of dilution on the dynamics . . . 152
IV.10 Transient monopole current: . . . 154
IV.11 Monopole density profile . . . 154

V.1 Experimental susceptibility . . . 156
V.2 Susceptibility crossover . . . 159
V.3 Scattering function . . . 162

V.4 Susceptibility $\chi(\mathbf{q}, T)$ 163

List of Tables

I.1 Ground state electronic configuration 25
I.2 Crystal field level 25
I.3 Nearest neighbour interactions 32

II.1 Probabilities of the Worm algorithm 61

IV.1 Mapping from the dipolar spin ice to the dumbbell model 133
IV.2 Energy scales resulting from a single spin flip 141

Acknowledgements

Ces trois dernières années ayant été assez pleines (voire intenses), cela risque de me prendre pas mal de temps pour remercier ou saluer tout ceux qui m'ont aidé ou que j'ai rencontré au fil de ma thèse. Je compatis donc par avance pour ceux qui vont devoir fouiller ces prochaines pages à la recherche d'un nom connu[1] !

Le premier nom qui me vient à l'esprit est bien sûr Peter, qui vient de me supporter presque quotidiennement pendant 37 mois (oui je sais, un mois de trop) ! En outre d'avoir été initié à l'Histoire centenaire des *Ashes*, je tiens à le remercier sincèrement de ces trois années de discussions et d'échange autour de quelques tableaux noirs et tasses de thé, pour son encadrement sans faille (malgré la lourde charge d'enseignement et d'administration) et pour la liberté qu'il m'a donné dans mon travail. En commençant cette thèse, je me doutais déjà que j'avais fait le bon choix de directeur[2] et ce fût amplement confirmé depuis. Cette thèse lui doit évidemment beaucoup, sans compter que j'ai beaucoup aimé travaillé sur ce sujet et passer quelques mois à Oxford, dans ses bagages !

Of course Oxford has been a central place in my thesis, where many projects have been either initiated or concluded and where I enjoyed crossing the University Park every day to go to work (despite the floods !). I would like to express my deep gratitude to Roderich[3] and to John, from whom I have learned several extremely useful theoretical techniques and who always found the time for explanations and discussions. I would also like to thank Claudio, with whom I have enjoyed many pleasant and interesting discussions[4], as well as advices. My stay in England would not have been complete without the discovery of the wonderful world of neutron scattering from the company of Tom[5], Mark and Steve, who ensure that my research remains on a firm experimental ground and who are my reference for any experimentally oriented problems. In the british team, I have also been particularly happy to collaborate with Adam, the other spin ice student !

Even if our collaboration is still "work in progress" and thus not in this thesis, I would like to thank Paul, Roger[6] and Michel for my visit in Waterloo, and the forthcoming ones,

[1] especially my non-french friends and colleagues who will enjoy alternating between Molière's and an ersatz of Shakespeare's language !

[2] après tout c'est déjà un peu à cause de tes cours de Phy Stat que je suis là.

[3] who even endeavoured to explain to me the subtleties of spin ice in Paris before my PhD.

[4] and not only about physics

[5] who proved to be extraordinarily patient with the mere theoretician that I am: "Hey Tom, what is this button for ?" and knows a lot about italian mafia pizza

[6] as well as Lori for their great hospitality and their moose stew !

with whom it is particularly agreeable and enlightening to do physics.

And because all these collaborations and conferences would be impossible without a financial support, I would also like to thank the ENS Lyon, the research group "Highly Frustrated Magnetism" - part of the European Science Fundation - and the French Canada Research Fund.

D'un point de vue général je voudrais saluer les membres du labo de physique, en particulier ceux de l'équipe 4 avec qui j'ai partagé ce petit bout de couloir tout au fond et sans oublier Laurence, Nadine et Laure, qui font de ce labo un endroit agréable, détendu et efficace pour travailler.

Ces trois années de thèses furent aussi trois années d'enseignement, grandement simplifiées par un excellent encadrement administratif d'Edith et technique de Jérôme, Adrien et Pascal ; un grand merci aussi à Hervé et Eric pour leurs journées (et aussi souvent leurs nuits) passées à préparer les plannings, Guillaume avec qui j'ai préparé et encadré plus d'un TP, Patrick et Guillaume pour les tutorats de Méca Q et Thibaut pour l'organisation de la meilleure "Journée des Thésards" du labo !

Last but not least, concerning the scientific aspect of my thesis, I am greatly thankful to my referees Fabien Alet, Leon Balents, Benjamin Canals, Philippe Mendels and Frédéric Mila to have come all the way to Lyon for my PhD defense and for their insightful comments and questions that have enriched this thesis, with a special acknowledgement to my *rapporteurs* who had to write a report despite a "slightly" delayed deposit of my manuscript !

A un degré plus éloigné mais non moins essentiel, je voudrais également saluer M. Lasserre[7], M. Blanchard, M. Dettwiller, Max[8] et Mme V[8].

D'un point de vue plus personnel, je voudrais saluer et chaleureusement remercier mes coloc de thèse, Karol, Guillaume et Sébastien pour la bonne humeur, l'effervescence et la douce odeur de café qui imprégnait notre bureau, mais aussi bien sûr Arnaud *&* Charles (s'il y a eu procrastination, j'en suis responsable ☕ ✷—), Tommaso , Johannes et l'équipe des Hell's Angels qui ont subi mes talents de goal pendant tout ce temps !

There is also naturally a long list of people I have met in various labs, workshops, summer school and with whom I will always be happy to enjoy a glas of wine, beer, tea, coke or whatever the local beverage will be: Andrew, Tim, Marion, Laura, Fabien, Daniel, Adel, Jérôme, Sid, Chris, Andrea (×2), Simon, Benoît, Ben, Tom, Andreas, Stuart, Thomas, Robert, Maxime, Arnaud *etc.*

Un merci tout particulier à mes amis pour leur présence permanente : Marie, Claire *&* Xavier, Aurélie, Justine *&* Romain[9], Maud *&* Fred[10], Damien[11], ma famille et surtout mes parents, toujours présents.

[7]un grand merci pour ses conseils de lecture.

[8]les meilleurs profs que j'ai connu.

[9]tant qu'il y aura des restos sur Lyon, on pourra en profiter ensemble !

[10]à très bientôt entre Paris, Dresde et Munich !

[11]celui qui copie tout ce que je fais avec un an d'avance ☺ et un très grand merci pour ta relecture sans faille de cette thèse !

Cette thèse fût réalisée et rédigée en musique : "*Alive*" de Daft Punk, Y.A.S., White Stripes, The Delano Orchestra (best band ever !), Nirvana, Aaron, Yann Tiersen, Black Eyed Peas, Timbaland, Charlie Winston, Lily Allen, Marilyn Manson, "*Mad World*", Lady Gaga (it was late and I was tired)... et fut sponsorisée par les madeleines "St-Michel©" et le thé "Lipton©".

Pour finir, j'aimerais remercier Pr. Trinh Xuan Thuan d'avoir écrit "*La mélodie secrète*".

I Introduction

I.1 Magnetic Materials

Before presenting the main features of magnetic materials, we should answer a legitimate question: "*Why are they interesting ?*" The reason is simple: because they are everywhere, from the simple compass that helped wanderers throughout the ages to navigate on Earth (which is itself one giant turbulent magnet [Ber07]), to the hard disk in MP3 players, passing by electric motors, voltage transformers, metal detectors and of course the magnet holding the shopping list on the fridge. The research in this domain is extremely vast, bringing together one of the largest community of physicists, so let me briefly present two of the main axes of current research.

Spintronics

This domain appeared 20 years ago with the discovery of the *giant magnetoresistance* effect observed in Fe/Cr multilayers by the groups of A. Fert [Bai88] and F. Grünberg [Bin89] (Nobel Prize 2007). The origin of this effect comes from the possibility to control the mobility of the electrons, and thus the resistivity of the material, by acting on the spins of these electrons through an external magnetic field. Its most remarkable application certainly is the production of read heads for hard disk drives more than 100 times more sensitive than the former sensors, opening the way to the race for miniaturisation of electronic devices during the last decade.

Superconductivity

It was observed for the first time by Onnes in 1911, when the resistivity of solid mercury suddenly disappeared below a critical temperature $T_C = 4.2$ K [Onn11], making it a perfect conductor. This phenomenon has been explained by Bardeen, Cooper & Schrieffer in 1957, by the creation of *Cooper pairs* between two electrons [Bar57] (Nobel Prize 1972). However this theory only explains the so-called *conventional* superconductivity that exists below 30 K, but is unable to justify the observation of higher critical temperature, firstly at 35 K in 1986 in copper oxydes [Bed86] (Nobel Prize in 1987) and up to the record of 138 K a few years later [Dai95], which has remained a theoretical challenge for the past 20 years. Moreover, a new wave of interest has followed the discovery of an Iron-based family of High T_C superconductor.

From a more fundamental view point, magnetic materials have the advantage of presenting a myriad of different behaviours that can be investigated by a wide range of experimental techniques and be described by surprisingly "simple" theoretical models in comparison to the *a priori* messy nature of the original many-body problem. Their study usually requires a multi-lateral approach, using methods from quantum mechanics, statistical physics, optics, *etc*, making them an intriguing puzzle for scientists and a laboratory for testing new concepts.

My thesis has been devoted to one of these materials, *spin ice*, whose remarkable properties have driven a great deal of interest during the past 12 years. The goal of this introduction is double. First of all, we present some fundamental aspects of magnetism relevant to spin ice and give the necessary foundations of the theory of phase transitions. We then briefly explain the key concept of *geometrical frustration*, before presenting the core of this work: spin ice. My purpose, or at least my aspiration, has been to go beyond a mere introduction of this material and to give a complete but yet concise and hopefully clear review on spin ice[1].

I.1.a Origin of magnetism in condensed matter

In this section, we will focus on the electronic aspect of magnetism due to the valence electrons of the atoms, because it is of particular relevance for spin ice. We start with the fundamental origin of magnetism, discussing the joint importance of its spin and orbital components and the influence of an external magnetic field, before illustrating the interactions of atoms through direct exchange coupling.

Spin-orbit coupling

An electron has two angular momenta; an orbital one $\mathbf{L} = \mathbf{r} \times \mathbf{p}$ and an intrinsic spin $\mathbf{S}$. From a semi-classical point of view, it is moving at a velocity $\mathbf{v} = \mathbf{p}/m_e$ in a radial potential $V(r)$ created by the nucleus of the atom or ion and screened by the internal electrons. We learn from special relativity that the intrinsic magnetic momentum of the electron $\mu \approx \frac{e}{m_e}\mathbf{S}$ feels a magnetic field generated by its motion proportional to $\mathbf{L}$

$$\mathbf{B} = \mathbf{E} \times \frac{\mathbf{v}}{c^2} = \left(-\frac{\mathbf{r}}{er}\frac{\mathrm{d}V}{\mathrm{d}r}\right) \times \frac{\mathbf{p}}{m_e c^2} = -\frac{1}{m_e e\, c^2}\left(\frac{1}{r}\frac{\mathrm{d}V}{\mathrm{d}r}\right)\mathbf{L} \tag{I.1}$$

where the massive nucleus is supposed motionless with respect to the dynamic electron, giving rise to an energy

$$W = -\mu \cdot \mathbf{B} = \frac{1}{m_e^2 c^2}\left(\frac{1}{r}\frac{\mathrm{d}V}{\mathrm{d}r}\right)\mathbf{L}\cdot\mathbf{S} = f(r)\,\mathbf{L}\cdot\mathbf{S} \tag{I.2}$$

If we take into account Slater's screening rules, $V(r) = -\dfrac{Z^* e^2}{4\pi\epsilon_0\, r}$ where $Z^* e$ is the effective nuclear charge seen by the valence electron, and we define the typical size of an atomic

[1] with a few restrictions, since we chose not to discuss diluted, "stuffed" or artificial spin ice.

orbital $r_0 \sim n^{*2}\, a_B/Z^*$, where n^* is the effective principal quantum number and a_B is the Bohr radius, the mean value of $f(r)$ is

$$\langle f(r)\rangle \propto \frac{Z^*}{r_0^3} \propto \frac{Z^{*4}}{n^{*6}} \tag{I.3}$$

Hence, the spin-orbit coupling will be especially important for heavy atoms (large Z^*) of small size. At first sight, these seem to be two antagonist conditions, but it is exactly the case for rare-earth elements. Their valence electrons are on the $4f$ layers, *i.e.* inside the electron cloud and thus strongly feel the attraction of the nucleus, diminishing their radius r_0 as Z is increasing: this phenomenon is known as the *Lanthanide contraction*. As we shall see in section I.3, spin ice is made of rare earth ions and this strong spin-orbit coupling imposes the *total* angular moment $\mathbf{J} = \mathbf{L} + \mathbf{S}$ as a good quantum number.

Paramagnetic phase

If there is no interactions between spins[2], the system is in a *paramagnetic* phase. Let us consider a system of N independent spins with total angular and magnetic quantum number J and $m = \{-J, ..., +J\}$ respectively; the magnetic moment along z is thus $\mu = m\, g_J \mu_B$ where μ_B is the Bohr magneton. The absence of coupling enables a straightforward calculation of the total magnetisation $\mathcal{M}$ in a field B by weighting each value of m with the corresponding Boltzmann factor; the result is expressed with the Brillouin functions $\mathcal{B}_J$:

$$\begin{aligned}
\mathcal{M} &= N\, g_J J \mu_B\, \mathcal{B}_J(\beta g_J J \mu_B B) \qquad \text{(I.4)}\\
\mathcal{B}_J(x) &= \frac{\sum_{m=-J}^{J} m/J\, \exp(-m\, x/J)}{\sum_{m=-J}^{J} \exp(-m\, x/J)}\\
\mathcal{B}_J(x) &= \frac{2J+1}{2J} \coth \frac{(2J+1)x}{2J} - \frac{1}{2J} \coth \frac{x}{2J}\\
\mathcal{B}_{1/2}(x) &= \tanh(x)
\end{aligned}$$

A Taylor expansion for small field gives the so-called Langevin susceptibility

$$\chi(T) = N\mu_0 \frac{(g_J \mu_B)^2 J(J+1)}{3k_B T} = \frac{C_J}{T} \tag{I.5}$$

This is the Curie law for a paramagnet and C_J is known as the Curie constant. In the case $J = 1/2$, the same result is easily obtained by minimising the Gibbs potential $\mathcal{G}^*$ with respect to the mean value of the magnetisation per spin $M = \mathcal{M}/(N\, g_J J \mu_B)$ which can vary from -1 to +1. One briefly presents this approach here, as it will prove to be useful in chapter III. Being in the paramagnetic phase imposes the absence of internal energy; the Helmholtz potential is then

$$\mathcal{G}^*(M) = -T\, \mathcal{S}(M) - \frac{1}{2} g_{\frac{1}{2}} \mu_B\, B\, M \tag{I.6}$$

[2]even if it is rigourously impossible, it is often a good approximation at high enough temperature

Let us define N_+ and N_-, the number of spins with respectively $m = +1/2$ and $m = -1/2$, related by $N = N_+ + N_-$ and $M = (N_+ - N_-)/N$. This allows us to write the entropy $\mathcal{S}(M)$ as

$$\begin{aligned}\mathcal{S}(M) &= -k_B \left[\frac{N_+}{N}\ln\frac{N_+}{N} + \frac{N_-}{N}\ln\frac{N_-}{N}\right] \\ &= -k_B \left[\left(\frac{1+M}{2}\right)\ln\left(\frac{1+M}{2}\right) + \left(\frac{1-M}{2}\right)\ln\left(\frac{1-M}{2}\right)\right] \end{aligned} \tag{I.7}$$

Minimising the Gibbs potential (I.6) gives the same expression of the magnetisation than equation (I.5) for $J = 1/2$.

However the approximation of non-interaction only holds at high temperature and spin coupling must be considered otherwise.

Exchange coupling

The origin of exchange interaction comes from an interplay between Coulomb interactions and Pauli's exclusion principle. In the interest of being clear, we have decided to illustrate this concept with a toy model, the molecule of hydrogen H_2.

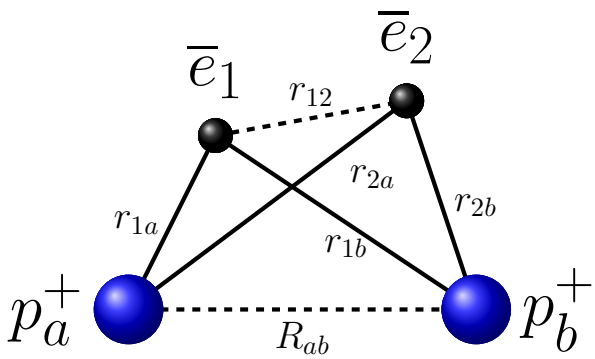

Figure I.1: **Hydrogen molecule:** The solid (resp. dashed) lines are attractive (resp. repulsive) interactions.

In the Heitler-London approximation, the relative difference of mass between protons and electrons allows us to fix the position of the nucleus while the electrons are positioned in $\mathbf{r}_1$ and $\mathbf{r}_2$. The Hamiltonian of this model is

$$\mathcal{H} = \mathcal{H}_{1a}(\mathbf{r}_1) + \mathcal{H}_{2b}(\mathbf{r}_2) + V_{int}(\mathbf{r}_1, \mathbf{r}_2) \tag{I.8}$$

$$\mathcal{H}_{\nu i} = \frac{p_\nu^2}{2m_e} - \frac{e^2}{4\pi\epsilon_0\, r_{\nu i}} \qquad \nu = 1, 2,\ i = a, b \tag{I.9}$$

$$V_{int} = \frac{e^2}{4\pi\epsilon_0}\left(\frac{1}{R_{ab}} + \frac{1}{r_{12}} - \frac{1}{r_{2a}} - \frac{1}{r_{1b}}\right) \tag{I.10}$$

Let $\phi_a(\mathbf{r}_1)$ and $\phi_b(\mathbf{r}_2)$ be the ground states of energy E_0 of the Hamiltonians $\mathcal{H}_{1a}$ and $\mathcal{H}_{2b}$ respectively. Following Pauli's exclusion principle, the fermionic nature of the electrons imposes a global antisymmetric wave function:

$$\Psi_1 \;=\; \Phi_A(\mathbf{r}_1, \mathbf{r}_2,) \otimes \chi_T \quad \text{and} \quad \Psi_2 \;=\; \Phi_S(\mathbf{r}_1, \mathbf{r}_2,) \otimes \chi_S \tag{I.11}$$

where χ_T and χ_S are the well-known triplet (symmetric) and singlet (antisymmetric) functions in spin space respectively, and:

$$\begin{aligned} \Phi_A(\mathbf{r}_1, \mathbf{r}_2,) &= \frac{1}{\sqrt{2\,(1+\ell^2)}}\,(\phi_a(\mathbf{r}_1)\phi_b(\mathbf{r}_2) + \phi_b(\mathbf{r}_1)\phi_a(\mathbf{r}_2)) \\ \Phi_S(\mathbf{r}_1, \mathbf{r}_2,) &= \frac{1}{\sqrt{2\,(1-\ell^2)}}\,(\phi_a(\mathbf{r}_1)\phi_b(\mathbf{r}_2) - \phi_b(\mathbf{r}_1)\phi_a(\mathbf{r}_2)) \end{aligned} \tag{I.12}$$

$$\ell \;=\; \int \mathrm{d}\mathbf{r}\, \phi_a^*(\mathbf{r})\phi_b(\mathbf{r}) \tag{I.13}$$

are the symmetrised spatial wave functions, normalised by the factor ℓ that takes into account the non-orthogonality of ϕ_a and ϕ_b. In the sub-space $\{\Psi_1, \Psi_2\}$, the Hamiltonian (I.8) can be diagonalised:

$$\mathcal{H} \;=\; \begin{pmatrix} 2\,E_0 \,+\, \dfrac{\upsilon+\omega}{1+\ell^2} & 0 \\ 0 & 2\,E_0 \,+\, \dfrac{\upsilon-\omega}{1-\ell^2} \end{pmatrix} \tag{I.14}$$

$$\upsilon \;=\; \int\!\!\int \mathrm{d}\mathbf{r}_1\mathrm{d}\mathbf{r}_2\, V_{int}(\mathbf{r}_1, \mathbf{r}_2)\; |\phi_a(\mathbf{r}_1)\phi_b(\mathbf{r}_2)|^2 \tag{I.15}$$

$$\omega \;=\; \int\!\!\int \mathrm{d}\mathbf{r}_1\mathrm{d}\mathbf{r}_2\, V_{int}(\mathbf{r}_1, \mathbf{r}_2)\, \phi_a^*(\mathbf{r}_1)\phi_a(\mathbf{r}_2)\phi_b^*(\mathbf{r}_2)\phi_b(\mathbf{r}_1) \tag{I.16}$$

where υ is Hartree's direct term and ω is Fock's exchange term. Hence the energy difference between the triplet Ψ_1 and the singlet Ψ_2 is:

$$\Delta E \;=\; J \;=\; 2\frac{\omega - \upsilon\ell^2}{1-\ell^4} \tag{I.17}$$

and it is straightforward to check that the Hamiltonian can be rewritten in the sub-space $\{\Psi_1, \Psi_2\}$:

$$\mathcal{H} \;=\; 2\,E_0 \,+\, \frac{\upsilon - \omega\ell^2}{1-\ell^4} - \frac{J}{4} - \frac{J}{4}\sigma_1\cdot\sigma_2 \;=\; E_{\mathrm{ref}} - \frac{J}{4}\,(\sigma_1^x\sigma_2^x \,+\, \sigma_1^y\sigma_2^y \,+\, \sigma_1^z\sigma_2^z) \tag{I.18}$$

where $\sigma_{x,y,z}$ are Pauli's matrices representing the spin 1/2 of the electrons. Before analysing our result, we should underline that we did not choose this model for its quantitative description of a solid; using atomic orbitals (AO) to construct molecular wave functions (I.12) means neglecting the deformation of these AO due to electronic correlations, an approximation that becomes even worst for a solid. However it is a excellent tool

to show how the electronic interactions work together with Pauli's principle to determine the nature of the exchange coupling.

Since ℓ is usually smaller than 1 (weak superposition of the AO), the sign of ΔE is fixed by $(\omega - \upsilon\ell^2)$ and will give rise to *ferromagnetism* ($\Delta E > 0$) or *antiferromagnetism* ($\Delta E < 0$). It is thus the Coulomb potential, through υ and ω, that imposes the nature of the coupling, but it is the global antisymmetry of the wave function (imposed by the exclusion between fermions) that enables this unique parallel between spatial correlations and a spin configuration. This is why we can write the complex many-body Hamiltonian (I.8) as a simple product of spins (I.18).

If we follow the same argument for two different valence electrons in the same atom, we can choose $\phi_a(\mathbf{r}_1)$ orthogonal to $\phi_b(\mathbf{r}_2)$, and thus $\ell = 0$ and $\Delta E = \omega$. Since ω is a positive electrostatic energy of the charge density $e\,\phi_a^*(\mathbf{r})\phi_b(\mathbf{r})$, in absence of crystal field terms, spins on the same atomic orbital want to be parallel to each others; this is Hund's first rule (see [Kit96], §14).

In a solid, the argument is more subtle, but the result is qualitatively the same, except that crystal field terms created by the surrounding atoms can make this Hamiltonian anisotropic with a direction-dependent coupling $J^{x,y,z}$:

$$\mathcal{H} \,=\, -\sum_{i>j} \left(J_{ij}^x\, S_i^x S_j^x \,+\, J_{ij}^y\, S_i^y S_j^y \,+\, J_{ij}^z\, S_i^z S_j^z \right) \tag{I.19}$$

where $\mathbf{S}_i$ is the total electronic spin of atom i which is not necessarily 1/2. One can also see this crystal field anisotropy as directly acting on the spherical symmetry of the spin

$$\mathcal{H} \,=\, -\sum_{i>j} J_{ij}\, \mathbf{S}_i \cdot \mathbf{S}_j \,+\, \sum_i \sum_{\nu=x,y,z} A_\nu\, |\mathbf{S}_i \cdot \hat{\mathbf{e}}_\nu|^2 \tag{I.20}$$

where $\hat{\mathbf{e}}_\nu$ are the Cartesian unity vectors. The above summations run over all pairs of spins but Hartree's and Fock's integral are non-zero on short distances only. The coupling between two atoms can be made stronger if it is mediated by a third non-magnetic anion, as *e.g.* in the salt $\{Mn^{2+}O^{2-}\}$ where nearest neighbours (NN) magnetic ions Mn^{2+} are not coupled, but next nearest neighbours (NNN) are antiferromagnetically ordered at low temperature because they can interact through the anion O^{2-} between them: this is called the *superexchange* and has been first proposed by Kramers [Kra34] with the help of Bloch, and later refined by Anderson [And50].

From a classical point of view, we can distinguish three limits:

- **Ising model**: the lowest energy corresponds to one of two discrete values (a doublet), *e.g.* $\mathbf{S} = \pm S\hat{\mathbf{e}}_z$ with $A_z \ll A_x, A_y$ in equation (I.20). The first excited states are not accessible by thermal or quantum fluctuations.

- **XY model**: the crystal field hinders he development of one the three spin component, *e.g.* $A_z \gg A_x, A_y$. Theoretically speaking, the spin can visit the whole circumference of the unity disc.

- **Heisenberg model**: no orientation is favoured $A_x \approx A_y \approx A_z$. The spin can wander on the surface of the unity sphere.

However we should notice that a small easy-axis anisotropy can quickly favour a XY bulk behaviour, as for Rb_2CrCl_4 [Kaw86, Vol91, Bra93] or even an Ising behaviour such as in cobalt substances K_2CoF_4 or Rb_2CoF_4 [Bre69].

We shall now turn our attention towards collective phenomena induced by this exchange coupling, namely the phase transitions. For reasons of simplicity, we will mainly use Ising spins, but we will also present the XY model as its physics happens to display many similar points with spin ice.

I.1.b Phase transitions

Landau theory

Interactions between the constituents of matter lead to collective behaviour that can be hindered by thermal perturbations for example. Hence from this competition between interactions and temperature, we can expect macroscopic thermodynamic changes upon cooling; this is the *phase transition*. For magnetic materials, the standard observable used to characterise such phenomena is the mean value of the magnetisation M. At high temperature fluctuations are strong enough to make the system (configuration of spins) completely disordered and $M = 0$ on average, whereas at zero temperature, *e.g.* nearest neighbour ferromagnetic interactions will force all spins to point in the same direction resulting in a saturated value of the normalised magnetisation $M = 1$; this is why M is called the *order parameter*. In absence of symmetry breaking field, this ordering is spontaneous and occurs at a well-defined temperature (apart from hysteresis considerations).

In order to conceptualise the phenomenon of phase transitions, Landau constructed a remarkable theory based on the Gibbs free energy $G(M,T)$ function of the order parameter and temperature, with the general idea that for a given temperature T_0, the magnetisation M should correspond to the global minimum of $G(M,T_0)$; for a presentation of Landau theory, see [Pli06, Car02]. In absence of symmetry breaking field, the Gibbs energy should be an even function of G, giving the following general expansion

$$\Delta G(M,T) = G(M,T) - G(0,T) = \frac{1}{2}b(T)M^2 + \frac{1}{4}c(T)M^4 + \frac{1}{6}d(T)M^6 + \dots \quad \text{(I.21)}$$

By considering the average value of M only, one explicitly neglects the fluctuations. They can be added in the theory by following Ginzburg's method (see [Pli06, Car02]). We shall not present the details of Ginzburg's approach here, but we can nonetheless precise that fluctuations can be correctly neglected for high dimensional systems, as the number of neighbours increases together with the dimension and a local fluctuation on one of the spins for example becomes relatively less important. The highest dimension where Landau theory is not quantitatively valid is called the *upper-critical dimension* and we note it d_c.

According to the different expressions of the pre-factor $b(T)$, $c(T)\ldots$, this function G can describe many different types of phase transitions; we focus here on the three most standard examples, namely a transition of 2nd order, 1st order and a tri-critical point. For each kind of transition, ΔG is plotted on figure I.2.

Transition of 2nd order We assume that $b(T) = b_o(T - T_c)$ and $c(T), d(T), \cdots > 0$. For $T > T_c$, ΔG only has one minimum at $M = 0$ whereas below T_c, that corresponds then to the transition temperature, the favoured value of the magnetisation is finite and doubly degenerate, behaving close to T_c^- like $M \sim \pm\sqrt{b/c}\sqrt{T - T_c}$. At T_c the potential is quartic instead of being quadratic, which means that even if there is a unique minimum, the potential is relatively "flat" compared to other temperatures and soft fluctuations around $M = 0$ are more likely yo occur; in this sense, T_c is called a *critical* point. All relevant thermodynamic quantities are computable this way, but here we simply want to emphasise that since the system cannot be in a superposition of states with opposite magnetisation, there is spontaneous symmetry breaking below the transition in favour of one of the two values; this is typical of the ferromagnetic phase transitions. The magnetisation being the variable conjugate with the magnetic field H, we have $-(\partial G/\partial H)_{H=0} \equiv M$. Hence the first derivative of G is continuous but not the second one; the transition is said to be of 2nd order.

Transition of 1st order Now, let us assume that $c(T)$ becomes negative at a temperature $T_n > T_c$ while $d(T)$ remains positive. As illustrated in figure I.2, local minima in ΔG are then appearing above T_c for magnetisation values $\pm M_o \neq 0$ and there is a temperature T_1 such that $G(\pm M_o, T_1) = G(0, T_1)$, imposing the conditions

$$\left.\frac{\partial G}{\partial M}\right|_{M_o} = 0 = bM_o + cM_o^3 + dM_o^5 \tag{I.22}$$

$$\Delta G(M_o, T_1) = 0 = \frac{b}{2}M^2 + \frac{c}{4}M^4 + \frac{d}{6}M^6 \tag{I.23}$$

giving the value of $M_o^2 = -3c/4d > 0$ and temperature T_1 is fixed by a relation between the pre-factors $16d(T_1)b(T_1) = 3c^2(T_1)$. Hence local minima appears as soon as $c(T)$ is negative at T_n, but they only become global for $T < T_1$ giving rise to a magnetisation jump from 0 to M_o and the other minimum $M = 0$ disappears below T_c. We have *metastable* states from T_n to T_c, *i.e.* even if the transition occurs at T_1 at equilibrium, there might be hysteresis effects depending on the height of the energy barrier to overcome between $M = 0$ and M_o. Even the first derivative of G (*i.e.* the magnetisation) is discontinuous here and the transition is thus called 1st order.

Tri-critical point If we assume that both coefficients $b(T)$ and $c(T)$ become negative at the same temperature (*i.e.* $T_n = T_c$), there is no metastability anymore and the magnetisation is again continuous. In fact we can follow the same reasoning as for the transition of the critical point presented previously with the only difference that the potential is now proportional to M^6 at the transition instead of being quartic ($G \propto M^4$): soft fluctuations

are even more favoured then and this transition is called a *tri-critical* point. In a real system the condition $b = c = 0$ is rather unlikely to occur if there is no external parameter Λ available to tune the value of these coefficients in order to bring them to zero at the same temperature. As Λ varies the pre-factor $c(T)$ will become negative either at higher or lower temperature than $b(T)$, giving rise respectively to a transition of 1st or 2nd order; in the phase diagram (T, Λ), the tri-critical point represents the frontier between these two lines of phase transition. This is exactly what happens for the superfluid transition in a mixture of ^{3}He and ^{4}He; at low ^{3}He concentration, the mixture remains homogeneous and the transition is continuous whereas there is a phase separation and discontinuity for higher density of ^{3}He.

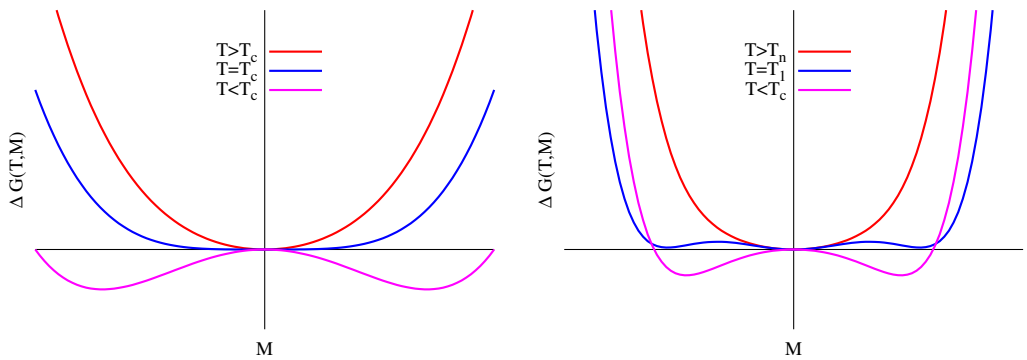

Figure I.2: **Gibbs energy for Landau theory** vs magnetisation M. Each curve represents a different temperature characteristic of the phase transition of 2nd (*left*) or 1st (*right*) order.

Critical exponents As observed for the magnetisation of a critical point $M \propto \sqrt{T - T_c}$, thermodynamic observables usually follow a power law scaling close to the transition temperature T_c characterised by *critical exponents*,

$$\begin{aligned} \text{susceptibility } \chi(0,T) &\propto |T - T_c|^{-\gamma} \\ \text{specific heat } C_h(0,T) &\propto |T - T_c|^{-\alpha} \\ \text{correlation length } \xi(0,T) &\propto |T - T_c|^{-\nu} \\ \text{magnetisation } M(0,T) &\propto |T - T_c|^{\beta} \\ |M(H,T_c)| &\propto |H|^{-1/\delta} \end{aligned} \tag{I.24}$$

For example in Landau theory we have found $\beta = 1/2$. These critical exponents $\gamma, \alpha, \nu, \beta, \delta$ turn out to be independent of the microscopic details of the system and fall into universality classes, *i.e.* different phase transitions can be described by the same family of exponents. Landau theory belongs to the so-called *mean field* universality class, a particularly powerful approach whose basic hypothesis is to neglect or to approximate the influence of the fluctuations in the system. By considering the mean value of the magnetisation

M, fluctuations have been indeed completely ignored in Landau theory, but they can be added phenomenologically through a new term in the Gibbs energy (I.21); $+|\nabla \cdot \mathbf{M}(\mathbf{r})|^2$, giving rise to Landau-Ginzburg theory. We shall not discuss the latter point (see [Pli06] for further details), but will rather turn our attention towards a model-dependent example of mean field theory.

Mean Field Theory: ferromagnet

The mean field approach is very general in various domains of physics and remains one of the first method employed to investigate a new model, as its qualitative insight is usually particularly accurate, despite an apparent simplicity and absence of fluctuations.

Intuitively we expect these fluctuations to become less and less relevant for systems of higher dimensions; a local fluctuation on a spin is more likely to propagate in a $1d$ chain (with two nearest neighbours) than in a $3d$ cubic lattice (with 6 nearest neighbours). Hence the mean field approximation should be valid at high enough dimension. We define the upper-critical dimension d_c as the highest dimension where non-mean field contributions are observed, like for example logarithmic corrections to scaling.

We first illustrate this approach with an Ising ferromagnet. Let us consider a system of N magnetic moments $\mu\,\mathbf{S}$ ($|\mathbf{S}| = 1$) in a magnetic field B_0, with NN ferromagnetic exchange coupling and a coordination number q:

$$\mathcal{H} \;=\; -J \sum_{\langle i,j \rangle} \mathbf{S}_i \cdot \mathbf{S}_j \;-\; \mu \sum_i \mathbf{S}_i \cdot \mathbf{B}_0 \tag{I.25}$$

where $\langle i, j \rangle$ represents each pair of NN spins i and j. At high temperature, it should be in a disordered paramagnetic phase, whereas at zero Kelvin we expect a completely ordered with all spins parallel even for zero field as $J > 0$. The mean field approach consists in linearising this equation, and we obtain up to a constant:

$$\mathcal{H}_{mf} \;=\; -\mu \sum_i \mathbf{S}_i \cdot \left(\mathbf{B}_0 \;+\; \frac{Jq}{\mu} \mathbf{M} \right) + \frac{Nq}{2}\, J\, M^2 \tag{I.26}$$

where from translation invariance, the normalised magnetisation per spin $\mathbf{M} \;=\; \langle \mathbf{S}_i \rangle$ is uniform. The additional term JqM/μ acts like an effective atomic field due to the mean value of the surrounding spins allowing us to follow the same argument as for a paramagnet (equation (I.5)):

$$M \;=\; \tanh \left(\frac{\mu B_0 \;+\; JqM}{k_B T} \right) \tag{I.27}$$

This is a self-consistent equation that must be solved numerically or graphically. If $B_0 = 0$, it gives rise to a phase transition of second order at $k_B T_c / J = q$ and the susceptibility above T_c is:

$$\chi(T > T_c) \;=\; \left(\frac{\partial \mathcal{M}}{\partial H} \right)_{H \to 0} \;=\; N \mu_0 \mu \left(\frac{\partial M}{\partial B} \right)_{B \to 0} \;=\; \frac{N \mu_0 \mu^2}{k_B (T - T_c)} \;=\; \frac{C_{\mathrm{CW}}}{T - \Theta_{\mathrm{CW}}} \tag{I.28}$$

where C_{CW} and Θ_{CW} are the Curie-Weiss constant and temperature respectively[3].

[3] we notice that C_{CW} is equal to the Curie constant for an Ising spin 1/2

Mean Field Theory: antiferromagnet

Let us consider the same Hamiltonian as (I.25) on a bipartite lattice (square or cubic...) with $J < 0$. The ground state is the so-called Néel ordered state with alternating spins *up* and *down* revealing two interpenetrating sublattices. Reasoning on each subset of spins, we obtain two coupled equations unveiling another 2nd order phase transition at $T_N = \frac{|J|q}{k_B}$ and a susceptibility $\chi(T > T_N) = \frac{C_{\rm CW}}{T+T_N}$ that is maximal at the transition but does not diverge, as the magnetic field B_0 is not conjugate to the staggered Néel order parameter.

Experimental susceptibility

We must not forget here that the MF theory neglects fluctuations and is thus unable to describe the physics near a critical point. In fact, exact results (for $2d$ systems) and numerical simulations (for $3d$) tell us that for a ferromagnet near the transition $\chi \propto |T - T_c|^\gamma$ where $\gamma = 1.75$ ($2d$) or $\gamma = 1.250 \pm 0.002$ ($3d$) [LB02]. However, away from the transition, the MF theory becomes valid and we can summarise our results as follows:

$$\chi \sim \frac{1}{T - \Theta_{\rm CW}} \qquad \text{where} \begin{cases} \Theta_{\rm CW} = 0 & \text{in the paramagnetic phase} \\ \Theta_{\rm CW} > 0 & \text{for ferromagnetic bonds} \\ \Theta_{\rm CW} < 0 & \text{for antiferromagnetic bonds} \end{cases} \tag{I.29}$$

Hence, an experimental measure of the susceptibility will give the sign of $\Theta_{\rm CW}$ and then the nature of the interactions in the compound, as well as an estimate of their strengths J. However this method must be used with caution since $\Theta_{\rm CW}$ represents the energy of the *effective* bond between spins, which might not be completely described by the bare exchange coupling, as in spin ice for example (cf. section I.3).

I.1.c 2-dimensional XY-model

As discussed in the context of the Landau theory, fluctuations become more and more relevant as the dimensionality d of the system is decreasing. In fact, following a rigourous theorem by Mermin & Wagner [Mer66], long range order (LRO) is impossible for continuous spins and for $D \leqslant 2$. This is indeed correct: for $D = 2$ the classical Heisenberg model has no transition, while the Ising model undergoes a transition into an ordered phase as proved by Onsager [Ons44]. As for the XY model, it is unique in the sense that there is a line of critical point terminating at finite temperature by the specific Berezinskii-Kosterlitz-Thouless transition, but without any LRO for any $T > 0$ [Ber70, Kos73].

Correlation function $g(r)$

If we note θ_i the angle of a spin with respect to a fixed direction (say the x-axis), then the Hamiltonian of this model is written as:

$$\mathcal{H} \;=\; -J \sum_{\langle i,j \rangle} \mathbf{S}_i \cdot \mathbf{S}_j \;=\; -J \sum_{\langle i,j \rangle} \cos(\theta_i - \theta_j) \tag{I.30}$$

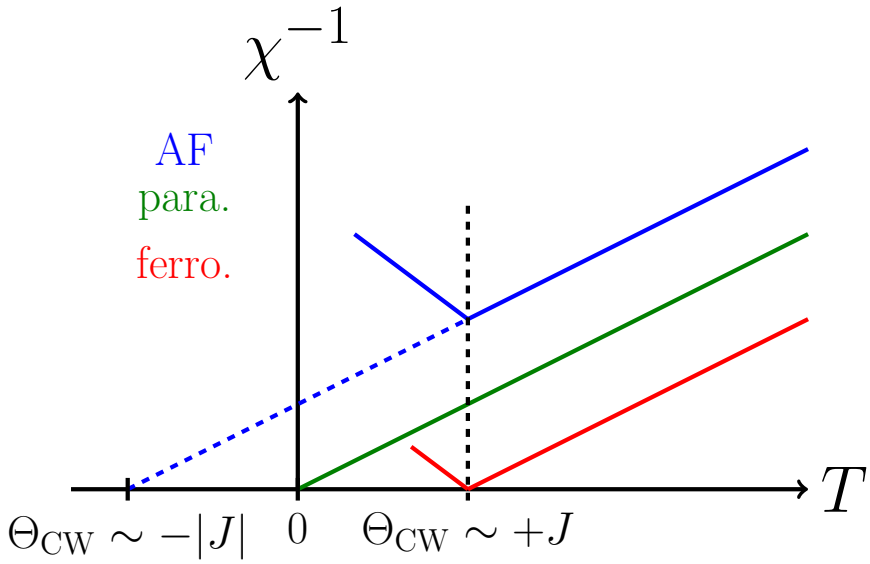

Figure I.3: **Signature of phase transitions in the susceptibility:** Schematic evolution of χ^{-1} as a function of the temperature T. Its behaviour highly depends on the interactions between spins: ferromagnetic (red), antiferromagnetic (blue) or paramagnetic phase (green). The dashed line is an imaginary prolongation of the linear behaviour of χ^{-1} down to negative temperature. For real materials, fluctuations usually drives the transition to slightly lower temperature than Θ_{CW}.

with $J > 0$. At low temperature, the main fluctuations are spin waves of long wave length, *i.e.* the difference $\theta_i - \theta_j$ is smoothly varying for nearest neighbours. We can then take the continuous limit of $\theta_i \to \theta(\mathbf{r})$ and rewrite the Hamiltonian (I.30) up to a constant:

$$\mathcal{H} = \frac{1}{2} J \sum_{\langle i,j \rangle} (\theta_i - \theta_j)^2 = \frac{1}{2} J \int \mathrm{d}\mathbf{r}\, (\nabla\theta)^2 \tag{I.31}$$

Let us define the NN distance a and the spin-spin correlation function $g(r) = \langle \mathbf{S}(0) \cdot \mathbf{S}(\mathbf{r}) \rangle$. The manifestation of the transition occurring in this system is particularly clear through the evolution of this function (see *e.g.* [Gol92, LB02, Arc97])

- low temperature: $g(r) = \left(\frac{a}{r}\right)^{\frac{k_B T}{2\pi J}}$ and $\langle (\theta(r) - \theta(0))^2 \rangle = \frac{k_B T}{\pi J} \ln \frac{r}{a}$;
- high temperature: $g(r) = e^{-\frac{r}{a} \ln\left(\frac{k_B T}{J}\right)}$.

At high temperature, we recover the general feature of a paramagnet with an exponential decay and a correlation length $\xi = \frac{a}{\ln(k_B T/J)} \xrightarrow[T \to \infty]{} 0$, but in the low temperature regime, the correlations become algebraic as for a critical point, although there is no LRO and finite size corrections to the thermodynamic limit remain in the window of experimental observation [Bra93] since the angular deviation diverges logarithmically with distance

r; we thus expect a transition that would account for this change of behaviour from high to low temperature regime. A complete analysis of this transition would require an extensive use of the renormalisation group technique, whose details are beside the scope of this introduction. However, it is still possible to describe this phenomenon qualitatively.

Vortices

Excitations out of the ordered ground state[4] can be either extensive (spin waves) or local vortex excitations, the latter being responsible for the above mentioned transition.

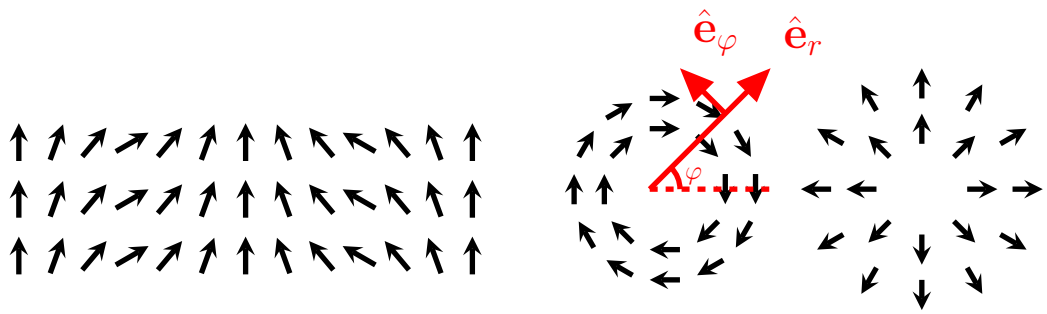

Figure I.4: **Excitations out of the XY ground state:** Spin waves (*left*) and vortices (*right*) whose charges are $Q = +1$.

In figure I.4 we give a few examples of such excitations. For the vortices, it is possible to express the field θ in polar coordinates (r, ϕ): *e.g.* $\theta(r, \varphi) = \text{cst} + \varphi \Rightarrow \nabla\theta = \frac{\hat{\mathbf{e}}_\varphi}{r}$. If $\mathcal{C}$ is a contour enclosing the centre of the vortex, then:

$$\oint_{\mathcal{C}} \nabla\theta \cdot \mathrm{d}\ell \;=\; 2\pi Q, \quad \text{where} \quad Q \in \mathbb{Z} \tag{I.32}$$

This type of excitation is called a *topological defect* bearing a *topological charge* Q and represents a singularity in the field θ. This name comes from the topology of the system that prevents these defects being destroyed by simple perturbations, but only by annihilation with other defects of opposite charge. Since equation (I.32) is reminiscent of Ampere's law with a magnetic field $\nabla\theta$ and a current $2\pi Q/\mu_0$, and the Hamiltonian (I.31) is also a function of the square of $\nabla\theta$, the vortices can be seen as the intersection of current lines with the $2d$ plane. This analogy enables the direct calculation of the potential of interaction between two charges $Q_1(\mathbf{r}_1)$ and $Q_2(\mathbf{r}_2)$:

$$V(Q_1(\mathbf{r}_1), Q_2(\mathbf{r}_2)) \;=\; -2\pi\, J\, Q_1 Q_2 \ln\left|\frac{\mathbf{r}_2 - \mathbf{r}_1}{a}\right| \tag{I.33}$$

The $2d$ XY model appears to be similar to a $2d$ *Coulomb gas* of topological charges. For a system of size $L \gg a$, a rough estimate of the entropy associated with a couple of

[4] with all spins parallel and a $O(2)$ symmetry due to their degree of freedom

opposite charges is $S_{\text{pair}} \sim 2\ln(L/a)^2$. Since this quantity diverges with L, whereas the energy of creation of a pair of defects is finite, we expect these vortices to exist for all temperatures, although their concentration will fall exponentially to zero as $T \to 0$. As for a single vortex of minimal charge, since $\nabla\theta = \frac{\hat{\mathbf{e}}_\phi}{r}$ and according to equation (I.31), its energy is $E = \pi J \ln(L/a)$ and its entropy $S \approx S_{\text{pair}}/2$, giving rise to a free energy

$$F = E - TS = (\pi J - 2T) \ln\left(\frac{L}{a}\right) \tag{I.34}$$

Hence, the vortices remain bounded until they become entropically deconfined at the Kosterlitz-Thouless transition temperature $T_{\text{KT}} = \pi J/2$ which is responsible for the exponential decay of the correlation function.

Within the last two sections of this introduction, we will introduce the key concept of *frustration* and then present in details the physics of spin ice, and see *e.g.* how a gauge theory reminiscent of this Coulomb gas can emerge from an Ising model.

I.2 Frustration in Physics

One of the common point of the systems presented so far is that the ground state possesses the same symmetry as the Hamiltonian, *i.e.* a global $\mathbb{Z}_2$ (Ising) or O(2) (XY) symmetry, due to their particular microscopic description. However, this is far from being a universal feature as illustrated below.

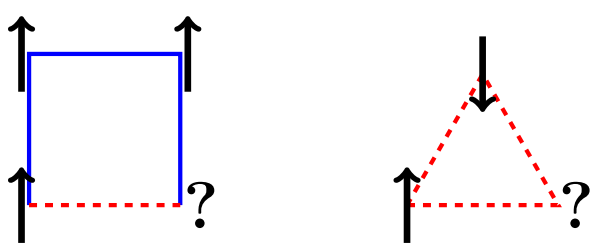

Figure I.5: **Frustration:** Ising spins on a square lattice with random bonds (blue = ferromagnet, dashed red = antiferromagnet) and on an antiferromagnetic triangular lattice.

In both examples shown in figure I.5, the total energy is independent of the orientation of the last spin (marked by **?**), which gives rise to **frustration**.

Definition: *Frustration arises when it is impossible to satisfy all interactions on the lattice at the same time.*

Hence frustration is a natural consequence of the competition between different interactions, each of them endeavouring to impose their own spatial correlations. In this sense, it is in fact a relatively common feature of magnetic compounds and more generally in

condensed matter, but its effects usually remain hidden if one energy scale prevails over the others in the material. The apparition of frustration requires either *randomness* or a specific lattice *geometry*. In this section, we will briefly present the influence of the first condition, before explaining in more details the importance of the latter.

I.2.a Randomness

The notion of frustration in condensed matter first appeared in the context of *spin glasses* [Gar10], in articles by Toulouse [Tou77] and Villain [Vil77] in 1977. However, Anderson seems to have been the first one to notice its importance and to write on a blackboard in Aspen in 1976 "*Frustration is the name of the game*". In order to illustrate the concept of random frustration, let us consider *e.g.* a square lattice with randomly distributed nearest neighbour exchange coupling:

$$\mathcal{H} = \sum_{<i,j>} J_{ij}\, \mathbf{S}_i \cdot \mathbf{S}_j \qquad \text{where} \langle J_{ij} \rangle = 0 \text{ and } \langle J_{ij}^2 \rangle > 0 \tag{I.35}$$

This is the Edwards-Anderson model proposed more than 30 years ago in an attempt to explain the susceptibility of dilute magnetic alloys [Edw75]. This has become the canonical model to study spin glasses. As illustrated on the left of figure I.5, frustration emerges from the interplay between antiferro- and ferromagnetic interactions: the energy landscape in the configurational space appears extremely rugged, with numerous local minima separated by energy barriers. At low temperature, the spin configuration will eventually get pinned in these local minima, leading among other things to a drastic relaxation slow down of the system; the Edwards-Anderson model therefore captures the relevant features of experimental spin glass materials. However we are interested in non-disordered systems here. Of course no crystal is perfect and there is always a residual amount of impurities or randomness, but they usually do not present spin glass behaviour and can thus be neglected, as for example for spin ice materials, where the source of frustration is in fact geometrical.

I.2.b Geometrical frustration

For a theoretical introduction on this subject, the interested reader may consult the papers by Collins & Petrenko [Col97], Moessner [Moe01] and Moessner & Ramirez [Moe06]. Experimental reviews have been written by Ramirez [Ram94] and Greedan [Gre01] while a recent review dedicated to pyrochlore oxydes is to appear in *Reviews of Modern Physics* [Gar10]. There are also several books, *e.g.* [Lie86, Die04] and another one coming soon [Lac10].

In 1950, Wannier [Wan50] and Houtappel [Hou50] studied the Ising antiferromagnet on the triangular lattice (see figure I.5) and noticed its extensive ground state degeneracy, preventing the setting up of long range order (LRO) for any temperatures, in opposition to its ferromagnet counterpart (cf. section I.1). A few years later, Anderson discovered the same property for the Ising antiferromagnet on the 3-dimensional (3d) pyrochlore lattice [And56] (see figure I.6). In the 1960's, the theoretical problems of vertex models

drew a great deal of interest, the highlight being the exact solutions by Lieb of the 2-dimensional (2d) 6-vertex model in 1967 [Lie67a, Lie67b, Lie67c], which can be seen as frustrated in comparison with the 16-vertex model. This model was explicitly built as a two dimensional version of water ice [Pau35] (see subsection I.3.a) and KH_2PO_4, also known as KDP (see subsection III.4) which are non-magnetic materials presenting specific frustrated features. Work on frustration in the 1970's was dominated by the discovery of spin glass by Cannella and Mydosh in 1972 [Can72]. The specific domain of geometrical frustration emerged on its own in the late 1980's, motivated by novel experiments on $SrCr_{9-x}Ga_{3+x}O_{19}$ (SCGO), a remarkable compound that remains paramagnetic down to 3.5 K despite a high Curie-Weiss temperature of $\Theta_{CW} = -515$ K associated with an effective decrease of the lattice dimensionality [Obr88, Ram90, Bro90]. This field of research has exploded during the past 20 years, with the discovery of a plethora of materials sharing a set of common properties.

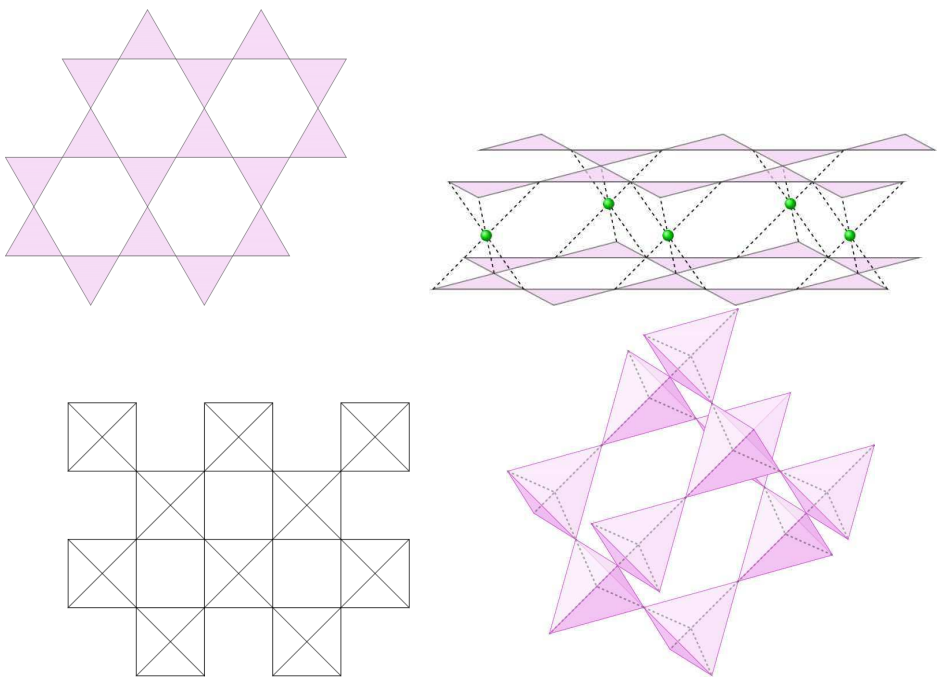

Figure I.6: **Frustrated lattices** encountered in geometrically frustrated systems in 2 or 3 dimensions: (*clockwise*) the Kagome lattice, SCGO formed by a triangular layer (green balls) sandwiched between two Kagome lattices, the pyrochlore lattice and its two dimensional projection, the checkerboard lattice.

General Features

As discussed in figure I.3, each type of interaction in a compound is characterised by susceptibility measurements. The remarkable thing is that frustration has its own signature also. Since most of the frustrated systems are antiferromagnet, we consider a negative Curie-Weiss temperature in the example of figure I.7, where the linear behaviour of χ^{-1}

persists below Θ_{CW}: frustration hinders or ideally completely precludes the occurrence of a phase transition into a long range order down to temperature T_F set by perturbation terms with respect to the original Hamiltonian.

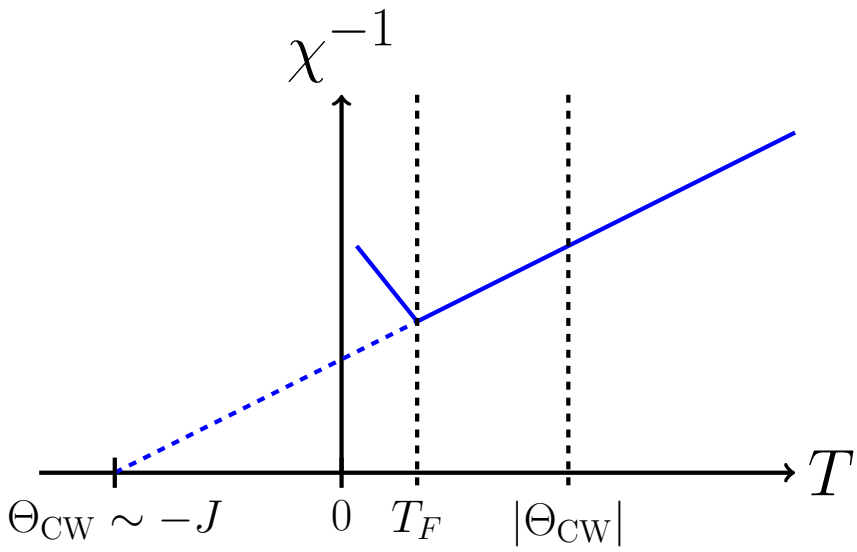

Figure I.7: **Signature of frustration in the susceptibility:** Schematic evolution of χ^{-1} as a function of the temperature T for a frustrated system. The dashed line is an imaginary prolongation of the linear behaviour of χ^{-1} down to negative temperature. The main point here is that geometrical frustration drives the ordering temperature T_F orders of magnitude below the Curie-Weiss temperature $|\Theta_{\mathrm{CW}}|$. This phenomenon cannot be induced by mere thermal fluctuations.

Figure I.7 brings to light the existence of three different regimes:

- $\Theta_{\mathrm{CW}} < T$: the usual paramagnetic phase, where thermal fluctuations are strong enough to keep the spin configurations disordered.

- $T_F < T < \Theta_{\mathrm{CW}}$: the interaction energy scale set by Θ_{CW} should be able to project the system into an ordered phase, but this is prevented by a subtle organisation of the correlations. This intermediate phase is known as *collective or cooperative paramagnetic regime* [Vil79], a term usually used for classical models, or *spin liquid* [And73, And87].

- $T < T_F$: In ideal spin liquids, this regime should not exist and the system should remain disordered down to 0 K. However in real materials, perturbations that should be negligible in comparison to the main interactions of order Θ_{CW} become relevant thanks to frustration and will cause a phase transition or crossover or even a spin freezing at a temperature T_F fixed by their energy scale. This phase below T_F is thus not necessarily ordered.

This threefold feature is so general in frustrated systems that it led to the definition of a simple and convenient *frustration index* introduced by Ramirez [Ram94] $f \equiv |\Theta_{\mathrm{CW}}|/T_F$, which eventually goes to infinity for ideal spin liquids. However we must be cautious as the absence of order at finite temperature in low dimensional systems is not necessarily a proof of frustration, but can rather be a consequence of thermal or quantum fluctuations; it remains nonetheless valid and useful for $3d$ models. As an example of non-trivial origin of a collective paramagnetic behaviour, we discuss classical models of continuous spins on corner sharing lattices.

Collective paramagnet

Let us define the dimension of the ground state D as the difference between the number of degrees of freedom F and the dimension of the constraints K; it is one of the most relevant property of classical models because if D is extensive, then the system should *a priori*[5] remain macroscopically dynamic in a collective paramagnetic phase [Vil79, Moe98b]. In order to understand this physics more intuitively, we will define a model as general as possible that allows an estimate of these numbers [Moe01].
A common point of the corner sharing lattices displayed in figure I.6 is the possibility to divide them into frustrated units including q mutually interacting spins: corner-sharing tetrahedra for SCGO and the pyrochlore lattice, triangles for Kagome and squares for the checkerboard lattice. In this case, a nearest neighbour antiferromagnetic Hamiltonian can be rewritten as

$$\mathcal{H} \;=\; J \sum_{\langle i,j \rangle} \mathbf{S_i} \cdot \mathbf{S_j} \;=\; \frac{J}{2} \sum_{\alpha=1}^{N} \mathbf{L}_\alpha^2 \qquad \text{where} \quad \mathbf{L}_\alpha \;=\; \sum_{\substack{i=1 \\ i \in \alpha}}^{q} \mathbf{S_i} \tag{I.36}$$

where $\mathbf{L}_\alpha$ is the total spin of one of the N units, indexed by α and $\mathbf{S}_i$ is a spin of unit length with n components. Hence $\mathbf{L}_\alpha = 0$ locally minimises the Hamiltonian and imposes n constraints ($L_\alpha^{x_1} = L_\alpha^{x_2} = ... = L_\alpha^{x_n} = 0$), while there are $(n-1)\ q$ degrees of freedom per unit [6], which gives for the entire system

$$D \;=\; F - K \;=\; \frac{N}{2}\ (n(q-2) - q) \tag{I.37}$$

where the 1/2 factor comes from the fact that each spin belongs to two units. According to this argument, the only *a priori* realistic model with $D \propto N$ is the Heisenberg Hamiltonian on the pyrochlore lattice ($n = 3, q = 4$). This is nonetheless only a good indication of degeneracy, because the different units of a lattice are connected, making the constraints non-independant and the degeneracy possibly extensive ($D \propto N$), as *e.g.* for the Heisenberg Kagome ($n = 3, q = 3$) or XY pyrochlore model ($n = 2, q = 4$) also: there is thus a subset of NN models that have macroscopically degenerate ground states, either discrete or continuous. However there is a subtle point here that has been occulted so far: the whole ground state manifold is not necessarily "uniform", in the sense that

[5] If we neglect further perturbations responsible for the transition at T_F.
[6] because of the unit length of $\mathbf{S}_i$, there is one degree of freedom lost per spin.

even if the internal energy is the same, the free energy may differ from one configuration to another, because of the presence of zero modes, *i.e.* of connected subspaces accessible at zero energy cost (at least in the harmonic approximation). If the entropy of such subspace dominates the entropy of the rest of the ground state manifold, then fluctuations (*e.g.* thermal or quantum) will lift the macroscopic degeneracy and select this subspace through an ordering transition; this phenomenon is known as *order by disorder* and has been introduced by Villain [Vil80] and its application to the present case comes from [Cha92] and [Moe98b]. The Heisenberg Kagome or XY pyrochlore models undergo such transition whereas the Heisenberg ptrochlore remains theoretically disordered down to zero Kelvin.

Following this overview, one sees the original contributions geometrical frustration can make to condensed matter: on a lower energy scale than the main nearest neighbour (NN) interactions, the 2nd or 3rd NN or long range (dipolar, quadrupolar) interactions, spin-lattice couplings, quantum fluctuations will act as perturbations, lifting the ground state degeneracy and being responsible for the transition at T_F. Since these effects are usually hidden in non-frustrated systems, it is then a unique occasion to see their full influence through exotic phase transitions or crossovers into non-trivial long range order or spin glass. Furthermore the collective paramagnet or spin liquid is also by itself an interesting feature of these materials, especially when this phase prevails down to 0 K (or more precisely, to the lowest accessible temperature), as maybe in the case of $Tb_2Ti_2O_7$ [Gar99, Gar03].

Since my thesis will focus on *Spin Ice*, where the spins are considered as Ising at low temperature within a very good approximation, the aim of this introduction was to briefly present the richness of frustration that can arise in classical models in general. As a consequence, we have been able to introduce the notion of *unit* which is particularly relevant in frustrated systems; the main physics can usually be qualitatively understood by studying these simple units at first, whereas a more complete picture will eventually require the consideration of the dependance between them, as presented in the next section.

I.3 Spin Ice

I.3.a Origin

Spin ice brings together a group of rare-earth oxide insulator $R_2M_2O_7$ with space group $Fd\overline{3}m$ where R^{3+} is a rare-earth magnetic ion whereas M^{4+} (Ti^{4+} or Sn^{4+}) is non-magnetic. Each type of cation sits on the vertices of one of two interpenetrating pyrochlore lattice formed by corner-sharing tetrahedra (see figure I.8). The well-established members of this family are $Dy_2Ti_2O_7$, $Ho_2Ti_2O_7$ and $Ho_2Sn_2O_7$, the latter being less studied because it is only available under polycrystalline form hindering the study of the characteristic anisotropy of spin ice: its melting is indeed incongruent, *i.e.* its liquid phase is not uniform but is polluted by microscopic crystals that prevent a uniform crystallisation.Although this thesis will focus on these three compounds, one should not forget their promising

quantum counterparts $Tb_2Ti_2O_7$ and $Tb_2Sn_2O_7$ (see below for a short discussion) and potential candidates for spin ice materials such as $Dy_2Sn_2O_7$ or $Pr_2Sn_2O_7$.

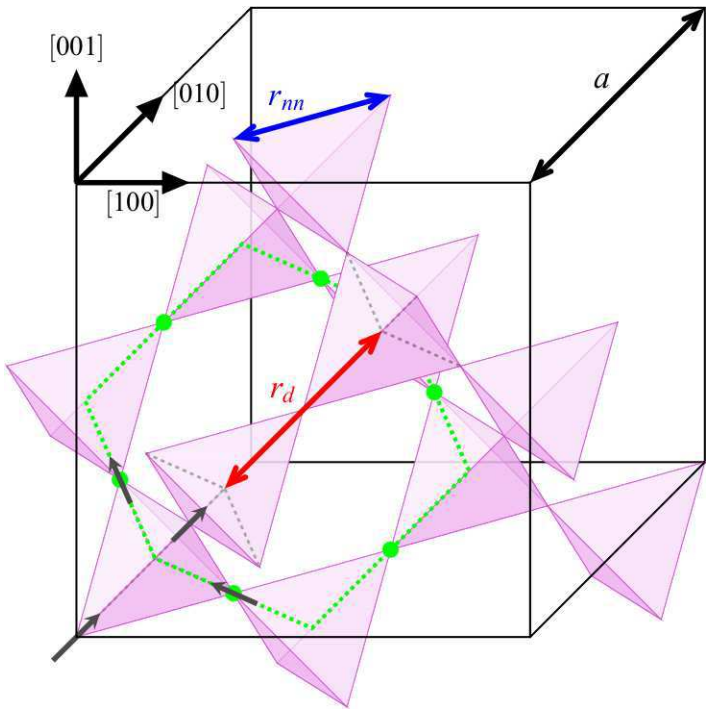

Figure I.8: **Pyrochlore lattice:** The spins are located on the corner of every tetrahedra and are fixed along their local [111] axis represented by the dashed lines. There are two types of tetrahedra that we shall call the *down* tetrahedra (bottom left with the four spins) and the *up* tetrahedra. Each *down* tetrahedra is connected to four *up* ones, and vice-versa. The cube represents a unit cell with 8 tetrahedra (four of each kind) and 16 spins, and defines the [100] (x), [010] (y) and [001] (z) axes. We introduce the length of the unit cell $a \approx 10$ Å as well as the distance between nearest neighbour $r_{nn} = \frac{\sqrt{2}}{4}\,a \approx 3.5$ Å and between the centres of two connected tetrahedra $r_d = \frac{\sqrt{3}}{4}\,a \approx 4.3$ Å. The smallest close loop encompasses 6 spins (see green loop).

As explained in detail in section I.1, the total angular momentum $\mathbf{J} = \mathbf{L} + \mathbf{S}$ is a good quantum number for rare earth elements and their electronic ground states is determined by the Hund's rules (see [Kit96], §14).

The free ion Dy^{3+} (resp. Ho^{3+}) then has a 16-fold (resp. 17-fold) degeneracy that is lifted by the surrounding crystal field; the corresponding energy levels have been estimated by neutron time-of-ight spectroscopy [Ros00], revealing an almost pure ground state doublet.

Thanks to the large energy level of the first excited state, the low temperature behaviour of these materials can be approximated by classical Ising spins with a very large magnetic moment ($\approx 10\,\mu_B$). This is the main difference with $Tb_2Ti_2O_7$ and $Tb_2Sn_2O_7$ where the ground state level is also a doublet, but Δ is much smaller (~ 10 K), and of the same order of magnitude as the interactions between spins [Gin00]. The admixing with

	[R]	[R^{3+}]	S	L	J
Dy	[Xe] $4f^{10}\,6s^2$	[Xe] $4f^9$	5/2	5	15/2
Ho	[Xe] $4f^{11}\,6s^2$	[Xe] $4f^{10}$	2	6	8

Table I.1: **Ground state electronic configuration** of the atom [R={Dy,Ho}], the free ion [R^{3+}], and the corresponding quantum numbers S, L and J

	GS	g_J	μ	Δ (meV)	Δ (K)
Dy	$\lvert 15/2, \pm 15/2\rangle$	4/3	$\approx 10\,\mu_B$	~ 0.033	~ 380
Ho	$\lvert 8, \pm 8\rangle$	5/4	$\approx 10\,\mu_B$	~ 0.020	~ 240

Table I.2: **Crystal field level:** The ground states $|J, J_z\rangle$ (GS), the Landé factor g_J, the estimated magnetic moment $\mu = g_J\, J\, \mu_B$ and the energy level of the first excited state Δ. $\left(g_J = 1 + \frac{J(J+1)-L(L+1)+S(S+1)}{2J(J+1)}\right)$

exciting CF states is thus not negligible and the spins are not perfectly Ising anymore. Quantum corrections are required for a complete picture of these two compounds with Tb rare-earth ions. [Mol07].

One last point about the single ion geometry in spin ice is that the cubic symmetry of the pyrochlore lattice does not allow a global Ising symmetry but rather a local easy-axis anisotropy: each spin points along the line joining the centres of two connected tetrahedra.

An important fact that we should keep in mind is that the geometrical frustrated systems we have presented so far are all antiferromagnets: Ising spins on the triangular lattice, Heisenberg model on the Kagome and pyrochlore lattice, *etc.* One reason why spin ice made such a noticeable entry in 1997 is that it is a frustrated *ferromagnet*: Mark Harris, Steven Bramwell and collaborators used muon spin resonance (μSR) and neutron scattering to show the absence of phase transition in $Ho_2Ti_2O_7$ down to 50 mK, but with a positive Curie-Weiss temperature $\Theta_{\rm CW} \approx 1.9$K [Har97]. Hence, with a frustration index $f \sim 40$, $Ho_2Ti_2O_7$ thus appeared as the first example of a *frustrated ferromagnet*, whose origin is elegantly understood through mappings with water ice [Pau35] or Anderson's model for spinels [And56] (see figure I.9), the former being responsible for the name of *spin ice* [Har97]. These analogies have been introduced by Harris et al. [Har97] and explained in details in [Bra98, Moe98a] and to understand them, we must first find the ground state configuration of a single tetrahedron where the spins are aligned along their

local [111] direction

$$\mathbf{S}_1 = \pm\frac{1}{\sqrt{3}}\begin{pmatrix}-1\\-1\\+1\end{pmatrix} \quad \mathbf{S}_2 = \pm\frac{1}{\sqrt{3}}\begin{pmatrix}+1\\+1\\+1\end{pmatrix} \quad \mathbf{S}_3 = \pm\frac{1}{\sqrt{3}}\begin{pmatrix}+1\\-1\\-1\end{pmatrix} \quad \mathbf{S}_4 = \pm\frac{1}{\sqrt{3}}\begin{pmatrix}-1\\+1\\-1\end{pmatrix} \tag{I.38}$$

where the indexes follow the notation of figure I.9 and an *out* spin, *i.e.* a spin pointing out of the tetrahedron, corresponds to the above vector with a positive sign. By convention the spin vector is of unit length and its actual magnetic moment ($\sim 10\mu_B$) will be included in the constants of the Hamiltonian. As we shall see in the next subsection, long

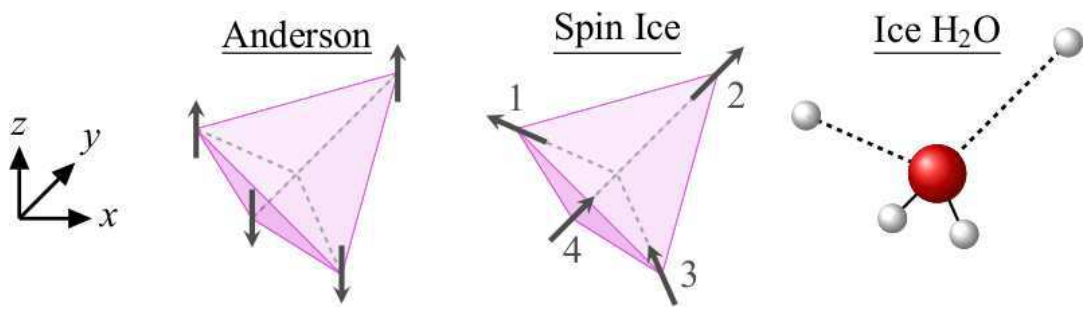

Figure I.9: **Models equivalent to spin ice:** The different mappings between Anderson's model for antiferromagnetic spinels, spin ice and water ice: the white spheres are the hydrogen atoms and the red one is the oxygen. A spin pointing *inside* (resp. *outside*) the tetrahedron corresponds to a *down* (resp. *up*) spin in the Anderson model and a short covalent bond (resp. long H-bond) for water ice.

range interactions are necessary for a complete description of these materials, but nearest neighbour interactions are a surprisingly good approximation able to qualitatively explain most of their properties. In this context, the spin ice Hamiltonian is

$$\mathcal{H} = -J_F \sum_{\langle i,j\rangle} \mathbf{S}_i \cdot \mathbf{S}_j \tag{I.39}$$

where J_F is a positive ferromagnetic constant. Equation (I.38) directly gives

$$\mathbf{S}_i \cdot \mathbf{S}_j = \begin{cases} -1/3 & \text{if both spins are } \textit{out} \text{ or } \textit{in} \\ +1/3 & \text{if one is } \textit{out} \text{ and the other is } \textit{in} \end{cases} \tag{I.40}$$

enabling one to rewrite the Hamiltonian [Moe98a]

$$\mathcal{H} = \frac{J_F}{3} \sum_{\langle i,j\rangle} \sigma_i\, \sigma_j \quad \text{where} \begin{cases} \sigma_i = +1 & \text{for an } \textit{out} \text{ spin} \\ \sigma_i = -1 & \text{for an } \textit{in} \text{ spin} \end{cases} \tag{I.41}$$

This Hamiltonian matches that of an antiferromagnet with a global Ising symmetry and has been first studied in the more general case of ordering in the spinel structure by Anderson [And56]; the equivalence is fully detailed in figure I.9. According to equation (I.36), the energy of the antiferromagnetic Anderson model is minimised when the magnetisation for each tetrahedron is zero, *i.e.* with two spins *up* and two spins *down*. For the spin ice model, it corresponds to two spins pointing inward and the remaining two pointing outward, giving rise to a finite magnetisation, either positive or negative, along one of the three cartesians axes: as this configuration will be of particular importance, we should name it the 2 *in* - 2 *out* state. Among the $2^4 = 16$ possible configurations per tetrahedron, 6 of them respect this condition, as depicted in figure I.10 The mapping between

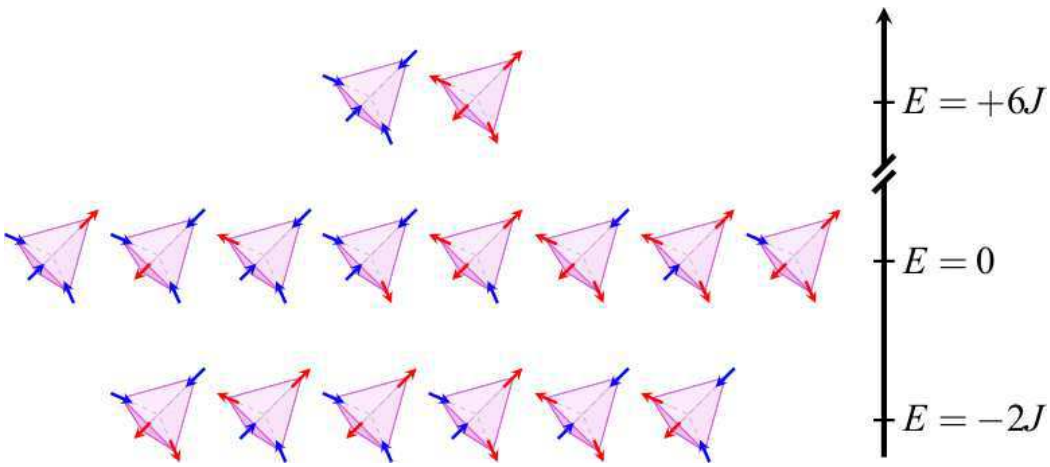

Figure I.10: **Degeneracy in spin ice:** The 16 possible configurations for a single tetrahedron where $J = J_F/3$ here (see equation (I.41). The blue (resp. red) arrows represent spins pointing inside (resp. outside) the tetrahedron.

these magnetic models and water ice is both cunning and straightforward (see figure I.9). In its solid phase, the oxygen atom of H_2O is connected to four hydrogen: two of them are close to the oxygen, linked by covalent bonds (arbitrarily chosen as analogue of *out* spins) whereas the others two are further apart and connected to the oxygen by a weaker hydrogen bond (the *in* spins). Hence we say that the ground state respect the so-called *ice-rules* first defined by Bernal & Fowler [Ber33]. From this mapping, we would expect spin ice to reproduce some of the thermodynamic properties of water ice.

In apparent opposition with the third law of thermodynamics, Pauling predicted in 1935 a finite entropy for water ice down to zero Kelvin that has been measured three years later by Giauque & Stout [Gia36]. More than 60 years later, Ramirez and colaborators found the same zero point entropy in spin ice [Ram99] as a consequence of geometrical frustration: the spins would like to be parallel to each other, but because they are forced to remain along their local [111] axis they can only form a 2 *in* - 2 *out* state which gives rise to the same highly degenerate ground state manifold. Here it is particularly interesting to notice that antiferromagnetic interactions would erase this frustration and favour the 4 *in* or 4 *out* states [Har97, Bra98], as for FeF_3 [Fer86]. The exact expected value of this entropy is still not known due to the analytical challenge to perform an exact

computation for a $3d$ system, but a mean field calculation as introduced by Pauling is nonetheless possible and noticeably accurate. There are $N/2$ tetrahedra in a system of N spins with a total number of 2^N configurations. For each tetrahedron 16 configurations are possible but only 6 of them are part of the ground state which means that from a mean field point of view 6/16 of the configurations per tetrahedron remain available down to zero Kelvin. Hence the zero-point entropy should be [Pau35]

$$S(T=0) \approx k_B \ln\left(2^N \left(\frac{6}{16}\right)^{N/2}\right) = \frac{N}{2} k_B \ln\left(\frac{3}{2}\right) \tag{I.42}$$

This estimation falls in semi-quantitative agreement (within a few percent) with experimental results on water ice [Gia36] and spin ice by Ramirez and collaborators [Ram99] (see figure I.11). They computed the entropy change by integration of the specific heat C_h measured between 0.2 K and 12 K

$$\Delta S = S(T_2) - S(T_1) = \int_{T_1}^{T_2} \frac{C_h}{T}\, dT \tag{I.43}$$

This experiment not only proved the spin ice nature of $Dy_2Ti_2O_7$ but was also a brilliant confirmation of the validity of this model. However, as we have already suggested, nearest neighbour spin ice is not the most accurate model, but its relevance happens to be a stunning consequence of dipolar interactions on the specific geometry of the pyrochlore lattice.

I.3.b Dipolar Interactions

As suggested by Harris *& al.* [Har98] and Moessner [Moe98a] and discussed in the introduction, dipolar interactions are of particular importance for rare earth ions Ho^{3+} and Dy^{3+}. Indeed, since this material is made of rare earth atoms, the exchange coupling is due to $4f$ electrons, buried behind $5s$ and $5p$ layers[7], and is thus very weak ($\sim$ 1K) in comparison with usual ferromagnet ($\sim 10^3$ K for iron). Additionally the magnetic moments in spin ice are really strong ($\approx$ 10 Bohr magneton). This is why the dipolar interactions, that are negligible on short length scale for iron, become preponderant in spin ice.

Siddharthan and collaborators were the first ones to highlight their influence and to suggest the dipolar origin of NN ferromagnetic coupling in $Ho_2Ti_2O_7$ [Sid99], the exchange coupling between Ho^{3+} ions being in fact antiferromagnetic. They obtained a dipolar interaction driven 1st order transition into an ordered phase that they matched with the peak of the specific heat in $Ho_2Ti_2O_7$ (see figure I.12). However this interpretation proved to be wrong and the peak was shown to be a manifestation of the large nuclear moment of Ho^{3+} ($I = 7/2$) [Blo69, dH99, Bra01b]). Once this hyperfine Schottky anomaly was substracted, the specific heat recovers the same shape and same Pauling's entropy as for $Dy_2Ti_2O_7$ [Bra01b, dH00]. In fact, even if the degeneracy lift is of particular importance,

[7] The $6s$ layer is empty because Ho^{3+} and Dy^{3+} lost three electrons.

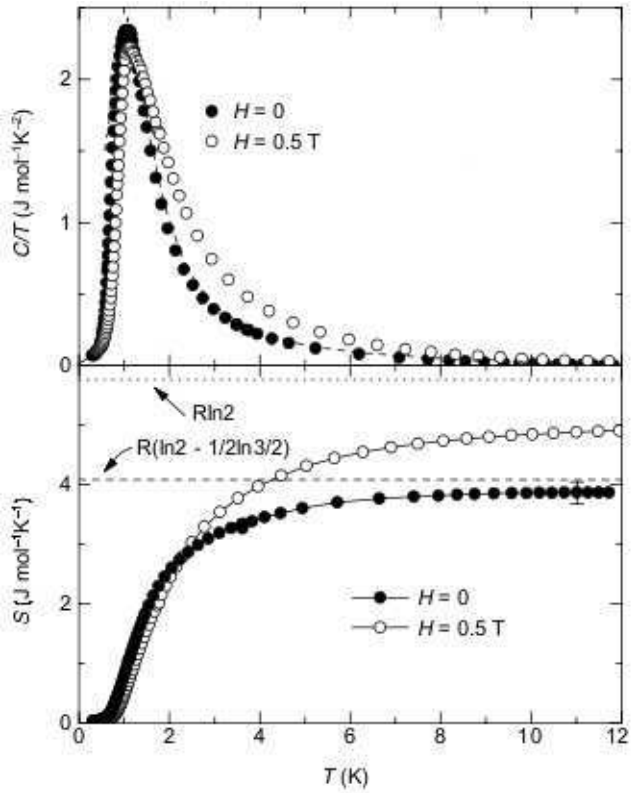

Figure I.11: **Zero-point entropy in $Dy_2Ti_2O_7$:** Specific heat (*top)* and entropy (*bottom*) per mole as a function of temperature [Ram99]. The entropy is arbitrarily fixed to be zero at zero Kelvin and should be equal to $R \ln 2$ at high temperature which means that the difference with this value corresponds to the zero point entropy that agrees with Pauling's estimate (black dots). However this degeneracy is lifted in presence of an external magnetic field (open circles, see I.3.d).

the 1st order transition happened to be an artefact of the truncation of the long range interactions after the 5th [Sid99] or 12th [Sid01] NN, as explained by den Hertog *&* Gingras [dH99, dH00]. These authors used the Ewald method (see section II.4) in order to take into account the infinite range of the dipolar interactions and showed the absence of a phase transition with a Monte Carlo algorithm using *single spin flip* Metropolis updates. They also performed a mean field calculation explaining how a finite truncation radius R_c of the dipolar interactions leads to a brutal degeneracy lifting while the 2 *in* - 2 *out* ground state degeneracy is *almost* completely recovered as $R_c \to \infty$ by *self-screening* of the dipolar interactions.

Dipolar spin ice (DSI) finally became the most relevant model when Bramwell and collaborators showed it was able to reproduce the features of the scattering function of $Ho_2Ti_2O_7$ measured by neutron scattering at 50 mK [Bra01b] (see figure I.13). The dipolar contribution turns out to be indispensable for understanding certain magnetic field induced transitions [Mel04, Yos04, Ruf05] (see I.3.d) as well as the quantitative feature of magnetic monopole excitations [Jau09b] (see I.3.c). The Hamiltonian of DSI is written

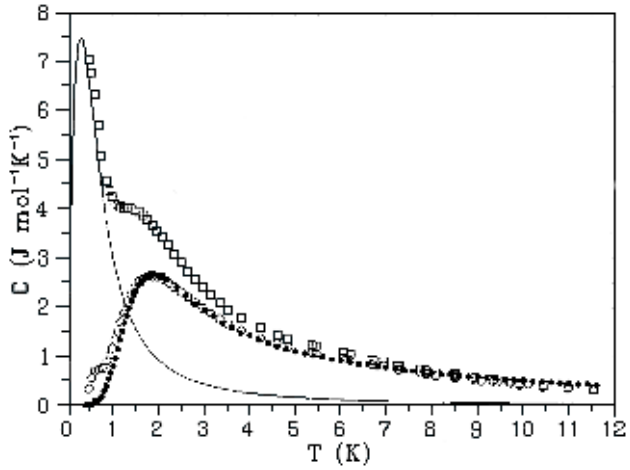

Figure I.12: **Hyperfine coupling in $Ho_2Ti_2O_7$:** Specific heat vs temperature: experimental data (□), estimated nuclear component (straight line), resulting electronic component (○) and Monte Carlo simulations for the electronic component (●) [Bra01b]. The peak is of nuclear origin rather than a signature of a phase transition and the electronic component of the specific heat is very similar to the one for $Dy_2Ti_2O_7$.

as.

$$\mathcal{H} \;=\; -J \sum_{\langle i,j \rangle} \mathbf{S}_i \cdot \mathbf{S}_j \;+\; D\, r_{nn}^3 \sum_{i>j} \left[\frac{\mathbf{S}_i \cdot \mathbf{S}_j}{|\mathbf{r}_{ij}|^3} - \frac{3\,(\mathbf{S}_i \cdot \mathbf{r}_{ij})\,(\mathbf{S}_j \cdot \mathbf{r}_{ij})}{|\mathbf{r}_{ij}|^5} \right] \tag{I.44}$$

where J, D and $r_{nn} \approx 3.5$ Å are respectively the antiferromagnetic exchange, the dipole-dipole coupling and the nearest neighbour distance between rare earth ions (see figure I.8). By definition of the dipolar interactions, we have

$$D = \frac{\mu_0\, \mu^2}{4\pi\, r_{nn}^3} \approx 1.4K \tag{I.45}$$

The remarkable property of this Hamiltonian is that it explains the surprising quantitative relevance of the NN model comes from the geometry of the pyrochlore lattice. Let us consider the dipolar interaction between the spins 1 and 2 defined in figure I.9.

$$\begin{aligned}
& D\, r_{nn}^3 \left[\frac{\mathbf{S}_1 \cdot \mathbf{S}_2}{|\mathbf{r}_{12}|^3} - \frac{3\,(\mathbf{S}_1 \cdot \mathbf{r}_{12})\,(\mathbf{S}_2 \cdot \mathbf{r}_{12})}{|\mathbf{r}_{12}|^5} \right] \\
= \;& D \left[\frac{\sigma_1}{\sqrt{3}} \begin{pmatrix} -1 \\ -1 \\ +1 \end{pmatrix} \cdot \frac{\sigma_2}{\sqrt{3}} \begin{pmatrix} +1 \\ +1 \\ +1 \end{pmatrix} - 3 \left\{ \frac{\sigma_1}{\sqrt{3}} \begin{pmatrix} -1 \\ -1 \\ +1 \end{pmatrix} \cdot \frac{1}{\sqrt{2}} \begin{pmatrix} 1 \\ 1 \\ 0 \end{pmatrix} \right\} \left\{ \frac{\sigma_2}{\sqrt{3}} \begin{pmatrix} +1 \\ +1 \\ +1 \end{pmatrix} \cdot \frac{1}{\sqrt{2}} \begin{pmatrix} 1 \\ 1 \\ 0 \end{pmatrix} \right\} \right] \\
= \;& \frac{5D}{3} \sigma_1 \sigma_2
\end{aligned}$$

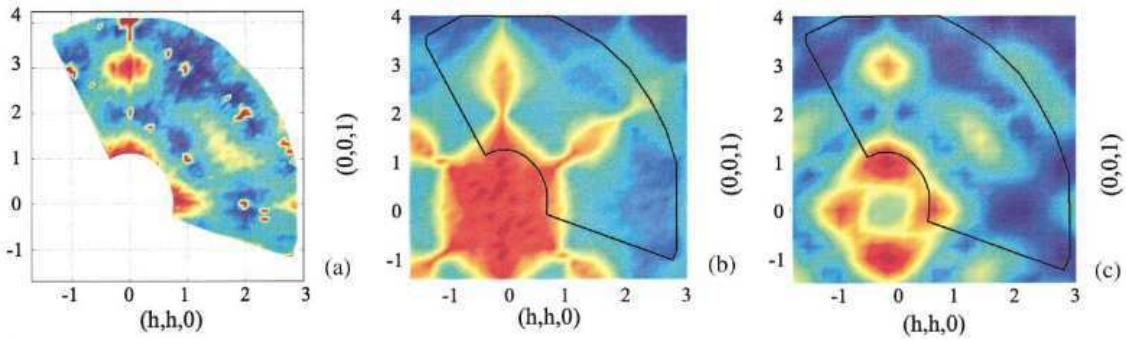

Figure I.13: **Scattering function in spin ice:** *(a)* Experimental neutron scattering pattern $S(q)$ of $Ho_2Ti_2O_7$ in the (hhl) plane of reciprocal space at T ∼50 mK. Dark blue shows the lowest intensity level, red-brown the highest. Temperature dependent measurements have shown that the sharp diffraction spots in the experimental pattern are nuclear Bragg peaks with no magnetic component. *(b)* $S(q)$ for the nearest neighbor spin ice model at $T = 0.15\,J$. *(c)* $S(q)$ for the dipolar spin ice model at $T = 0.6$ K, which is visibly more adequate to describe the experimental feature of the scattering function than the NN model. The areas dened by the solid lines denote the experimental data region of (a). Figure and caption from [Bra01b].

where σ_i was defined in equation (I.41). By symmetry, the result is the same for all pairs of spins in a tetrahedron. Hence the NN term of the dipolar interaction is equivalent to an exchange term and the NN Hamiltonian is recovered as follows

$$\mathcal{H} \;=\; J_{\text{eff}} \sum_{\langle i,j \rangle} \sigma_i\, \sigma_j \quad \text{where} \quad J_{\text{eff}} \;=\; D_{nn} + J_{nn} \;=\; \frac{5D}{3} + \frac{J}{3} \tag{I.46}$$

A numerical value of J has been obtained by comparison between Monte Carlo simulations and experimental data of the specific heat for $Dy_2Ti_2O_7$ [dH00] or of neutron scattering for $Ho_2Ti_2O_7$ [Bra01b] and $Ho_2Sn_2O_7$ [Kad02]. In the latter case, the uncertainty of around 50% is considerably higher than in the cases of $Ho_2Ti_2O_7$ and $Dy_2Ti_2O_7$. The complete serie is summarised in the following table.

A complete understanding of the self-screening of the dipolar interactions requires more refinements that will be presented in the next subsection, but nonetheless we now have a good idea about the origin of frustration in these materials: the AF exchange is made effectively ferromagnetic by the dipolar interaction and the resulting system maps onto a frustrated AF model. However one question remains unanswered; if the extensive degeneracy of the NN model is, even only slightly, lifted by dipolar interactions, how is it that neither experiments [Ram99, Sid99, Bra01b] nor numerical simulations [dH00, Bra01b] manage to find a transition or crossover into an ordered phase ? The reason, at least in the case of numerical simulations, is *spin freezing*: there is in fact a dramatic slowing down of the dynamics at low temperature (below 1 K for $Dy_2Ti_2O_7$) that prevents the equilibration of the system and thus the observation of an ordered state. We will come back to the origin of this freezing later in this introduction and in the chapter IV, but

	D	D_{nn}	J	J_{nn}	J_{eff}
Dy [dH00]	1.41	2.35	-3.72	-1.24	1.11
HoTi [Bra01b]	1.41	2.35	-1.65	-0.55	1.8
HoSn [Kad02]	1.41	2.35	≈ 1.0	≈ 0.33	≈ 2.7

Table I.3: **Nearest neighbour interactions:** Exchange, dipolar and effective antiferromagnetic couplings in Kelvin.

without studying the actual dynamics of spin ice, we can nonetheless find a (theoretical) way to force the system to equilibrate. This is the method used by Melko and collaborators, using a non-local algorithm, able to remain in the 2 *in* - 2 *out* manifold by flipping loops of spins [Mel01b, Mel04]. They obtained a 1st order transition towards an ordered state described by the scattering vector $q = (0, 0, 2\pi/a)$ as depicted on figure I.15. The phase diagram on the same figure shows the influence of the ratio J_{nn}/D_{nn}

- $J_{nn}/D_{nn} \lesssim -0.91$: the AF nature of the exchange is too strong and dominates the dipolar interactions; the system is not frustrated anymore;
- $J_{nn}/D_{nn} \gtrsim -0.91$: there is a crossover between the paramagnetic phase and the spin ice regime where the NN model rules the world, at a temperature depending on J_{nn}/D_{nn}[8], before entering into the $q = (0, 0, 2\pi/a)$ phase dictated by the long range dipolar interactions at low temperature (see figure I.15).

As usual in condensed matter, it is always possible to look for a more detailed Hamiltonian able to reproduce more microscopic features of a material and spin ice does not derogate from this rule. Fennell *& al.* were the first ones to suggest the limit of the DSI model that bears some discrepancies with neutron scattering experiments [Fen04], closely followed by Ruff *& al.* and Tabata *& al.* when they tried to quantitatively fit theory with a magnetic field driven transition [Ruf05, Tab06]. This point has been recently strengthened by the neutron scattering experiments that are precise enough to pinpoint the tiniest differences with simulations [Yav08]. As shown in figure I.8, the pyrochlore lattice can be seen as an entanglement of interpenetrating $3d$ hexagons formed by 6 tetrahedra while at the same time, hexagon-like shapes are observed in the scattering function of $Dy_2Ti_2O_7$ [Fen04]. Yavors'kii and collaborators tested the degree of coincidence between these two observations [Yav08] and found that even if simulations of independent hexagons are able to give a semi-quantitative fit of the experimental results, suggesting the emergence of clusters in frustrated systems as in $ZnCr_2O_4$ [Lee02], the inclusion of 2nd

[8] Since D_{nn} is known, J_{nn} can be deduced by the position of the Schottky peak in the specific heat [dH00]

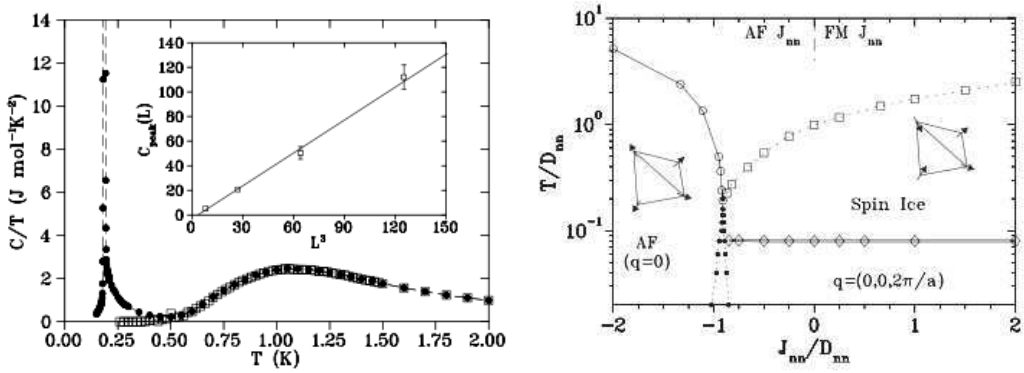

Figure I.14: **Phase transition in dipolar spin ice:** *Left:* Simulations of the specific heat obtained by a combination of single spin flip moves (SSF) and the loop algorithm (•) and SSF only (□) [Mel01b]. The sharp peak at ~ 200 mK as well as the linear scaling of its maximum value C_{peak} as a function of the system volume L^3 (*inset*) are clear indications of the first order nature of this transition. The SSF algorithm is not able to equilibrate the system and the transition is thus not observed. *Right:* Phase diagram of dipolar spin ice T/D_{nn} vs J_{nn}/D_{nn} [Mel04] (see figure I.15 and equation (I.46) for the notations). The open squares correspond to the crossover between the paramagnetic phase and the spin ice regime located at the maximum of the broad peak in the specific heat C_h (see *left*). The open diamonds represents the sharp peak due to the 1st order transition. The y-axis is displayed on log scale.

and 3rd nearest neighbours, *i.e.* between hexagons, are necessary for an almost perfect fit. Hence if we write the Hamiltonian as

$$\mathcal{H} = \sum_{n=1}^{3} \sum_{\langle i,j \rangle_n} J_n \, \mathbf{S}_i \cdot \mathbf{S}_j \tag{I.47}$$

where $\langle \cdot, \cdot \rangle_n$ are the nth NN pairs, we obtain for $Dy_2Ti_2O_7$, $J_1 \approx 3,41K$, $J_2 \approx -0,14K$, $J_3 \approx 0,025K$.

However, even if promising and certainly necessary for a complete understanding of these materials, this model is so far a refinement of dipolar spin ice at very low temperature ($\sim$ 0.5 K) and is only available for $Dy_2Ti_2O_7$. The DSI model remains quantitatively robust for a wide range of temperature and magnetic field and the best compromise between simplicity and efficiency.

The last model we must present has been defined recently by Castelnovo, Moessner & Sondhi [Cas08] and aroused the curiosity of the community, as an incubator for effective magnetic monopoles.

I.3.c Magnetic Monopoles in Spin ice

This work is built on a serie of papers [Hus03, Moe03b, Her04, Isa04b, Hen05] which have shown how a family of $3d$ frustrated systems could exhibit algebraic correlations; a

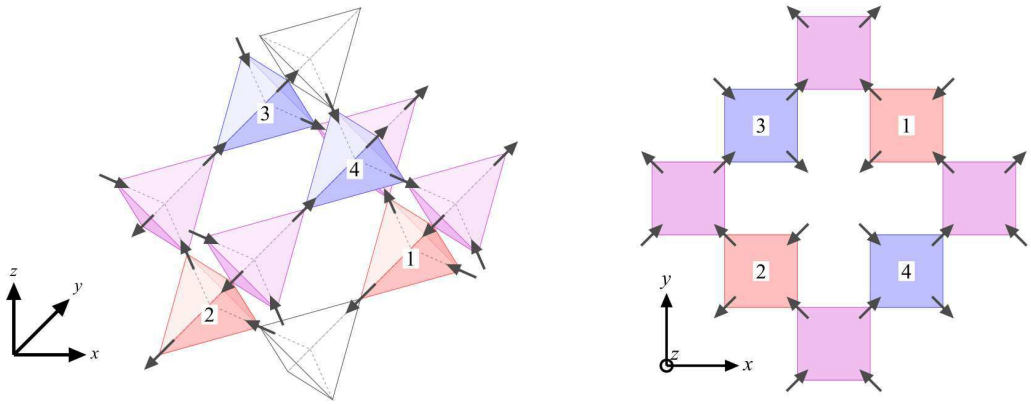

Figure I.15: **Ground state of the dipolar spin ice model** in $3d$ (*left*) and its $2d$ projection along the z-axis (*right*), also called the MHG phase (Melko, den Hertog, Gingras from [Mel01b]). It respects the ice-rules. All spins in the same (001) layer points towards the same direction. There is a rotation of $\pi/2$ from one plane to the one above and the same pattern is thus reproduced by a translation of length a along the z-axis: this is why this phase is expected to give a Bragg peak at $q = (0, 0, 2\pi/a)$. This transition is symmetry breaking because the net magnetisation is rotating within the (x, y) and has no component along the vertical direction: since this phase is totally defined by a rotation axis x, y or z and a chirality (sense of rotation), it is 6-fold degenerate.

concept elegantly shown in the nearest neighbour spin ice model [Hen05]. Let us consider the magnetisation of a tetrahedron α: $\mathbf{M}(\mathbf{r}_\alpha) = \sum_{i\in\alpha} \mathbf{S}_i$ and define the coarse-grained field $\mathbf{M}(\mathbf{r}) = \frac{1}{V}\sum_{\alpha\in V} \mathbf{M}(\mathbf{r}_\alpha)$ averaged over a volume V large enough to make $\mathbf{M}(\mathbf{r})$ a smoothly varying function.The proof of algebraic correlations requires two-stage and its arguments are based on the frustrated 2 *in* - 2 *out* ground state.

On this manifold, the Gibbs free energy G is purely entropic and can be expressed as a distribution function of $\{\mathbf{M}(\mathbf{r})\}$. For a tetrahedron respecting the ice-rules, $\mathbf{M}(\mathbf{r}_\alpha)$ can only take 6 values proportional to $(\pm1, 0, 0), (0, \pm1, 0)$ or $(0, 0, \pm1)$. Hence computing the entropy density for a volume V is equivalent to the problem of a completely random polymer made of monomers fixed on the cubic lattice and whose extremities are separated by $\mathbf{M}(\mathbf{r})$. A large value of $|\mathbf{M}(\mathbf{r})|$ will force most of the spins/monomers to point towards this direction and only allow a relatively small number of configurations, with the example of a unique state for a saturated magnetisation or straight polymer. On the other hand, zero magnetisation fixes a minimum of degrees of freedom. Hence the Gibbs free energy functional and its Fourier transform are expressed to the lowest order and up to a constant as

$$G\left[\{\mathbf{M}(\mathbf{r})\}\right] = \frac{T}{V}\int d^3\mathbf{r}\,\frac{1}{2}\,K\,|\mathbf{M}(\mathbf{r})|^2 \tag{I.48}$$

$$\Leftrightarrow \tilde{G}\left[\left\{\tilde{\mathbf{M}}(\mathbf{k})\right\}\right] = T\sum_{\mathbf{k}}\frac{1}{2}\,K\,\left|\tilde{\mathbf{M}}(\mathbf{k})\right|^2 \tag{I.49}$$

which gives a temperature independent Gaussian probability $e^{-G/T}$ and $\langle \tilde{M}_\mu(-\mathbf{k})\tilde{M}_\nu(\mathbf{k})\rangle =$

$\delta_{\mu\nu}/K$. However this argument neglects the ice-rules. If we regard the spins as local fluxes of magnetisation then these constraints impose a flux conservation for each tetrahedron (2 spins *in* and 2 spins *out*); from a coarse-grained point of view, it is equivalent to a divergence free condition.

$$\nabla \cdot \mathbf{M}(\mathbf{r}) = 0 \quad \Leftrightarrow \quad \mathbf{k} \cdot \tilde{\mathbf{M}}(\mathbf{k}) = 0 \tag{I.50}$$

which imposes $\tilde{\mathbf{M}}(\mathbf{k})$ to be orthogonal to $\mathbf{k}$ and thus

$$\langle \tilde{M}_\mu(-\mathbf{k}) \tilde{M}_\nu(\mathbf{k}) \rangle = \frac{1}{K} \left(\delta_{\mu\nu} - \frac{k_\mu k_\nu}{|\mathbf{k}|^2} \right) \tag{I.51}$$

where the Greek indices μ, ν are Cartesian coordinates labels. After a final Fourier transform back to real space, we obtain the desired correlations

$$\langle M_\mu(\mathbf{0}) M_\nu(\mathbf{r}) \rangle \propto \frac{1}{K} \frac{\delta_{\mu\nu} - 3\,\hat{r}_\mu \hat{r}_\nu}{r^3} \qquad \text{where} \quad \hat{r}_\mu = \frac{r_\mu}{|\mathbf{r}|} \tag{I.52}$$

This result deserves a few comments. First of all, we have lost the details of the pyrochlore lattice as soon as we used a coarse-grained field and this result can be generalised to models others than spin ice [Hus03, Moe03b, Her04, Isa04b, Hen05], the only hypothesis being

- a *Coulomb phase* gauge theory imposed by equation (I.49);
- a divergence free condition, consequence of the ice-rules constraints (I.50).

The magnetisation field $\mathbf{M}(\mathbf{r})$ is then equivalent to a magnetic field without monopoles which explains the specific form of the correlations similar to those generated by a *dipole-dipole interaction*. One might think that the $1/r^3$ long-distance behaviour in a $3d$ crystal should lead to a logarithmic divergence in the scattering function; nevertheless, this does not happen because of the dipolar angular dependance that cancels the overall divergence in the integral. Spin ice thus appears as a potential experimental realisation of a *critical-like* phase, since algebraic correlations are usually characteristic of critical phase transitions. Its manifestation should be seen in the scattering function measured by neutron scattering, through the existence of *pinch points* [You81] which have indeed been observed by Fennell and collaborators in $Ho_2Ti_2O_7$ [Fen07, Fen09]. We refer the reader to appendix C for an introduction to pinch points.

This analogy between the nearest neighbour model and dipolar correlations has been brought one step further by Isakov *& al.* when they explained "Why Spin Ice Obeys the Ice Rules ?" [Isa05]. This question remained indeed unanswered so far: why is the extensive 2 *in* - 2 *out* degeneracy quasi-recovered by addition of long range dipolar interactions [Gin01] ? Is it a coincidence or not ? We will here briefly summarise the arguments of [Isa05], starting by rewriting the DSI Hamiltonian (I.44) as a matrix

$$\mathcal{H} = \sum_{i<j} \sum_{\ell<\ell'} \sigma_i^\ell \, \mathcal{H}_{i,j}^{\ell,\ell'} \, \sigma_j^{\ell'} = \sum_{i<j} \sum_{\ell<\ell'} \sigma_i^\ell \left(J \, \mathcal{J}_{i,j}^{\ell,\ell'} + D \, r_{nn}^3 \, \mathcal{D}_{i,j}^{\ell,\ell'} \right) \sigma_j^{\ell'} \tag{I.53}$$

where σ_i^ℓ is the scalar spin defined in eq. (I.41) located on one of the four sites ℓ of the tetrahedron i. $\mathcal{J}_{i,j}^{\ell,\ell'}$ and $\mathcal{D}_{i,j}^{\ell,\ell'}$ take into account respectively the whole geometry of the exchange coupling and dipolar interactions. Following the method of [Can01], one need to define the following Fourier transformation

$$\sigma_i^\ell = \frac{1}{N}\sum_{\mathbf{q}} \sigma_{\mathbf{q}}^\ell \, e^{i\mathbf{q}\cdot\mathbf{r}_\mathbf{i}^\ell} \qquad \sigma_{\mathbf{q}}^\ell = \sum_i \sigma_i^\ell \, e^{-i\mathbf{q}\cdot\mathbf{r}_\mathbf{i}^\ell} \tag{I.54}$$

where $\mathbf{r}_i^\ell$ is the position of the spin σ_i^ℓ. The above Hamiltonian can now be rewritten in the Fourier representation

$$\mathcal{H} \;=\; \sum_{\mathbf{q}} \sum_{\ell<\ell'} \sigma_{\mathbf{q}}^\ell \left(J\,\tilde{\mathcal{J}}_{\mathbf{q}}^{\ell,\ell'} + D\, r_{nn}^3\, \tilde{\mathcal{D}}_{\mathbf{q}}^{\ell,\ell'} \right) \sigma_{-\mathbf{q}}^{\ell'} \tag{I.55}$$

As $\ell = 1..4$, $\mathcal{J}_\mathbf{q}$ and $\mathcal{D}_\mathbf{q}$ are 4×4 matrices and function of the wave vector $\mathbf{q}$. They can be diagonalised in a basis of $\mathbf{q}$-dependent eigenvectors $|v_\ell(\mathbf{q})\rangle$.

$$\mathcal{J} \;=\; \begin{pmatrix} 0 & 0 & 0 & 0 \\ 0 & 0 & 0 & 0 \\ 0 & 0 & \epsilon_3(\mathbf{q}) & 0 \\ 0 & 0 & 0 & \epsilon_4(\mathbf{q}) \end{pmatrix} \tag{I.56}$$

where $\epsilon_3(\mathbf{q}) > 0$, $\forall\mathbf{q}$ and $\epsilon_4(\mathbf{q}) > 0$, $\forall\mathbf{q}$ except for $\mathbf{q} = \mathbf{0}$. Hence, the ground state with eigenvalue zero is two dimensional and $\mathbf{q}-$independent (flat energy bands), whereas the excited states manifold is dispersive. At $T = 0$, the physics is solely determined by the lowest energy modes and we can therefore carry our reasoning on the following projector $\mathcal{P}$ instead of $\mathcal{J}_\mathbf{q}$ without loss of generality, keeping the same eigenbasis $|v_\ell(\mathbf{q})\rangle$.

$$\mathcal{P} \;=\; \begin{pmatrix} 0 & 0 & 0 & 0 \\ 0 & 0 & 0 & 0 \\ 0 & 0 & 1 & 0 \\ 0 & 0 & 0 & 1 \end{pmatrix} \tag{I.57}$$

The main result of [Isa05] is that working backwards from [Hus03, Moe03b, Her04, Isa04b, Hen05], one obtains in real space

$$\mathcal{D}_{i,j} \;=\; \frac{8\pi}{3}\mathcal{P}_{i,j} + \Delta_{i,j} \tag{I.58}$$

with $\Delta_{i,j} \sim \mathcal{O}\left(r_{ij}^{-5}\right)$. Hence the Hamiltonian is made up of a sum of three matrices $\mathcal{H}_{i,j} = J\,\mathcal{J}_{i,j} + D\,r_{nn}^3\,\frac{8\pi}{3}\mathcal{P}_{i,j} + D\,r_{nn}^3\,\Delta_{i,j}$ whose long distance behaviour is dominated by the first two terms, that is the long range $1/r^3$ interactions are screened, giving rise to an effective NN coupling and corrections to $\mathcal{O}\left(r_{ij}^{-5}\right)$. In the long distance limit, $\mathcal{J}_{i,j}$ and $\mathcal{D}_{i,j}$ are equivalent under projection to the flat energy bands, *i.e.* they have the same eigenvectors and same ground state manifold; they are said to be *projectively equivalent*. By definition, this ground state is the 2 *in* - 2 *out* manifold and the above results shows how it is slightly lifted by $\Delta_{i,j}$ that will favour the ordered state discovered with the loop algorithm [Mel01b]. However since this term is a correction of order $1/r^5$, we do not know its relative importance with respect to other perturbations of quadrupolar or quantum origin for example. The main result of Isakov *& al.*'s paper is that DSI and NNSI have the same ground state, up to $\mathcal{O}\left(r_{ij}^{-5}\right)$ corrections. To summarise these remarkable analogies, I would like to quote [Isa05]: "*Dipolar spins are ice because ice is dipolar.*"

Our last point will be that this "self-screening" of long range interactions [dH00] can be generalised to other models as long as they have a pair of projectively equivalent interactions $\mathcal{J}'$ and $\mathcal{D}'$. Finally, we will see in the rest of this subsection a manifestation of this equivalence through the creation of effective magnetic monopoles.

Our analysis so far only concerns the very low temperature properties of spin ice on the ice-rules manifold, but in fact defects which break the divergence free condition can be thermally activated. Flipping a single spin in a 2 *in* - 2 *out* configuration leads to the creation of a pair of different defects (3 *in* - 1 *out* and 3 *out* - 1 *in*) that can be separated at no energy cost in the NN model (the tetrahedra in between recover the ice-rules), but which feel an effective Coulomb attraction in DSI [Cas08] (see figure I.16). In the same way that electric dipoles are formed by two electric charges, spins can be seen in a thought experiment as two separated magnetic charges sitting on the vertices of the diamond lattice, dual of the pyrochlore one; this is the *dumbbell* model for which projective equivalence is exact [Cas08] (see figure I.17). In order to reproduce the value of the magnetic moment μ of the rare-earth ions, one needs to define the magnetic charge as $|Q| = \mu/r_d$, where r_d is the distance between two neighbouring charges. Hence each centre of tetrahedron will be occupied by four charges (one per spin) and the 2 *in* - 2 *out* condition imposes magnetic neutrality (figure I.17). In analogy with electrostatics a magnetic moment points towards the positive charge, meaning that a 3 *in* - 1 *out* (resp. 3 *out* - 1 *in*) defect will bear a net difference of two positive (resp. negative) charges: the total charge carried by a local excitation is then $\pm\, q_m = \pm\, 2\mu/r_d$. The notion of positive and negative magnetic charges has also been introduced by Ryzhkin in the context of the Zeeman energy required to move a defect in a magnetic field [Ryz05]. Since the spins interact through dipolar interactions in the DSI model, the charges defined on the extremities of these spins *must* interact through an effective magnetic Coulomb interaction and behave like *classical magnetic monopoles*. If we start with a 2 *in* - 2 *out* manifold (vacuum of monopoles) and then flip a spin, we shall create a pair of charges of opposite sign; now if we flip a continuous chain of neighbouring spins, we shall separate the two

charges by a distance r which will then feel a Coulomb potential up to $\mathcal{O}\left(r^{-5}\right)$ corrections

$$V(r) \;=\; -\frac{\mu_0}{4\pi}\frac{q_m^2}{r} \tag{I.59}$$

Last but not least, a pair of monopoles are created at *finite* distance and cost a *finite* amount of energy, and since the Coulomb potential is not diverging for infinite separation, the monopoles are *not confined*: this is the first example of fractionalisation in a $3d$ magnetic system (figure I.16).

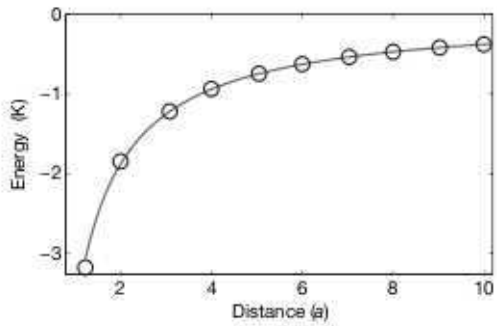

Figure I.16: **Coulomb potential:** Magnetic energy required to separate two monopoles of opposite charges by a distance a [Cas08]: numerical computation (○) where the charges remain on a Kagome plane (see figure I.20) perfectly fitted by a $1/a$ Coulomb law. It is arbitrarily scaled to zero for infinite distance $a \to \infty$.

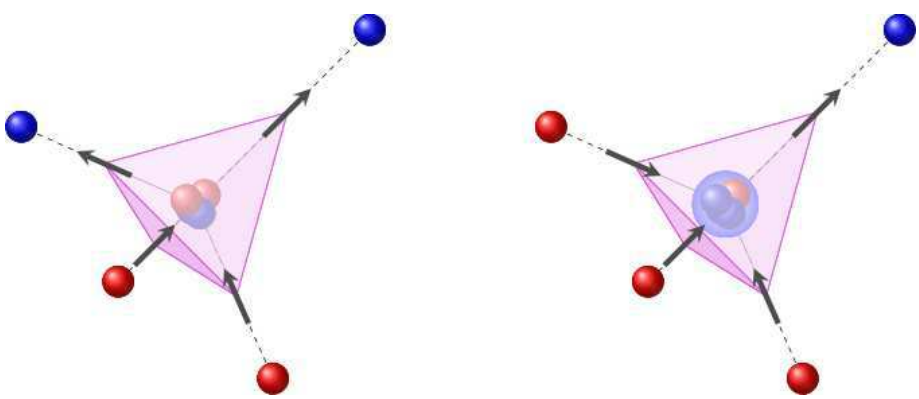

Figure I.17: **Dumbbell model:** Each magnetic dipole is seen as two charges sitting on the vertices of the dual diamond lattice (dashed lines). 2 *in* - 2 *out* is a vacuum whereas 3 *in* - 1 *out* is a positive charge.

Summary

Here I want to present my point of view about these three models. We should start with the $T = 0$ behaviour. On the one hand, the 2 *in* - 2 *out* ground state manifold of

the NNSI model exactly corresponds to a vacuum of monopoles in the dumbbell model. Here we see how an extensive set of spin configurations is made unique in the monopole language; this will prove to be of crucial importance for quantitative comparisons with experiments [Jau09b] (see chapter IV). On the other hand, the only difference between DSI and the dumbbell model is that a spin is a point dipole, localised on the pyrochlore lattice, and not a pair of magnetic charges on the vertices of the diamond lattice. If not for this dissimilarity, the ground state of all three models (NNSI, DSI, dumbbell) would be the same 2 *in* - 2 *out* manifold, but the ground state degeneracy of the DSI model is in fact slightly lifted by the term $\Delta_{i,j}$ of quadrupolar order $1/r^5$ due to the difference between two forms of dipoles (or the position of four charges). From this approach, the projective equivalence of the exchange term $\mathcal{J}_{i,j}$ and the dipolar interaction $\mathcal{D}_{i,j}$ at long distance [Isa05] thus has a deep physical interpetration due to the specific geometry of spin ice which is particularly transparent in the language of monopoles.

At finite temperature, this difference still holds between DSI and NNSI/dumbbell model, but we must also take into account the creation of 3 *in* - 1 *out* or 3 *out* - 1 *in* excitations. In the DSI or dumbell model, they interact through an effective Coulomb potential of *magnetic* origin directly due to the dipoles or charges [Cas08], whereas in the NNSI model they feel a weak effective Coulomb interaction of *entropic* origin as they appear as excitations out of a divergence free ground state[9] [Isa04a]. This entropic contribution also exists in the DSI model but is totally dominated by the magnetic term.

In the rest of this manuscript, we will endeavour to use the notion of *defects* for NN spin ice and the term of *monopoles* for dipolar spin ice or the dumbbell model. The difference of energy scale between the entropic and magnetic contributions makes the defects almost free to move in comparison with the monopoles.

The next subsections of this presentation of spin ice will be devoted at first to the influence of an external magnetic field and then to the dynamics of these materials, two aspects that attracted a great deal of experimental and theoretical interest and that make up the core of this thesis.

I.3.d Magnetic field

In the previous subsections, we have presented the strong easy-axis spin anisotropy along the local (111) direction (*cf.* equation (I.38)). As theoretically predicted by Harris *& al.* [Har98] and experimentally confirmed for $Dy_2Ti_2O_7$ [Fuk02] and $Ho_2Ti_2O_7$ [Pet03], an external magnetic field can couple in many different ways with these Ising spins, favouring a unique or a set of configurations, solely depending on the field orientation. The low temperature specific heat of $Dy_2Ti_2O_7$ in zero field is a simple Schottky peak due to the crossover from the paramagnetic phase to the ice-rules regime (see figure I.11), but the addition of a magnetic field in a powder sample produces three *field independent* and relatively sharp peaks at 0.34, 0.47 and 1.12 K; this degeneracy lift strongly indicates the existence of phase transitions [Ram99], as confirmed in a single crystal by Higashinaka *&*

[9] Equation (I.50) becomes $\nabla \cdot \mathbf{M}(\mathbf{r}) = \rho(\mathbf{r})$ where $\rho(\mathbf{r})$ is the coarse-grained density of defects. The dipolar correlation between spins gives rise to an effective Coulomb interaction between defects.

al. [Hig03a]. The presence of such peaks has attracted a great deal of interests, and their origin requires the consideration of specific field orientations.

Magnetic field [001]

This orientation and its five other cubic symmetries ([00$\bar{1}$], [010]...) are the only directions having the same influence on all four spins of each tetrahedron, *i.e.* $\pm\frac{1}{\sqrt{3}}\mu\, H_{001}$, favouring a unique state with saturated magnetisation along the z-axis, as displayed by the tetrahedron of figure I.8. Monte-Carlo simulations using a local update algorithm showed the presence of what appeared to be a liquid-gas like transition with a line of first order transition ending by a critical point, However the linear field dependance of the transition temperature has not been observed experimentally for any of the above mentioned peaks [Har98].

For the model system, if we allow the spins to partially lose their Ising nature and to fluctuate around their local easy-axis vector $\mathbf{e}_i$ following an energy term $-A\sum_i(\mathbf{S}_i\cdot\mathbf{e}_i)^2$, we can continuously tune the parameter A to favour either Ising ($A\to+\infty$) or Heisenberg ($A=0$) spins. Treating J/A as a small parameter, we observe the persistance of the liquid-gas transition down to a given value of $A=A_{tc}$ where the critical point becomes tricritical for $H_{001}=0$ [Cha02].

However no transition has been observed in specific heat measurements on a single crystal of $Dy_2Ti_2O_7$ but rather a changeover of the Schottky peak, from a nearest neighbour ferromagnetic origin to a Zeeman one for increasing field [Hig03b]. Neutron scattering experiments showed the presence of a $q=0$ Bragg peak in the scattering function of $Dy_2Ti_2O_7$ and $Ho_2Ti_2O_7$ [Fen05], a signature of the expected ordered state with all spins *up*, but even if the magnetisation seems to become discontinuous at low enough temperature ($T<0.5$K), its origin remains unclear: is it a 1st order transition as predicted by Harris and collaborators [Har98], or a consequence of a spin freezing preventing the equilibration of the material ? This question has been at the origin of my thesis and will thus be developed in the following chapters.

Magnetic field [110]

As one can see in figure I.18, a large enough magnetic field in the [110] direction will fix the position of two spins per tetrahedron, but will not couple to the other two which are perfectly orthogonal ; However these two spins are not free because they are forced by the ice-rules to have a given projection in the same direction, *i.e.* to the left or the right of the field H_{110}. Hence the system can be considered as an ensemble of $1d$ chains of spins: the α- and β-chain. The α-chains are all aligned with the magnetic field whereas the β-chains are parallel to each other and orthogonal to the field: the pyrochlore lattice can be seen as a pileup of $\alpha-\beta-\alpha-\beta-\alpha-...$ layers in the [001] direction (see figure I.18).

For the NN model at $T=0$, the α-chains are pined by the field while each β-chain is formed by spins all pointing in the same direction but free to choose the left or right orientation. For a system of size $L\times L\times L$, there is of the order of L^2 β-chains and the ground state entropy, although still diverging with L, is no longer extensive: $S_{\rm GS}\sim L^2\sim N^{2/3}$ [Hig03a].

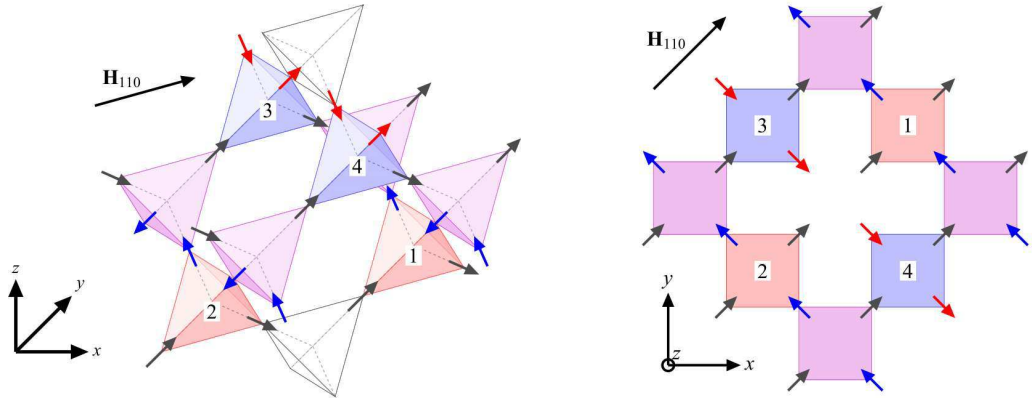

Figure I.18: **Ground state in a [110] field:** The α-chains (black spins) are aligned along the field, as opposed to the MHG phase of figure I.15, while the β-chains (blue and red spins) are antiferromagnetically ordered (α-F β-AF). This gives rise to Bragg peaks at the X points of the Brillouin zone in the scattering function and is thus referenced as the $q = X$ phase [Har97, Fen05].The ice-rules are respected.

Dipolar interactions will antiferromagnetically couple the β-chains, leading to the $q = X$ ground state displayed on figure I.18. In fact, a rather complex phase diagram was obtained by Monte Carlo simulations with Ewald summation and loop algorithm [Yos04, Mel04, Ruf05], given in figure I.19. At high enough temperature ($T \gtrsim 1$K), the ice-rules are no longer respected and we simply see a crossover from the paramagnetic phase to a phase with all α-chains oriented along the field (α-F). Upon cooling, we either enter the spin ice regime (low field) or the above mentioned $q = X$ ground state (high field, noted α-F β-AF on the diagram). Of course, for small field and temperature, the dipolar interactions predominate and impose the MHG phase predicted by [Mel01b] (see figure I.15).

Even if this phase diagram has been qualitatively confirmed by specific heat measurements [Hir03], a completely $q = X$ ordered phase has not been observed experimentally so far; α-chains are easily coupled with the field, but even if β-chains are robust on a non-negligible length scale (~ 130Å*i.e.* over 13 unit cells for $Dy_2Ti_2O_7$ at 0.05 K and 1.5 T) their antiferromagnetic arrangement does not hold over more than 4 or 5 neighbours, leading to diffuse scattering instead of a Bragg peak in the scattering function for the $q = X$ phase [Fen05, Cla09]. As suggested by [Mel04, Cla09], this absence of long range order may be due to the difficulty (or maybe even impossibility) of perfect alignment of the crystal with respect to the field; the β-chains will be frustrated by a parasite component of the external field, breaking their AF order.

Our last point is that for large enough magnetic field, the transition into the ordered $q = X$ state, even if not complete, occurs at a field-independant temperature of ~ 1.2 K and may be the origin of one of the three peaks observed by Ramirez *& al.* [Ram99].

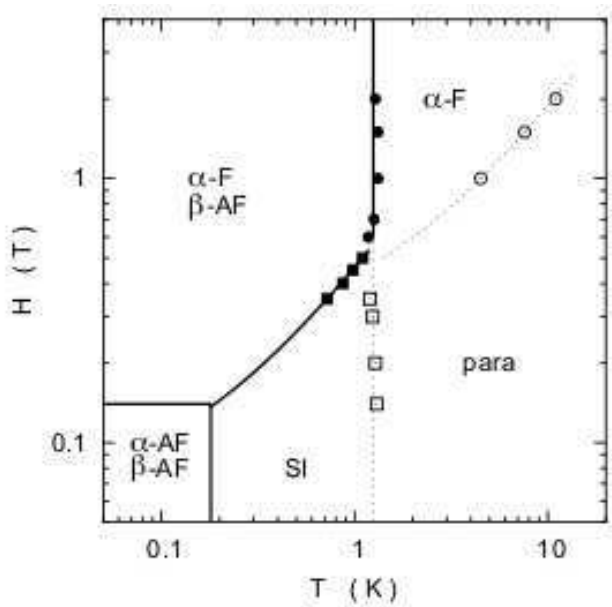

Figure I.19: **Phase diagram of dipolar spin ice in a [110] field** on a log-log scale, computed numerically from [Yos04]. The solid lines show the first order transitions whereas the dotted ones are crossover. However Hiroi *& al.*'s experiment [Hir03] seem to suggest a continuous transition from the spin ice regime to the α-F β-AF phase; the absence of discontinuity may be due to misalignment that is extremely difficult to get rid of.

Magnetic field [111]

Both orientations we have presented so far have in common that the magnetic field does not break the ice-rules, which is not he case anymore for a field in the [111] direction, which favours 3 *in* - 1 *out* and 3 *out* - 1 *in* configurations. Our discussion will gain in clarity if we consider for the time being the pyrochlore as an alternating stack of triangular and Kagome planes (see figure I.20).

Again, the action of the field is quite different for the four spins: three of them (in the Kagome plane) are only partially coupled to it, while the fourth one (in the triangular lattice) is parallel to the field. This suggests a two-stage evolution of the magnetisation (see figure I.21). The spins in the triangular layers will be the first to be fixed by the field (typically 2 kOe for $Dy_2Ti_2O_7$ at 0.5 K) but the three others will remain disordered thanks to the competition between the ice-rules striving to keep a disordered state in the Kagome plane and the Zeeman energy [Har98, Mat02b]. Since the 2 *in* - 2 *out* manifold imposes ones "Kagome" spin per tetrahedron to have a component opposite to the field, the magnetisation will be independent of the field, giving rise to a *magnetisation plateau* (see figure I.21 for T=0.48 K). For increasing field, the Zeeman energy will eventually overcome the exchange energy, forcing the ice-rules to be broken and saturating the magnetisation ($\approx$ 10 kOe for $Dy_2Ti_2O_7$ at 0.5 K). Of course, if the temperature is not low enough, the defects can be thermally activated and the magnetisation plateau disappears. This region of competition where the triangular planes are saturated and the Kagome layers are

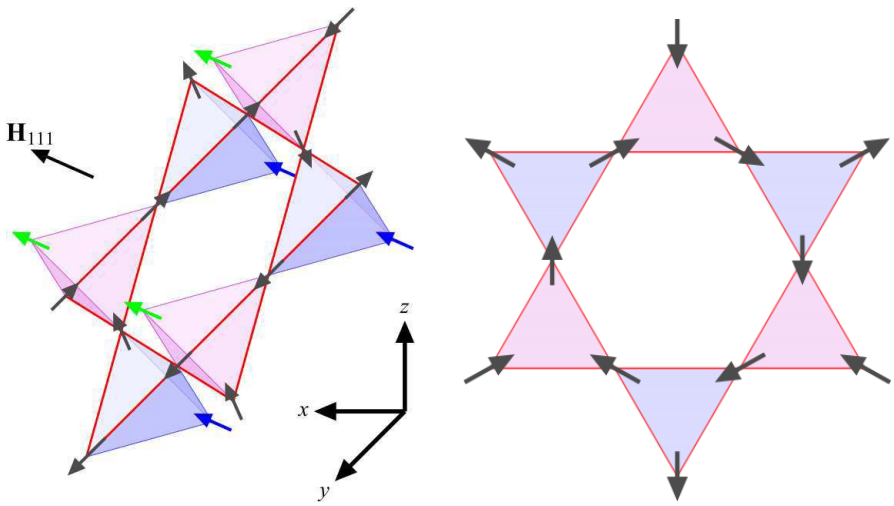

Figure I.20: **Ground state of Kagome Ice:** *Left:* For convenience, the $x-$ and $y-$axes are reversed with respect to the other figures. The emerging $2d$ Kagome Ice is drawn in red, surrounded by two triangular lattices made of green and blue spins aligned with the field. We can see that the Kagome Ice-rules are different depending of the spin out of the Kagome plane: it is 2 *in* - 1 *out* for violet *up* tetrahedra and 2 *out* - 1 *in* for blue *down* tetrahedra. For large magnetic field, the ice-rules are broken and all spins are in the field direction. *Right:* A possible configuration of the Kagome layer: 2 *in* - 1 *out* for the *up* (violet) triangles, and 2 *out* - 1 *in* for the down (blue) triangles, imposed by the ice-rules and the fourth spin in the triangular layer, in opposition with the Kagome Ice defined by Wills *& al.* where all six possibilities 2 *in* - 1 *out* and 2 *out* - 1 *in* are accessible for any triangles [Wil02].

decoupled is called *Kagome Ice* [Mat02b]. This term was first introduced by Wills *& al.* as a theoretical $2d$ analogue of spin ice [Wil02], but their model describes a less constrained system than $3d$ spin ice in a [111] field, as explained in the caption of figure I.20.

The Kagome Ice problem maps exactly onto a dimer problem on the honeycomb lattice which is a critical phase with algebraic correlations and a finite entropy [Moe03a], as measured by [Mat02b, Hir03, Aok04] If we slightly tilt the field from the [111] towards the [001] direction, this phase should order at low temperature via the novel Kasteleyn transition discussed in more details in later chapters [Kas63, Moe03a]: an experimental signature of this transition has been observed by neutron scattering [Fen07].

Once again, the field temperature diagram is quite complex [Hir03, Sak03, Aok04, Hig04b, Sai05] (see figure I.21). In a nutshell, increasing the field will first fix the spins on the triangular layer and then the ones on the Kagome planes; for low temperature, this will be done on the 2 *in* - 2 *out* manifold when possible, inducing the Kagome Ice phase for intermediate field values, whereas at high temperature the field-decoupled spins are thermally random. All "phase transitions" are crossovers, except between Kagome Ice and the fully saturated state which is 1st order ending with a critical point at (H_{111}, T) =(0.93 T, 0.36 K) [Sak03]; this liquid-gas phase transition is unexplainable within the nearest neighbour model, but has been recently understood as a $2d$ condensation of magnetic

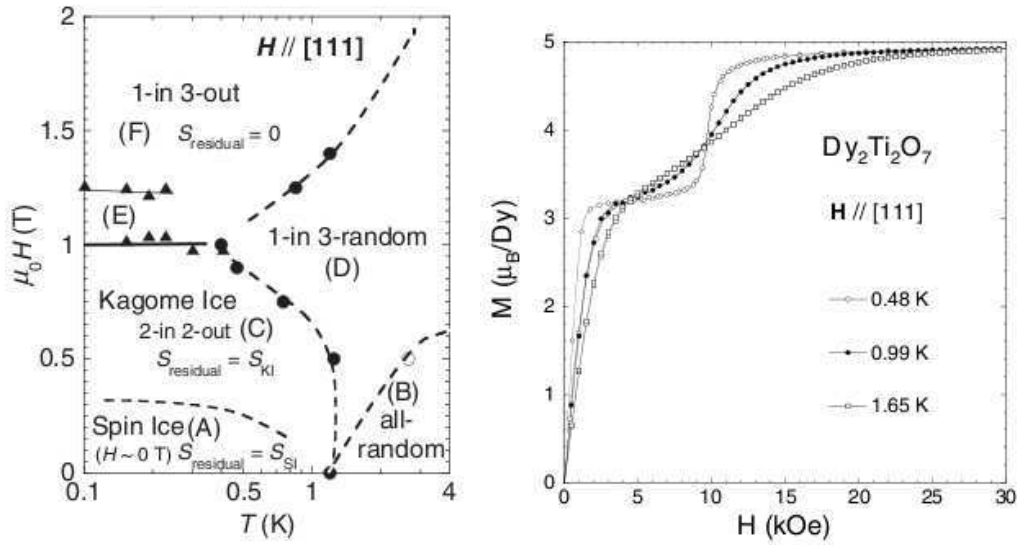

Figure I.21: **Phase Diagram and Kagome Ice plateau in a [111] field:** *Left:* Phase diagram of $Dy_2Ti_2O_7$ obtained by specific heat measurements [Hig04a]. The solid line at $\mu_0 H \approx 1$ T is first order and ends with a critical point. The dashed lines are crossovers. The Kagome Ice and 1 *in* - 3 *out* ordered phase are displayed in figure I.20. *Right:* Magnetisation in "Bohr magneton per ion" units vs the field for different low temperatures. The plateau is clearly visible when $T = 0.48$ K.

monopoles where the field acts as a chemical potential. The critical ending point corresponds to one of the three peaks measured by Ramirez *& al.* [Ram99].

Last but not least, Kagome Ice represents a $2d$ frustrated system with a divergence free condition and enabled the first known observation of a *pinch point* or *bow tie* in the scattering function of a magnetic material: this is a manifestation of the algebraic dimer correlations [Fen07].

Magnetic field [112]

As discussed above, the $3d$ pyrochlore lattice viewed along the [111] direction is a stack of alternating $2d$ Kagome and triangular layers. By cubic symmetry, this is also true for $[1\overline{1}\overline{1}]$, $[\overline{1}1\overline{1}]$ and $[\overline{1}\overline{1}1]$. A field along the [112] direction happens to be orthogonal to the latter orientation, which means its effect will be in some sense opposite to the [111] case; in the ground state, the three spins of the Kagome lattice will be pinpointed by the field whereas the fourth one, in the triangular plane, will not couple to the field. However the ice-rules, acting as an *internal* field, will fix its orientation in a global $q = 0$ state, with all spins *up* as if the field were along the [001] direction.

New and particularly interesting physics arises from spin ice if we tilt this [112] field towards the [110]; for a given angle the three Kagome spins remains fixed in the same orientation, but the internal field they produce on their neighbours on the triangular lattices is *canceled*. This spin that lies on a $3d$ face-centred cubic lattice (fcc) does not feel the

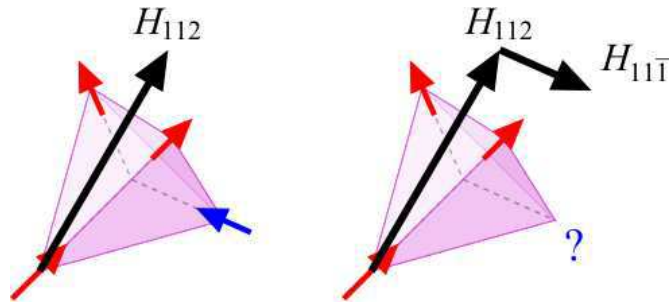

Figure I.22: **Decoupled spin in a [112]-tilted field:** A [112] field fixes the orientation of the red spins while the blue one is pinned in a 2 *in* - 2 *out* state (*left*). If we add a field along the $[11\bar{1}]$ direction, it will counterbalance the internal field acting on the blue spin which will be freed from the ice-rules and will only feel the long range dipolar interactions.

influence of either the ice-rules, or the field: we thus end up with an fcc Ising dipolar magnet [Ruf05] whose ground state is ferromagnetic [Bec30, Tes54]. Ruff *& al.* numerically predicted a 1st order transition, observed experimentally by Higashinaka *&* Maeno [Hig05], even if the 1st order nature was only confirmed following a delicate field-angle dependent magnetization measurement performed by Sato and collaborators [Sat06]. The transition is expected to be responsible for one of the specific heat peaks, even if further work with 2nd and 3rd nearest neighbours is required in order to determine precisely the transition temperature.

Summary

As discussed in [Mel04] and in a recent paper by Moessner [Moe09], the addition of strong anisotropy and finely tuned field orientations are responsible for "*dimensional reduction and conversion*":

- if some spins are not coupled to the field ([110]), we create two sets of independent $1d$ chains: one of them pinned by the field (α-chains) whereas the others (β-chains) are free to interact through dipolar interactions, at least on short distances;

- if the field tends to favour configurations out of the 2 *in* - 2 *out* manifold ([111]), it will result in a two-stage process: the first orients the spins in a way respecting the ice-rules, which fixes all spins on the $2d$ triangular lattice, while the second breaks the ice-rules in favour of the Zeeman energy, with a magnetisation plateau in between, characteristic of the $2d$ Kagome Ice;

- it is even possible to cancel the internal field felt by a sub-set of spins by its nearest neighbour surrounding (tilted from [112]), creating $0d$ isolated spins, free to interact through long range interactions and giving rise to an effective $3d$ fcc Ising dipolar magnet.

From this point of view, the [001] direction does not look as interesting as its counterparts: all spins are coupled to the field and the favoured state does not even break the ice-rules ! But in this case, where does this numerical liquid-gas transition come from and why has it not been observed experimentally ? As we shall explain it in great details in this thesis, it is in fact precisely the conjunction of ice-rules and of finely tuned external perturbations that interacts exactly in the same way with all spins, that will be the source of exotic phase transitions on the constrained 2 *in* - 2 *out* manifold.

I.3.e Dynamics

Already in the first paper on spin ice [Har97], it was noticed that the nature of the disordered ground state is *static*, as opposed to antiferromagnetic frustrated magnets such as SCGO that conserves spin fluctuations down to the lowest temperatures [Obr88, Uem94, Sch96]. The authors of this article suggested the importance of the easy-axis anisotropy that gives rise to large energy barriers between ground states.

The complexity of spin ice dynamics is well illustrated through considering the relaxation time of $Dy_2Ti_2O_7$ that displays three characteristics features [Sny04a] (see figure I.23).

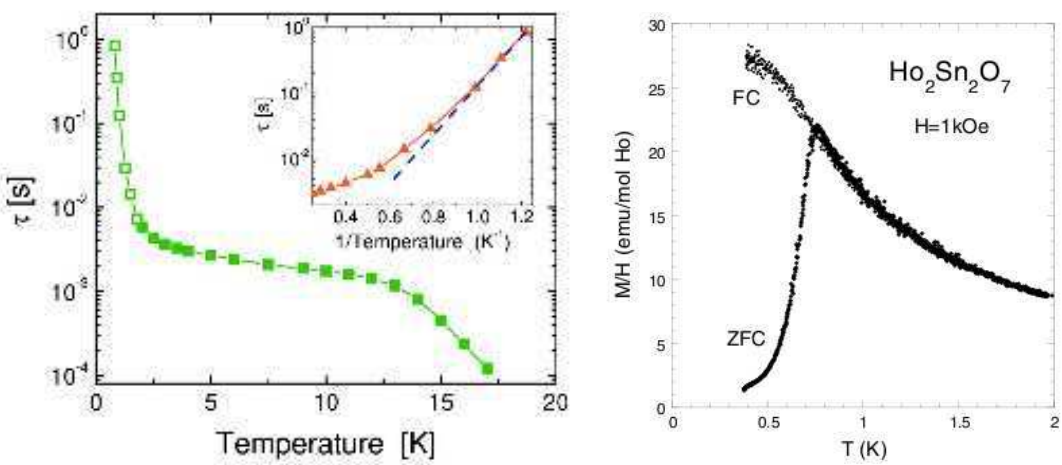

Figure I.23: **Spin ice dynamics:** *Left:* Relaxation time τ of $Dy_2Ti_2O_7$ vs the temperature T from Snyder *& al.* [Sny04a] with the characteristic double crossover at ≈ 12 K and ≈ 1 K. The inset shows a zoom of τ vs $1/T$ at low temperature on a log-lin scale and shows the divergence from an Arrhenius law. *Right:* Temperature dependence of DC-magnetization of $Ho_2Sn_2O_7$ at 1 kOe. ZFC and FC denote zero field cooling and field cooling, respectively [Mat00]. Hysteresis appears at ≈ 0.7 K but the FC curve is not flat below, as expected for a regular spin glass.

The high temperature regime has been described as an Arrhenius process whose energy barriers is of the order of the first excited states of the CEF levels, *i.e.* $\sim 200 - 300$ K [Mat01, Sny01, Ehl03, Sut07, Lag07] and Neutron Spin Echo (NSE) measurements have shown a q-independence of the scattering, suggesting a single-ion process [Ehl04]. The

origin of this high temperature relaxation must then come from the single-ion anisotropy of the spins which becomes apparent above 12 K for $Dy_2Ti_2O_7$ and ≈ 25 K for $Ho_2Ti_2O_7$. From a semiclassical point of view, it is only above this temperature that one begins to see the Heisenberg nature of the spins.

However if such behaviour was permanent for all temperatures, the relaxation time $\tau(T)$ should increase exponentially and go beyond the characteristic time scale of DC-measurements ($\sim 10^2$ s) for $T \approx 8$ K, whereas equilibration remains possible down to ≈ 1 K [Mat01]. This suggests a modification of this process or the apparition of a second regime that takes over this one, as observed on figure I.23 where the Arrhenius law gives way to a quasi-temperature-independent relaxation. Using NSE techniques, Ehlers *& al.* rejected the possibility of two different regimes and proposed a quantum tunnelling origin of this *relaxation plateau* [Ehl03]: the internal dipolar field felt by each spin has a component orthogonal to the spin that allows a finite inversion rate whose dynamic becomes predominant below 12 K.

But now comes a brutal slowing down of the relaxation below $T_f \approx 1$ K, responsible for the spin freezing mentioned before that leads to magnetic hysteresis. But even if this phenomenon has been confirmed by many experiments [Mat00, Mat01, Sny01, Ehl03, Lag07, Ore07, Cla09], no consensus has been made and in fact no theory has been able to successfully explain its nature until now. The only certitude is that it can *not* be a regular spin glass transition:

- DC-measurements performed on $Ho_2Sn_2O_7$ indicate an irreversibility below 0.75 K between the field cooled (FC) and zero field cooled (ZFC) magnetisation, as expected for a spin glass, *but* the FC curve continues to increase monotonically instead of remaining flat, characteristic of a blocking phenomena rather than a glass effect (see figure I.23 extracted from [Mat00]);

- In a typical spin glass, an external magnetic field would tend to suppress the spin freezing whereas T_f is slightly enhanced for spin ice [Sny01];

- The most striking element against glassy behaviour is the very existence of figure I.23,*i.e.* the possibility to extract a single characteristic time relaxation. Spin glasses have a wide window of time scales, whereas AC-measurements on spin ice show a narrow range of relaxation times with a clear maximum of the imaginary part of the susceptibility χ'' as a function of the frequency response [Mat01, Sny01].

Analogies with spin-freezing in dilute dipole glasses, superparamagnetic blocking or dielectric relaxation in glycerine have been made but it has not been possible to explain why spin ice should follow such behaviour. The development of magnetic correlations imposing the inversion of a cluster of spins or the importance of the ice-rules have also been suggested. Hence, many questions remain open. For example,

- why do $Ho_2Ti_2O_7$ and $Ho_2Sn_2O_7$ relaxation times follow an Arrhenius law around 1 K with an activated energy of ~ 25 K [Mat00, Ehl04], but not $Dy_2Ti_2O_7$ [Mat01, Sny04a], except for very low temperature magneto-calorics measurements that could be explained by a Raman or Orbach process with a typical energy scale of 3.6 K ?

- why is the frozen regime suppressed by a magnetic field but favoured by a small amount of non-magnetic dilution ?

- how can one explain the drastically different time scales characteristic of the plateau region as measured by different experimental techniques and compounds: ~ 5 ms for bulk measurements on $Dy_2Ti_2O_7$, $\sim 0.5\,\mu$s for muon spin resonance (μSR) on $Dy_2Ti_2O_7$ and ~ 10 ns for neutron scattering on $Ho_2Ti_2O_7$?

- what kind of single process can explain this double crossover ?

All these questions will be addressed in the last section of this thesis from the point of view of constrained monopole dynamics.

In the next subsection, we briefly present a few magnetic compounds with a pyrochlore structure that are potential candidates to enlarge the spin ice family.

I.3.f Spin ice candidates

Despite more than 100 papers solely dedicated to spin ice, only three materials have been *officially* recognised: $Ho_2Ti_2O_7$ by neutron scattering as the first spin ice compound [Har97], $Dy_2Ti_2O_7$ by specific heat measurements and the proof of zero-point entropy [Ram99] and $Ho_2Sn_2O_7$, whose specific features have been first recognised in susceptibility measurements [Mat00] and then confirmed by neutron scattering [Kad02]. As already mentioned, the latter has been much less studied because of the impossibility to obtain a single crystal. But other materials may join this group.

$Pr_2Sn_2O_7$ was first suggested as a spin ice compound by Matsuhira *& al.* because of an apparent Ising nature of the spins and a dynamical behaviour reminiscent of spin ice [Mat02a, Mat04]. Recent neutron scattering experiments validated the ground state doublet with a large energy gap of $\gtrsim 100$ K to the first excited state [Zho08a]. With a magnetic moment of 2.6 μ_B per ion and a NN distance of 3.75 Å, we can estimate the effective NN parameters from specific heat measurements: $D_{nn} = 0.13$ K and $J_{nn} \approx 0.9$ K. $Pr_2Sn_2O_7$ also displays a zero-point entropy that is at least partially lifted with a magnetic field, but its numerical value disagrees with Pauling's entropy. More work needs to be done to understand this compound, but if it proves to be a spin ice material, its absence of freezing down to the lowest temperatures would make it of great interest as discussed at the end of this manuscript.

$Dy_2Sn_2O_7$ displays the same dynamical behaviour and zero-point entropy as its titanate counterpart and is thus a solid candidate for being spin ice. Same result holds for reasonable dilution of $Dy_2Sn_{2-x}Sb_xO_{7+x/2}$ (x=0.5). Dy_2NbScO_7 also has a finite entropy at $T = 0$, but noticeably smaller than Pauling's, suggesting a stronger constraint on the. ground state manifold.

A recent poster by Zivkovic, Lago and Rojo recognised a potential spin ice signature in the spinel $CdEr_2Se_2$, but we know too little about it to give any more details. If it happens to be confirmed, this would be the first non pyrochlore oxides spin ice.

This review on spin ice is now over. I have tried to be as exhaustive as possible, but I chose not to present the effect of dilution or "stuffing" (even if this will be briefly discussed within the manuscript) and the rising subject of $2d$ *artifical spin ice*, made of elongated magnetic islands of size 0.5 μm that should hopefully reproduce some of the characteristics of spin ice at room temperature. Even if these themes open new possibilities for the physics of spin ice, they are mostly out of subject for my thesis which is focused on the topological constraints in a $3d$ classical system.

I.4 Plan

During the three years of this PhD, we have striven to consider as many aspects of the spin ice model as possible, *always* keeping in mind the experimental relevance of the problems we studied.

The core of this manuscript is divided in four chapters, the next one (§ II) being dedicated to the presentation of the methods we have used; we shall define the models investigated and introduce the necessary background for a self-sufficient understanding of both the analytical and numerical results obtained in this thesis.

Our first study is presented in chapter III and concerns the influence of perturbations such as a [001] magnetic field or an anisotropic bond distortion, on the topologically constrained 2 *in* - 2 *out* manifold for the nearest neighbour spin ice model. The divergence free condition allows the use of the very efficient Worm algorithm whose outcome will be perfectly confirmed by exact analytical results on the Husimi tree and with the transfer matrix method in $3d$. The ground state degeneracy lift imposed by these perturbations provokes topologically driven phase transitions, namely the Kasteleyn and the KDP transition, that will be extensively studied [Jau08]. Our results in a field will be compared with experimental results, whereas the realisation of bond distortion in spin ice crystals will be discussed in the context of uniaxial pressure.

In the fourth chapter (§ IV) we are interested in dynamical aspects of spin ice, our goal being to explain the peculiar temperature dependance of the magnetic time relaxation; not only was it an open question for the last nine years, but this behaviour proves to be a direct consequence of the deconfinement of quasi-particles interacting through a Coulomb potential, *i.e.* magnetic monopoles ! This study has been the first dynamical signature of the presence of monopoles in spin ice [Jau09b].

Finally, in the last chapter V, we investigate the non-standard behaviour of the susceptibility in $Ho_2Ti_2O_7$ as a function of the temperature and the scattering vector $\mathbf{q}$ in reciprocal space, displaying the complex crossover between the paramagnetic phase and the low temperature spin ice regime respecting the topological constraints.

II Methods

Both numerical and analytical techniques were required to investigate the multiple facets of spin ice. If a classical Metropolis - Monte Carlo algorithm is sufficient and a priori accurate to simulate the temperature dependent dynamics of spin ice, long range interactions need a specific treatment: the *Ewald method* presented in section II.4. On the other hand, as discussed in the introduction I.3.c, dipolar interactions can be neglected in a first approximation if we are only interested in the 2 *in* - 2 *out* constrained manifold, but a "single spin flip" move is not adequate anymore and will require a cluster technique; we chose the *Worm algorithm* for reasons that will be made clear in section II.3.

Since spin ice materials are very well described by Ising spins at low temperature and we will see that this can be accurately treated by analytical approaches such as a *Husimi tree* calculation (section II.6) and even an exact treatment for one of the transition we are going to investigate, the multi-critical point of $\infty-$order, using a $3d$ version of the *transfer matrix* (section II.5).

This chapter is divided into six parts. We first introduce the problems investigated in this thesis, namely the influence of magnetic field and bond distortion, and the emergence of magnetic monopoles at finite temperature. The following three sections are devoted to numerical methods; after a very brief presentation of the Metropolis argument in Monte Carlo simuations, we develop the Worm algorithm applied to spin ice and then explain the mathematical foundations of the Ewald summation. In the remaining sections, we introduce the transfer matrix method for $1-$ and $2-$dimensional statistical problems before presenting the general form of the Husimi tree and adapt it to the pyrochlore lattice.

II.1 Presentation of the model

In this thesis, we will be interested in the effects of an external magnetic field along the [001] direction and of bond distortion, as illustrated in figures II.1. The experimental realisation of bond distortion using uniaxial pressure will be discussed in details in subsection III.4.f. As one can see in figures II.2 and II.3, both perturbations lift the ground state degeneracy, but with the crucial difference that a field favours a unique configuration with all spins *up*[1] whereas the distortion conserves a global $\mathbb{Z}_2$ symmetry. It will turn out that the main physics seems to happen on the constrained 2 *in* - 2 *out* manifold, where

[1] An *up* (resp. *down*) spin has a positive (resp. negative) $z-$component.

these external perturbations will induce symmetry breaking phase transitions.

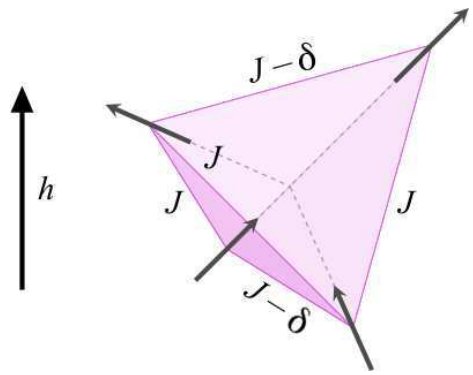

Figure II.1: **Presentation of the model:** The magnetic field is vertical and the bonds in the horizontal planes are weaker than the others.

We should note here that the 6 types of tetrahedra respecting the ice-rules have a net magnetic moment along one of the 3 cartesian directions ($x-$, $y-$, $z-$axis) or in the opposite way.

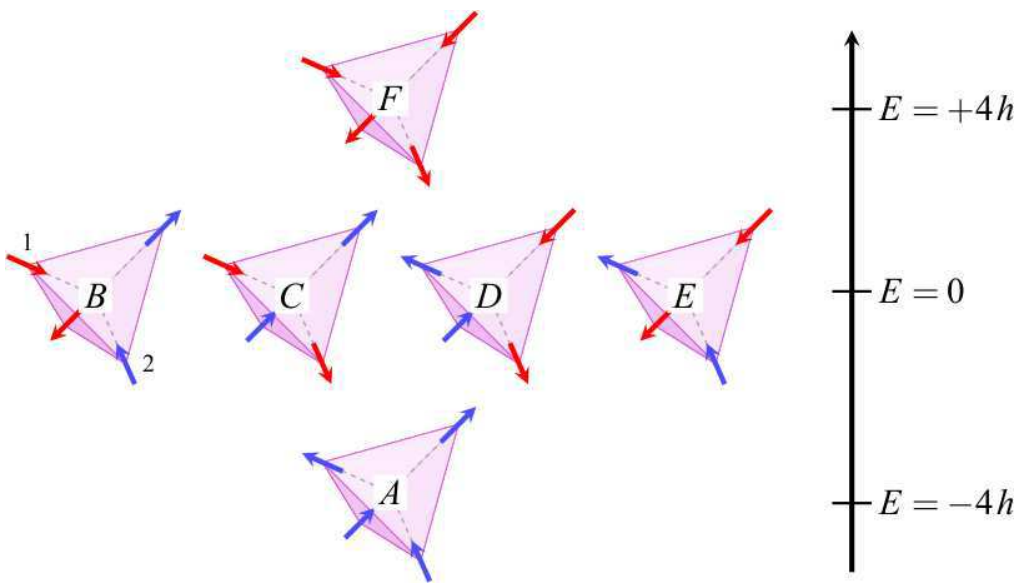

Figure II.2: **Degeneracy lift of the 2 *in* - 2 *out* tetrahedra in a [001] magnetic field.**

Since we will mainly focus on the 2 *in* - 2 *out* manifold, we will only use the nearest neighbour model as it is projectively equivalent with dipolar spin ice up to corrections of

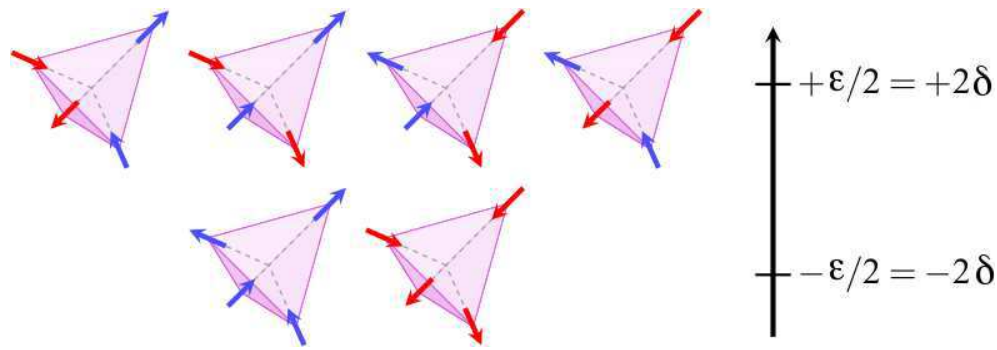

Figure II.3: **Degeneracy lift of the 2 *in* - 2 *out* tetrahedra with bond distortion.**

order $1/r^5$ (see subsection I.3.c).

$$\mathcal{H} = -\mu^2 \sum_{\langle i,j \rangle} J'_{i,j}\, \mathbf{S}_i \cdot \mathbf{S}_j - \mu_0\, \mu \sum_i \mathbf{H} \cdot \mathbf{S}_i \tag{II.1}$$

$$= -\frac{\mu^2}{3} \sum_{\langle i,j \rangle} J'_{i,j}\, \sigma_i\, \sigma_j - \mu_0 \frac{\mu}{\sqrt{3}} |\mathbf{H}| \sum_i \sigma'_i \tag{II.2}$$

$$= -\sum_{\langle i,j \rangle} J_{i,j}\, \sigma_i\, \sigma_j - h \sum_i \sigma'_i \tag{II.3}$$

where $\mu \approx g_J J \mu_B$ is the magnetic moment of a rare earth ion, $\mathbf{H}$ is the [001] magnetic field and $J'_{i,j}$ is the effective nearest neighbour exchange coupling defined in equation (I.46) whose value varies due to bond distortion. The scalar spin σ_i has been defined in equation (I.41): $\sigma_i = +(-)1$ if the spin is *out* (*in*), whereas the new scalar spin definition σ'_i simply represents the sign of the $z-$component of spin i (parallel to the field). $J_{i,j}$ and h are the effective parameters of our model, homogeneous to an energy

$$h = \mu_0 \frac{\mu}{\sqrt{3}} |\mathbf{H}| \quad \text{and} \quad J_{i,j} = \begin{cases} \frac{\mu^2}{3}(J_{\text{eff}} - \delta_{eff}) \;=\; J - \delta \;\; \text{for a bond in the (001) planes} \\ \frac{\mu^2}{3} J_{\text{eff}} \;=\; J \;\; \text{otherwise} \end{cases} \tag{II.4}$$

We use here the short notation of J instead of J_{eff} for convenience. The contribution of each term of equation (II.3) in the energy of different tetrahedra configurations is given in figures II.2 and II.3.

II.2 Monte Carlo

The Monte Carlo (MC) algorithm invented by Metropolis *& al.* [Met53] could well be the most famous numerical method in physics[2], essentially because its key concepts are particularly simple and after more than 50 years of evolution, it has proven to be able

[2]this article is incidently the most cited one of my bibliography, with more than 11000 citations according to ISI Web of Knowledge !

to adapt to a very large range of problems. This subject has been treated in numerous books and articles in a more detailed and clearer way that we can afford here. We invite the interested reader to consult for example the reference book by Binder and Heermann [Bin97] or the more recent book by Krauth [Kra06] (a succinct version of the first chapter dedicated to Monte Carlo basis is available on arxiv [Kra96]). In this section we only present the main aspects of this technique.

The Monte Carlo technique is dedicated to simulations of *stochastic* processes, *i.e.* whose evolution is non-deterministic: randomness will allow the system to fluctuate among different microstates. Hence a microscopic picture is numerically accessible and enables one to compute thermodynamic observables easily. Such a method raises a few questions: "How can one implement the influence of randomness ? What kind of *probability* is pertinent for the evolution between microstates ? That is, is it possible to simulate dynamic as well as static properties ? How can one make the simulation as close to the physical system as possible ?" In both dynamic and static aspects, we need to consider a system with a finite number of microstates referenced by roman letters i and with respective weights $w_i(t)$ whose time-evolution is dictated by the so-called *Master equation*

$$\frac{d\,w_i(t)}{dt} = \sum_j P_{ji}\,w_j(t) - P_{ij}\,w_i(t) \tag{II.5}$$

where P_{ij} is the transition probability to go from microstate i to microstate j. This is a Markov process because the transition rate $a_{ij} = P_{ij}\,w_i$ only depends on the present state of the system; the process retains no memory. The evolution is thus imposed by the relative balance between the production of probability w_i at the expense of the other microstates w_j and its disappearance in favour of the same microstates w_j. The system will eventually reach a steady state where $\frac{d\,w_i(t)}{dt} = 0$ $(\forall i)$. This condition can be fulfilled if

$$a_{ij} = a_{ji} \Leftrightarrow \frac{P_{ji}}{P_{ij}} = \frac{w_i(t\to\infty)}{w_j(t\to\infty)} \tag{II.6}$$

By imposing the transition probabilities P_{ij}, the above equation ensures that after a transient time (typically expressed as T_{eq}) the system will reach a steady state where the probability distribution will be fixed by the weights w_i. The Monte Carlo time t is *a priori* unrelated to the physical real time. In fact this MC time will highly depend on the algorithm used ("single spin flip", "cluster", *etc*) and its aim is not necessarily to reproduce the physical time evolution, but rather to provide an efficient way to visit the phase space, usually in the canonical ensemble.

Equation (II.6) is of course a *sufficient* condition to impose $\frac{d\,w_i(t)}{dt} = 0$ $(\forall i)$ but is not a *necessary* hypothesis: one could imagine much more complex dynamics that would also result in setting $\sum_j P_{ji}\,w_j(t) - P_{ij}\,w_i(t)$ to zero. The above choice is subjective but is widely used as it offers a particularly elegant symmetry, coupling all pairs of microstates

in the same manner and facilitating the tractability of future computations. This equation (II.6) is called the **detailed balance condition** (DBC) and is one of the cornerstones of Monte Carlo algorithms.

The DBC is primordial in MC simulations, but it only assures a correct probability transition between configurations and does not guarantee they are *all* accessible. We must make sure that starting with a chosen or arbitrary microstate does not technically prevent the simulation to visit any other configuration; this is the condition of **ergodicity**, and together with detailed balance, they ensure an adequate representation of the different microstates.

Of course, from a practical point of view, the simulation must be sufficiently long in order to be able to visit all configurations with a frequency imposed by the DBC. If the initial microstate is far from equilibrium, one also needs to wait for equilibration before computing thermodynamical observables. Hence, one can define two characteristic Monte Carlo times T_{eq} and T_{tot}, required for equilibration and to guarantee a correct coverage of the configurational space respectively[3].

Spin ice turns out to be a good example to illustrate the details of the Monte Carlo algorithm. The source of randomness here is the thermal noise, because the physics under interest is at finite temperature, and quantum fluctuations are negligible in spin ice. Let us consider a finite system of N spins; since they are of Ising nature, the simplest Monte Carlo move that respects ergodicity is a "single spin flip" (SSF); one can visit all 2^N configurations by flipping the spins one by one. A MC step is usually defined as N SSF attempts and represents the unity of the MC time t running from 0 to T_{tot}. The algorithm is detailed in the following diagram. The elements inside the dashed rectangle represent the core of the program and are called the Metropolis argument [Met53]. The energetic term ΔE is defined as the difference of energy between the new microstate with a spin flipped and the former one: one can immediately check that a move towards a more stable configuration is always accepted. β is the well-known effective inverse temperature $\beta = 1/k_B T$.

This SSF method happens to be a good algorithm to simulate the actual dynamics of some materials such as spin ice, as Nature seems to be well reproduced by *local* dynamical moves. However this locality may as well be a problem for systems with topological constraints (see III.1.b) where the only possible excitations are macroscopic. In this case a cluster method involving an extensive number of spin is required and we chose to use the so-called Worm algorithm introduced in the next section in order to investigate the 2 *in* - 2 *out* ground state manifold of spin ice.

[3]One must not confuse with the time defined in equation (II.5) since we are in the steady state for the probability distribution and $w_i = \text{cst}\ \forall i$.

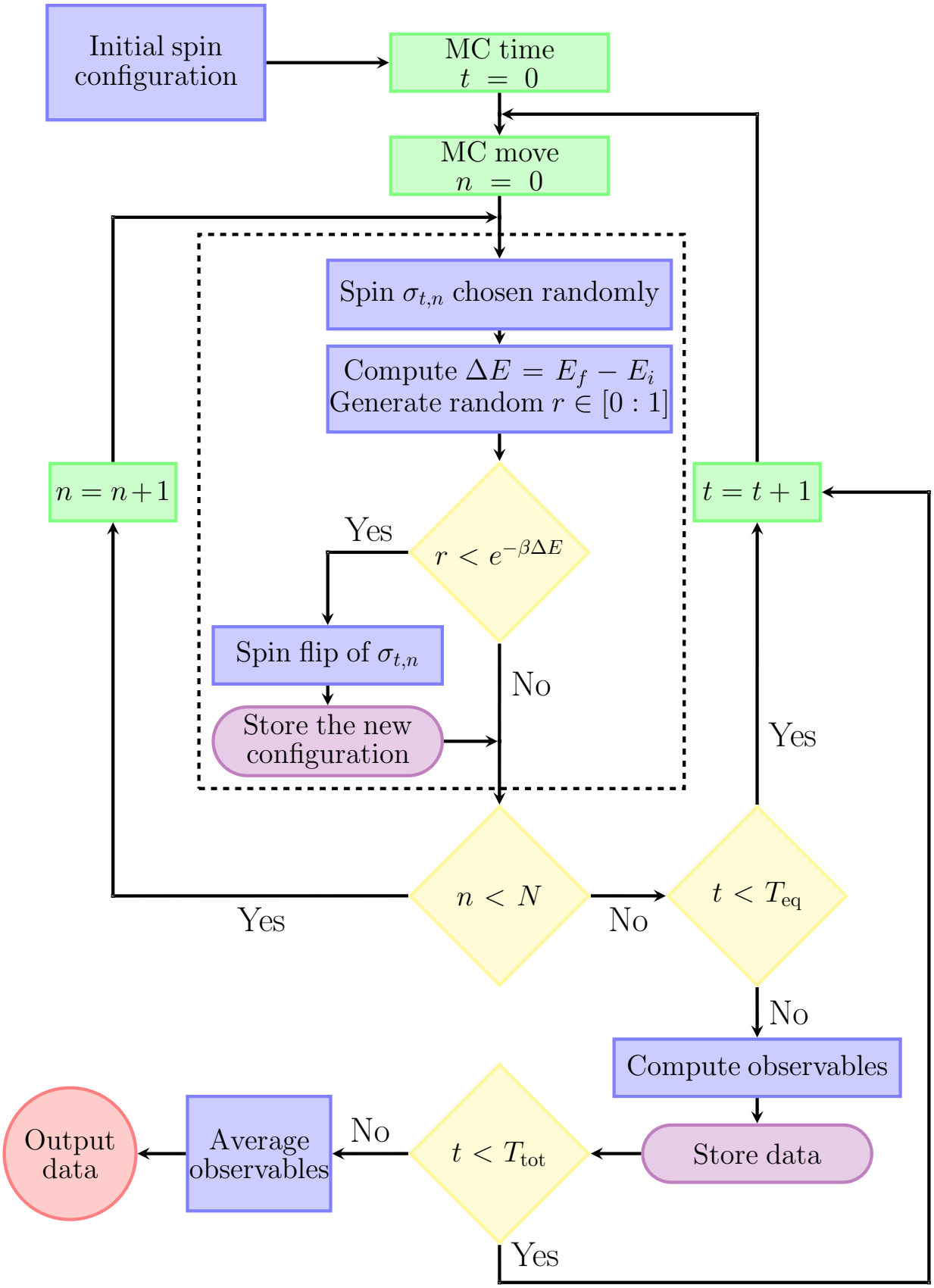
Initial spin configuration
MC time $t = 0$
MC move $n = 0$
Spin $\sigma_{t,n}$ chosen randomly
Compute $\Delta E = E_f - E_i$
Generate random $r \in [0:1]$
$r < e^{-\beta\Delta E}$
Yes
No
Spin flip of $\sigma_{t,n}$
Store the new configuration
$n = n+1$
$t = t+1$
Yes
$n < N$
Yes
No
$t < T_{\text{eq}}$
No
Compute observables
Store data
$t < T_{\text{tot}}$
No
Yes
Average observables
Output data

II.3 Worm algorithm

When we decided to study the influence of external perturbations on spin ice, we had two goals in mind. First of all, we wanted to explain the discrepancy between theoretical expectations [Har98] and experimental results [Ram99, Fen05] and to predict further phenomena under pressure. As we shall discuss it in chapter IV, this has required the use of algorithms adequate to simulate spin ice materials such as the single spin flip move. Additionally we found out that the underlying physics has ramifications for fundamental statistical problems which necessitate the consideration of topological constraints (the ice-rules), which are impossible to study with a local simulation. That is, if we want to force the system to remain on the 2 *in* - 2 *out* manifold, we cannot flip a single spin as it will create a pair of topological defects. We must then use non-local moves able to connect two configurations respecting the ice-rules and to restrain the phase space to the whole 2 *in* - 2 *out* manifold; this has been accomplished with the Worm algorithm that has been discussed in [Bar98, Isa04b, San06]. This method is also sometimes referenced as the loop algorithm, but in this manuscript, we keep this denomination for the loop algorithm used by Melko and collaborators [Mel01b, Mel04]. In the *loop* algorithm, a loop is randomly created in the system and is flipped according to a single Metropolis argument, *i.e.* it depends on the energy difference involved between the two states of the the loop move and can be rejected; whereas for the *Worm* algorithm, the detailed balance condition is imposed all along the construction of the loop, which allows us to flip loops of arbitrary length even in the presence of a field, without rejection ! This crucial difference makes the latter algorithm particularly attractive for our application.

Before going any further, we should explain what we mean by *loops*. Their existence comes from the divergence free condition: if we are on a 2 *in* - 2 *out* configuration, there is a local flux conservation (see subsection I.3.c ensuring that if we enter in a tetrahedron through an *in* spin, there are always two possibilities to go out through an *out* spin. By repeating this process step by step (*in-out-in-out-in...*) in a finite size system, we will eventually close the loop that can then be flipped without breaking the ice-rules and define the next microstate of the system (see figure III.1 for an illustration). The loop can propagate until either the initial spin is encountered; this is a long loop. Or a previously visited spin is encountered and the dangling end of the loop can be neglected; a short loop (see figure II.4). For the same reasons as given in the detailed analysis of reference [Mel04, Mel01a], we chose to use a majority of short loops, which is the best compromise between CPU time economy and coverage of the phase space. Now that we have established a way to remain on the 2 *in* - 2 *out* manifold, we must check if it is acceptable for a Monte Carlo move.

We will arbitrarily focus our argument onto the $z-$axis, but the 6-fold degeneracy of the 2 *in* - 2 *out* spin ice ground state ensures an equivalence for both $x-$ and $y-$axis. The pyrochlore lattice can be seen as a stack of (001) layers of spins connected by tetrahedra (see figure III.19). The ice-rules impose that the $z-$component of the two spins at the top of a tetrahedron (upper layer) must be the same one as for the two other spins at the bottom (lower layer). Hence the magnetisation along the $z-$axis must be the same

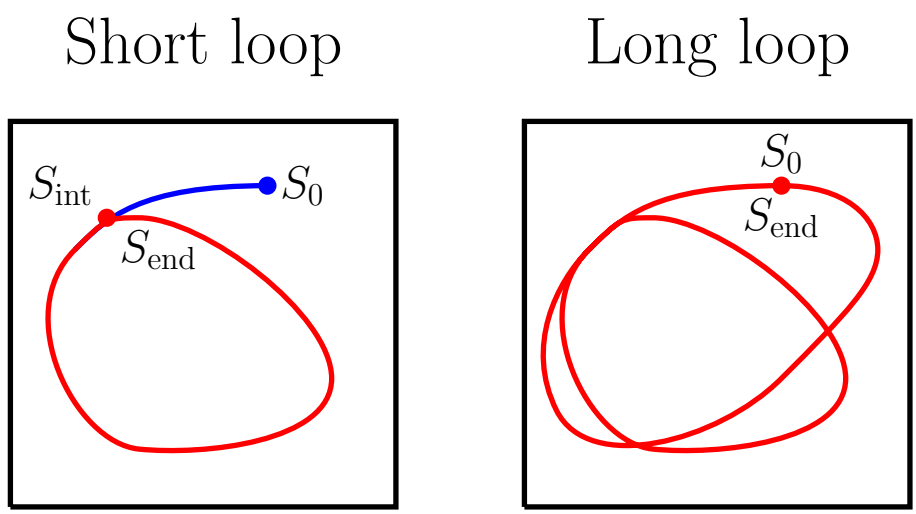

Figure II.4: **Loops from the Worm algorithm:** We use a $2d$ representation for convenience. *Left:* The loop begins at S_0 and finally hits an intermediate site S_{int} where it closes; this is a *small* loop. The red loop is flipped while the dangling blue part is left unchanged. *Right:* we prevent the loop to close on an intermediate site and can only close on the initial spin S_0; this is a *long* loop.

for all (001) layers and the *up* and *down* spins form an ensemble of strings spanning the whole system in both [001] and [00$\overline{1}$] directions: a spin configuration on the pyrochlore lattice can then be exactly mapped onto a fully-packed configuration of strings on the dual diamond lattice (see figure II.5). With periodic boundary conditions on the 2 *in* - 2 *out* manifold the strings have no ends and must be closed; they can therefore be constructed by the Worm algorithm and flipping an entire string does not break the ice-rules. Let us consider two random microstates with N_i^+ strings of *up* spins and N_i^- strings *down* ($i = 1, 2$). To go from configuration 1 to 2, we can simply "erase" the N_1^- strings *down*, giving rise to a configuration with saturated magnetisation (all spins *up*), and re-form the necessary N_2^- strings *down* to obtain the second microstates with $N_1^- + N_2^-$ MC moves. This proves that all the 2 *in* - 2 *out* configurations are connected to each other by creating or erasing a finite number of MC loops: ergodicity is thus respected !

We will now investigate the most difficult part of the Worm algorithm, *i.e.* how to construct a loop respecting detailed balance and without rejection ? The solution consists in imposing different probabilities for the propagation of the loop depending on the type of tetrahedron visited and respecting the DBC (II.6). The notation refers to figure II.2 or II.3

The Boltzmann weight w_i for each configuration is made up from bond (internal energy) and site (Zeeman energy) contributions. As each spin is shared between two tetrahedra, the Zeeman energy can be considered to be shared between them. Here we choose equal shares. The Zeeman energies for vertices (B, C, D, E) defined in figure II.2 add to zero and their exchange energies are equal, giving equal weights: $w_B = w_C =$

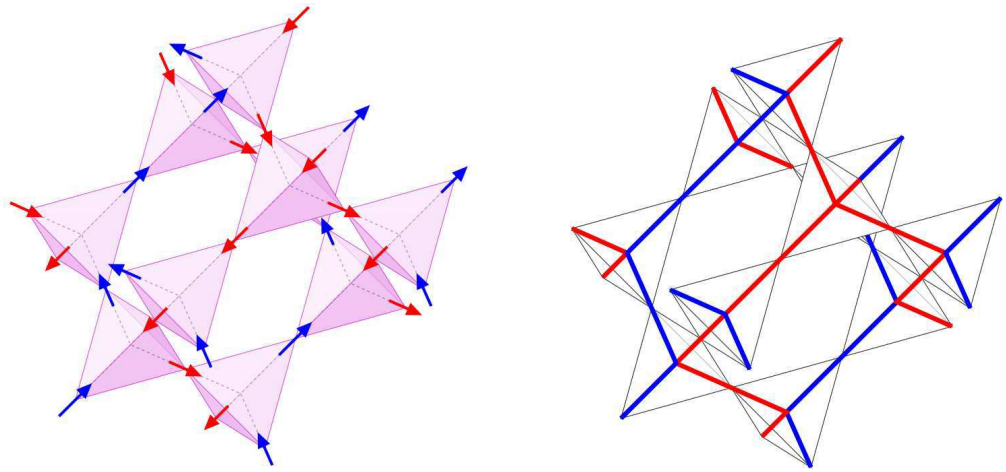

Figure II.5: **Mapping from a spin configuration to an ensemble of strings:** The blue (resp. red) strings are made of *up* (resp. *down*) spins respecting the ice-rules.

$w_D = w_E = w_o$. The field lifts the degeneracy between A ($w_A = w_\uparrow$) and F ($w_F = w_\downarrow$):

$$\begin{aligned} \frac{w_\uparrow}{w_0} &= \exp\left[\beta\left(+2h + 4\delta\right)\right] \\ \frac{w_\downarrow}{w_0} &= \exp\left[\beta\left(-2h + 4\delta\right)\right] \end{aligned} \tag{II.7}$$

To construct a loop we first choose a spin at random. The spin shares two tetrahedra, pointing into one and out of the other. We choose the tetrahedron with the spin pointing in as the starting point of the loop. Its initial state is I. This is a convention that could change from one loop construction to another. We now make a virtual flip of the spin, breaking the ice rules on both tetrahedra and creating a pair of topological defects: 3 *out* - 1 *in* for our chosen tetrahedron and 3 *in* - 1 *out* for the other. We now flip a second spin on the chosen tetrahedron to re-establish the ice rules. As this has to be an "out spin" there are three possibilities: either we can flip the same spin back again - a backtrack - or we can choose one of two possible forward directions, taking the tetrahedron to constrained state J and moving the defect elsewhere. We can construct the transition probabilities $P^{kl}_{IJ} = a^{kl}_{IJ}/w_I$ such that

$$w_I = \sum_J a^{kl}_{IJ}, \tag{II.8}$$

$k = 1, 2$ indicates by which of the two "in" spins the loop entered the tetrahedron. For the first step this corresponds to the initially selected spin. Indice $l = f, b$ indicates if the move is forward or backtracking. There are thus $6 \times 2 = 12$ such equations but because of the symmetries discussed above it turns out that only four are independent:

$$w_\uparrow = a^b_{\uparrow\uparrow} + a^f_{\uparrow o} + a^f_{\uparrow o} \tag{II.9}$$

$$w_o = a^{1f}_{oo} + a^{1b}_{oo} + a^{1f}_{o\uparrow} \tag{II.10}$$

$$w_o = a^{2f}_{oo} + a^{2b}_{oo} + a^{2f}_{o\downarrow} \tag{II.11}$$

$$w_\downarrow = a^{b}_{\downarrow\downarrow} + a^{f}_{\downarrow o} + a^{f}_{\downarrow o}, \tag{II.12}$$

where the index k has been dropped in equations (II.9) and (II.12) as the transition probabilities $A \to B, C, D$ or E and $F \to B, C, D$ or E are independent of the starting point for the loop. Transitions from the four degenerate states do depend on k. Take for example the vertex B: spins 1 and 2 are illustrated in figure II.2. Starting from B^1 the loop can take the vertex to E, A or back to B, while B^2 can be transformed into C, F or back to B. The index $l = b, f$ is used explicitly here to distinguish between backtracking and forward processes among the four degenerate vertices B, C, D, E and is rather redundant elsewhere. The symmetry between the two series of transition probabilities is broken by the external field but all other similar paths are equivalent to one of these. This leads to the two equations for the evolution of a vertex off the degenerate set B, C, D, E {(II.9), (II.10)} and {(II.11), (II.12)}.

The number of independent parameters is reduced further by implementing the detailed balance condition

$$\frac{P^{kl}_{IJ}}{P^{k'l}_{JI}} = \frac{w_J}{w_I}, \tag{II.13}$$

which leads to: $a^{f}_{\uparrow o} = a^{1f}_{o\uparrow}$ and $a^{f}_{\downarrow o} = a^{2f}_{o\downarrow}$ (note that even though the reverse process involves flipping the same spins the index k is not necessarily the same for vertex I or J). Hence we finally obtain two independant sets of two equations, each with four unknown variables. The equations are therefore under-determined; a property we can use to our advantage to *optimize* our algorithm, choosing the most efficient way to construct the loops. It is clear that an optimal loop algorithm will exclude backtracking if possible, hence wherever possible we set the transition probabilities for backtracking equal to zero giving the minimal set of equations to be solved:

$$\begin{aligned} w_\uparrow &= 2a^{f}_{\uparrow o} \\ w_o &= a^{1f}_{oo} + a^{f}_{\uparrow o}, \end{aligned} \tag{II.14}$$

and

$$\begin{aligned} w_\downarrow &= 2a^{f}_{\downarrow o} \\ w_o &= a^{2f}_{oo} + a^{f}_{\downarrow o}. \end{aligned} \tag{II.15}$$

The solutions yield positive probabilities for $T > T_\uparrow$ and $T > T_\downarrow$ respectively, where

$$T_{\uparrow(\downarrow)} = \frac{4\delta + (-)2h}{\ln 2} \tag{II.16}$$

For lower temperatures backtracking must be included for the relevant transitions to ensure a physically meaningful solution. Note that for $\delta = 0$, $T_\downarrow$ is always negative. A resume of the vertex transition probabilities is given in table II.1.

Once the process described above is completed the 3 *out* - 1 *in* defect is moved to a new tetrahedron K and the process is repeated, propagating the loop until closure.

$T \leqslant T_\uparrow$	$T \geqslant T_\uparrow$
$P^b_{\uparrow\uparrow} = 1 - 2\dfrac{w_o}{w_\uparrow}$	$P^b_{\uparrow\uparrow} = 0$
$P^f_{\uparrow o} = \dfrac{w_o}{w_\uparrow}$	$P^f_{\uparrow o} = \dfrac{1}{2}$
$P^{1f}_{oo} = 0$	$P^{1f}_{oo} = 1 - \dfrac{1}{2}\dfrac{w_\uparrow}{w_o}$
$P^{1f}_{o\uparrow} = 1$	$P^{1f}_{o\uparrow} = \dfrac{1}{2}\dfrac{w_\uparrow}{w_o}$

$T \leqslant T_\downarrow$	$T \geqslant T_\downarrow$
$P^b_{\downarrow\downarrow} = 1 - 2\dfrac{w_o}{w_\downarrow}$	$P^b_{\downarrow\downarrow} = 0$
$P^f_{\downarrow o} = \dfrac{w_o}{w_\downarrow}$	$P^f_{\downarrow o} = \dfrac{1}{2}$
$P^{2f}_{oo} = 0$	$P^{2f}_{oo} = 1 - \dfrac{1}{2}\dfrac{w_\downarrow}{w_o}$
$P^{2f}_{o\downarrow} = 1$	$P^{2f}_{o\downarrow} = \dfrac{1}{2}\dfrac{w_\downarrow}{w_o}$

Table II.1: **Probabilities of the Worm algorithm** for different ranges of temperature.

The algorithm can be modified at higher temperature to take into account a finite concentration of topological defects, which begin to occur as T approaches the scale set by the exchange coupling J. As the loop construction involves the virtual propagation of a 3 *out* - 1 *in* defect we allow the line to terminate if it encounters a 3 *in* - 1 *out* defect and the loop move involves flipping the connected line of spin from the initial to the final position of the defect. The net result of the move is to catapult the 3 *in* - 1 *out* defect from the position of the final encounter to that of the initial spin flip, providing a kind of "worm hole" for topological defects across the system. Dealing with defects makes the algorithm more complex and slows it down making it no more efficient than a simple Metropolis algorithm for high defect concentrations. This is why we did not consider the possible translation of double defects *four in* or *four out* through a loop move since their presence is only relevant at relatively high temperature.

The results obtained from the Worm algorithm are detailed in the chapter III and among other things, bring to light the nature of the temperatures $T_\uparrow$ and $T_\downarrow$ and the relevance of the picture of strings spanning the system. However in this thesis, we have not limited ourselves to the 2 *in* - 2 *out* manifold. We have also studied the monopole creation/anihilation and the influence of long range interactions. The latter requires a

special treatment, as presented in the following section.

II.4 Ewald Method

II.4.a General presentation

If we want to go beyond the nearest neighbour model, we must take into account long range interactions that happen to be particularly subtle to implement numerically. Let us consider a central potential $u(r)$ in a system of size $V = L^3$ with a uniform density ρ of interacting particles. A (very) naive estimate of the total energy is

$$\begin{aligned} \mathcal{U} &= \frac{1}{2}\rho^2 L^3 \int_{\lambda_c}^{L} \mathrm{d}r\; u(r)\; 4\pi\, r^2 && \text{(II.17)} \\ &= \frac{1}{2}\rho^2 L^3 \left(\int_{\lambda_c}^{r_c} \mathrm{d}r\; u(r)\; 4\pi\, r^2 + \int_{r_c}^{L} \mathrm{d}r\; u(r)\; 4\pi\, r^2 \right) && \text{(II.18)} \\ &= \mathcal{U}_{\text{core}} + \mathcal{U}_{\text{tail}} && \text{(II.19)} \end{aligned}$$

where λ_c is an UV cut-off describing hard core repulsion and r_c is an eventual numerical cut-off. Computers are of course unable to simulate macroscopic crystals with of the order of 10^{23} elements and we can only consider finite system size (typically 10^4 or 10^5 atoms). Unfortunately, as one can see from equation (II.19), the contribution of the tail of the energy diverges for potential decaying as $1/r^\nu$, $\nu \leqslant 3$; *e.g.* for Coulomb potential, $\mathcal{U}_{\text{tail}}$ diverges quadratically with L. For dipolar interactions the divergence should be logarithmic, but in fact the angular dependance integrates to zero[4]. The arrangement of spins or charges may lead to screening effects with an effective potential decaying much faster than the original algebraic interaction, as *e.g.* for free ions in electrolytes feeling an effective Yukawa potential $V(r) \propto \exp(-r/\ell_D)/r$ (where l_D is the Debye length of the solutions). For spin ice this gives rise to the projective equivalence presented in section I.3.c [Isa05]. Gingras & den Hertog showed the importance of considering the whole range of the dipolar interactions to reveal this screening [dH00, Gin01], at the risk of obtaining non-physical phase transitions for a finite cut-off radius r_c [Sid99]. This phenomenon is a many-body effect requiring interactions on all length scales whose implementation in finite numerical systems is quite subtle. This is why long range interactions require a specific treatment by using, for example, the Ewald summation.

This method has been developped by Ewald in 1921 in the context of ionic crystals [Ewa21] and has been since then extended to magnetic materials, as well as molecular simulations, soft matter, *etc* and remains one of the most widely used techniques to deal with long range interactions. For a rigourous discussion on this subject, we refer the reader to a very detailed series of articles by de Leeuw & *al.* [dL80a, dL80b, dL83], while a more pedagogical introduction can be found in the book by Frenkel & Smit [Fre02]. We

[4]This is the same reason why $3d$ pinch points due to dipolar correlations are not divergent in the scattering function [Isa04a].

start by considering the Coulomb interaction between magnetic monopoles and we use SI units in this section.

Let us consider a magnetically neutral system of N charges ($\sum_i q_i = 0$) in a cube of diameter $V = L^3$. We impose periodic boundary conditions giving rise to an infinite succession of *images* of the system surrounding the central cube and indexed by the vector $\mathbf{n}$ between the image and the origin. The global energy is then

$$\mathcal{U}_{\text{coul}} = \frac{1}{2}\sum_{i=1}^{N} q_i\,\phi(\mathbf{r}_i) \quad \text{where} \quad \phi(\mathbf{r}_i) = \sum_{j=1}^{N}{}' \sum_{\mathbf{n}} \frac{\mu_0}{4\pi}\,\frac{q_j}{|\mathbf{r_{ij}} + \mathbf{n}L|} \tag{II.20}$$

where the last sum runs over all images $\mathbf{n}$ and the prime indicates that $j \neq i$ when $\mathbf{n} = \mathbf{0}$. Hence, we are interested in the energy of the N charges interacting between them *and* with all their images. As opposed to equation (II.19), the above sum is convergent because the system is globally neutral; if we look far enough from the central cube, it will be seen as a vacuum of charges. However it is only conditionally convergent and we must consider a very large number of images to obtain a correct estimate of $\mathcal{U}_{\text{coul}}$; the key concept of the Ewald method is to substitute for this poorly converging series a sum of absolutely converging ones. Let us illustrate this idea with figure II.6. The monopoles are considered as point charges on a square lattice with an energy given by equation (II.20). Now the idea is to add a diffuse charge distribution of opposite charge around every monopole, making a net local neutrality over all the system. As we shall see below, the new corresponding energy is quickly convergent. One now needs to subtract this artificial contribution by adding a potential with opposite diffuse charge distribution, *i.e.* of the same sign as the point charges; this term happens to be exactly computable in Fourier space if we consider a Gaussian distribution for the compensating magnetic cloud:

$$\rho_G(r) = -q_i \left(\frac{\alpha}{\pi}\right)^{\frac{3}{2}} \exp(-\alpha\, r^2) \tag{II.21}$$

The result should be independent of α that will be chosen for numerical efficiency as explained shortly.

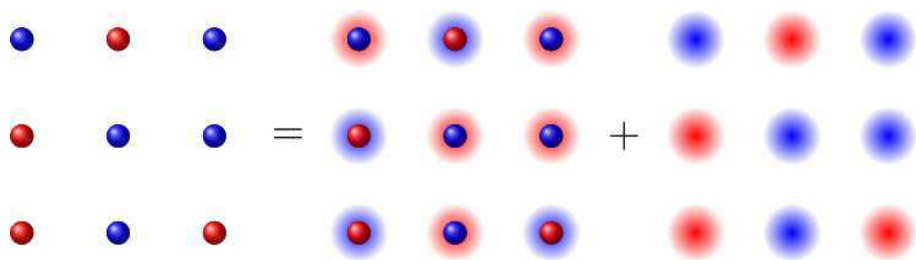

Figure II.6: **Illustration of the Ewald sum:** The left hand side term is a conditionally convergent sum of point charge potentials that is impossible to compute numerically in a reasonable amount of time. This is why we transform this term in two absolutely convergent series by adding a Gaussian charge distribution of opposite sign to the point charges (2nd term) and subtracting the same Gaussian charge distribution (3rd term).

II.4.b Analytical calculation of the series

Fourier space: diffuse charge distribution

Our problem can be reduced to solving Poisson's equation for a given magnetic charge distribution $\rho(\mathbf{r})$

$$-\nabla^2\phi(\mathbf{r}) \;=\; \mu_0\,\rho(\mathbf{r}) \tag{II.22}$$

which can be re-written in Fourier space

$$k^2\tilde{\phi}(\mathbf{k}) \;=\; \mu_0\,\tilde{\rho}(\mathbf{k}) \tag{II.23}$$

One obtains $\tilde{\phi}(\mathbf{k}) = q_i/k^2$ for a single point charge. Now we can follow the same reasoning for the diffuse charge distribution defined as

$$\rho_{\mathbb{F}}(\mathbf{r}) \;=\; \sum_{j=1}^{N}\sum_{\mathbf{n}} q_j \left(\frac{\alpha}{\pi}\right)^{\frac{3}{2}} \exp\left(-\alpha\left|\mathbf{r}-(\mathbf{r}_j+\mathbf{n}L)\right|^2\right) \tag{II.24}$$

$$\Leftrightarrow\; \tilde{\rho}_{\mathbb{F}}(\mathbf{k}) \;=\; \sum_{j=1}^{N} q_j\,\exp(-i\,\mathbf{k}\cdot\mathbf{r}_j)\,\exp\left(-\frac{k^2}{4\alpha}\right) \tag{II.25}$$

where the index $\mathbb{F}$ is for "Fourier" space. By implementing this expression in the Poisson equation (II.23), one can compute the potential due to the whole charge distribution felt at point $\mathbf{r}$, and then the total energy $\mathcal{U}_{\mathbb{F}}$

$$\phi_{\mathbb{F}}(\mathbf{r}) \;=\; \frac{\mu_0}{V}\sum_{\mathbf{k}\neq\mathbf{0}}\sum_{j=1}^{N}\frac{q_j}{k^2}\,\exp\left(-i\,\mathbf{k}\cdot(\mathbf{r}-\mathbf{r}_j)\right)\,\exp\left(-\frac{k^2}{4\alpha}\right) \tag{II.26}$$

$$\mathcal{U}_{\mathbb{F}} \;\equiv\; \frac{1}{2}\sum_{i=1}^{N} q_i\,\phi_{\mathbb{F}}(\mathbf{r}_i) \;=\; \frac{\mu_0}{2V}\sum_{\mathbf{k}\neq\mathbf{0}}\frac{1}{k^2}\left|\rho(\mathbf{k})\right|^2\,\exp\left(-\frac{k^2}{4\alpha}\right) \tag{II.27}$$

where

$$\rho(\mathbf{k}) \;=\; \sum_{i=1}^{N} q_i\exp(i\mathbf{k}\cdot\mathbf{r}_i) \tag{II.28}$$

Within a few paragraphs, we shall explain the consequences of our arbitrary choice $\mathbf{k}\neq\mathbf{0}$ in equation (II.27). Another important point is that $\mathcal{U}_{\mathbb{F}}$ has been defined with a self-interaction term that should be subtracting in the end, as explicated below.

Self-Interaction

This spurious contribution comes from the interaction of the point charges with the Gaussian charge distribution located exactly around them. The magnetostatic potential of each

diffuse distribution $\phi_G(r)$ can be be calculated directly in real space using the Poisson equation in spherical coordinates.

$$-\frac{1}{r}\frac{\partial^2 r\phi_G(r)}{\partial r^2} = \mu_0\,\rho_G(r) \tag{II.29}$$

With two successive partial integration, one obtain

$$\phi_G(r) \;=\; \frac{\mu_0}{4\pi}\frac{q_i}{r}\,\mathrm{erf}\left(\sqrt{\alpha}\,r\right) \quad \text{where} \quad \mathrm{erf}(x) \;=\; \frac{2}{\sqrt{\pi}}\int_0^x \exp\left(-u^2\right)\,\mathrm{d}u \tag{II.30}$$

$\mathrm{erf}(x)$ is the so-called error function. Since we are interested in the interaction with a magnetic charge at $r = 0$, one can define $\phi_{self}(\mathbf{r}_i) = \phi_G(r = 0) = 2q_i\,\sqrt{\alpha/\pi}$ and compute the total self-interaction energy

$$\mathcal{U}_{\text{self}} \;\equiv\; \frac{1}{2}\sum_{i=1}^{N} q_i\,\phi_{self}(\mathbf{r}_i) \;=\; \frac{\mu_0}{4\pi}\sqrt{\frac{\alpha}{\pi}}\,\sum_{i=1}^{N} q_i^2 \tag{II.31}$$

Real space: point charge screened by oppositely charged distribution

From equation (II.30), we can already write the potential of a charge located at the origin, surrounded by a Gaussian cloud of opposite charge.

$$\phi_{\mathbb{R}}(r) \;=\; \frac{\mu_0}{4\pi}\left(\frac{q_i}{r} \;-\; \frac{q_i}{r}\mathrm{erf}\left(\sqrt{\alpha}r\right)\right) \;=\; \frac{\mu_0}{4\pi}\frac{q_i}{r}\mathrm{erfc}\left(\sqrt{\alpha}r\right) \tag{II.32}$$

giving rise to an energy

$$\mathcal{U}_{\mathbb{R}} \;=\; \frac{1}{2}\,\frac{\mu_0}{4\pi}\sum_{i,j}^{N}{\sum_{\mathbf{n}}}' \; q_i q_j \frac{\mathrm{erfc}\left(\sqrt{\alpha}\,|\mathbf{r}_{ij} - \mathbf{n}L|\right)}{|\mathbf{r}_{ij} - \mathbf{n}L|} \tag{II.33}$$

Hence the total energy of our system with N magnetic charges is

$$\mathcal{U}_{\text{coul}} \;=\; \mathcal{U}_{\mathbb{F}} \;-\; \mathcal{U}_{\text{self}} \;+\; \mathcal{U}_{\mathbb{R}} \tag{II.34}$$

$$= \;\frac{\mu_0}{4\pi}\left[\sum_{\mathbf{k}\neq\mathbf{0}}\frac{4\pi}{2V}\,\frac{|\rho(\mathbf{k})|^2}{k^2}\,e^{\left(-\frac{k^2}{4\alpha}\right)} \;-\; \sqrt{\frac{\alpha}{\pi}}\,\sum_{i=1}^{N} q_i^2 \;+\; \frac{1}{2}\,\sum_{i,j}^{N}{\sum_{\mathbf{n}}}' \; q_i q_j \frac{\mathrm{erfc}\left(\sqrt{\alpha}\,|\mathbf{r}_{ij} - \mathbf{n}L|\right)}{|\mathbf{r}_{ij} - \mathbf{n}L|}\right] \tag{II.35}$$

The central term (self-interaction) may not be constant in a system where particles can be created or annihilated, but it can at least be easily and exactly computed, while the two other series are now absolutely convergent and the error due to truncation can thus be controlled. This expression is a function of α, the width of the Gaussian distribution, that is an adjustable parameter. Unfortunately, its influence is exactly opposite for $\mathcal{U}_{\mathbb{F}}$ and $\mathcal{U}_{\mathbb{R}}$; if it improves the convergence of $\mathcal{U}_{\mathbb{F}}$, it will inevitably slow down the one of $\mathcal{U}_{\mathbb{R}}$, and *vice-versa*: $\alpha = 1.0$ is a good compromise. This parameter α is also an excellent numerical check of the validity of the algorithm, because there must be a bug in the program if $\mathcal{U}_{\text{coul}}$ is not independent of α.

Dipolar interactions between spins

For an ensemble of magnetic dipoles μ_i, the potential of interaction can be written as

$$\phi_{dip}(\mathbf{r}_{ij}) \;=\; \frac{\mu_0}{4\pi}\left[\frac{\mu_i\cdot\mu_j}{|\mathbf{r}_{ij}|^3} - \frac{3\,(\mu_i\cdot\mathbf{r}_{ij})\,(\mu_j\cdot\mathbf{r}_{ij})}{|\mathbf{r}_{ij}|^5}\right] \;=\; \frac{\mu_0}{4\pi}\;(-\mu_i\cdot\nabla_i)\;(-\mu_j\cdot\nabla_j)\;\left(\frac{1}{|\mathbf{r}_{ij}|}\right) \tag{II.36}$$

When compared to the Coulomb potential between magnetic charges (II.20), we see one can obtain the Ewald decomposition for dipoles by replacing q_i by $-\mu_i\cdot\nabla_i$ in equation (II.35) (see [Fre02, Wan01] and reference herein).

$$\begin{aligned}\mathcal{U}_{\text{dip}} \;=\; & \frac{\mu_0}{4\pi}\Bigg\{\sum_{\mathbf{k}\neq\mathbf{0}}\frac{4\pi}{2V}\,\frac{|\mathbf{M}(\mathbf{k})|^2}{k^2}\,e^{\left(-\frac{k^2}{4\alpha}\right)} \;-\; \frac{2\pi}{3}\left(\frac{\alpha}{\pi}\right)^{\frac{3}{2}}\sum_{i=1}^{N}\mu_i^2 \\ & +\frac{1}{2}\sum_{i,j}^{N}{\sum_{\mathbf{n}}}'\left[(\mu_i\cdot\mu_j)\,B(r_{ijn}) \;-\; (\mu_i\cdot\mathbf{r}_{ijn})(\mu_j\cdot\mathbf{r}_{ijn})\,C(r_{ijn})\right]\Bigg\}\end{aligned} \tag{II.37}$$

where $\mathbf{r}_{ijn}\equiv\mathbf{r}_i-\mathbf{r}_j-\mathbf{n}L$ and

$$B(r) \;\equiv\; \frac{\operatorname{erfc}(\sqrt{\alpha}\,r)}{r^3} \;+\; 2\sqrt{\frac{\alpha}{\pi}}\,\frac{\exp(-\alpha\,r^2)}{r^2} \tag{II.38}$$

$$C(r) \;\equiv\; 3\frac{\operatorname{erfc}(\sqrt{\alpha}\,r)}{r^5} \;+\; 2\sqrt{\frac{\alpha}{\pi}}\left(2\alpha+\frac{3}{r^2}\right)\frac{\exp(-\alpha\,r^2)}{r^2} \tag{II.39}$$

$$\mathbf{M}(\mathbf{k}) \;\equiv\; \sum_{i=1}^{N} i\,\mu_i\cdot\mathbf{k}\,\exp(i\,\mathbf{k}\cdot\mathbf{r}_i) \tag{II.40}$$

Demagnetisation effect

A general presentation of demagnetisation can be found in the appendix B. Here we simply want to point out that if we want to take into account this effect in our simulations, we need to impose some boundary conditions by adding a term representing the energy required to magnetise the system despite the counter-influence of the surface [dL80a, Mel04]

$$\mathcal{U}_{\text{demag}} \;=\; \frac{2\pi}{(2\mu'+1)V}\left|\sum_{i=1}^{N} q_i\mathbf{r}_i\right|^2 \quad \text{for magnetic charges} \tag{II.41}$$

$$\mathcal{U}_{\text{demag}} \;=\; \frac{2\pi}{(2\mu'+1)V}\left|\sum_{i=1}^{N} \mu_i\right|^2 \quad \text{for magnetic dipoles} \tag{II.42}$$

where μ' is the magnetic permeability surrounding the system. Note that equation (II.41) is independent of the origin defining the vector $\mathbf{r}_i$ for a neutral system. We decided not to add this term for two reasons, clearly exposed in [Mel04]:

i we have only been interested in simulations with long range interactions in zero field, *i.e.* with no net magnetic moment on average in which case the demagnetisation term can be left out. However, as we shall see, the addition of a magnetic field with long range interactions may be one of the next promising steps of my research.

ii the inconvenience of this term is that once it is added in the simulations, then the outcome can only be compared with experiments respecting the same settings, *i.e.* measurements on spherical samples embedded in a material of permeability μ'; whereas if we use the standard Ewald decomposition of equations (II.35) and (II.37), then we can compare our results to any measurements as long as the specific demagnetisation effects can be dealt with.

Now that we know how to compute the energy due to Coulomb or dipolar interactions, we can implement it in a Monte Carlo algorithm and simulate our system of interest with a simple Metropolis algorithm for example.

II.4.c Numerical application to spin ice

As spin ice materials can be described by magnetic monopoles with Coulomb interaction on the diamond lattice or by spins with dipolar interactions on the pyrochlore lattice, we need two different algorithms using both equations (II.35) and (II.37); we chose to illustrate our approach with the Coulomb potential, the parallel with dipolar interactions being direct.

For monopoles, the value of the charges on the lattice can be either -1, 0 or $+1$ (we will not consider double defects 4 *in* or 4 *out*), whereas it is simply ± 1 for spins. The Metropolis move we consider will include two sites on the diamond lattice (transfer of a monopole from one site to another, or creation/anihilation of a pair of monopoles) and only one on the pyrochlore lattice (single spin flip).

If we look at equation (II.35), we see that the Fourier term is much faster to compute as it only has two sums (over i in $\rho(\mathbf{k})$ and over $\mathbf{k}$) whereas the Real term has three sums. Since our computation time will be dominated by the Real series, it will turn out to be more efficient to transform the Fourier series in a triple sums and compute everything in the same way, as detailed below.

So far our discussion on the Ewald summation has been very general and we did not use one of the fundamental and trivial properties of spin ice materials, that is they are well-ordered crystals with well-defined respective distances $\mathbf{r}_{ij}$, apart from lattice defects that we neglect here. Hence the term

$$u_{\mathbb{R}\ i,j} \equiv \sum_{\mathbf{n}}{}' \frac{\operatorname{erfc}\left(\sqrt{\alpha}\,|\mathbf{r}_{ij} - \mathbf{n}L|\right)}{|\mathbf{r}_{ij} - \mathbf{n}L|} \tag{II.43}$$

can be computed and stored beforehand and will always be the same in the algorithm. Then computing $\mathcal{U}_{\mathbb{R}}$ requires a N^2 sum

$$\mathcal{U}_{\mathbb{R}} = \frac{\mu_0}{4\pi}\,\frac{1}{2}\sum_{i,j}^{N} q_i q_j\, u_{\mathbb{R}\ i,j} \equiv \frac{\mu_0}{4\pi}\,\frac{1}{2}\sum_{i}^{N} q_i\, u_{\mathbb{R}\ i} \tag{II.44}$$

Once this total energy is computed, as a Metropolis move is local and only concerns two sites, updating the move if accepted will only result in a sum of $2N$ terms for the Real series $\mathcal{U}_{\mathbb{R}}$. On the other hand for the Fourier series $\mathcal{U}_{\mathbb{F}}$, this update will be of order $\mathcal{O}(1)$ for $\rho(\mathbf{k})$ (see equation (II.28), but will then also require another sum over $\mathbf{k}$. We shall soon discuss the size of this last sum, but we see here that this method requires two different sums of non-negligible size. This is why we decided to re-write the Fourier series

$$\sum_{\mathbf{k}\neq\mathbf{0}} \frac{4\pi}{2V} \frac{|\rho(\mathbf{k})|^2}{k^2} e^{\left(-\frac{k^2}{4\alpha}\right)} = \sum_{i,j}^{N} \sum_{\mathbf{k}\neq\mathbf{0}} \frac{4\pi}{2V} \frac{q_i q_j}{k^2} e^{i\mathbf{k}\cdot\mathbf{r}_{ij}} e^{\left(-\frac{k^2}{4\alpha}\right)} \tag{II.45}$$

in a way similar to the Real series in equation (II.35)). We notice here that the vector $\mathbf{k}$ in the Fourier series plays the same role as $\mathbf{n}$ in the Real series. By running the sum over $\mathbf{n}$ and $\mathbf{k}$, we are then left with a double sum over i and j of order $\mathcal{O}(N^2)$ only and we can follow the same reasoning as for the Real series alone with equation (II.43) and (II.44), *i.e.* we compute the effective interaction between two sites u_{ij}, and then sum over N to define $u_i = \sum_j q_j u_{ij}$ and finally compute the total energy $\mathcal{U}_{\text{coul}} = (1/2)\sum_i q_i u_i$. The self-interaction term is included in u_{ij} when $i = j$. This way of computation will allow us to have a Metropolis update of order $\mathcal{O}(N)$.

We can further improve the method because the computation of the N^2 terms u_{ij} are time consuming. Even if this is only done once at the beginning of the algorithm, this computation becomes rapidly sluggish for systems with more than 10^3 sites typically. Thanks to the translational invariance of the diamond or pyrochlore lattice, we can rather compute the energy term $u(\mathbf{r}_{ij})$ for pairs of monopoles/dipoles separated by vector $\mathbf{r}_{ij}$ as explained in figure II.7. Hence the summations over $\mathbf{n}$ and $\mathbf{k}$ only need to be done an order of N times instead of N^2. The correspondence $u_{ij} \equiv u(\mathbf{r}_{ij})$ and the computation of the total energy remains or order N^2, but the gain of time is nonetheless noteworthy: we can easily consider systems of size 10^4 now.

We have not discussed yet the limits $\mathbf{k}_{lim}$ and $\mathbf{n}_{lim}$ of the sums over $\mathbf{k}$ and $\mathbf{n}$ respectively. As they are absolutely convergent, we simply need to carry the summation until $\mathcal{U}_{\text{coul}}$ reaches its asymptotic value and neglect the rest of the series that can be made as small as possible. The best way to know if we reached the asymptotic limit is, as we have written before, to compute the energy for the same configuration but different values of α as the outcome should be independent of this parameter. However varying α will modify the convergence speed of the series: if α increases, the Fourier term will be slower (and the limit $\mathbf{k}_{lim}$ must be pushed further) while the Real one will be faster to compute. A good compromise is $\alpha = 1$.

Another choice would have been to take a large enough value of α, in order to be able to neglect the Real series $\mathcal{U}_{\mathbb{R}}$ completely. This would require a very large value of $\mathbf{k}_{lim}$, but as the Fourier series $\mathcal{U}_{\mathbb{F}}$ can be more easily computed than its Real counterparts (see discussion above). The initial computation of the total energy $\mathcal{U}_{\text{coul}}$ might be longer, but the Metropolis update would then only be of order $\mathcal{O}(k_{lim}^3)$, *i.e.* independent of the system size ! In our case the CPU time gain is negligible or even inexistent, but it could

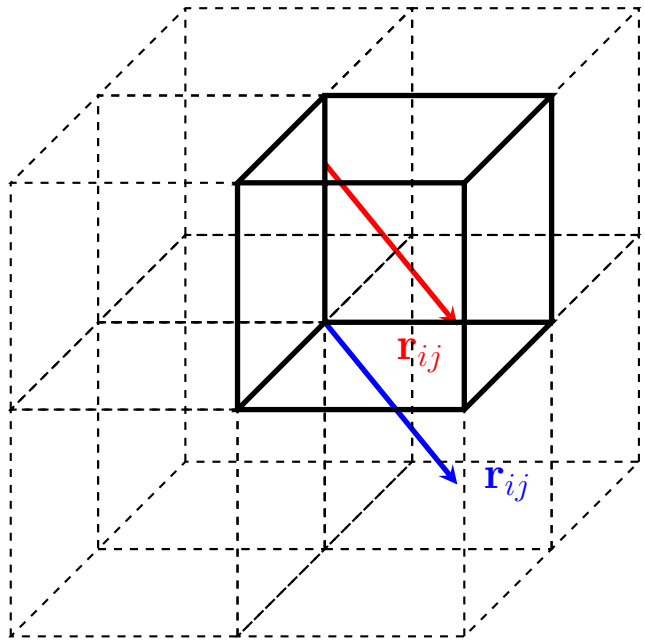

Figure II.7: **Periodic boundary conditions in the Ewald method:** The initial system cube of size $L \times L \times L$ (solid lines) surrounded by its 7 images around the origin $(0, 0, 0)$. All vectors $\mathbf{r}_{ij}$ starting at the origin and ending in one of these 8 cubes (like the blue one) can be translated into the initial system cube (and becomes the red vector) and are able to connect every possible pairs of sites in this initial cube. However one must consider two different origins for the diamond lattice (there are two types of vertices, corresponding to the two types of tetrahedra) and four different origins for the pyrochlore lattice. In fact, the calculation of $u(\mathbf{r}_{ij})$ can be obtained for the 7 images by symmetry arguments in equation (II.35) from the initial cube.

become essential for larger systems.

Our section on the Ewald summation and numerical techniques is finished and we now turn our intention towards the analytical methods used in this thesis, namely the transfer matrix and the Husimi tree.

II.5 Transfer matrix

II.5.a One dimensional Ising model

The Ising model has been proposed in 1925 by Ising, a student of Lenz, who solved it in the $1d$ case [Isi25][5]. Its exact solution can be attained using several approaches but happens to be particularly elegant with the transfer matrix method. We consider a ferromagnetic

[5] we should note here that this world-wide known model bears the name of the PhD student...

Ising chain with periodic boundary conditions in presence of an external magnetic field $\mathbf{H}$ and exchange coupling J (see figure II.8). The discussion below can be found in Baxter's book [Bax07]. The periodic boundary conditions guarantees translational invariance and

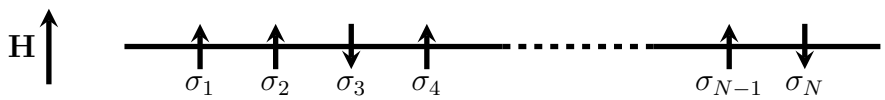

Figure II.8: **Ising chain** with N sites and $\sigma_{N+1} = \sigma_1$

enables one to define a unique magnetisation $M = \langle \sigma_i \rangle$. The partition function can be formally written

$$\mathcal{Z}_N \;=\; \sum_{\{\sigma\}} \exp\left[\sum_{i=1}^{N} (K\,\sigma_i\sigma_{i+1} \;+\; h\,\sigma_i)\right] \quad \text{where} \quad K = \beta J, \;\; h = \beta|\mathbf{H}| \tag{II.46}$$

where the first sum runs over all configurations $\{\sigma\}$. Thanks to the small connectivity of a $1d$ chain, the above exponential can be factored into terms that are functions of two neighbouring spins only

$$\mathcal{Z}_N \;=\; \sum_{\{\sigma\}} \prod_{i=1}^{N} V(\sigma_i, \sigma_{i+1}) \tag{II.47}$$

where

$$V(\sigma, \sigma') \;\equiv\; \exp\left[K\,\sigma\sigma' \;+\; \frac{h}{2}\,(\sigma + \sigma')\right] \;=\; V(\sigma', \sigma) \tag{II.48}$$

Hence $\mathcal{Z}_N$ appears like the sum of all possible 2^N arrangements of the product of N terms $V(\sigma, \sigma')$. Now if we define the matrix

$$\bar{\mathbf{V}} \;=\; \begin{pmatrix} V(+,+) & V(+,-) \\ V(-,+) & V(-,-) \end{pmatrix} \;=\; \begin{pmatrix} e^{K+h} & e^{-K} \\ e^{-K} & e^{K-h} \end{pmatrix} \tag{II.49}$$

the summations over σ_2, σ_3... can be seen as matrix multiplications; the final summation over σ_1 being taken as the trace of the product

$$\mathcal{Z}_N \;=\; \mathrm{Tr}\,\bar{\mathbf{V}}^N = \lambda_+^N + \lambda_-^N \tag{II.50}$$

where

$$\lambda_\pm \;=\; e^K\,\cosh(h) \;\pm\; \sqrt{e^{2K}\sinh^2(h) + e^{-2K}} \tag{II.51}$$

are the eigenvalues of $\bar{\mathbf{V}}$: $\lambda_+ > \lambda_-$. Equation (II.50) can be easily obtained recursively if we understand that the components $\nu_{\sigma,\sigma'}$ defined as

$$\bar{\mathbf{V}}^N = \begin{pmatrix} \nu_{+,+} & \nu_{+,-} \\ \nu_{-,+} & \nu_{-,-} \end{pmatrix} \tag{II.52}$$

represents the Boltzmann weight of all configurations beginning with a spin σ and ending with σ': taking the trace of $\bar{\mathbf{V}}^N$ yields the projection onto the manifold of configurations respecting the periodic boundary conditions, whereas $\nu_{\sigma,-\sigma}$ does not respect the periodic boundary conditions for N spins, but are necessary for the recursive iteration in order to take into account the degrees of freedom of an additional spin $N+1$.

Together with equations (II.50) and (II.51), one can obtain the Gibbs free energy per particle $g(H,T)$ and the magnetisation $m(H,T)$ in the thermodynamic limit $N \to \infty$

$$g(H,T) = -k_B T \ln\left(e^K \cosh(h) + \sqrt{e^{2K}\sinh^2(h) + e^{-2K}}\right) \tag{II.53}$$

$$m(H,T) = -\left(\frac{\partial g}{\partial H}\right) = \frac{e^K \sinh(h)}{\sqrt{e^{2K}\sinh^2(h) + e^{-2K}}}. \tag{II.54}$$

The analyticity of the free energy proves the essential result of the Ising chain, *i.e.* the absence of a phase transition for finite temperature, as opposed to higher dimensions [Ons44, Pli06]. However one can exactly calculate the correlation length $\xi = [\ln(\lambda_+/\lambda_-)]^{-1}$ which tends to infinity as $T \to 0$ for $H = 0$. This divergence indicates the presence of a critical point at $T = 0$.

We shall not study this model any further, as we are not directly interested in the Ising chain but in the method employed. We will see in the next chapter how one can generalise this technique in higher dimension, but the principle will remain the same: one connects the degrees of freedom between spins thanks to a *transfer matrix* and the partition function can be solely expressed in terms of its eigenvalues, the goal being to know its maximal eigenvalue as it is the dominant one in the thermodynamic limit.

II.5.b 6-vertex model

The 6-vertex model, also sometimes referred as ice-type models, is of great interest in this thesis as it can be seen as a $2d$ version of spin ice and is exactly solved by the transfer matrix method [Lie67d, Lie67b, Lie67c, Lie67a, Sut67]. We shall however not give its solution here as this would require a whole chapter by itself and is well detailed in [Bax07], but we will outline its similarities (and differences) with our $3d$ model and introduce how to deal with the transfer matrix in a statistical problem of dimensions higher than one.

Presentation of the 6-vertex model

The goal of this model is to describe materials such as ice or potassium dihydrogen phosphate $\left[K^+ (H_2PO_4)^-\right]$ (usually referred as KDP [Sla41]) where the hydrogens arrangement respects Bernal & Fowler ice-rules [Ber33] in a tetrahedral structure with two hydrogens close to the oxygen or PO_4^{3-} forming the molecule H_2O or anion, and the others two further apart (see illustration in figure I.9). Such compounds are of course three-dimensional, but have been extensively studied in their present $2d$ version that allows an exact treatment. In this regard the work presented in the next chapter (III.4.c) is an original attempt to extend this study for higher dimensions.

As discussed in the introduction for spin ice, there are 6 possible configurations respecting the ice-rules, which can be mapped onto a configuration of strings following the schema of figure II.9. We will assume this model in zero field and should thus be equiva-

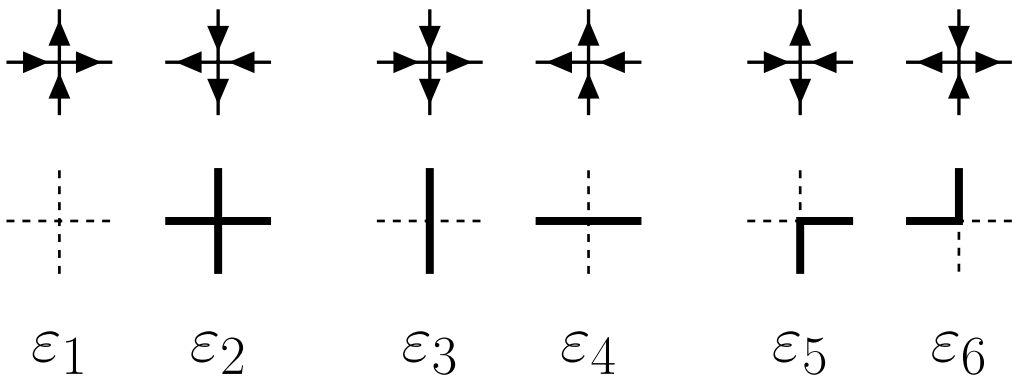

Figure II.9: **6-vertex model**: As for spin ice, each arrow can be seen as a dipole (either electric or magnetic). All 6 vertices respect the ice-rules and can be mapped onto a configuration of strings (second line). Each vertex has an energy ε_i that goes by pair (see equation (II.55).

lent under reversal of the arrows. This imposes certain conditions on the energies of the vertices.

$$\varepsilon_1 = \varepsilon_2, \quad \varepsilon_3 = \varepsilon_4, \quad \varepsilon_5 = \varepsilon_6 \tag{II.55}$$

Depending on the ratio of these energies, we can have very different behaviours:

- $\varepsilon_{i=1..6} = 0$: we recover Pauling's degeneracy of the *ice model*, solved by Lieb [Lie67d, Lie67c];
- $\varepsilon_{i=5,6} = 0$, $\varepsilon_{i=1..4} > 0$: this is the so-called F model proposed to describe antiferroelectrics because its ground state has a staggered polarisation;
- $\varepsilon_{i=1,2} = 0$, $\varepsilon_{i=3..6} > 0$: a given orientation of the polarisation is favoured (see left panel of figure II.10), characteristic of an ordered ferroelectric such as potassium dihydrogen phosphate and is known as the KDP model [Sla41, Lie67a].

This model shares many common points with spin ice: in absence of perturbations, they are both ice-models in 2 or $3d$, and the bond distortion defined in figure II.3 is equivalent to the KDP model. There is however an interesting difference as the third dimension restores a perfect symmetry between the three different pairs of vertices; favouring any one of these pairs will always result in symmetry breaking through a ferromagnetically ordered state with magnetisation along one of the three Cartesian axes, as opposed to the F model which is staggered.

Transfer matrix

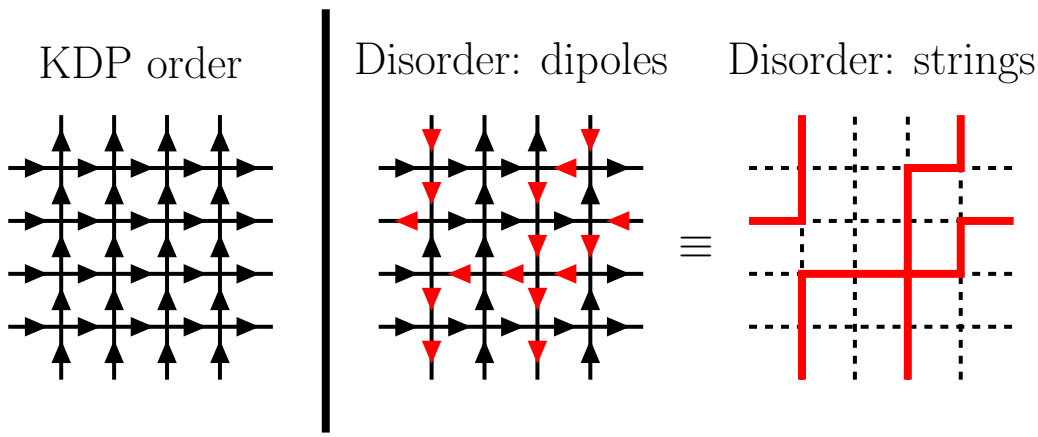

Figure II.10: **Configurations of the 6-vertex model:** *Left:* One of the two ground states of the KDP model with a net polarisation pointing north-east. *Right:* an example of disordered state represented with both dipoles and strings. We impose periodic boundary conditions.

As illustrated on figure II.10 on a lattice with R rows and C columns, one can visualise the problem as an arrangement of strings spanning the entire system. As for the Ising chain presented previously, the goal of the transfer matrix is to write the partition function as a product of matrices $\bar{V}$, but with the additional complexity that $\bar{V}$ now connects the degrees of freedom of two successive *rows* and not simply sites and is thus of size $2^R \times 2^R$. Let us define σ_r the configuration of row r. The partition function can then be formally written

$$\mathcal{Z} \;=\; \sum_{\{\sigma_r\}} \bar{V}(\sigma_1,\sigma_2)\ldots\bar{V}(\sigma_{R-1},\sigma_R)\,\bar{V}(\sigma_R,\sigma_1) \;=\; \mathrm{Tr}V^R \tag{II.56}$$

where

$$\bar{V}(\sigma_i,\sigma_j) \;=\; \exp\left[-\beta\left(c_1\varepsilon_1+\cdots+c_6\varepsilon_6\right)\right] \tag{II.57}$$

and c_ν is the number of vertices of type ν between rows i and j. As for the Ising chain, in the limit of large R, the partition function will be dominated by the maximal eigenvalue

λ_{max} of degeneracy g

$$\mathbf{Z} \sim g\lambda_{max}^{R} \tag{II.58}$$

The exact calculation of the eigenspectrum of $\bar{V}$ is feasible here but particularly complex: we refer the interested reader to Baxter's book for further details [Bax07]. The goal of this section was simply to give a hint of the transfer matrix technique as we shall give all the details of the method in a consistent way in the next chapter III.4.c for the specific case of spin ice.

Unfortunately, the mathematical complexity of this technique might hinder its usefulness for more general problems and approximations may be required, such as the Husimi tree presented below.

II.6 Husimi tree

Exact solutions are particularly elegant and satisfying, but in our 3−dimensional world, it remains a mathematical challenge, the above mentioned Ising model in $3d$ being one of the "Holy Grails" of statistical physics. This is why more and more complex approximated methods have been developed during the past century and an exhaustive treatment of these would require an *Encyclopædia*. The standard Mean Field (MF) theory presented in the introduction I.1.b is the most famous one and widely used. Here, we will introduce more elaborated techniques whose improvements compared to MF methods are both transparent and remarkable: the Bethe approximation [Bet35, Pli06], Bethe lattice [Bet35, Bax07] and its direct parent, the Husimi tree [Cha94, Mon98].

II.6.a Bethe approximation

The fundamental characteristic of the MF approach is to neglect spatial fluctuations, the action of the environment on a single spin being restricted to a uniform molecular field (equation (I.26)). The Bethe approximation is similar, except for the first nearest neighbour exchange that will be considered exactly with the atomic field $\mathbf{h}_a$ only being applied to the outer spins (see figure II.11). Hence, as opposed to general MF, the microscopic nature of the lattice is taken into account with the coordination number q. The Hamiltonian of this cluster is

$$\mathcal{H} \;=\; -J\,\mathbf{S}_0 \cdot \left(\sum_{i=1}^{q} \mathbf{S}_i\right) \;-\; \mathbf{h}_a \cdot \left(\sum_{i=1}^{q} \mathbf{S}_i\right) \tag{II.59}$$

where $\mathbf{S}$ are Ising spins. The partition function $\mathcal{Z}_c$, as well as the expectation value of the spins $\langle \mathbf{S}_0 \rangle$ and $\langle \mathbf{S}_{i=1..q} \rangle$ can be directly obtained and the macroscopic size of the system can be implemented *a posteriori* by imposing translational invariance: $\langle \mathbf{S}_0 \rangle = \langle \mathbf{S}_{i=1..q} \rangle$

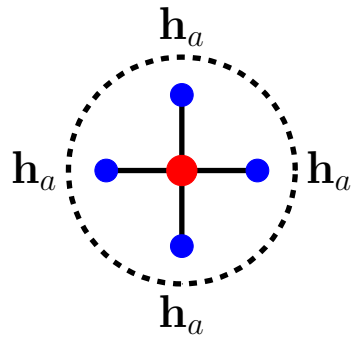

Figure II.11: **Bethe approximation:** We consider a finite cluster with a central spin (indexed by 0) and its $q = 4$ nearest neighbours, connected to their environment by an atomic field $\mathbf{h}_a$.

giving the following self-consistent equation, only function of $h_a = |\mathbf{h}_a|$

$$\begin{aligned}
\mathbf{Z}_c &= 2\cosh^q\left(\beta(J+h_a)\right) + 2\cosh^q\left(\beta(J-h_a)\right) && \text{(II.60)}\\
\langle \mathbf{S}_0 \rangle &= \frac{2}{\mathcal{Z}_c}\left[\cosh^q\left(\beta(J+h_a)\right) - \cosh^q\left(\beta(J-h_a)\right)\right]\\
&= \frac{2}{\mathcal{Z}_c}\Big[\sinh\left(\beta(J+h_a)\right)\cosh^{q-1}\left(\beta(J+h_a)\right)\\
&\quad - \sinh\left(\beta(J-h_a)\right)\cosh^{q-1}\left(\beta(J-h_a)\right)\Big] = \langle \mathbf{S}_i \rangle\\
\Leftrightarrow e^{2\beta h_a} &= \frac{\cosh^{q-1}\left(\beta(J+h_a)\right)}{\cosh^{q-1}\left(\beta(J-h_a)\right)} && \text{(II.61)}
\end{aligned}$$

As for equation (I.27), this can be solved numerically or graphically, and a Taylor expansion for small h_a gives the transition temperature:

$$\beta_c J = \frac{1}{2}\ln\left(\frac{q}{q-2}\right) \qquad \text{(II.62)}$$

For a square lattice, this gives $k_B T_c/J = 2.885$, relatively close to Onsager's exact result $k_B T_c/J = 2.269$ [Ons44], compared to the MF result of the introduction I.1.b $k_B T_c/J = 4$. Another noticeable improvement is the absence of a transition at finite temperature for a $1d$ problem (*i.e.* $q = 2$), in agreement with the exact result of the precedent section.

However, as already discussed in sections II.3 and II.5, we want to take into account non-local excitations, which is impossible with a small cluster with nearest neighbours only; this is why we will extend this method to the infinite Bethe lattice.

II.6.b Bethe lattice

This method has been developed in the early years of statistical mechanics by Bethe [Bet35] in a recursive manner, while a variational approach has been introduced a few years later

by Fowler & Guggenheim [Fow40], and led to a multitude of approximation techniques such as Husimi trees (see below) or the Kikuchi method [Kik51]. A discussion concerning these two approaches can be found in [Pre03]. The Bethe lattice and its generalisations have been used in many different fields such as *e.g.* polymer physics [Mor76, Guj84], water [AB08], spin liquids with the remarkable paper of Chandra & Douçot [Cha94], spin glasses [Mel96, Lau08] *etc.* Its interest is double; it is often a reliable approximation and a substantial improvement compared to mean field calculations [Bax07, Guj95], especially applied to frustrated systems [Mon98], and usually allows the efficiency and satisfaction of exact results.

In fact, a variational version of the Bethe lattice has already been used in the context of spin ice by Yoshida & *al.* in order to compute the zero-point entropy that a simple MF treatment fails to reproduce, and to obtain an analytical expression of the scattering function with reasonable success [Yos02]. In this thesis, we personally chose to use a recursive approach, that we find clearer and more elegant. In the next chapter III, we will reproduce the results of [Yos02], but we shall also go further and take advantage of this technique to investigate the influence of external perturbations and of topological constraints. For pedagogical reasons, we will first present the general form of the Bethe lattice before implementing the microscopic pyrochlore structure.

In figure II.11, the degrees of freedom of the outer spins are only coupled by the presence of the central spin. Hence, once the value of σ_0 is fixed, the contribution of the q other spins can be factorised in the partition function (II.60). This is exactly the idea of the Bethe lattice that is constructed by allowing one and only one path connecting two different spins, as depicted on figure II.12

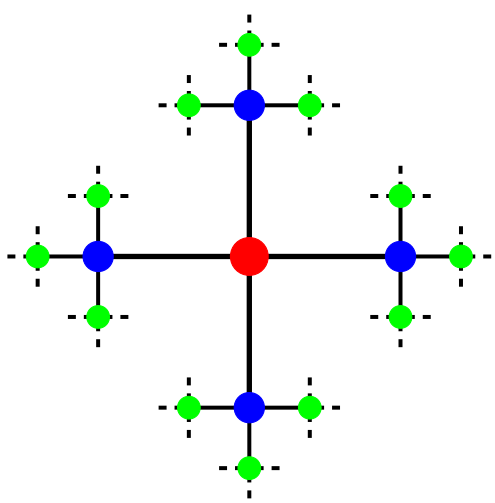

Figure II.12: **Bethe lattice:** Each spin on shell n is connected to $q = 4$ others, one towards the interior of the lattice $n - 1$, and three outer spins $n + 1$, with only one path between each pair of spins.

The Bethe lattice is entirely defined by its coordination number q. The central spin (red, shell $n = 0$) is surrounded by a first shell of q nearest neighbours (blue, $n = 1$),

and then a second shell of next nearest neighbours (green, $n = 2$), and so on... Once a *branch* is created, it never crosses another one; this absence of intersection allows the factorisation of the degrees of freedom shell by shell and to compute the partition function recursively.

There are $N_n = q(q-1)^{n-1}$ spins in shell $n > 0$ and for a system of L shells other than a simple $1d$ chain (*i.e.* $q > 2$), there is a total of $N = \dfrac{q\left[(q-1)^L - 1\right]}{q-2}$ spins. The ratio of spins on the surface over their total number is $\dfrac{N_L}{N} \xrightarrow[L\to\infty]{} \dfrac{q-2}{q-1} \sim 1$: since this coefficient should scale like $N^{-1/d}$ on a regular lattice of dimension d, it means that the Bethe lattice is equivalent to a system of *infinite dimension* [Bax07]. This remark is far from being innocent since it means that roughly half of the spins (the ones on shell L) are only connected to one neighbour instead of q, making a huge difference in the resulting physics (see *e.g.* [Che74]). In fact, such a graph that takes into account *all* sites, including the outer shell, is known as the *Cayley tree*. But if we are more interested in the approximation of a real lattice rather than an intriguing but more abstract surface effect, we will only consider the spins in the core of the graph, far from the boundary that should be ideally rejected to infinity; these spins should all be equivalent and form the so-called Bethe lattice [Che74, Bax07].

We will not pursue the calculations of thermodynamic quantities here, because the final result happens to give the same value of the transition temperature as the Bethe approximation; we shall rather directly illustrate this method for the $3d$ pyrochlore lattice.

II.6.c Husimi tree

The major problem of a Bethe lattice is that it is not able to reproduce the geometrical frustration due to competitive interactions since there is no closed loops. This is why we need to define a cluster version where we replace every vertices by a frustrated geometrical unit, giving rise to a *Husimi tree* (see figure II.13).

> **Terminology:** The term *Husimi tree* has been introduced by Harary and Uhlenbeck [Har53] in honour of previous work by Husimi [Hus50] and defined as "a connected graph in which no line lies on more than one cycle" (see figure II.13). If all cycles are triangles, then it is called a *cactus*. Hence, strictly speaking, if the unit of the graph is a tetrahedron, we should not call it a Husimi tree but in fact a *block graph*. However the rigourous definition has been forgotten for a long time and Husimi tree or cactus has become a general term including all variants where the typical units can be a triangle, square, tetrahedron, *etc.* In this manuscript we shall invariably use the term "Husimi tree".

We can compute a few characteristic quantities for such a Husimi tree of L shells:

$$N = 4\sum_{n=0}^{L} 3^n = 2\left(3^{L+1} - 1\right) \qquad \text{total spins}$$

$$N_t = 1 + 4\sum_{n=1}^{L} 3^{n-1} = 2\,.\,3^L - 1 \quad \text{tetrahedra} \tag{II.63}$$

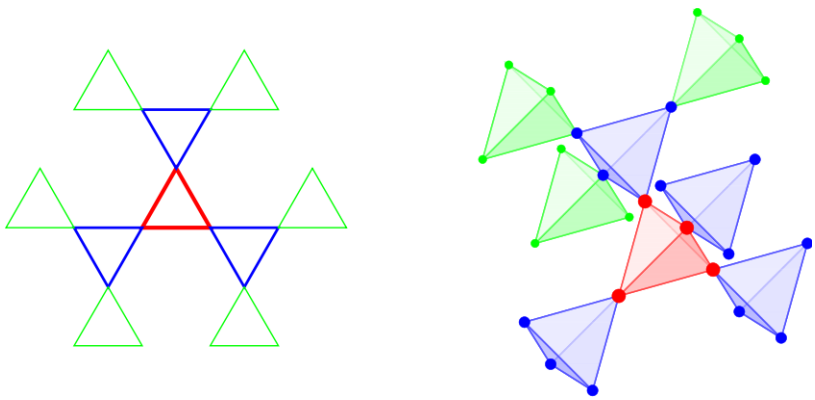

Figure II.13: **Husimi tree:** *Left:* A pure Husimi cactus as defined by [Har53] whose blocks are triangles. *Right:* the modified Husimi tree that will be used for spin ice with tetrahedral units. Each colour represents a given shell. We must emphasise here that it is different from the pyrochlore lattice, because the next shells $n = 3, 4, ...$ will *never* close to make loops with the other ones, because this tree is growing in an infinite dimension.

Even if a Husimi tree is locally identical to a pyrochlore lattice (up to 3 shells), its nature is in fact fundamentally different since it is of infinite dimension, as the centres of the tetrahedra form a Bethe lattice and there is on average three spins per tetrahedron ($N/N_t \to 3$) instead of only two for the pyrochlore lattice. We can now compute thermodynamic quantities recursively, but for convenience, we shall reverse the indices of the shells: they are labeled from 0 on the boundary inwards, such that the last shell before the central tetrahedron (blue on Fig. II.13) has index L. We will use the Hamiltonian of the nearest neighbour spin ice model in a [001] magnetic field h and with a bond distortion δ (see equation (II.3) and figure II.1).

II.6.d Recursion on the Husimi tree for spin ice

The first step is to couple the degrees of freedom between two consecutive shells n (*e.g.* green on figure II.13) and $n+1$ (*e.g.* blue). The applied magnetic field breaks the global $\mathbb{Z}_2$ symmetry and makes this coupling different whether the spin in the inner shell $n+1$ is *up* or *down*:

$$\begin{aligned} Z_\uparrow &= 3\,e^{\beta h} + 2\,e^{2\beta(J-\delta)-\beta h} + e^{2\beta(J+\delta)+3\beta h} + e^{-3\beta h} + e^{-\beta(6J-2\delta)-\beta h} \\ Z_\downarrow &= 3\,e^{-\beta h} + 2\,e^{2\beta(J-\delta)+\beta h} + e^{2\beta(J+\delta)-3\beta h} + e^{3\beta h} + e^{-\beta(6J-2\delta)+\beta h} \end{aligned} \tag{II.64}$$

The different terms of the R.H.S represent the $2^3 = 8$ possible configurations of the 3 spins on the outer shell n. Let us define A_n and B_n the partition function of a branch starting on shell n with an *up* and *down* spin respectively, and germinating all the way up to the surface (the shell 0). The power of the Husimi tree is to allow a recursive exact

expression of these functions thanks to the above equations (II.64)

$$\begin{aligned} A_{n+1} &= 3A_n^2 B_n\, e^{\beta h} \;+\; A_n^3\, e^{2\beta(J+\delta)+3\beta h} \\ &\quad + B_n^3\, e^{-3\beta h} \;+\; 2A_n B_n^2\, e^{2\beta(J-\delta)-\beta h} \\ &\quad + A_n B_n^2\, e^{-\beta(6J-2\delta)-\beta h} \\ B_{n+1} &= 3A_n B_n^2\, e^{-\beta h} \;+\; B_n^3\, e^{2\beta(J+\delta)-3\beta h} \\ &\quad + A_n^3\, e^{3\beta h} \;+\; 2A_n^2 B_n\, e^{2\beta(J-\delta)+\beta h} \\ &\quad + A_n^2 B_n\, e^{-\beta(6J-2\delta)+\beta h} \end{aligned} \tag{II.65}$$

where $h \geqslant 0$. For example, the term $3A_n^2 B_n\, e^{\beta h}$ on the R.H.S. means that the 3 configuration with energy h have two spins *up* (A_n^2) and one *down* (B_n) in the shell n. To calculate the energy, one considers all six bonds in the tetrahedron, but the Zeeman contribution of the three outer spins only, as the Zeeman energy of the inner spin will be taken into account in the next iteration between $n+1$ (*e.g.* blue on Fig. II.13) and $n+2$ (*e.g.* red).

The complete partition function for a Husimi tree of L shells is obtained by connecting four branches on the central tetrahedron:

$$\begin{aligned} Z_L &= 2A_L^2 B_L^2\, e^{-\beta(6J-2\delta)} \;+\; 4A_L^2 B_L^2\, e^{2\beta(J-\delta)} \\ &+ 4A_L B_L^3\, e^{-2\beta h} \;+\; B_L^4\, e^{2\beta(J+\delta)-4\beta h} \\ &+ 4A_L^3 B_L\, e^{2\beta h} \;+\; A_L^4\, e^{2\beta(J+\delta)+4\beta h} \end{aligned} \tag{II.66}$$

Following the same argument as for the Bethe lattice, we can get rid of the surface effect by considering a site deep within the graph [Bax07], *e.g.* on the central tetrahedron. Hence, the component of the magnetisation along the field M_L is:

$$M_L = \frac{1}{Z_L}\left[2A_L B_L\left(A_L^2\, e^{2\beta h} \;-\; B_L^2\, e^{-2\beta h}\right) \;+\; e^{2\beta(J+\delta)}\left(A_L^4\, e^{4\beta h} \;-\; B_L^4\, e^{-4\beta h}\right)\right], \tag{II.67}$$

For convenience, we dropped the prefactor of $10\mu_B/\sqrt{3}$ in front of the magnetisation: $M_L \in [-1:1]$. However, as it is, equation (II.67) is useless because it is the ratio of *a priori* two diverging sequences. We will come back later to the relevant values of A_0 and B_0 on the boundaries, but we already know they are Boltzmann factors, and must then be strictly positive for finite temperature. From equation (II.65), we know that $A_{n+1} > A_n^3\, e^{2\beta(J+\delta)+3\beta h}$ and $B_{n+1} > A_n^3\, e^{3\beta h}$, making them divergent. But since A_n is non-zero, we can define a new sequence

$$\boxed{\begin{aligned} Y_n &= \frac{B_n}{A_n}\, e^{-2\beta h}, \quad \forall n \in \mathbb{N} \\ Y_{n+1}\, e^{2\beta h} &= \mathcal{F}(Y_n) \\ &= \frac{3Y_n^2 \;+\; Y_n^3\, e^{2\beta(J+\delta)} \;+\; 1 \;+\; 2Y_n\, e^{2\beta(J-\delta)} \;+\; Y_n\, e^{-\beta(6J-2\delta)}}{3Y_n \;+\; e^{2\beta(J+\delta)} \;+\; Y_n^3 \;+\; 2Y_n^2\, e^{2\beta(J-\delta)} \;+\; Y_n^2\, e^{-\beta(6J-2\delta)}} \end{aligned}} \tag{II.68}$$

By definition, the elements of $\{Y_n\}_{n\in\mathbb{N}}$, are all positive or null. It implies that the above defined function $\mathcal{F} : [0; +\infty[\rightarrow \mathbb{R}$ is continuous at finite temperature, and since $\mathcal{F}(0) = e^{-2\beta(J+\delta)/3} > 0$ and $\lim_{+\infty} \mathcal{F} = \exp(2\beta(J+\delta)/3)$, the sequence $\{Y_n\}_{n\in\mathbb{N}}$ is necessarily convergent and its limit will be noted Y. The magnetisation can also be rewritten in term of Y_L

$$\boxed{M_L = \frac{2Y_L\,(1 - Y_L^2) + e^{2\beta(J+\delta)}\,(1 - Y_L^4)}{2Y_L^2\,e^{-\beta(6J-2\delta)} + 4Y_L^2\,e^{2\beta(J-\delta)} + 4Y_L^3 + Y_L^4\,e^{2\beta(J+\delta)} + 4Y_L + e^{2\beta(J+\delta)}}} \quad \text{(II.69)}$$

$\{M_n\}_{n\in\mathbb{N}}$ is also converging to a limit M. Both equations (II.68) and (II.69) are the basis of our work n the Husimi tree. The general solution can only be obtained numerically, but for a few specific cases, especially on the 2 *in* - 2 *out* manifold, analytic expressions of thermodynamic quantities such as the magnetisation, specific heat, entropy, *etc* can be extracted, as presented in the next chapter.

III Topological phase transitions

III.1 Constrained Manifold

III.1.a Nature of the transitions

We will study here the model presented in section II.1, *i.e.* the nearest neighbour spin ice system in presence of an external magnetic field along the [001] direction and with bond distortions. Let us briefly recall the Hamiltonian

$$\mathcal{H} = -\sum_{\langle i,j \rangle} J_{i,j}\, \sigma_i\, \sigma_j - h \sum_i \sigma'_i \tag{III.1}$$

$$\text{where} \quad J_{i,j} = \begin{cases} J - \delta & \text{for a bond in the (001) planes} \\ J & \text{otherwise} \end{cases}$$

The scalar spin σ_i and σ'_i have already been defined in the previous chapters

- $\sigma_i = +(-)1$ if the spin is *out* (*in*) for an *up* tetrahedron;
- $\sigma'_i = +(-)1$ if the sign of the $z-$component of the spin is positive (negative).

Equation (III.2) is illustrated in figure II.1. In order to compare our theory to experiments, we will need to consider local excitations, such as *e.g.* 3 *in* - 1 *out* defects, but we shall at first mainly focus our intention on the 2 *in* - 2 *out* manifold where the ice-rules constraints are source of exotic phase transitions. As presented in figures II.2 and II.3, the external perturbations are responsible for an important degeneracy lift, favouring only one or two configurations.

Let us now briefly explain the reasons of this work and give a hint of the upcoming results. Our first motivation was to understand numerical predictions of 1st order transition in presence of a [001] field h [Har98] where we realised the intriguing influence of the ice-rules constraints that led us to consider the effect of a perturbation δ respecting the *up/down* symmetry. In absence of field $h = 0$, we thus expect a symmetry breaking phase transition into one of the two ordered phase; this is indeed what we obtain, through an apparent 1st order transition. However we shall prove that an infinitesimal field h will surprisingly immediately makes this transition continuous, whereas the standard picture from Landau theory in the phase diagram (T, h) would have been a line of 1st order transition becoming 2nd order after a tri-critical point (see subsection I.1.b and [Car02]).

But the most remarkable result happens for $\delta = 0$, where a symmetry breaking field h provokes a continuous phase transition: these unusual properties are direct consequences of the topological constraints of the 2 *in* - 2 *out* manifold (see subsection III.1.b).

Let us now consider the above defined model on the 2 *in* - 2 *out* manifold, with $N = (2L_z).(2L_\perp^2)$ spins, where L_z (resp. $L_\perp$) is the number of *up* tetrahedra in the vertical (resp. horizontal) direction: there are thus $2L_z$ spins in the vertical direction, and $2L_\perp^2$ in a (001) plane (which is not a simple square lattice, see figure III.19). There are $N/2$ tetrahedra ($N/4$ of each kind), and $3N$ bonds between nearest neighbours. In absence of perturbations, the internal energy for each microstate in the reduced phase space has therefore the same value, $U = -NJ$. At finite temperature, there is a competition between the Zeeman energy or bond distortion and the entropic term $-T\,S$ in order to minimise the total Gibbs free energy. If we start our reasoning at $T = 0$ in presence of perturbations, then all spins are *up*[1], the only configuration favoured by both perturbations (see figure III.1). The total free energy is $G(T = 0) = -\left[(J + \delta) + h\right] N$. Let us now flip a single spin out of the ordered state. This breaks the ice rules creating a pair of local defects at a free energy cost of $\delta G = 4J + 2h + 4\delta$. Flipping another neighbouring spin results in separating the defects and costs no further energy to order J, but a perturbation energy $\delta G = 2h + 4\delta$ per spin. This succession of *down* spins form a *string* spanning the entire system thanks to periodic boundary conditions and can eventually reach the first tetrahedron, "closing" the string and annihilating the defects: we thus recover the 2 *in* - 2 *out* manifold and the internal energy of $4J$. In order to respect the ice-rules all along the construction of the string (except at its extremities), one has two possibilities to go out of each tetrahedron, representing an entropy gain of $\ln(2)$ per spin. The total free energy change for placing a string in the system is then

$$\begin{aligned} \Delta G &= (2L_z)\,(2h + 4\delta \,-\, T\ln 2) \\ &\propto L_z\,(T_\mathrm{K} - T) \end{aligned} \tag{III.2}$$

where

$$T_\mathrm{K} = \frac{2h + 4\delta}{\ln 2} \tag{III.3}$$

The Boltzmann constant is included in the temperature. From this naive but surprisingly accurate argument, one can deduce that:

- for $T < T_\mathrm{K}$, the free energy cost of a single string is divergent in the thermodynamic limit and is thus impossible. The system remains frozen in the ordered saturated state and both specific heat C_h and susceptibility χ are zero;
- for $T > T_\mathrm{K}$, such strings are entropically favoured and the system can finally relax.

There is thus a violently asymmetric transition mediated by the ice-rules constraints taking place at T_K, with fluctuations above the transition but not below. Through this

[1] we recall that spin *up* means a positive z-component

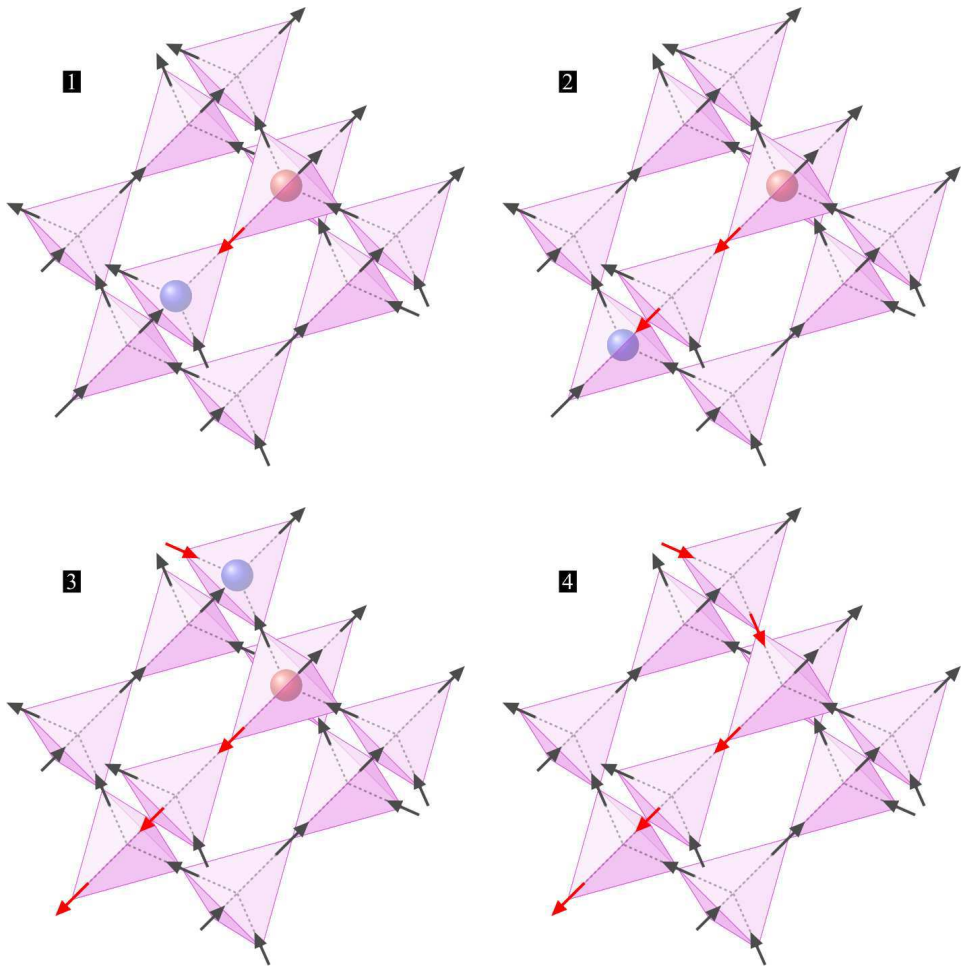

Figure III.1: **Construction of a string:** We start by creating a pair of defect by flipping a spin randomly (1); depending on the competition between energy cost (due to the perturbations) and entropic gain, the defects may be able to propagate (2); cross the entire system thanks to periodic boundary conditions (3); and get annihilated, restoring the 2 *in* - 2 *out* manifold but with an additional (red) string (4).

asymmetry the transition has often been described as having both 1st and 2nd order characteristics, "averaging" the two sides giving rise to $3/2-$order transition [Nag73a]. However we will see in the following sections that the nature is really consistent with a 2nd order transition, but could become 1st if the strings attract each other.
One should note that the transition temperature T_{K} has already been obtained in the calculations of the probabilities of the Worm algorithm: $T_{\text{K}} = T_{\uparrow}$ defined in equation (II.16). It is indeed not so surprising to think that this transition can have direct consequences on the detailed balance condition, as we shall explain them in the next section III.2.
The concept of creation, diffusion and annihilation of a pair of defects, similar to the physics of magnetic monopoles but in *absence* of long range interactions, should only be considered here as a useful but abstract picture to illustrate the concept of string construction: the constraints forbid such defects and the string is in fact a non-decomposable

entity connecting two configurations. Furthermore we have so far only discussed the apparition of strings spanning the whole system from top to bottom and the impossibility of local defects because of the ice-rules, but what about small closed loops [Yav08] ? Such moves including at least six spins forming a hexagon can connect two configurations on the 2 *in* - 2 *out* manifold at zero energy cost, neither to order J nor to order δ or h (see figure III.3). However even if small closed loops are essential for the ergodicity of the system, the topology of the constrained regime makes them inaccessible out of the initial fully saturated state. We shall discuss this point in details in the next subsection.

The remarkable thing about this transition is that it occurs when the system is rigorously constrained to the manifold of spin ice states such that the internal energy for each microstate in the reduced phase space has the same value. This allows for a phenomenological mean field approach which we present below. Just as for a paramagnet the magnetic Helmholtz potential for the constrained system has an entropic component only: $\mathcal{F}^*(M) = -T\,\mathcal{S}(M)$, where $\mathcal{S}$ is the standard entropy of an Ising paramagnet defined in equation (I.7). $\mathcal{S}$ goes to zero, as M reaches its maximum value, $M = 1$ but it does so with infinite slope and hence an infinite value for h/T as h is the field conjugate to M. The minimisation of the Gibbs potential $\mathcal{G}^* \equiv \mathcal{F}^* - h\,M$ thus provides a magnetisation that is an analytical function of h/T unable to reach its maximum value for finite field or temperature (see equation (I.5) or the left panel of figure III.2): there is no phase transition.

However if one assumes that the hidden divergence free condition can drive the entropy to zero for finite $h/T = h_{\mathrm{K}}/T$, then $\mathcal{S}(M \to 1) \to 0$ with a *finite* slope as illustrated in the right panel of figure III.2). This is of crucial importance as for $h > h_{\mathrm{K}}$, the configuration with saturated magnetisation is the unique possible microstate with *zero* fluctuations as $\partial\mathcal{G}^*/\partial M$ is finite and negative at $M = 1$. This simple argument allows us to reproduce the characteristics of this transition obtained previously from microscopic considerations. It remains although a phenomenological approach as the hypothesis of zero entropy for finite h/T is an *ad hoc* assumption. In order to implement it naturally in the theory, one needs to consider explicitly the effect of the ***topological ice-rules constraints*** in this collective paramagnet which is not simply thermally disordered but with algebraic dipolar correlations (see section I.3.c), properties that incompatible with the standard Landau Ginzburg Wilson theory.

III.1.b Topological constraints

As the notion of topology will be extensively used in this thesis, we shall briefly justify it beforehand. Let us for the time being forget about the external perturbations, and simply consider the nearest neighbour spin ice model with periodic boundary conditions.

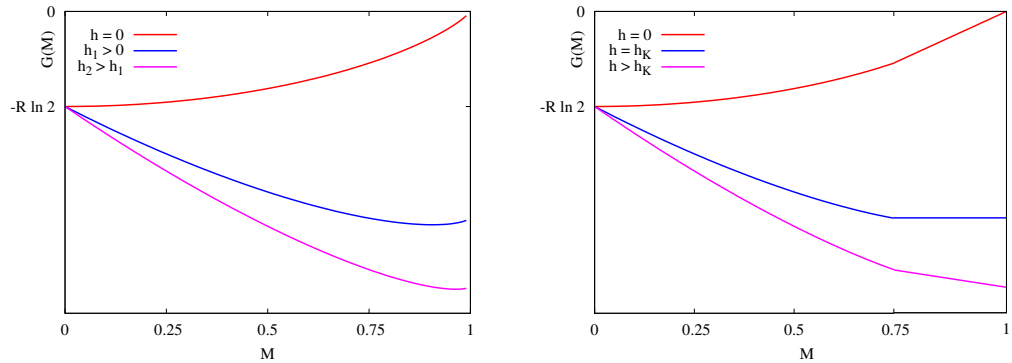

Figure III.2: **Gibbs potential** $\mathcal{G}^*$ as a function of M. For a paramagnetic phase (*left*), the magnetisation M goes continuously from 0 to 1 as h increases, reaching saturation only for infinite field, whereas for the constrained spin ice phase (*right*), saturation is obtained for $h \geqslant h_{\mathrm{K}}$ (blue and pink curve). On the right panel, the straight region of the Gibbs potential ($M > 0.75$) is voluntarily exaggerated to illustrate our discussion; it should be infinitesimal.

On the ground state manifold

The ground state manifold of spin ice is highly degenerate and long range ordered, because of the algebraic dipolar correlations (see subsection I.3.c) but does not break any symmetry in the system. In that sense, this phase that is not thermally disordered cannot be described by a Landau theory. This is very similar to the notion of *topological order*, introduced 20 years ago in order to take into account the original ordering observed in Fractional Quantum Hall liquids [Tsu82, Wen95]. We refer the interested reader in topological order to Wen's book [Wen04]. As a classical system, the 2 *in* - 2 *out* manifold of spin ice is *not* strictly speaking a topological order, but we shall nonetheless outline their remarkable analogies. In order to define the important notion of "sector", we will continue to use the above mentioned strings spanning the system in the [001] direction but we shall keep in mind that in absence of perturbations h and δ, the 2 *in* - 2 *out* manifold does not break any symmetry and there is no reason to particularise a specific orientation.

As mentioned previously, one can visit the whole 2 *in* - 2 *out* manifold simply by creating and erasing strings spanning the entire system along the vertical axis. The crucial point is that, as explained at the beginning of the methodology section on the Worm algorithm II.3, the magnetisation is preserved from one (001) plane to another, preventing the strings to end abruptly in the bulk of the system. As we have arbitrarily chosen to define a string as a continuous line of *down* spins surrounded by *up* spins, it means that $n = 0$ corresponds to the fully saturated states with magnetisation in the $z-$axis $M_{n=0} = +1$, whereas for an arbitrary value of n, we have

$$M_n = \frac{L_\perp^2 - n}{L_\perp^2} \tag{III.4}$$

since there are $2\,L_\perp^2$ spins per horizontal plane. Hence a given number of strings n rep-

resents a sub-ensemble of the 2 *in* - 2 *out* phase space and corresponds to a given value of the magnetisation: we shall call this reduced manifold a *sector*. The same reasoning can be made to define sectors with respect to the $x-$ and $y-$axis. Two different sectors are solely connected by macroscopic moves and one needs a non-local measure to determine the sector; *e.g.* counting the number of strings crossing an entire (001) plane, the outcome being independent of the chosen plane. This is in fact an immediate consequence of the periodic boundary conditions. Without them, a string could start on one side (*e.g.* $x = 0$) and end on the same side a few layers above, flipping only a finite and small number of spins and it would be impossible to define sectors. According to [Cas07], the existence of such sectors that are not indistinguishable by local measurements is one of the fundamental properties of *classical topological order*, a classical generalisation of its quantum analogue mentioned previously. However to identify topologically ordered phases for certain, one would need to compute the topological entropy defined in [Cas07] which may be an impossible task for a $3d$ system like spin ice [Cas09]. Interestingly, because of the extensive strings required to go from one sector to another, classical topological order should induce *topological ergodicity breaking* that may well be accompanied by glassy behaviour [Cas07]. We shall briefly discuss this point in the next chapter on the dynamics of spin ice, as this material becomes indeed frozen at low temperature where we expect the ice-rules constraints to be respected. One should note that ergodicity within a sector is ensured by local closed loops carrying zero magnetisation (see figure III.3); local perturbations can thus have an effect within a given sector, but cannot change the sector.

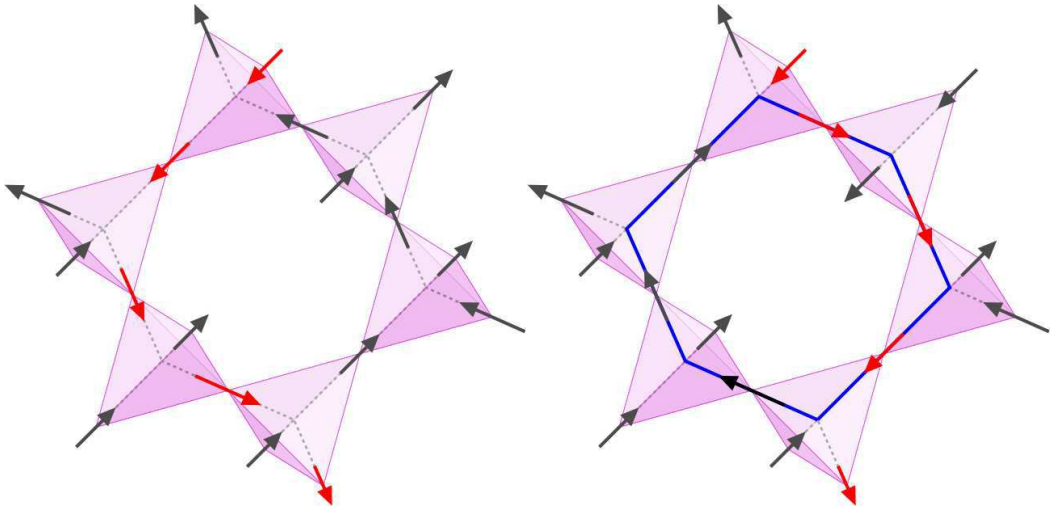

Figure III.3: **Small closed loop:** We see a piece of an extensive (red) string that can fluctuate around an *hexagon* of spins (in blue). This is the smallest possible move on the constrained manifold and costs rigourously no energy (except of $\mathcal{O}(\delta)$ if it leads to strings intersection). There is no magnetisation change involved and we thus remain in the same sector.

Topological defects

An additional feature of topological order is the emergence of fractionalised particle-like excitations. As presented in the introduction I.3.c, spin ice on the 2 *in* - 2 *out* manifold can be elegantly described by a divergence free gauge theory, where local excitations out of the ground state appear as sources or sinks of the flux of magnetic field $\bar{\mathbf{B}}$ and break the topological constraints (3 *in* - 1 *out* and 3 *out* - 1 *in* tetrahedra). In analogy with the emergence of magnetic monopoles because of dipolar interactions between spins, these defects feel an effective entropic Coulomb interaction due to the dipolar correlations prevailing in the vacuum and are thus deconfined (see introduction I.3.c). Following Gauss theorem, one immediately shows that a defect bears a topological charge

$$Q \equiv \oiint_V \bar{\mathbf{B}} \cdot \mathrm{d}\mathbf{S} \tag{III.5}$$

in analogy with the vortices in the Kosterlitz-Thouless transition. The periodic boundary conditions prevent the apparition or disappearance of the defects on the borders; they can only be created or annihilated in pairs of opposite charge, thereby respecting the neutrality of the system. The beauty of spin ice is that this gauge theory becomes "real" when one considers the complete Hamiltonian with dipolar interactions, and the topological defects become magnetic monopoles up to corrections of order $1/r^5$ [Isa05, Cas08].

Hence even if we cannot give a definite answer and must thus be cautious with the terminology, the ground state of spin ice seems to share many characteristic features of a classical version of a topological ordered phase[2]. However the notion of sectors, topological defects (as compared to the XY model) and topological constraints are particularly relevant.

Topologically driven phase transitions

In presence of macroscopic perturbations h or δ, we explicitly break the symmetry of the system in favour of one direction and lift the degeneracy of the ground state: the different sectors are not equivalent anymore and are defined with respect to this symmetry-breaking axis z. This is why the resulting phase transitions we have studied in this thesis can be described using the $z-$component of the magnetisation M as an order parameter. The notion of sectors will nonetheless prove to be especially relevant.

As the new ground state induced by the perturbations has a saturated magnetisation with no strings $n = 0$ (the same reasoning holds by symmetry for a fully packed ensemble of strings $n = 2\,L_\perp^2$), the corresponding sector is necessarily constituted by a unique configuration. Since local closed loops can only connect two microstates within the same sector, they are not allowed here and the system can only relax through string excitations. Of course, once a single string appears at the transition, closed loops will proliferate in order to respect the ergodicity for each sector.

[2]This subsection has benefited of enlightening discussions with Paul McClarty, Claudio Castelnovo and Pierre Pujol.

Periodic boundary conditions are necessary if we want to prevent the formation of small strings on the border of the system, but are of course absent in real materials; however as a crystal is in the "thermodynamic limit", we expect these surface effects to be negligible and the strings to appear essentially in the bulk of the compound.

The divergence free constraint is a necessary condition for the existence of such excitations but it is not sufficient. For example, hard core dimers on a square lattice do not show such transitions, as the system can leave the crystalline ordered state (valence bond solid) by flipping a pair of dimers through 90°, creating an excitation of finite energy and extent (resonating valence bond [And87]).

III.2 Kasteleyn transition: $\delta = 0$

In this section, we shall focus on the effect of the [001] magnetic field *without* bond distortion. The 6-fold symmetry of the 2 *in* - 2 *out* manifold is thus broken and the low temperature ordering occurs through the so-called Kasteleyn transition, introduced by Kasteleyn in the context of ordering of hard core $2d$ dimers lying on the bonds of a honeycomb lattice [Kas63]. Applying local chemical potentials, μ_i, for dimers oriented in one of the $i = 1, 2, 3$ possible directions leads to a singular ordering transition for finite values of the fugacities $z_i = exp(-\beta\mu_i)$. The transition can also occur for dimers on three dimensional equivalents of the honeycomb lattice such as the brick lattice [Bha83], while the exponents can be determined in dimension d through mapping onto a directed polymer problem [Bha91a]. It has been extensively used to describe trans-gauche structural transitions in polymerized lipid bilayers and the resulting theory provides a good qualitative description of the singular density change occurring in solvent bilayer systems as a function of temperature [Nag73b] (see figure III.4 extracted from [Nag73a]).

It has been shown that the same Kasteleyn transition exists in the nearest neighbour model for spin ice materials on a pyrochlore lattice, with magnetic field directed close to the body centred cubic [111] direction[Moe03a] (see section I.3.d). Placing the field along this direction isolates the Kagome layers orthogonal to the field. The magnetic field fixes only one out of the four sublattices with the result that the extensive ground state degeneracy of zero field is only partially lifted, as it maps onto the antiferromagnetic Ising model on Kagome lattice in a field, as well as on Kasteleyn's original dimer problem on the Honeycomb lattice. Tilting the field off the [111] direction, giving a finite perpendicular field component $h_\perp$, is equivalent to applying chemical potentials μ_i to the dimers and the spins order in the Kagome planes for a finite value of $h_\perp/T$ via a Kasteleyn transition.

The study of the [001] orientation of the field has first been motivated by previous numerical work that found indications of a 1st order phase transition at finite field [Har98]. In his paper [Wat99], Watson suggested the clever parallel between this numerical prediction and the theory of the 6-vertex model [Bax07], but the exact $2d$ calculation for the square ice model in a field is unable to explain the discontinuity of the order parameter obtained numerically, or to reproduce experimental magnetisation curves [Fuk02]. In this thesis, we shall show explicitly that the observed first order nature was in fact a consequence of the loss of ergodicity due to the single spin flip dynamics used at that time.

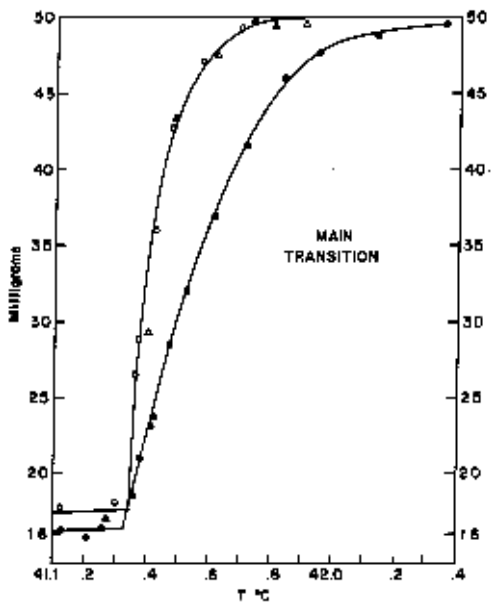

Figure III.4: **Kasteleyn transition for biomembranes:** This figure is directly extracted from [Nag73b] and represents the relative difference in weight between an equal volume of water and 1 g of dipalmitoyl lecithin dispersion. The open circles are a sequence of increasing temperatures and the triangles are a sequence of decreasing temperatures, both for about a 10% dispersion. The solid circles are for a 25% dispersion.

Interestingly experimental results reflect the same out-of-equilibrium features [Fen05], as natural dynamics is also local rather than the non-local dynamics discussed here. However, with the introduction of the Worm algorithm and the Husimi tree method, our results very clearly confirm that the transition is in fact a Kasteleyn transition very similar to that observed for dimers on the brick lattice [Bha83]. These results have been published in [Jau08, Jau09a].

III.2.a Husimi Tree

We will now pursue the calculations of the thermodynamic observables on the Husimi tree, starting from equations (II.68) and (II.69) with $\delta = 0$ and in the limit $J \gg h, T$ in order to impose the ice-rules, which can be written[3]:

$$Y_{n+1}\, e^{2\beta h} = \frac{Y_n^3 + 2Y_n}{1 + 2Y_n^2} \tag{III.6}$$

$$M_L = \frac{1 - Y_L^4}{4Y_L^2 + Y_L^4 + 1} \tag{III.7}$$

[3]We should recall that the different pre-factors due to the fact that the spins are not parallel to the z-axis have been included in the parameters or constants; *e.g.* , the magnetisation $M \in [-1 : +1]$ instead of $[-1/\sqrt{3} : +1/\sqrt{3}]$.

where M_L is the magnetisation of a central spin in a Husimi tree made of L shells, function of $\{Y_n\}_{n\in\mathbb{N}}$, a sequence constructed in order to have a finite limit. In our case, there are in fact three fixed points

$$Y\,e^{2\beta h} \;=\; \frac{Y^3+2Y}{1+2Y^2} \Rightarrow Y=0, \quad Y^2 = \frac{2-e^{2\beta h}}{2\,e^{2\beta h}-1} \tag{III.8}$$

We shall only keep the positive values of Y as M is an even function of Y. A Taylor expansion of the left equation immediately tells us that a non-trivial solution exists and is stable for $2 > e^{2\beta h} \Leftrightarrow T > T_{\mathrm{K}}$, whereas $Y = 0$ for $T < T_{\mathrm{K}}$. If we inject this solution in equation (III.7), one get the magnetisation as a function of temperature and magnetic field:

$$\boxed{\begin{array}{lcl} T < T_{\mathrm{K}} & \rightarrow & M \;=\; +1 \\ T > T_{\mathrm{K}} & \rightarrow & M \;=\; \dfrac{\sinh(2\beta h)}{2\;-\;\cosh(2\beta h)} \end{array}} \tag{III.9}$$

This result is plotted in figure III.5 and respects the expected signature of the Kasteleyn transition. On can see from equation (III.8) that the transition occurs when $2 \equiv e^{2\beta h}$, *i.e.* when the Boltzmann weight of the two configurations of tetrahedra crossed by a string going towards the centre of the Husimi tree is equal to the Boltzmann weight of the configuration with all spins *up*. Hence at T_{K} we have indeed the propagation of a string spanning the whole Husimi tree from one boundary to the other (rejected to infinity) and passing by the centre.

In order to study the critical behaviour at T_{K}, it is convenient to define the reduced magnetisation $\Delta M \equiv 1 - M \geqslant 0$. Its temperature dependence at the transition is

$$\Delta M \sim \frac{4}{3}(\ln 2)^2 \left(\frac{T}{h} - \frac{T_{\mathrm{K}}}{h}\right) \tag{III.10}$$

giving a critical exponent $\boxed{\beta = 1}$ as previously obtained by [Bha83, Bha91b]. The magnetisation M is in fact a function of a unique parameter, namely h/T which implies a simple relation between the specific heat and the susceptibility

$$C_{\mathrm{h}} \;=\; \frac{\partial E}{\partial T} \;=\; \frac{h}{T^2}\,\frac{\partial M}{\partial \beta} \;=\; \frac{h}{T^2}\,(h\,T)\,\frac{\partial M}{\partial h} \;=\; \frac{h^2}{T}\,\chi \tag{III.11}$$

where

$$\boxed{C_{\mathrm{h}} \;=\; 2\beta^2 h^2 \frac{2\,\cosh\,(2\beta h)\;-\;1}{[2\;-\;\cosh\,(2\beta h)]^2}.} \tag{III.12}$$

above T_{K} and $C_{\mathrm{h}} = \chi = 0$ in the frozen state. The specific heat is plotted on figure III.7. As expected from equation (III.10), C_{h} undergoes a finite jump at the transition: $\Delta C_{\mathrm{h}} = 4(\ln 2)^2/3$ and $\alpha = \gamma = 0$.

The last thermodynamic quantity we consider here is the entropy $S(T,h)$. For the Husimi tree, Pauling's argument for the estimate of the 2 *in* - 2 *out* manifold degeneracy

is exact [Pau35]; since we impose the ice-rules for all temperatures here, we get $S(T \to +\infty, h) \to \frac{1}{2}\ln\frac{3}{2}$. The entropy change per spin between the high temperature regime and T is defined as

$$\begin{aligned}\Delta S(T_0) &\equiv S_\infty - S(T_0) = \int_{T_0}^{+\infty} \frac{C_\mathrm{h}}{T}\,\mathrm{d}T \\ &= \int_0^{\beta_0} \frac{C_\mathrm{h}}{\beta}\,\mathrm{d}\beta = \frac{1}{2}\int_0^{x_0} x\,\frac{\mathrm{d}M}{\mathrm{d}x}\,\mathrm{d}x\end{aligned}$$

where $x \equiv 2\beta h$. A partial integration of the last expression gives the complete expression of the entropy change

$$\boxed{\Delta S(\beta h) = \frac{1}{2}\left[\ln\left(2-\cosh(2\beta h)\right) + \frac{(2\beta h)\,\sinh(2\beta h)}{2-\cosh(2\beta h)}\right]} \tag{III.13}$$

One can check that $S\left(T \to T_\mathrm{K}^+\right) \to 0$ consistently with the phase space being reduced to a unique configuration at T_K; since there is no latent heat at the transition, it is of 2$^\mathrm{nd}$ order according to Ehrenfest's definition [Sta71]. As we are on the constrained manifold with constant internal energy, the Gibbs energy is $G \equiv -TS - hM$

$$G(\beta h) = \frac{T}{2}\ln\left(\frac{4-2\,\cosh(2\beta h)}{3}\right) \tag{III.14}$$

This result is exact on the Husimi tree in the asymptotic limit $T/J, h/J \to 0$. However we were not able to extract further analytical results outside this limit, *i.e.* if we consider the inclusion of defects; one must then solve equations (II.68) and (II.69) numerically, as displayed in figure III.5. The transition has then disappeared and the evolution of the magnetisation becomes more and more rounded as we increase the ratio h/J: we should note here that the magnetic field does *not* break the ice-rules, but since the temperature is scaled after the field (we plot T/T_K in the figure), a larger field strength means a higher temperature regime with more thermally activated topological defects.The reason for this rounding is quite straightforward. For finite J, the topological constraints are lifted and strings of finite size, terminated by topological defects of opposite charges, can appear in the bulk of the system; such excitations require a finite amount of energy and enable the system to leave the frozen configuration before the Kasteleyn temperature T_K. Above a characteristic scale fixed by the separation between defects, the system will become regularly paramagnetic and this is just what is observed in the rounding of the transition in figure III.5.

The Husimi tree gives us the satisfaction of asymptotic analytical solutions, that are exact on this lattice of infinite dimension, but remains an approximation with respect to the geometry of the pyrochlore lattice that should be tested with the help of the Worm algorithm.

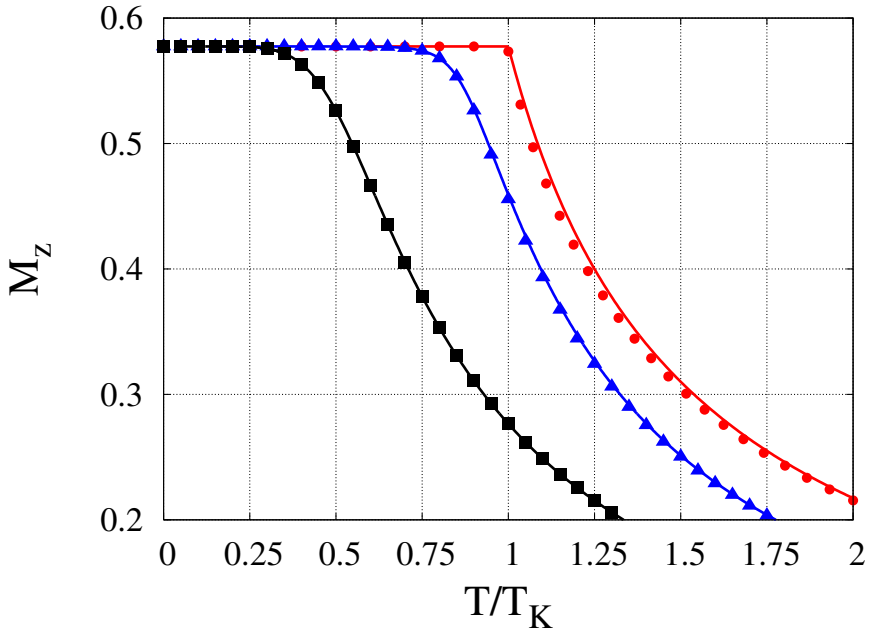

Figure III.5: **3d Kasteleyn transition in spin ice:** Magnetization per spin M_z vs. T/T_{K} obtained from simulations for the pyrochlore lattice (dots) and analytically on the Husimi tree (solid lines) for $h/J \to 0(\bullet)$, $0.075(\blacktriangle)$ and $0.33(\blacksquare)$. We have plotted the $z-$component of the magnetisation that differs from M by a factor of $1/\sqrt{3}$. The behaviour of M_z reminds us of the Kasteleyn transition in biomembranes, seen in figure III.4 [Nag73b].

III.2.b Worm algorithm

The method has already been detailed in the precedent chapter II.3 and we shall therefore only discuss the consequences of $\delta = 0$ with respect to the table II.1 where the different probabilities used in the loop construction are summarised. First of all, the temperature $T_\downarrow$ turns out to be negative and the bottom-left part of the table thus does not apply. The Boltzmann weights are now related by:

$$\frac{w_\uparrow}{w_0} = \frac{w_0}{w_\downarrow} = \exp(2\beta h) \tag{III.15}$$

$$= 2 \quad \text{at the transition } T_{\mathrm{K}} = T_\uparrow \tag{III.16}$$

giving the following set of probabilities at the transition

$$P^b_{\uparrow\uparrow} = 0, \quad P^f_{\uparrow o} = \frac{1}{2}, \quad P^{1f}_{oo} = 0, \quad P^{1f}_{o\uparrow} = 1, \tag{III.17}$$

$$P^b_{\downarrow\downarrow} = 0, \quad P^f_{\downarrow o} = \frac{1}{2}, \quad P^{2f}_{oo} = \frac{3}{4}, \quad P^{2f}_{o\downarrow} = \frac{1}{4}, \tag{III.18}$$

allowing us a phenomenological understanding of the simulations. If we randomly choose an *up* spin at first, which are in large majority at T_{K}, we will start constructing a string

(since there is no backtrack, $P^b_{\uparrow\uparrow} = 0$) respecting the entropic random choice for each tetrahedron ($P^f_{\uparrow o} = 1/2$). On the one hand, if we do not meet any pre-existing string, we will eventually cross the loop under construction, which will most likely end in forming a string ($P^{2f}_{oo} = 3/4$) or temporarily pursuing the construction ($P^{2f}_{o\downarrow} = 1/4$). On the other hand, if we meet a pre-existing string, we will inevitably *erase* it ($P^{1f}_{oo} = 0$ and $P^{1f}_{o\uparrow} = 1$). The same argument applies for an initial *down* spin, *i.e.* in a pre-exisiting string; the string will disappear.

If left alone, a string will always go forward along the z-axis and diffuse according to a $2d$ random walk in the (x, y) plane, which means it cannot close on itself before spanning the entire system at least once. Hence a typical string of size $\sim 2\,L_z$ (from top to bottom of the system) will *occupy* a cylindrical volume of radius $\sqrt{2\,L_z}$ and since two strings cannot intersect at T_K at the risk of being erased, there will be of the order of $L^2_\perp/L_z$ strings in the system once equilibrated at the transition temperature, giving rise to a magnetisation $M \approx (1 - 1/L_z)$ according to equation (III.4). Even if this confirms the expected saturated magnetisation in the thermodynamic limit, as observed in figure III.5, the finite size effects appear to be quite noticeable. However the absence of rejection of the Worm algorithm makes the equilibration process extremely efficient and allows the simulation of system up to $3,2.10^7$ of spins in a reasonable amount of time (a few days for the whole range of temperature from $T = 0$ to $T = 2\,T_\mathrm{K}$ – see figure III.5). This reasoning is of course a naive approach of the problem, as we neglect the microscopic details of the pyrochlore lattice and the possibility of multiple crossing of the system for a loop thanks to the periodic boundary conditions, but it captures nonetheless the essence of the physics of the Kasteleyn transition as shown on the right panel of figure III.6 where the fit is quantitatively correct (within error bars) despite an apparent small concavity.

One can pursue this reasoning by hands in order to understand the continuity of the transition. Let us consider the tetrahedron at the intersection between two strings; being crossed by a second string always costs a Zeeman energy but does not bring any entropic gain as this second string has a unique choice to propagate. There is thus an entropic repulsion between strings and the second string shall require a slightly higher temperature than T_K to be formed which will result in a continuous transition.

The situation is fairly similar below T_K, but with the crucial difference that backtracking ($P^b_{\uparrow\uparrow} > 0$) makes it more and more difficult to create a loop as the temperature is decreased: a loop can now erase its *own* path. It is particularly satisfying to visualise how the thermodynamic argument of equation (III.2) manifests itself through the necessity of backtracking imposed by the detailed balance condition in the simulations.

Finite size effects are here again quite noticeable. According to the value of $P^b_{\uparrow\uparrow} \to 0^+$ close to T_c^-, the numerical loop should be able to attain an average size ℓ before being erased; if the vertical size L_z of the system is smaller than ℓ, then the loop has a chance to be closed and to form a string below T_c. This argument can be made quantitative by noticing that δG is dominated by the energy $E_\mathrm{string} = (2h)\,(2L_z)$. Hence the Boltzmann weight for a string excitation decreases exponentially with system size: $w_\mathrm{string} \propto \exp\left(-\beta E_\mathrm{string}\right)$ [Isa04b]. As the reduced magnetisation $\Delta M \equiv 1 - M$ is pro-

portional to the number of loops, one can observe this exponential finite size scaling by making an accurate measure of ΔM below $T_{\rm K}$. In figure III.6) we show ΔM on a logarithmic scale, as a function of $h/h_{\rm K}$ for different system sizes[4]. The data, averaged over up to 10^7 configurations fit the exponential scaling remarkably well down to $\Delta M \sim 10^{-7}$. This analysis shows convincingly that the mechanism for the transition is exactly the generation of extensive excitations developed in this section.

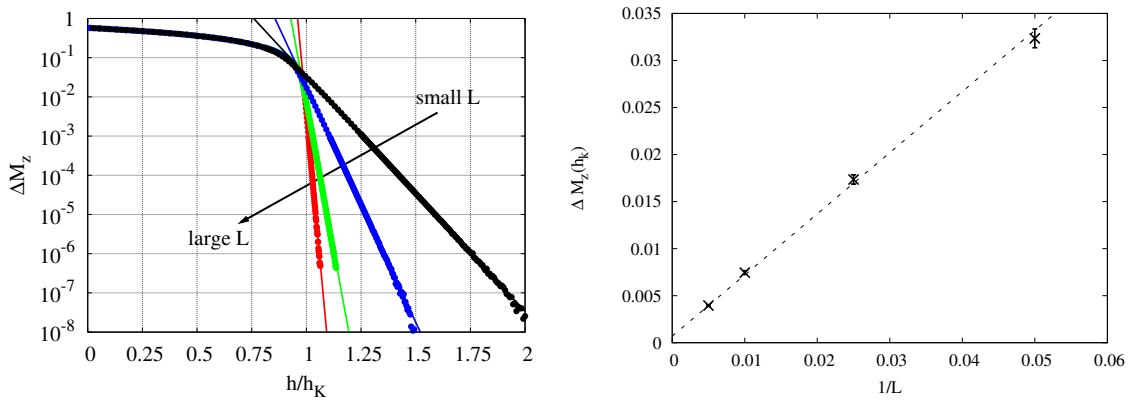

Figure III.6: **Finite size effects:** *Left:* Relative magnetisation ΔM_z as a function of $h/h_{\rm K}$ obtained numerically (•) for different sizes of the system: $L = 20, 40, 100, 200$. The straight lines are a fit to the Boltzmann factor $e^{(L\,\ln 2)\,h/h_{\rm K}}$. We have plotted the $z-$component of the magnetisation $\Delta M_z \equiv \Delta M/\sqrt{3}$. *Right:* We have extracted from the same data the $1/L_z$ behaviour of ΔM_z at the transition for a cubic system ($L = L_\perp = L_z$). The dashed line is a guide to the eye.

III.2.c Upper-critical dimension

As discussed above, each technique brings to light its own facet of the Kasteleyn transition, but the main success of this study is that the numerical and analytical approaches are in semi-quantitative agreement, as illustrated in figure III.5 showing the asymmetric singular behaviour of the magnetisation for $J \to \infty$. Thus, this figure is very similar to the one found in [Wat99], as the 6-vertex model in a field is identical to the original problem of closed-packed dimers on a hexagonal lattice discussed by Kasteleyn [Wu68], but with different critical behaviour. The upper-critical dimension of this transition is three [Bha83]. For $d = 3$, we expect logarithmic corrections in the magnetisation

$$\Delta M \propto t(1 - a \ln t) \quad \text{where} \quad t \equiv \frac{T - T_{\rm K}}{T_{\rm K}} \tag{III.19}$$

and a logarithmic divergence of the specific heat $C_{\rm h} \propto -\ln(t)$. For $d = 2$, the divergence is algebraic (critical exponent $\alpha = 1/2$) whereas for $d > 4$, as *e.g.* for the Husimi tree, there

[4] $h_{\rm K}$ is defined as $T\,\ln(2)/2$.

is no divergence anymore ($\beta = 1$ and $\alpha = 0$). This explains the small but nonetheless present mismatch between the simulations (red circles) and the analytics (red line) in figure III.5, that becomes clearer for the specific heat (see figure III.7).

With the inclusion of topological defects, one can make the transition vanished together with the logarithmic singularities. The results from both techniques then fit perfectly on top of each other. Furthermore in the context of low temperature series expansion, the Husimi tree is exact up to the 5th order, as it takes into account the geometrical term of 4th order (tetrahedron) and there is no 5th order term. The first degree of approximation corresponds to the hexagonal loop, which would appear at 6st oder.

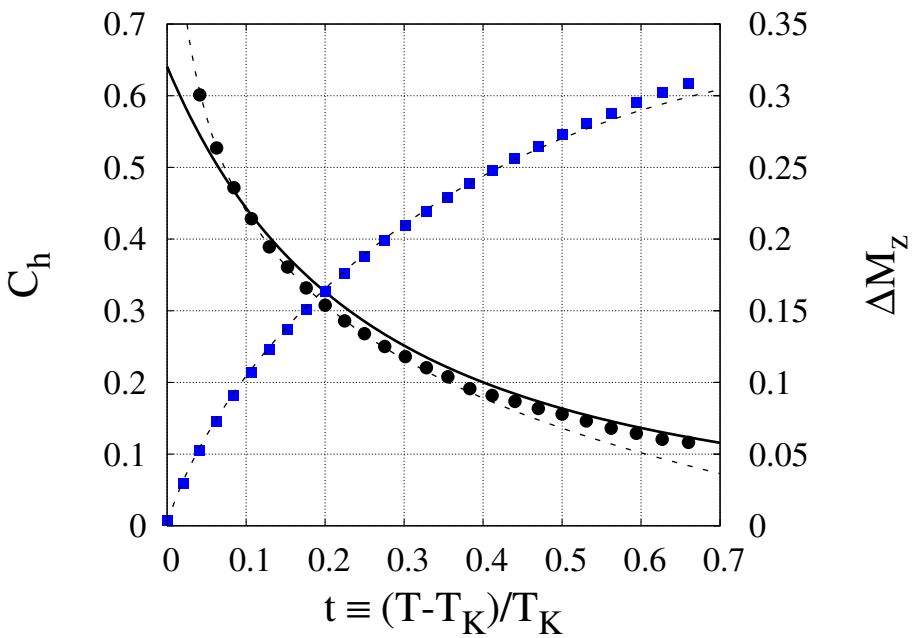

Figure III.7: **Logarithmic corrections at the upper-critical dimension:** Specific heat C_{h} and relative magnetisation ΔM_z as a function of t obtained from simulations (• for C_{h} and ■ for ΔM_z) and analytically (solid line for C_{h}) in the limit $J \gg h$. The dashed lines are a fit to logarithmic singularities given in equation (III.19).

III.2.d World lines for bosons

As shown in figure II.5, the topological constraints produce a one-to-one mapping between spins and strings configurations. A further analogy can be made through the definition of strings as *world lines for hard core bosons*, moving in $2d$ with the $z-$axis as an imaginary time. The $3d$ Kasteleyn transition then maps onto a $(2+1)$ quantum phase transition between a vacuum state and a Bose condensate at zero temperature, where the reduced magnetisation ΔM (resp. the reduced temperature $t \equiv (T/T_{\text{K}} - 1)$) is proportional to boson density (resp. bosons chemical potential) [Jau08]. Following [Fis88], one immediately recovers the critical behaviour of equation (III.19).

Powell & Chalker were able to incorporate the microscopic details of the pyrochlore lattice in this theory [Pow08] and to extract an analytical expression of the two-points spatial correlation function

$$C(\mathbf{r}_\perp, z) = \langle \mathbf{S}_i \cdot \mathbf{S}_j \rangle - \langle \mathbf{S}_i \rangle \cdot \langle \mathbf{S}_j \rangle \tag{III.20}$$

where the separation between lattice sites i and j is $\mathbf{r}_\perp$ within the (001) plane and z along the [001] direction. The authors of [Pow08] found an algebraic dipolar form of the correlations, similar to the zero field behaviour [Isa04a, Hen05]. We tested their result using the Worm algorithm and could confirm the $1/r^3$ scaling, as exposed in figure III.8. Close to the Kasteleyn transition, we observe a crossover to $1/z$ dependence, a characteristic signature of the self-interaction of the strings (*i.e.* bosons visiting the same site during their $2d$ evolution with time z), predominant in this regime where the concentration of strings/bosons is very diluted.

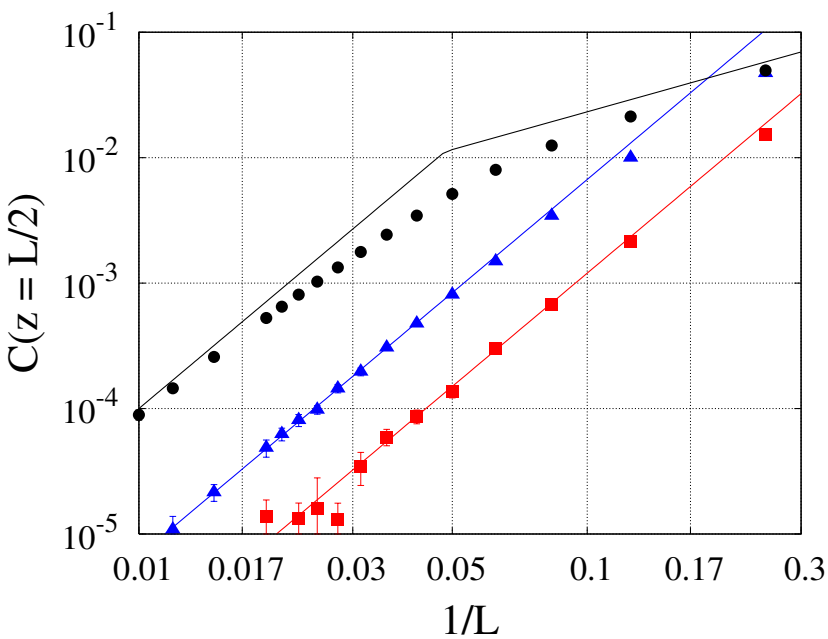

Figure III.8: **Correlations in a [001] field:** We show finite size scaling plots of $C(\mathbf{r}_\perp = 0, z = L/2)$ for three dimensional systems of size L and for magnetic field along the $z-$axis $h/h_{\mathrm{K}} = 0.33\,(\blacksquare)$, $0.66\,(\blacktriangle)$ and $0.93\,(\bullet)$ on a on log-log scale. We can extract the power law behaviour of $C(\mathbf{r}_\perp, z)$ in the thermodynamic limit: for small field we find a $1/z^3$ behaviour consistently with the dipolar correlations leading to the pinch points, whereas as we get closer and closer to the transition the self-interaction of strings becomes dominant, leading to a $1/z$ scaling.

III.2.e Experiments

As the experimental systems fall out of equilibrium at low temperature, it is difficult to compare theory with experiment very close to the Kasteleyn transition. But at rea-

sonably low temperatures, where the concentration of topological defects is low but sufficiently high to maintain ergodicity, it is possible to observe a rounded transition and to compare data with our theory. As an example we show in figures III.9 experimental magnetisation measurements in the [001] field scans performed at fixed low temperature in $Ho_2Ti_2O_7$ [Fen05] and $Dy_2Ti_2O_7$ [Fuk02]. For the left panel (Holmium Titanate), the temperature is $T_{\text{exp}} = 1.2$K, *i.e.* about 2/3 of the effective nearest neighbour exchange constant $J_{\text{eff}} \sim 1.8K$ (see table I.3), whereas for the right panel (Dysprosium Titanate), $T_{exp} = 1.8\text{K} \approx 3/2 J_{\text{eff Dy}}$. The magnetisation flattens off abruptly at the saturation value, $M_{\text{exp}} = 10\mu_B/\sqrt{3}$ in a way reminiscent of the Kasteleyn transition but is indeed rounded near saturation[5]. Demagnetisation effects have been taken into account for both experimental data (see appendix B). Also shown in the figure is our data calculated analytically from the Husimi tree approximation, up to a scale factor; the best fit has been obtained for $h_{\text{theo}} = 1.67\, h_{\text{exp}}$ for Holmium Titanate and $T_{\text{theo}} = 0.83\, T_{\text{exp}}$ for Dysprosium Titanate. At such temperatures, results from the Worm algorithm and the Husimi tree are indistinguishable and in qualitatively good agreement with experiments. However as we are at a temperature relatively far from the Kasteleyn transition and quite close to a non-collective paramagnetic regime, *i.e.* with a non-negligible concentration of topological defects, simpler models (such as a Brillouin function) can also give a correct fit to the experiments, but with a less accurate fitting parameter (*e.g.* 39% of T_{exp} for the Brillouin function instead of 83% for the Husimi tree for Fukazawa's data). Hence our theory is able to take into account more accurately the microscopic details of the pyrochlore lattice (see the agreement between simulations and the Husimi tree) and more importantly to shed a new light onto the underlying physics of topological sectors *modulo* the influence of local defects in the Kasteleyn transition.

The use of scaling factors is not surprising here as a more quantitative comparison would require the inclusion of Coulomb interactions between topological defects. The better agreement for the experiment on $Dy_2Ti_2O_7$ is also understandable. In spin ice compounds, the strings have a finite length and are terminated by magnetic monopoles. For lower concentration of monopoles, the strings can thus propagate on a longer distance before an eventual annihilation of the quasi-particles, and the influence of the Coulomb interactions attracting both monopoles is then stronger. Hence a higher effective temperature $T_{\text{exp}}/J_{\text{eff}}$ appears to be in favour of our nearest neighbour model that is perfectly able to reproduce the paramagnetic regime. For temperatures well below the scale set by the exchange constant J_{eff}, experiments indicate that spin ice materials are out of equilibrium, as expected if the actual dynamics is local [Fen05]: this notion will be extensively detailed in the next chapter.

This section on the influence of a magnetic field is now over and we will now consider the additional possibility of bond distortion. Both perturbations will result in a tuneable Kasteleyn transition, while the most intriguing physics will occur in zero field with restoration of the global $\mathbb{Z}_2$ symmetry.

[5]The $1/\sqrt{3}$ factor comes from the scalar product between the spins and the field.

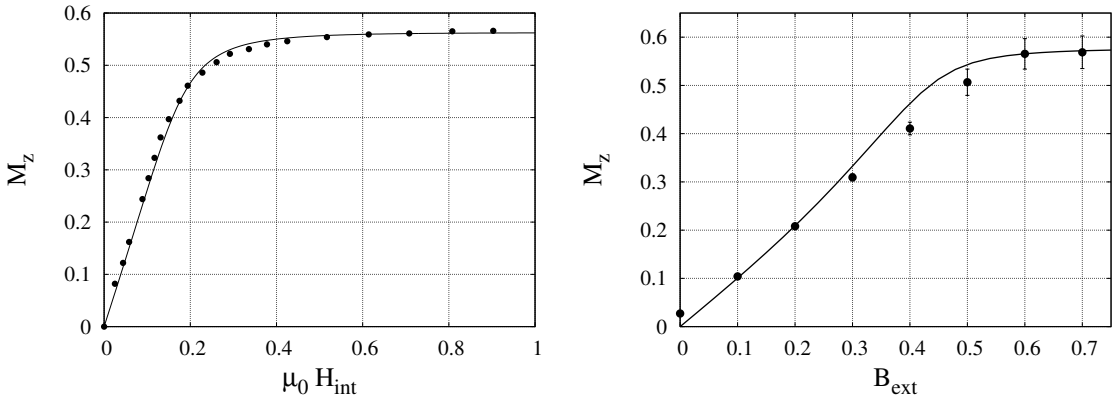

Figure III.9: **Magnetisation in a [001] field:** *Left:* Magnetisation M_z vs the internal magnetic strength $\mu_0 H_{\text{int}}$ obtained analytically for the Husimi tree (solid lines) and experimentally (•) for the compound $Dy_2Ti_2O_7$ at $T_{\text{exp}} = 1.8$K; data from [Fuk02]. *Right:* M_z vs the external magnetic field B_{ext} obtained analytically (solid lines) and experimentally (•) by neutron scattering on the compound $Ho_2Ti_2O_7$ at $T = 1.2$ K [Fen05]. For fitting details, see main text.

III.3 A tuneable Kasteleyn transition: $h > 0,\ \delta > 0$

As presented in subsection III.1.a, the argument for the Kasteleyn transition remains valid on the 2 *in* - 2 *out* manifold when both magnetic field h and bond distortion δ are non zero, resulting in a shifting of the transition temperature (III.3). From the point of view of the Worm algorithm, the main difference is that for small enough magnetic field ($h < 2\delta$), a second characteristic temperature $T_\downarrow$ becomes positive (see equation (II.16)) and introduces another set of probabilities for $T < T_\downarrow$ favouring tetrahedra crossed by two strings. $T_\downarrow$ being by definition always smaller than $T_\uparrow$, the influence of the new set of probabilities can then only be felt in the frozen phase where the field induced symmetry breaking prevents the formation of strings. However for very low temperature and $h < 2\delta$, one can expect a metastable state with all spins down, as the probability to erase a string is zero at $T = 0$ ($P^b_{\downarrow\downarrow} = 1$ and $P^f_{\downarrow o} = 0$). The energy barrier between both fully saturated states is held infinite by the topological constraints.

As observed on figure III.10, the asymmetric shape of the Kasteleyn transition is clearly conserved but with a more and more pronounced slope as $h/\delta \to 0$. This is a direct consequence of the energy recovered from bond distortion as a tetrahedron is spanned by a second string, making the entropic repulsion between them less efficient. The characteristic logarithmic singularity also prevails, as shown in figure III.11, where ΔM has been fitted with equation (III.19), only valid *a priori* for diluted concentration of strings [Bha83]: indeed, the fit turns out to be incorrect for large values of ΔM.

When the ice-rules are respected, it is again possible to extract analytical expressions for the magnetisation. Using equations (II.68) and (II.69) in the limit $J \gg h, T, \delta$, the

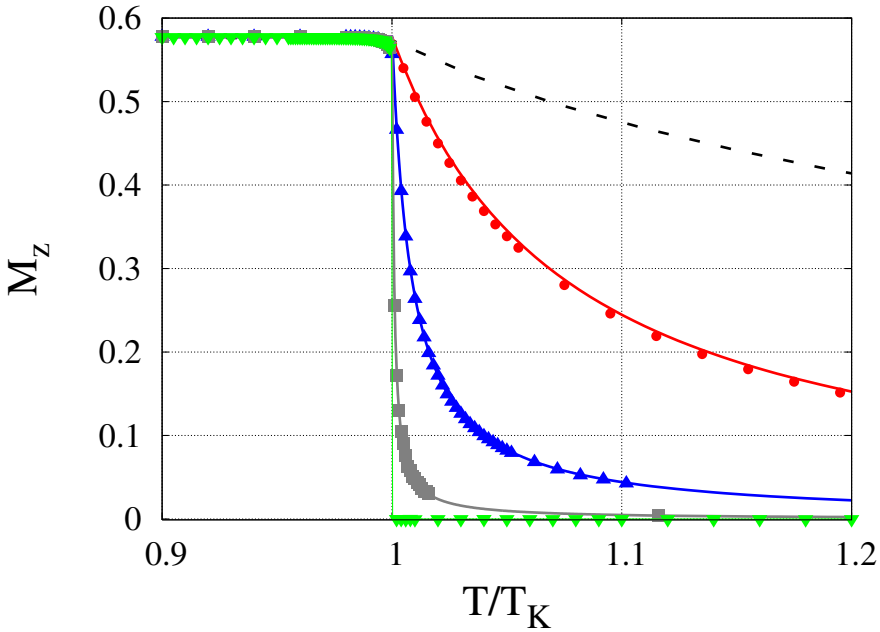

Figure III.10: **Tuneable Kasteleyn transition:** Magnetisation M_z vs. $T/T_{\rm K}$ using the Worm algorithm (dots) and calculations on the Husimi tree (solid lines) for different ratio $h/\sqrt{3}\delta = 0.1$(●), 0.01(▲), 10^{-3}(■) and 0(▼). The dashed line is a reminder of the magnetisation when $\delta = 0$.

limit Y of the sequence $\{Y_n\}$ must be solution of

$$Y\, e^{2\beta h} \;=\; \frac{Y^3\, e^{4\beta\delta} + 2Y}{e^{4\beta\delta} + 2Y^2} \tag{III.21}$$

and should be added in the expression of the magnetisation

$$M \;=\; \frac{1 \,-\, Y^4}{4\, e^{-4\beta\delta} Y^2 \,+\, Y^4 \,+\, 1} \tag{III.22}$$

Solutions of equation (III.21) for all temperatures are $Y = 0$ (corresponding to $M = +1$) and $Y \to +\infty$ (corresponding to $M = -1$). The non-trivial solution is not defined for all temperatures but only for $T > T_{\rm K}$ and $T < T_{\downarrow}$:

$$\breve{Y}^2 \equiv \frac{2 - e^{2\beta h}\, e^{4\beta\delta}}{2\, e^{2\beta h} - e^{4\beta\delta}} \tag{III.23}$$

Now we should study the stability of these different fixed points

- $T > T_{\rm K}$: the only stable point is $\breve{Y}$ giving rise to the non-trivial evolution of the magnetisation of equation (III.24) (see below);
- $T_{\downarrow} < T < T_{\rm K}$: the only stable point is $Y = 0$ corresponding to the fully saturated microstate $M = +1$;

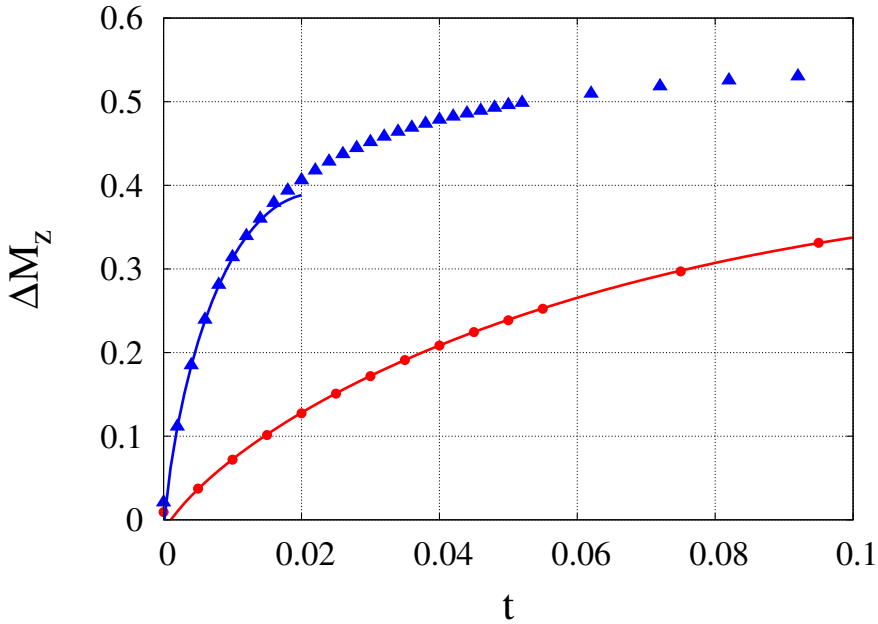

Figure III.11: **Logarithmic corrections at the upper-critical dimension:** Numerical values of $\Delta M_z \equiv M_{z\,sat} - M_z$ vs. the reduced temperature t fitted by equation (III.19) (solid lines) for different ratio $h/\sqrt{3}\delta = 0.1$(●) and 0.01(▲).

- $T < T_{\downarrow}$: both $Y = 0$ and $Y \to +\infty$ are stable points but as $\breve{Y} > 1$ then the whole ensemble $Y \in [0:1]$ corresponding to $M \in [0:1]$ belongs to the basin of attraction of $M = +1$. However $M = -1$ is nonetheless a metastable state as discussed previously.

Hence, the expression of the magnetisation is

$$\boxed{\begin{aligned} T < T_{\rm K} \quad &\to \quad M = +1 \\ T > T_{\rm K} \quad &\to \quad M = \frac{\sinh(2\beta h)}{2\,e^{-4\beta\delta} - \cosh(2\beta h)} \end{aligned}} \tag{III.24}$$

We recover equation (III.9) with $\delta = 0$ and more importantly, one easily checks that $M(T_{\rm K}) = +1$: there is thus no latent heat and the transition remains continuous with bond distortion. Hence by using δ as a free parameter, one can tune the transition in order to make the relaxation more or less fast. On the Husimi tree, the slope of ΔM at $T_{\rm K}^{+}$ is not diverging but follows a linear scaling similar to (III.10)

$$\Delta M \sim \frac{(\ln 2)^2}{2h + 4\delta} \frac{1}{1 - \exp\left(\frac{4h\,\ln 2}{2h+4\delta}\right)} (T - T_{\rm K}) \tag{III.25}$$

The main difference between the Husimi tree and the $3d$ simulations is the absence of logarithmic singularities, but their results remain very close to each other as shown in

figure III.10. Interestingly the slope of the magnetisation for the analytic calculation becomes infinite when there is no field, promising an intriguing new kind of physics for $h = 0$!

III.4 KDP transition: $h = 0$

III.4.a Apparent 1st order transition

Following equations (III.21), (III.22) and (III.23), the study of bond distortion for configurations respecting the topological constraints is quite straightforward. As $T_{\downarrow} = T_{\mathrm{K}}$ for $h = 0$, both microstates $M = \pm 1$ become stable and equiprobable at low temperature, while $\breve{Y} = 1 \Leftrightarrow M = 0$ is the stable fixed point above the transition

$$\boxed{\begin{array}{lcl} T < T_{\mathrm{K}} & \rightarrow & M = \pm 1 \\ T > T_{\mathrm{K}} & \rightarrow & M = 0 \end{array}} \tag{III.26}$$

The magnetisation thus jumps at the transition from zero to one of the fully saturated state, as displayed on figure III.10 from both the analytical and numerical results. Equations (II.7) and table II.1 show the perfect $\mathbb{Z}_2$ symmetry appearing in the probability set. Strings made of *up* and *down* spins are now equivalent, but we should keep the terminology of "strings" for the ones made by spins pointing *down* by convenience. This symmetry imposes zero magnetisation in the collective paramagnetic phase, down to the symmetry breaking phase transition in a way reminiscent of the ferromagnetic ordering in the Ising model presented in the introduction I.1.b; with the crucial difference though that the ice-rules constraints prevent a gradual building up of the magnetisation. They rather impose a brutal full magnetisation through strings excitations at $T_c = T_{\mathrm{K}}$. From now on, we shall call the transition temperature T_c in order to make a clear distinction with the Kasteleyn transition, even if the phenomena, with $h = 0$ and $h > 0$, do share some similarities.

As discussed in section II.5, this model with bond distortion is known as the KDP model, introduced by Slater in 1941 in order to explain the phenomenon of ferroelectricity in potassium dihydrogen phosphate $\left[\mathrm{K}^+ (\mathrm{H}_2\mathrm{PO}_4)^-\right]$ within a mean field approximation [Sla41]. The inclusion of defects have been first studied by Takagi [Tak48] and generalised by Silsbee *& al.* [Sil64]. The $2d$ version of the KDP model with constraints has become a special case of the 6-vertex model and has been solved exactly by Lieb in 1967 [Lie67a], showing what appears to be a 1st order phase transition and becoming one of the main *tour de force* of $2d$ statistical mechanics. A few years later, Nagle generalised this result to all dimensions, proving exactly by low and high temperature expansions the discontinuity of the energy and entropy at T_c.

In this section, we shall make an extensive use of the Husimi tree which will provide a complete analytical description of the KDP transition, with and without topological defects, re-deriving some of the results of [Sla41, Tak48, Sil64]. However our final goal is

to go beyond this mean field approach thanks to the Worm algorithm and the transfer matrix method in $3d$, and to try to show this venerable transition in a new light; the discontinuity of thermodynamic observables are in fact a consequence of the particular criticality of this transition, which is a multicritical point of $\infty-$order.

High temperature regime: in presence of defects

As discussed above, the symmetry of the system for *both* the constrained and non-constrained manifold imposes zero magnetisation at high temperature; this property allows analytical solutions for many thermodynamic quantities on the Husimi tree, even in the presence of topological defects.

We shall recall here that A_n and B_n represent the partition function of a "branch" of the Husimi tree of n shells, starting respectively with an *up* or a *down* spin. Hence for zero magnetisation, we can use the global symmetry to define $A_0 \equiv B_0$; using equation (II.65), one can then prove recursively for all integers n that

$$A_{n+1} \,=\, B_{n+1} \,=\, \alpha\, A_n^3 \,=\, \alpha^{-1/2}\, \left(\sqrt{\alpha} A_0\right)^{3^n} \tag{III.27}$$

$$\text{where} \quad \alpha \,=\, 4 \,+\, e^{-\beta(6J-2\delta)} \,+\, 2\, e^{2\beta(J-\delta)} \,+\, e^{2\beta(J+\delta)} \tag{III.28}$$

where topological defects have been taken into account. The complete partition function of the Husimi tree (II.66) becomes

$$Z_L \,=\, 2\,\alpha\, A_L^4 \,=\, \frac{2}{\alpha}\left(\alpha\, A_0^2\right)^{2\cdot 3^L} \tag{III.29}$$

giving also $M_L = 0$ from equation (II.67). In the thermodynamic limit, we recall that the number of tetrahedra is $N_t = 2 \cdot 3^L$ (see equation (II.63)), which gives the free energy

$$F = -T\, N_t\, \ln\left[\left(4 \,+\, e^{-\beta(6J-2\delta)} \,+\, 2\, e^{2\beta(J-\delta)} \,+\, e^{2\beta(J+\delta)}\right)\, A_0^2\right] \tag{III.30}$$

and the internal energy

$$E \,=\, -N_t\, \frac{(2\delta - 6J)\, e^{-\beta(6J-2\delta)} \,+\, 4(J-\delta)\, e^{2\beta(J-\delta)} \,+\, 2(J+\delta) e^{2\beta(J+\delta)}}{4 \,+\, e^{-\beta(6J-2\delta)} \,+\, 2\, e^{2\beta(J-\delta)} \,+\, e^{2\beta(J+\delta)}} \,-\, 2\, N_t \frac{\partial \ln A_0}{\partial \beta} \tag{III.31}$$

The entropy is deduced from $S = (E - F)/T$. If we were interested in the Husimi tree as a statistical problem by itself, we should study the influence of the boundary conditions through A_0, which are essential since $\sim 2/3$ of the spins are on the external shell. However if we want to use the BL as a tool for investigating what is happening in the spin-ice model, we can use this variable as a fitting parameter. We recall here that the Husimi tree is a very valid approximation of the pyrochlore lattice as they are equivalent down to 6th order (hexagon of spins) in a series expansion. We must though be cautious about the ratio "number of tetrahedra / number of spins": it is 1/2 for the pyrochlore lattice and 1/3 for the Husimi tree. This is why we always reason in terms of the number of tetrahedra N_t. In order to determine the fitting parameter A_0, we will use the asymptotic values of the

internal energy and the entropy as $T \to +\infty$. As we expect a random distribution of the 16 possible tetrahedra configuration, the energy is

$$\frac{E}{N_t}(T \to +\infty) \;=\; [-2(J+\delta)]\,\frac{2}{16} \;+\; [-2(J-\delta)]\,\frac{4}{16} \;+\; [0]\frac{8}{16} \;+\; [6J-2\delta]\,\frac{2}{16} \;=\; 0 \tag{III.32}$$

To obtain this result from equation (III.31), one must set

$$\frac{\partial \ln A_0}{\partial \beta} = 0 \tag{III.33}$$

which is understandable as A_0 represents the influence of the outer-shell of spins whose magnetisation should remain constant as in the core of the Husimi tree. The second asymptotic condition we can use is the entropy on the pyrochlore lattice, $S_{\text{pyro}}(T \to +\infty) = N \ln 2 = N_t \ln 4$, whereas the one on the Husimi tree extracted from equations (III.30) and (III.31) is $S_{\text{HT}} = N_t \ln(8\,A_0^2)$, giving the final condition

$$A_0^2 \;=\; \frac{1}{2} \tag{III.34}$$

The fitting parameter being defined, we can now write the expression of the entropy for all temperatures

$$\boxed{\begin{aligned} \frac{S}{N_t} \;&=\; \ln\left[\frac{1}{2}\left(4 \,+\, e^{-\beta(6J-2\delta)} \,+\, 2\,e^{2\beta(J-\delta)} \,+\, e^{2\beta(J+\delta)}\right)\right] \\ &-\; \beta\,\frac{(2\delta-6J)\,e^{-\beta(6J-2\delta)} \,+\, 4(J-\delta)\,e^{2\beta(J-\delta)} \,+\, 2(J+\delta)e^{2\beta(J+\delta)}}{4 \,+\, e^{-\beta(6J-2\delta)} \,+\, 2\,e^{2\beta(J-\delta)} \,+\, e^{2\beta(J+\delta)}} \end{aligned}} \tag{III.35}$$

with the surprising outcome that $S(T=0) < 0$! As this result is physically impossible, it means that our assumption of zero magnetisation must fail at some finite temperature; there is also an ordering phase transition occurring in the system with defects [Tak48]. However we do not know yet its temperature and thus cannot calculate its entropy.

We note that the expression (III.35) can be recovered from a Pauling's argument taking into account all 16 configurations weighted by their Boltzmann factor, as this type of reasoning is exact on the Husimi tree; for the details of the calculation, please see appendix A. By taking the derivative of the energy E with respect to temperature, we can also calculate the specific heat. These results have been obtained for the non-constrained problem, but as we are especially interested in the topologically driven multi-critical point, we shall also study these quantities in absence of defects, *i.e.* $J \to +\infty$.

High temperature regime: on the 2 *in* - 2 *out* manifold

The entropy then becomes

$$\boxed{\frac{S}{N_t} \;=\; \ln\left(e^{-4\beta\delta} \,+\, \frac{1}{2}\right) \,+\, \frac{4\beta\delta}{\frac{1}{2}\,e^{4\beta\delta} \,+\, 1}} \tag{III.36}$$

This expression has been obtained from a combinatorial approach by Slater [Sla41]. In the limit $T \to +\infty$ we recover Pauling's entropy for this collective paramagnet, whereas at the transition $T_c = 4\delta/\ln 2$, we find on the pyrochlore lattice

$$\boxed{S(T_c) \;=\; N_t\,\frac{1}{2}\ln 2 \;=\; N\,\frac{1}{4}\ln 2 \;=\; 0.1733\;N} \tag{III.37}$$

As demonstrated in appendix A, such entropy corresponds to a specific distribution of the tetrahedra configurations; 50% of them are in one of the two favoured states (25% with all spins *up* and 25% with all spins *down*) while the other half is made of a uniform repartition of 2 *in* - 2 *out* tetrahedra with zero magnetisation. The equality of the Boltzmann weights gives $4e^{-2\beta\delta} = 2e^{+2\beta\delta} \Leftrightarrow T = T_c$.

In figure III.12, we compare this estimation with the entropy S_{num} integrated from Worm algorithm based simulations. The most accurate $T \to +\infty$ reference we are aware of, has been obtained by Nagle using series expansion: $S_{\text{PN}}/N = 0.20501 \pm 0.00005$ [Nag66], whereas Pauling's entropy is $S_{\text{Pauling}}/N = 0.202733$. The difference between these two values essentially holds in the addition of hexagonal correlations for the series expansion. S_{num} jumps at T_c from zero to $S/N = 0.1737 \pm 0.0005$, through the apparition of a huge spike in C_{h}. The entropy at T_c^+ is therefore in extremely good agreement with the prediction from the Husimi tree (III.37) and the difference is a measure of the correlations that exist between tetrahedra, which disappear as the ordering transition is approached.

On the constrained manifold, the low temperature regime is simply characterised by a symmetry breaking onto one of the fully saturated microstate with zero fluctuations. However as for the Kasteleyn transition which has been rounded by addition of topological defects, the KDP transition becomes continuous [Tak48].

Low temperature regime: in presence of defects

Thanks to a numerical estimate of the limit of $\{Y_n\}_{n\in\mathbb{N}}$ (II.68) injected in the magnetisation (II.69), we obtain the behaviour of the Husimi tree for any finite values of J. At low enough temperature, we expect the density of 4 *in* or 4 *out* defects to be negligible. This is why the sole addition of 3 *in* - 1 *out* and 3 *out* - 1 *in* topological defects should be sufficient to give a useful hint of the transition. Within this approximation, it is then possible to carry out the computation of the magnetisation, starting with the limit $n \to \infty$ of $\{Y_n\}$:

$$Y \;=\; \frac{3Y^2 \;+\; Y^3\,e^{2\beta(J+\delta)} \;+\; 1 \;+\; 2Y\,e^{2\beta(J-\delta)}}{3Y \;+\; e^{2\beta(J+\delta)} \;+\; Y^3 \;+\; 2Y^2\,e^{2\beta(J-\delta)}} \;=\; f(Y) \tag{III.38}$$

The transition appears when the magnetisation becomes non-zero, *i.e.* when the stable point is no longer $Y = 1$. However it is always solution of equation (III.38); a graphical representation of $f(Y)$ shows that the transition occurs at the temperature corresponding to $f'(1) = 1$, equivalent to

$$e^{2\beta(J+\delta)} \;=\; 2 \;+\; 2\,e^{2\beta(J-\delta)} \tag{III.39}$$

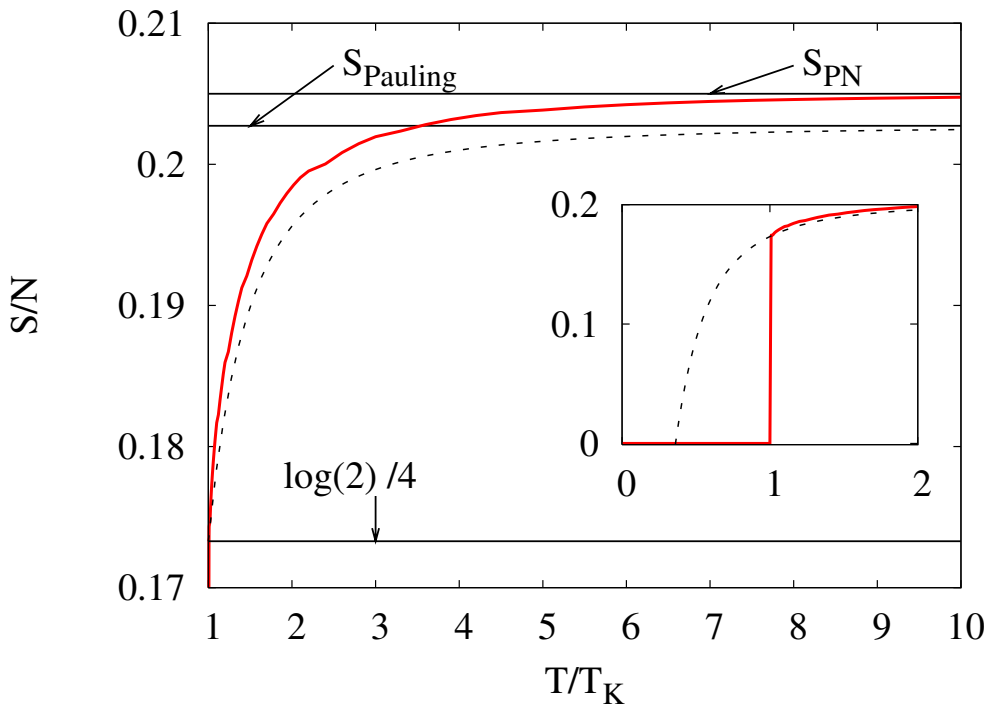

Figure III.12: **Entropy on the constrained manifold:** Evolution of the entropy per spin S/N vs temperature T/T_{K} using the Worm algorithm (red thick line with $N = 4.10^6$ spins) and formula (III.36) (dashed line). The inset shows the jump of the entropy at the transition.

suggesting the following change of variable $\kappa = e^{2\beta(J+\delta)} - 2 - 2\,e^{2\beta(J-\delta)}$ within equation (III.38). We then obtain a "reasonable" polynomial

$$\begin{aligned} Y^4 - (2+\kappa)Y^3 + (2+\kappa)Y - 1 &= 0 \\ \Leftrightarrow (Y-1)(Y+1)\left(Y^2 - (2+\kappa)Y + 1\right) &= 0 \end{aligned}$$

whose only solution strictly below 1 (*i.e.* we chose arbitrarily $M > 0$) is $Y = 1 + \kappa/2 - \sqrt{\kappa + \kappa^2/4}$. After a few calculations and by neglecting again the 4 *in* and 4 *out* tetrahedra, we finally obtain the magnetisation

$$\boxed{\begin{aligned} M &= \frac{1}{\varpi^2\left(1 - \sqrt{1 - 1/\varpi^2}\right)} - 1 \\ \text{where} \quad \varpi &= 1 + \kappa/2 = e^{2\beta(J+\delta)}/2 - e^{2\beta(J-\delta)} \end{aligned}} \tag{III.40}$$

A similar expression of the polarisation in a ferroelectric has been obtained by [Wad98] using the cluster variation method. With a critical exponent of $\beta = 1/2$, this phase transition seems to fall in the mean field Ising universality class, as one would expect for a calculation on the Husimi tree. As displayed on figure III.13, the collapse between the

numerical data and the analytical curve is semi-quantitative, as a mean field approach ultimately fails to reproduce critical behaviour of the $3d$ Ising universality class.

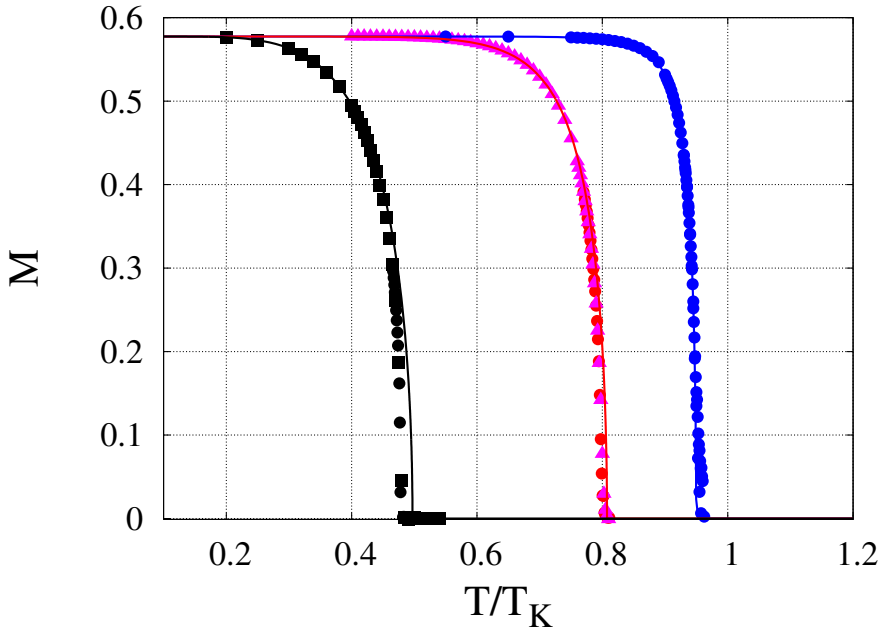

Figure III.13: **KDP transition with defects:** $z-$component of the magnetisation M_z vs temperature $T/T_{\rm K}$ obtained from simulations for the pyrochlore lattice (dots) and analytically on the Husimi tree (solid lines) for $\delta/J = 0.033(\bullet), 0.066(\blacktriangle)$ and $0.3(\blacksquare)$.

It is indeed an intriguing point that the Husimi tree allows quantitative comparisons with the $3d$ numerical results, such as the magnetisation discontinuity or the value of the entropy at T_c^+, but displays discrepancies with the inclusion of defects; this suggests a decrease of the upper-critical dimension on the constrained manifold, which we will confirm thanks to a more throughout study at T_c.

III.4.b Multicritical Point of ∞-order

Landau theory

Before studying the explicit nature of the KDP transition, we shall temporarily go back to the Landau theory presented in the introduction I.1.b in order to define a *multi-critical point of* $\infty-$*order* and to present some of its remarkable properties. Let us write the Gibbs free energy in a convenient way

$$G(M) \;=\; N\left[\frac{\alpha_2}{2}(T-T_c)\,M^2 \;+\; \sum_{n=n'}^{+\infty}\frac{\alpha_{2n'}}{2n'}\,M^{2n'}\right] \tag{III.41}$$

where α_2 was noted b_o in the introduction and $\alpha_{2n'} > 0,\ \forall n' \geqslant n$. Above T_c, the stable point is $M = 0$ and at the transition the leading contribution of the potential comes from

the first term in the sum $\frac{\alpha_{2n}}{2n} M^{2n}$; this is a multi-critical point of order n. For example, the tri-critical point is a special case with $n = 3$ and where the quartic term has disappeared at T_c. The important consequence of this Gibbs energy is that fluctuations around $M = 0$ become softer and softer as n increases as illustrated in figure III.14, until all values of the magnetisation eventually become equiprobable at T_c in the limit $n \to \infty$. We shall see it is exactly what is happening for spin ice with $\delta > 0$ and $h = 0$.

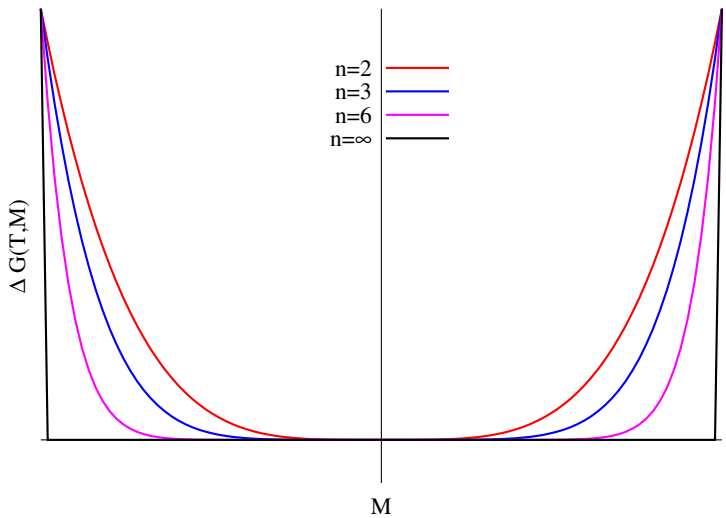

Figure III.14: **Gibbs energy for Landau theory (multi-critical point)** vs magnetisation M. Each curve represents a multi-critical point of order n, from $n = 2$ to ∞.

Benguigui studied this Gibbs energy and has obtained the following family of critical exponents [Ben77]

$$\beta = \frac{1}{2(n-1)} \quad \alpha = \frac{n-2}{n-1}, \quad \delta = 2n-1, \quad \gamma = 1, \quad \nu = \frac{1}{2} \tag{III.42}$$

The hyperscaling relation $2\beta + \gamma = d\nu$ provides the upper-critical dimension

$$d_c = \frac{2n}{n-1} \xrightarrow[n \to +\infty]{} 2 \tag{III.43}$$

hence we expect our $3d$ model to display mean field behaviour, which justifies *a posteriori* the use of the Husimi tree. We shall now go beyond the results presented in [Ben77], as being above the upper-critical dimension leads to surprising critical behaviour, expecially in the correlations.

Finite size effects using the Boltzmann probability

$$P(M) = \frac{1}{\mathcal{Z}} \exp\left(-\beta G(M)\right) \tag{III.44}$$

gives $\langle M^2 \rangle \sim N^{-1/n}$ at the transition $T = T_c$. It follows that the mean field correlator $g_{\mathrm{MF}} \equiv \langle M^2 \rangle - \langle M \rangle^2$ scales with system size as $N^{-1/n}$. Hence in the limit of $n \to \infty$ the averaged correlator is of order $\mathcal{O}(1)$.

However to these homogeneous fluctuations of a magnet of size N, extracted from Landau theory, one needs to add local fluctuations *à la* Ginzburg for a non-homogeneous critical system. Following the standard scaling hypothesis and the definition of critical exponent η, the correlator contribution due to critical fluctuations is [Car02, Pli06]

$$g_{\rm sc}(r) = \frac{1}{r^{d-2+\eta}} f_1\left(\frac{r}{\xi}\right) \tag{III.45}$$

where ξ is the characteristic correlation length. For system of finite size $L \times L \times L$ at the transition where $\xi \to L$, we get the scaling form

$$g_{\rm sc}(r) = \frac{1}{L^{d-2+\eta}} f_2\left(\frac{r}{L}\right), \quad \text{where} \quad f_2(x) = \frac{1}{x^{d-2+\eta}}\, f_{1(x)} \tag{III.46}$$

The total correlator $g(r)$ is therefore the sum of both contributions: a mean field term and a scaling function due to the critical fluctuations

$$\boxed{g(r) \;=\; g_{\rm MF} + g_{\rm sc}(r) \;=\; \frac{A}{L^{d/n}} + \frac{B}{L^{d-2+\eta}}\, f_2\left(\frac{r}{L}\right)} \tag{III.47}$$

For high dimensions, we have $\eta = 0$ and we can again calculate the upper critical dimension defined when fluctuations become irrelevant, *i.e.* when $g_{\rm MF}$ takes over $g_{\rm sc}$ in the thermodynamic limit

$$\frac{d_c}{n} = d_c - 2 \Leftrightarrow d_c = \frac{2n}{n-1} \tag{III.48}$$

We recover the result of (III.43). One of the direct consequence of equation (III.47) is the finite size behaviour of the susceptibility $\chi \equiv N\overline{g(r)}/T$ where $\overline{g(r)}$ is the spatial average of the correlator

$$\boxed{\chi \;=\; A\, N^{1-1/n} + B\, N^{2/d}} \tag{III.49}$$

Note that the term $B\, N^{2/d}$ can be directly obtained from the scaling hypothesis used to define the critical exponents (I.24) and their numerical values (III.42): $\chi_{sc} \sim L^{\gamma/\nu} \sim N^{\gamma/d\nu} \sim N^{2/d}$. Hence for our multi-critical point of $\infty-$order in $3d$, the leading term comes from the homogeneous Landau theory rather than from the local fluctuations, and we show that the susceptibility diverges linearly with N. This result is in fact not so surprising as the system can visit *all* values of the magnetisation with the same probability at the transition (see figure III.14).

Another important remark is that if we want to measure the scaling form of the correlator $g_{\rm sc}(r)$, we need to subtract the leading mean field contribution because we are above the upper-critical dimension. From a mean field point of view, we shall then compute

$$\begin{aligned} C(\mathbf{r}) \;&=\; g(r) \,-\, g_{\rm MF} \;=\; \left[\left\langle \overline{\sigma(\mathbf{r})\sigma(0)} \right\rangle \,-\, \langle\overline{\sigma}\rangle^2\right] \,-\, \left[\langle\overline{\sigma}^2\rangle \,-\, \langle\overline{\sigma}\rangle^2\right] \\ &=\; \left\langle \overline{\sigma(\mathbf{r})\sigma(0)} \right\rangle \,-\, \langle\overline{\sigma}^2\rangle \end{aligned} \tag{III.50}$$

where $\langle \dots \rangle$ is the statistic average over all microstates, $\overline{\cdots}$ is the spatial average and $\sigma(r)$ are the pseudo-spins. According to equation (III.49), spatial correlations produce corrections to scaling in a finite size scaling analysis above the upper critical dimension and the correlation function (III.50) is thus defined to capture these corrections. It turns out that it also correspond to the correlations within a given sector of the magnetisation, as explained below.

For a multi-critical point of order n, fluctuations due to soft modes around the minimum of the Gibbs energy become relevant (see figure III.14) and the system spends more and more time out of the reduced phase space with $M = 0$ (this is the famous critical opalescence for the liquid-gas transition). However this is not taken into account in the mean value of the magnetisation $M \equiv \langle \overline{\sigma} \rangle = 0$ and $g(r) = \left\langle \overline{\sigma(\mathbf{r})\sigma(0)} \right\rangle$ is then "artificially" more correlated, because in a sector of large magnetisation, most of the spins point in the same direction even if they are not correlated[6]. Hence the contribution of the finite value of the magnetisation should be subtracted *for each microstate* rather than on average. This gives

$$C(\mathbf{r}) = \left\langle \overline{\sigma(\mathbf{r})\sigma(0)} - \overline{\sigma}^2 \right\rangle \tag{III.51}$$

$$= \left\langle \overline{\sigma(\mathbf{r})\sigma(0)} \right\rangle - \left\langle \overline{\sigma}^2 \right\rangle \tag{III.52}$$

which is the same expression as (III.50): taking out the mean field divergence of the susceptibility is equivalent to subtract this "artificial" correlation.

We felt the necessity to present in details some aspects of this mean field theory of multi-critical point, as they are not so frequently discussed for an arbitrary value of n, especially in the limit $n \to \infty$. Keeping this image in mind, we can now turn our attention back to our problem of bond distortion in spin ice that will prove to be a multi-critical point of $\infty-$order.

Husimi tree

On the constrained manifold, one can directly use equation (III.21) with $h = 0$

$$Y = \frac{Y^3\, e^{4\beta\delta} + 2Y}{e^{4\beta\delta} + 2Y^2} \quad \Leftrightarrow \quad Y = Y \quad \text{at } T = T_c \tag{III.53}$$

which means that *all* positive values of Y, and therefore all physical values of $M \in [-1 : +1]$ are **equiprobable** at the transition. This corresponds to a flat free energy, which is very far from the standard picture of a 1st order transition with metastable microstates as commonly believed for the KDP transition, but is similar to the above mentioned multi-critical point of $\infty-$order ! Furthermore numerical simulations on cooling and heating display no hysteresis which definitely rules out the possibility of metastable states.

[6]For example a paramagnet in a high magnetic field should have no correlations (because there are no interactions) even if almost all spins are parallel to the field.

This flatness of the free energy has already been observed by Slater in its original paper on KDP within a mean field approximation but only as a side remark and he did not notice the multi-critical nature of this transition. The exact results for the $2-$ [Lie67a] and $d-$dimensional [Nag69] KDP transition, as well as the reference book by Baxter [Bax07], do not mention this flat free energy even if it is known to present a singularity at T_c. However in 1977, when Benguigui studied multi-critical points of $\infty-$order following the Landau-Ginzburg-Wilson approach [Ben77], he showed how this can result in the discontinuity of the order parameter and thus look like a 1st order transition with the above critical exponents (III.42) as for the $2d$ KDP model, but once again a proof of the multi-criticality of this transition is still lacking in three dimensions.

Our goal remains the study of bond distortion in spin ice materials, with respect to potential experiments (see subsection III.4.f), but its peculiar nature drew our attention and encouraged us to perform a throughout analysis of its characteristics. We shall first take advantage of the Worm algorithm to confirm the result of the Husimi tree (III.53) in $3d$ and then use the transfer matrix method to implement the structure of the pyrochlore lattice in an exact analytical treatment. Finally, we shall study the different contributions in the correlations.

Worm algorithm

Among the six tetrahedron configurations available on the 2 *in* - 2 *out* manifold, four of them with zero magnetisation along the $z-$axis can be grouped together, allowing the definition of only three relevant densities of tetrahedra:

- $n_\uparrow$ for configurations with all spins *up* (no strings are passing by);
- $n_\downarrow$ for configurations with all spins *down* (two strings are passing by);
- n_o for configurations with half spins *up* and half *down* (one string is passing by).

Except if specified otherwise, N is the total number of spins on the pyrochlore lattice. Additionally to these three quantities, we will also be interested in two thermodynamic observables, namely the mean value of the magnetisation and the energy, that can be expressed in terms of the above densities:

$$\begin{aligned} M &= (n_\uparrow - n_\downarrow) \in [-1 : +1] \\ E &= (n_o - n_\uparrow - n_\downarrow) \in [-1 : +1] \end{aligned} \tag{III.54}$$

The energy E is defined up to a constant and should be multiplied by a factor 2δ that is dropped here for convenience. Let us define the thermal average $\langle ... \rangle$. In the ordered phase, $\langle n_\uparrow \rangle = 1$, $\langle n_\downarrow \rangle = 0$, $\langle n_o \rangle = 0$ (we arbitrarily chose the *up* configuration), while in a disordered yet constrained phase, $\langle n_\uparrow \rangle = 1/6$, $\langle n_\downarrow \rangle = 1/6$, $\langle n_o \rangle = 2/3$.

In figure III.15 we show the probability distribution function (PDF) $P(M)$ calculated numerically from the loop algorithm at $T = T_c$. In a mean field-like system, its behaviour should reproduce the shape of the free energy with respect to the mean value of the magnetisation M, as $P(M) \propto \exp(-\beta G(M))$ in a mean field approach.

The data show strong evidence for $P(M)$ being completely flat in the thermodynamic limit. For small cubic system size, $P(M)$ looks flat over the major part of the domain, becoming rounded, as M approaches ± 1. For $N = 4000$ spins we have reduced the statistical noise in the interval $-0.7 < M < 0.7$ to $\Delta P/P < 10^{-3}$. We shall see from the mapping onto the quantum phase transition that the multi-criticality is rigourously obtained in the limit $L_z \gg L_\perp^2$. We have therefore plotted the same PDF of M for small perpendicular size and a very long vertical one (see second panel of figure III.15). The effect is even more dramatic than for a cube as we discover a perfectly flat PDF without rounding close to saturation. The distribution is flat within this resolution and there is no curvature that would indicate a 1st order transition. Increasing the system size increases the noise, but as can be seen from the figure, the function appears to approach the flat form predicted for the BL: $P(M) = 0.5, \quad -1 < M < 1$ and zero elsewhere. For finite system size, it will be useful to model $P(M)$ by a rectangular function

$$P(M) = \begin{cases} 1/2 + \varepsilon_N & \text{if } |M| \leq (1 - \lambda_N) \\ 0 & \text{if } |M| > (1 - \lambda_N) \end{cases} \tag{III.55}$$

From normalization conditions we find $\lambda_N = 2\varepsilon_N/(2\varepsilon_N + 1)$.

As a first consequence of the multi-criticality, the numerical dynamics become sluggish because a numerical loop takes an arbitrary long time to close on itself: since all sectors of M are equiprobable, a single loop move of the Worm algorithm can connect two microsates with very different magnetisation, requiring a extremely long numerical loop spanning the system many times through periodic boundary conditions. Furthermore in order to measure quantitatively the flatness of $P(M)$, one needs very good statistics with a very long Monte-Carlo time. This is why although millions of spins can be simulated for all other temperatures, we can only afford a typical number of 4000 spins at T_c

In figure III.16 we show a parametric plot of E vs M at the transition. The curve is parabolic and can be fitted accurately by

$$E = -A_N \, - \, (1 - A_N)M^2, \tag{III.56}$$

where A_N is a size dependent constant. From this, taking $P(M)$ as defined in equation (III.55) on the flat region, we can estimate the probability density $P(E)$:

$$P(E) \, = \, \frac{1/2 + \varepsilon_N}{\sqrt{1 - A_N}} . \frac{1}{\sqrt{-A_N - E}}. \tag{III.57}$$

This is compared with numerical data in figure III.17 for $N = 32000$ spins. The agreement is excellent away from the limit $E = -1$ where the approximation "$P(M) = \text{cst}$" breaks down. A first order transition would show up here as a double peaked structure and this is clearly not present, giving further evidence that the pyrochlore system has the same multi-critical behaviour as the Husimi tree.

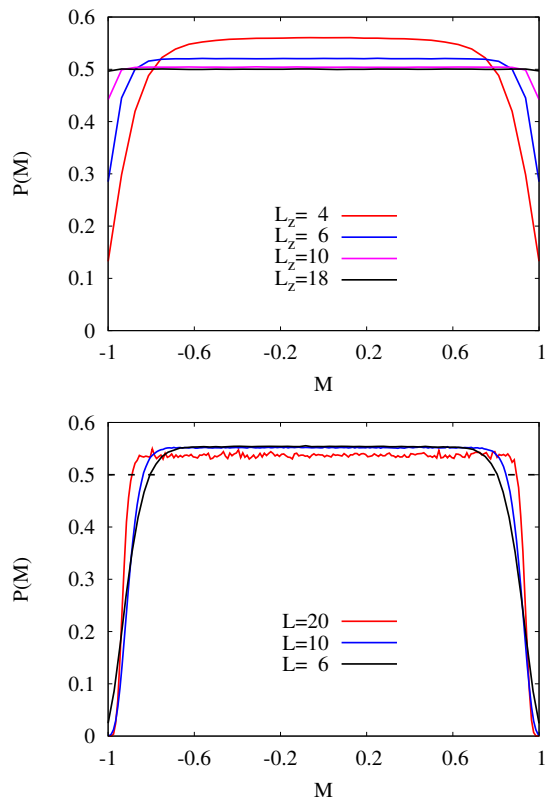

Figure III.15: **Equiprobability of the sectors:** Normalised probability distribution function (PDF) of measuring a given value of the magnetisation M. *Top:* $L_\perp$ is fixed at 4 tetrahedra while L_z is increased to reach the limit $L_z \gg L_\perp$ where the PDF is flattened. *Bottom:* The sample has a cubic shape $L = L_\perp = L_z$. The dashed line represents the expected flat probability at 0.5. The curve for $L = 20$ remains noisy because of a lack of statistics due to the large size of the system. We recover a flat PDF except close to saturation.

Finally, putting equation (III.54) into (III.56) and averaging over all M leads to an estimate for the thermal averages in the thermodynamic limit

$$\begin{aligned} \langle n_o \rangle &= \frac{1-A_N}{2}\left(1-\frac{(1-\lambda_N)^2}{3}\right) \\ \langle n_\uparrow \rangle = \langle n_\downarrow \rangle &= \frac{1}{4}\left((1-A_N)+(1+A_N)\frac{(1-\lambda_N)^2}{3}\right) \end{aligned} \tag{III.58}$$

By measuring A_N, λ_N, we obtain the same result as direct simulations on system sizes up to 3.10^5 spins, *i.e.* $\langle n_{o,\uparrow,\downarrow} \rangle \approx 0.333 \pm 0.005$. In the thermodynamic limit, we expect A_N, $\lambda_N \to 0$ and thus

$$\boxed{P(M) = 1/2, \quad E = -M^2, \quad P(E) = \frac{1/2}{\sqrt{-E}}, \quad \langle n_{o,\uparrow,\downarrow} \rangle = 1/3} \tag{III.59}$$

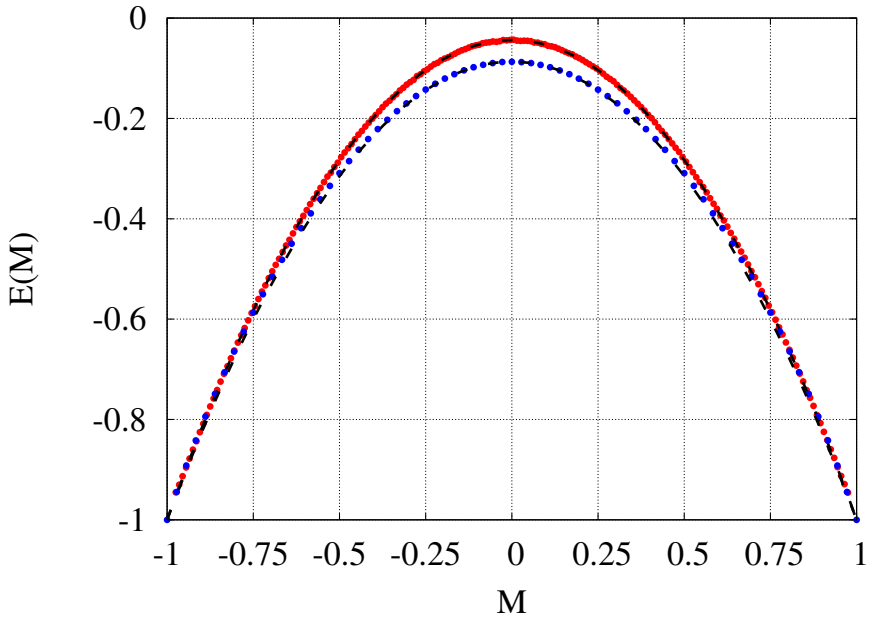

Figure III.16: **Energy E vs magnetisation M** for $N \simeq 16000$ spins (blue) and $N = 256000$ spins (red, above the blue curve). The dashed lines are a fit to the parabola (III.56).

This result is at first sight surprising, because it differs from the Husimi tree where $\langle n_o \rangle = 1/2$, $\langle n_{\uparrow,\downarrow} \rangle = 1/4$ (see below equation (III.37)), whereas both numerical and analytical entropies are equal at T_c^+ (see figure III.12). It would indeed be a remarkable coincidence that the hexagonal loop correlations missing in the Husimi tree could justify this discrepancy for two systems with the same flat free energy and entropy. The explanation comes in fact from the scaling limit of the tetrahedron density above T_c. Figure III.18 shows $\langle n_o(T > T_c) \rangle$ for different system sizes. As N increases, $\langle n_o \rangle$ approaches $1/2$, as $T \to T_c$. Defining $T_c(N)$ as the temperature for which $\langle n_o(N) \rangle = 1/2$, we find a power law scaling for the reduced temperature $t_0 = (T_c(N) - T_c)/T_c \sim N^{-\alpha}, \quad \alpha \approx 0.41$, as shown in the inset of figure III.18[7]. Hence in the thermodynamic limit $\langle n_o \rangle$ jumps discontinuously from 1/2 to 1/3.

Hence numerical analysis of the $3d$ spin ice system confirms our results from the Husimi tree, but as previous work by Lieb [Lie67a] and Nagle [Nag69] have shown the possibility to study this model exactly, we have endeavoured to construct a rigourous proof of its multi-critical nature, with the satisfaction to discover it was possible to implement the $3d$ structure of the pyrochlore lattice.

[7]We do not have an explanation for the value of this exponent. To understand it requires additional work.

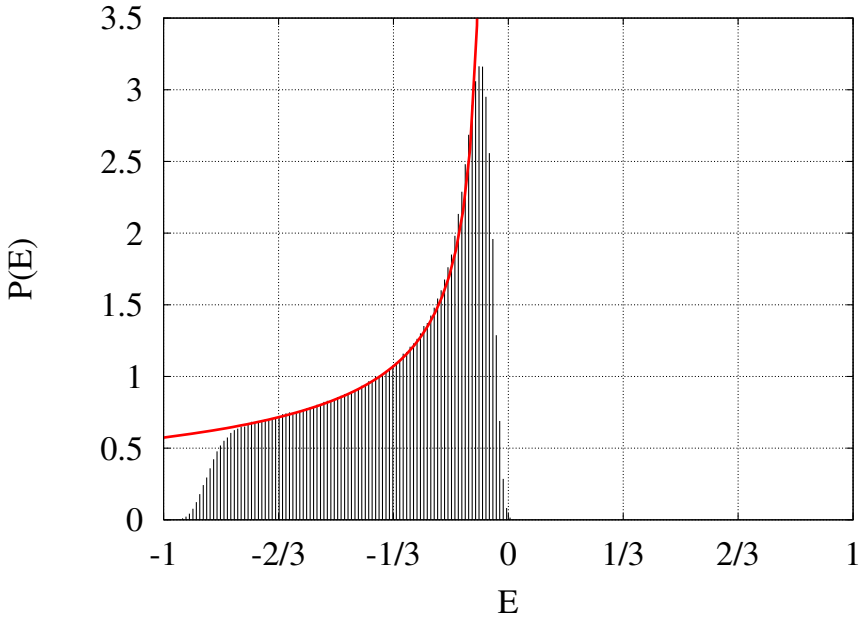

Figure III.17: **Probability distribution of the energy $\mathbf{P}(\mathbf{E})$** for $N \simeq 32000$ spins averaged over 9.10^6 loops. The red curve is a fit of equation (III.57).

III.4.c Rigourous proof: Transfer Matrix method

We have generalised the $2d$ transfer matrix method introduced in the precedent chapter II.5 for the $3d$ pyrochlore lattice, following the technique developped in [Pow08] where the authors constructed an effective hopping Hamiltonian characterising the Kasteleyn transition in spin ice. Here we shall nevertheless follow a different approach, considering the exact classical Hamiltonian on the constrained manifold as the symmetry of our problem allows a rigourous treatment.

We shall at first define the mathematical notations and present the Perron-Frœbenius (PF) theorem, an essential tool to determine the maximal eigenvalue of non-negative matrices. We shall then prove the necessary hypotheses of this theorem before discussing the physical interpretation of our result. Most of the mathematical theorems used here are extracted from the very detailed book by Minc on "Non-Negative Matrices" [Min88] while some definitions come from the "Handbook of Matrices" by Lütkepohl [L96].

Definitions

Our goal is to define a transfer matrix $\mathcal{T}$ that connects a layer in the (x, y) plane (or (001) plane) with N spins to the one just above[8]: the z direction is equivalent to an imaginary time for the quantum critical point (see [Pow08] and figure III.19). As presented in II.5,

[8]Now N represents the number of spins in a plane, not in the whole system. In general, most of the reasoning in this subsection will be made for $2d$ layers, the third dimension being recovered by piling the (001) planes up.

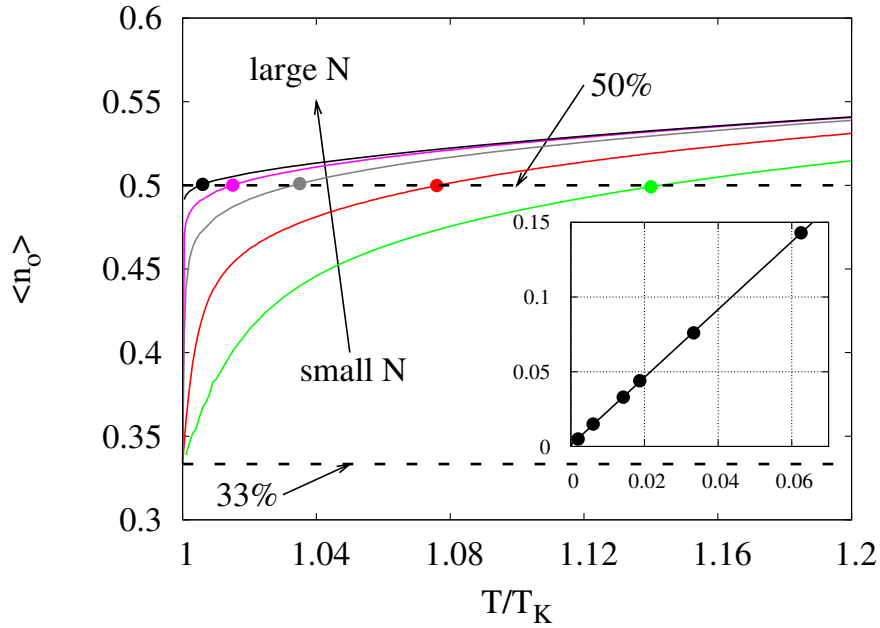

Figure III.18: **Density of tetrahedra:** Evolution of $\langle n_o \rangle$ with report to T/T_{K} obtained with the Worm algorithm for different sizes of the system: $N = \{864, 4.10^3, 3.210^4, 2.5610^5, 4.10^6\}$. The dashed line gives the 1/3 value at $T = T_{\mathrm{K}}$. The inset gives the evolution of the reduced temperature $(T_c(N) - T_c)/T_c$ as a function of $N^{-\alpha}$.

the coefficient $\mathcal{T}_{i,j}$ is the Boltzmann weight (or non-normalized probability) to go from configuration i on layer z to configuration j in the upper plane $z+1$. But since we are in a pyrochlore lattice, the upper plane is not directly above the one below, rather there is a rotation of $\pi/2$ [Pow08]. We can thus only recover the same lattice structure after four steps and it will be useful to consider the matrix $\mathcal{T}^4$ (see figure III.19).

From a mathematical point of view, the matrix $\mathcal{T}$ is an endomorphism since the image of the set of possible configurations $\mathcal{E}$ by action of $\mathcal{T}$ remains in the same set $\mathcal{E}$. This means that we are going to perform a reduction of endomorphism by considering the diagonal blocks $\mathcal{T}_\ell$ that describe the possible evolution of a configuration of ℓ strings from one plane to the next (see the matrix below).

$$\mathcal{T} = \begin{pmatrix} \boxed{\mathcal{T}_1} & & & \\ & \boxed{\mathcal{T}_2} & & \\ & & \ddots & \\ & & & \boxed{\mathcal{T}_\ell} & \\ & & & & \ddots \end{pmatrix}$$

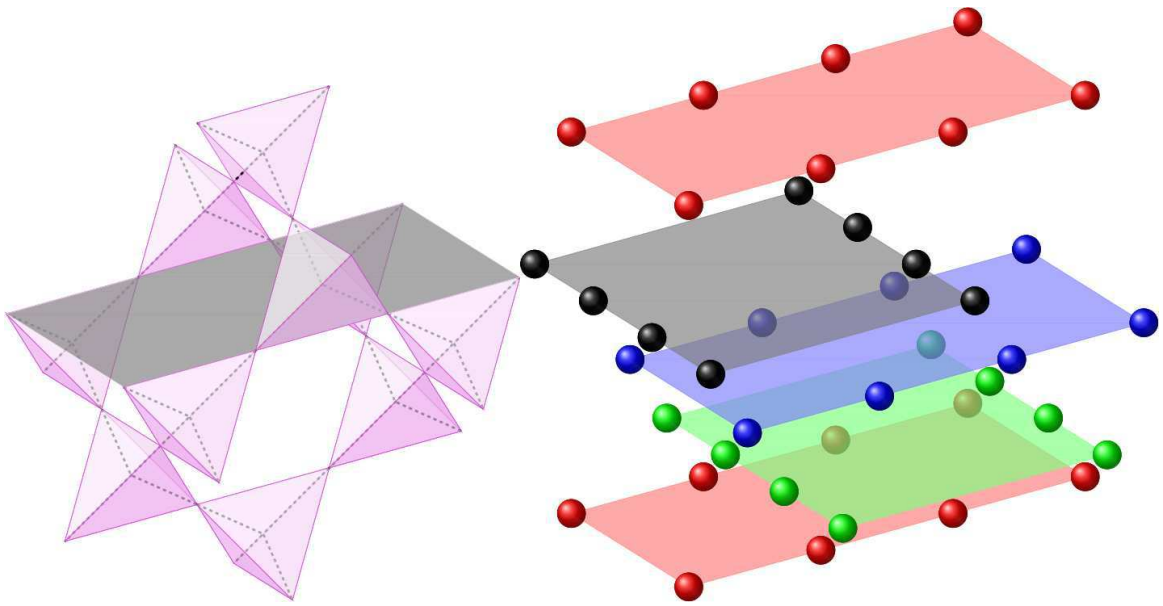

Figure III.19: **3d Transfer Matrix:** *Left:* The pyrochlore lattice where a (001) plane is depicted. *Right:* the pyrochlore lattice seen as a stack of (001) planes rotated by an angle of $\pi/2$: we recover the same plane after 4 steps. Each layer is a distorted square lattice with nearest neighbour distance r_{nn} in one direction and $2\,r_{nn}$ in the orthogonal one (see figure I.8 for the notation).

This reduction is only possible because the number of strings is conserved along the z direction in absence of topological defects; a string cannot be divided (and forms a ramification), nor can it melt itself into another one. The dimension of the subspace or sector $\mathcal{E}_\ell$ defined by a block T_ℓ is the number of ways to place ℓ indistinguishable strings among N sites, *i.e.* C_N^ℓ. If we label each site by an integer $r = 1..N$, it is then possible to define a configuration R_ℓ by the set of positions $[r_1, r_2, ..., r_\ell]$ where the strings crosses the plane. R_ℓ is of course a vector of $\mathcal{E}_\ell$, and the C_N^ℓ possible combinations of R_ℓ form a orthonormal basis of $\mathcal{E}_\ell$.

We can now define our model, using the same Boltzmann factors as in the $2d$ case :

- a tetrahedron with no strings has a weight of 1;
- a tetrahedron with 1 string has a weight of $\Gamma = e^{-\beta\epsilon}$ where $\epsilon = 4\delta$;
- a tetrahedron with 2 strings has a weight of 1.

Since this model respects a $\mathbb{Z}_2$ symmetry by flipping all the spins at once, the results should be the same for ℓ or $N - \ell$ strings. We shall thus only consider the matrices with $\ell \leq N/2$. Because of the structure of the unit cell of a pyrochlore lattice, N is always even.

Although the analytic expression of the eigenvalues for all sectors is tractable in $2d$ using the Bethe Ansatz [Lie67a], it turns out to be technically impossible (as far as we know) in $3d$. However in the limit $L_z \to \infty$, the maximal eigenvalue is the only relevant

one (see section II.5) and is computable using (a version of) the Perron-Frœbenius (PF) theorem :

Theorem: If a square matrix $\mathcal{T}$ of size n and coefficients $\mathcal{T}_{ij}$ is **non-negative**, **irreducible** and **primitive**, then there exists a *unique* positive maximal eigenvalue λ_{max} ($\forall$ eigenvalue $\lambda \in \mathbb{C}$, $|\lambda| < \lambda_{max}$), such that

$$\min_i \left(\sum_{j=1}^{n} \mathcal{T}_{ij} \right) < \lambda_{max} < \max_i \left(\sum_{j=1}^{n} \mathcal{T}_{ij} \right) \tag{III.60}$$

where the " $<$" sign becomes " $=$" if the minimum row sum is equal to the maximum one. The corresponding eigenspace is of dimension 1 and λ_{max} is a simple root of the characteristic polynomial.

First of all, we need to prove the different hypotheses of this theorem: the first one (non-negative) is trivial, since the coefficients of $\mathcal{T}$ are Boltzmann weights, they must be real and non-negative, but the proof of irreducibility and primitivity is a more subtle task.

Proof of the irreducible and primitive character

If all coefficients $\mathcal{T}_{ij}$ were strictly positive, the problem would be immediately solved. Unfortunately most configurations of two successive layers cannot be connected and $\mathcal{T}_{ij}$ can be equal to zero. We thus need to use another theorem:

Theorem : A necessary and sufficient condition for a non-negative matrix $\mathcal{T}_\ell$ to be irreducible and primitive is that $\mathcal{T}_\ell^k$ be positive for some positive integer k.

A physical interpretation of this condition is that from any initial configuration with ℓ strings, after a finite number of steps k in the z-direction, *all* configurations with ℓ strings are probable. This condition may look evident; if we consider a single string, since its evolution is a random walk in $2d$, then we can see that after a necessary finite time t (or step k) the string can go through any possible site, as long as the perpendicular size of the system in the (x, y) plane is finite. However its generalization with ℓ strings is rather tedious, essentially because the pyrochlore lattice is not a superposition of identical $2d$ lattices. The demonstration is illustrated with the following figure III.20.

This figure shows a 2d projection of four consecutive layers if one looks towards the z-direction ; the 5th layer is thus the same one as the first (red) one (see figure III.19 for a $3d$ version). On the left, we simply enumerate the way we arbitrarily chose to index the sites on each plane. It is important that the numbering remains the same on each layer after a clockwise rotation of $\pi/2$, as this is the condition to have the same expression for the transfer matrix $\mathcal{T}$ between each plane !

Let us consider an initial configuration $R_\ell = [r_1, r_2, ..., r_\ell]$ on the first (red) layer. Each site is paired with one of its neighbours (see the ellipses on the figure on the right) because they are part of the same tetrahedron in the 3d pyrochlore lattice. Thus, if each string

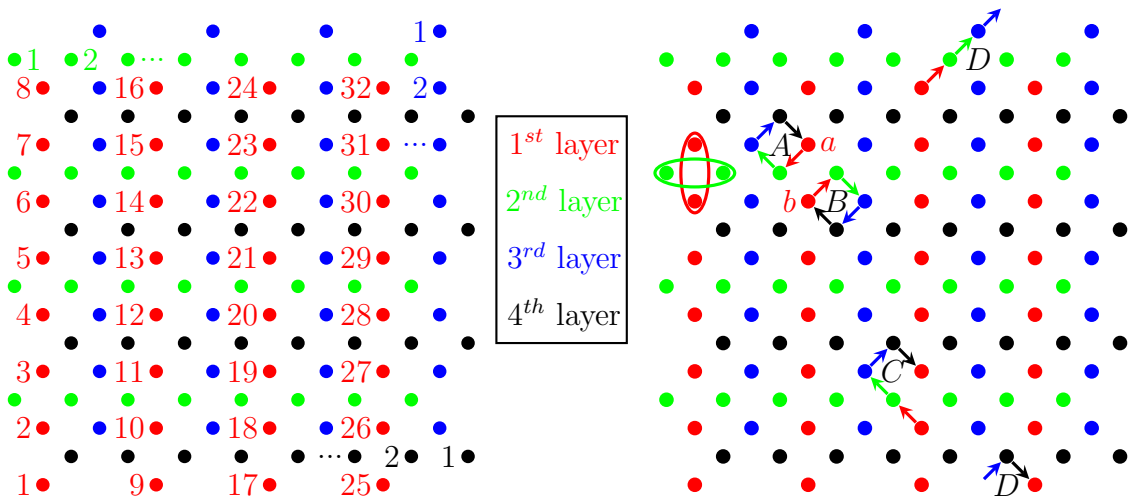

Figure III.20: **2d projection of the pyrochlore lattice:** Each site represents a spin and each color is a different layer. The $2d$ projection of a tetrahedron is given by the ellipses on the right panel.

going through a site a (resp. b) follows the clockwise spiral path A (resp. B), then we can recover the same configuration after 4 steps, because two strings will then never be in the same site at the same time during this process (which would be impossible). In fact, there are many different ways to remain in the same configuration after 4 steps, but here we only want to prove that there is always at least one. Since $\ell \leq N/2$, the plane is not completely filled with strings and there always exists a site r_j such that $r_j + 1$ is not part of the vector R_ℓ (see the numbering on the left figure). By following path C (or D because of periodic boundary conditions), r_j can go to $r_j + 1$ in 4 steps while the $\ell - 1$ other strings can end up on the same position following a spiral of type A or B, *without* crossing each other on the same site at the same "time". Thanks to the periodic boundary conditions, it is easy to show that by changing a site r_j into $r_j + 1$ every 4 steps, a vector R_ℓ can become any possible configuration after a finite number of k steps, where k is a multiple of 4 in our argument. Since there is a finite probability to remain in the same configuration after 4 steps, all the possible configurations become probable after k_{max} iterations; thus $\left(\mathcal{T}^{k_{max}}\right)_{ij} > 0 \, \forall i, j$. Hence $\mathcal{T}$ is irreducible and primitive !

Critical transition of ∞-order

Now that we can use the Perron-Frœbenius theorem (III.60), we need to calculate the row sums for each of the diagonal blocks of the transfer matrix. We can define for each configuration, ℓ_1 (resp. ℓ_2) the number of strings which are going to enter alone (resp. by pair) in a tetrahedron, giving $\ell = \ell_1 + \ell_2$ with ℓ_2 even. According to our model, the energy cost of such a configuration is $\ell_1 \, \epsilon$. If a tetrahedron is spanned by two strings, then both spins on the upper layer are necessarily *down*, whereas a single string leaves two possibilities. It means that the row corresponding to a given configuration or vector

contains 2^{ℓ_1} terms which are all equal to $\Gamma^{\ell_1} = e^{-\beta\,\ell_1\,\epsilon}$: its sum then gives $(2\Gamma)^{\ell_1}$. Whether 2Γ is larger or smaller than 1, this sum diverges or goes to zero with ℓ_1. We can then define a critical temperature $T_c = \dfrac{\epsilon}{\ln 2} \Leftrightarrow 2\Gamma|_{T_c} = 1$ such that :

- $\forall\, T < T_c$, $(2\Gamma)^{\ell} < \lambda_{max} < (2\Gamma)^0 = 1$: the maximal eigenvalue of any sector is vanishing in the thermodynamic limit except for $\ell = 0$. The partition function is $\mathcal{Z}(L_z \to \infty) = 1$ corresponding to the frozen state with no strings and saturated magnetisation.
- for $T = T_c$, $\lambda_{max} = 1$, $\forall \ell$: the maximal eigenvalue corresponds to an eigenspace of dimension 1 and is the same for all sectors: **all sectors are equiprobable in the limit** $L_z \to \infty$, whose direct consequence is a flat free energy for all values of the magnetisation. The transfer matrix is stochastic (and even ergodic, see definition in [L96]), which means that the corresponding eigenvector is $(1, 1, ..., 1)$ and hence **all configurations within a given sector are also equivalent**. These are the central results of our demonstration.
- $\forall\ T > T_c$, $1 < \lambda_{max} < (2\Gamma)^{\ell}$: the maximal eigenvalue for any non-zero number of strings is bigger than the one corresponding to the fully saturated state. The system is able to relax.

If ℓ is odd, we can replace the 1 by 2Γ in the above inequalities, but it does not make any difference in the result. Above T_c the block matrix with $N/2$ strings and zero magnetisation has the highest upper boundary and is thus the most reliable candidate to have the highest maximal eigenvalue, but our method is not sufficient to prove it. The perpendicular size of the (001) planes can be taken as large as desired but must remain finite in order to ensure irreducibility and primitivity of the matrix $\mathcal{T}$ and the specific nature of this transition thus only appears when $L_z \gg L_\perp$.

A comment on the diagonalisability

Since the transfer matrix is not real and symmetric, it is not clear if it is diagonalisable or not; in fact a rapid check for the simplest non-trivial case $N = 8$ and $\ell = 1$ shows $\mathcal{T}$ is not diagonalisable. However as for any real matrix, $\mathcal{T}$ is similar to a matrix J in Jordan form with complex numbers (see equation (III.61)). Hence $\mathcal{T}^k$ and J^k are also similar and the

trace being similarity-invariant, we have the partition function $\mathcal{Z}_k = \mathrm{Tr}\left(\mathcal{T}^k\right) = \mathrm{Tr}\left(J^k\right)$.

$$T \sim J \equiv \begin{pmatrix} J_1 & & & & \\ & J_2 & & 0 & \\ & & \cdot & & \\ & & & \cdot & \\ & 0 & & J_i & \\ & & & & \cdot \end{pmatrix} \quad \text{where} \quad J_i \equiv \begin{pmatrix} \lambda_i & 1 & & & 0 \\ & \lambda_i & 1 & & \\ & & \cdot & \cdot & \\ & & & \cdot & 1 \\ 0 & & & & \lambda_i \end{pmatrix} \tag{III.61}$$

By definition of the Jordan matrix, the diagonal terms of J^k must be λ_i^k where λ_i is one of the eigenvalues of J. Additionally since the maximum eigenvalue λ_{max} is a simple root of the characteristic polynomial of $\mathcal{T}$ (see PF theorem), and thus of J, there is one and only one Jordan block of size 1 with eigenvalue λ_{max}, all the other Jordan blocks having diagonal terms strictly smaller than λ_{max}. This proves that even if $\mathcal{T}$ is not diagonalisable, we have the following partition function for a system of k vertical layers

$$\mathcal{Z}_k = \mathrm{Tr}\left(\mathcal{T}^k\right) = \lambda_{max}^k + \sum \lambda_i^k \tag{III.62}$$

where the first term is dominant in the limit $k \to \infty$. As mentioned above, J can have complex coefficients but since $\mathcal{T}$ is a real matrix, each complex eigenvalue is paired with its conjugate and the global trace remains of course real.

Physical Insight

We have tried to be as rigourous as possible here but it may have been at the expense of clarity. This is why we shall try to summarize our method from a more physical point of view. The only energy excitation above the fully saturated ground state is the apparition of tetrahedra spanned by a single string, and *all* tetrahedra contribute to the same entropic gain, *i.e.* $T \ln 2$. This is the crucial difference with the Kasteleyn transition where tetrahedra occupied by two strings bring another energy level (see figure II.2) and no entropy. Hence at the transition when the unique entropic scale ($T_c \ln 2$) cancels the unique energy excitation (4δ), all types of tetrahedra, all sectors and all configurations within a sector become equivalent: this is why the maximum eigenvalue for each sector is the same and corresponds to a "uniform" eigenvector $(1, 1, ..., 1)$. Additionally the pyrochlore lattice is "ergodic" in the sense that any two configurations of $2d$ (001) layers within the same sector (*i.e.* crossed by the same number of strings) can be connected given a long enough vertical separation between them (or long enough "imaginary time to diffuse"): this is why the matrix is irreducible and primitive and the maximum eigenvalue is unique, preventing the promotion of one sector over another one.

Extension to other models

The Kasteleyn transition does not have this *up/down* symmetry which is the reason why the transition is different, and why a small but finite magnetic field immediatly lift the multi-critical point. However the same argument can be carried out and proves that the system remains frozen until T_K and can relax for higher temperature.

The 6-vertex model on a pyrochlore lattice is of course special because it describes real systems such as KH_2PO_4 or spin ice, but from a statistical point of view, it is interesting to note that this argument can be generalised for a more general (but less realistic) class of vertex models. Let us for example consider a lattice of vertices with p legs (p is even and equals 4 for KDP) in d dimensions. The transfer matrix will now connect the degrees of freedom of two consecutive hypersurfaces of $d-1$ dimensions. A first requirement is to have what we shall call an *ergodic* lattice, which means that any two configurations are related by a finite number of steps and ensures the hypotheses of irreducibility and primitivity of the transfer matrix. This is true for the square or checkerboard lattice in $2d$ or the cubic lattice in $3d$. This condition is useful for the application of the full version of the PF theorem, but the important point is for the matrix to be stochastic at a certain temperature T_c. Let us note ℓ_i the number of vertices crossed by i strings in a given configuration ($i = 0, \ldots, p/2$). For each vertex, there are $C^i_{p/2}$ combinations for i strings to go out, which gives $\prod_{i=0}^{p/2} \left(C^i_{p/2}\right)^{\ell_i}$ possible configurations for the entire hypersurface. Let us define ϵ_i the energy of a vertex spanned by i strings and Γ_i the corresponding Boltzmann weight. The total energy of a given hypersurface is

$$E_{hs} = \sum_{i=0}^{p/2} \ell_i \epsilon_i \tag{III.63}$$

and the sum of the coefficients in a column of this transfer matrix is

$$\left(\prod_{i=0}^{p/2} C^i_{p/2}\right)^{\ell_i} \exp\left(-\beta \sum_{i=0}^{p/2} \ell_i \epsilon_i\right) = \prod_{i=0}^{p/2} \left(C^i_{p/2}\, \Gamma_i\right)^{\ell_i} \tag{III.64}$$

Thus if the energy of a vertex is $\epsilon_i = T_c \ln C^i_{p/2}$ which makes zero for 0 or $p/2$ strings, then the transfer matrix is stochastic at T_c ! This condition looks quite peculiar, but in the case of the cubic lattice with $p = 6$ legs[9], we can define a single energy ϵ corresponding to one or two strings and we will obtain the same kind of KDP transition at $T_c = \epsilon / \ln 3$. This model has been studied by Ellout & Maaskant [Elo95] who showed that the transition was discontinuous using the same method as Nagle in [Nag69], but now we are in a position to expose the true multi-critical nature of this transition.

This method is very efficient since it enables us to study the so-called *inverse* KDP model introduced by Wu [Wu68] and Glasser [Gla69], where we consider $\epsilon < 0$. We immediatly see that the maximal eigenvalue is now always strictly larger than 1 (since

[9]The transfer matrix then connects two successive layers orthogonal to the [111] direction.

$2\Gamma > 2$) and the transition has disappeared, as predicted by Wu and proved by Glasser in $2d$. This is easy to see from a Kasteleyn argument, as there is no competition between entropy and energy.

This transfer matrix method can also be used in order to study the quantum analogue of the KDP model that allows among other things the extraction of analytical expression for the correlation functions, as for the Kasteleyn transition [Jau08, Pow08].

III.4.d Mapping onto a quantum phase transition

The calculations in this subsection have been performed by J.T. Chalker and are reproduced in this thesis for the purpose of completeness. Furthermore from these results, we managed to justify the multi-criticality not only in the limit of infinite vertical size L_z, but also in the "cubic" thermodynamic limit with $L_\perp = L_z$.

This method follows Lieb's original idea of 1967 [Lie67a] who mapped the $2d$ KDP model onto the XXZ Heisenberg chain that had been solved the year before by Yang & Yang [Yan66]. The same analogy can be carried out on our $3d$ system mapping onto the $2d$ XXZ Heisenberg ferromagnet with spin operators 1/2

$$\mathcal{H} = -\sum_{\langle i,j \rangle} J \left(\hat{s}_i^x \hat{s}_j^x + \hat{s}_i^y \hat{s}_j^y \right) + D\, \hat{s}_i^z \hat{s}_j^z \tag{III.65}$$

where the z-axis is taken as the imaginary time for the propagation of strings. Even if the details of the pyrochlore lattice can be implemented [Pow08], a more straightforward calculation on the square lattice with N sites is sufficient for obtaining an insight of this quantum phase transition that occurs at the isotropic Heisenberg point with $SU(2)$ symmetry when $D = J$, between the Coulomb phase with $U(1)$ symmetry ($D < J$ at high temperature T for the classical model) and the frozen phase ($D > J$ at low T). If we define the Fourier transform as

$$S_{\mathbf{k}}^\alpha = \sum_i \hat{s}_i^\alpha e^{-i\mathbf{k}\cdot\mathbf{r_i}} \tag{III.66}$$

where α is a cartesian coordinate and $\mathbf{k}$ is a $2d$ wave vector, then equation (III.65)can be rewritten at the critical point $J = D$

$$\mathcal{H} = \frac{1}{N} \sum_{\mathbf{k}} \epsilon(\mathbf{k}) \left(\frac{1}{2} \left(S_{-\mathbf{k}}^- S_{\mathbf{k}}^+ + S_{-\mathbf{k}}^+ S_{\mathbf{k}}^- \right) + S_{-\mathbf{k}}^z S_{\mathbf{k}}^z \right) \tag{III.67}$$

with

$$\epsilon(\mathbf{k}) = -\frac{J}{2} \sum_\delta e^{-i\mathbf{k}\cdot\delta} \tag{III.68}$$

where δ denotes the vector between nearest neighbours. Let $S(S+1)$ and M be respectively the eigenvalues of $S^2 = \sum_\alpha \left(\sum_i s_i^\alpha \right)^2$ and $S^z = \sum_i \hat{s}_i^z = S_{\mathbf{k=0}}$ where $0 \leqslant S \leqslant N/2$

and $-S \leqslant M \leqslant S$. One of the ground states is $|S = N/2,\, M = N/2\rangle$ with all spins aligned along the z-axis. Since $\left[\mathcal{H}, S_{\mathbf{0}}^{-}\right] = 0$, all eigenvectors $|S = N/2,\, M = -N/2 \cdots N/2\rangle$ have the same zero energy: a spin flip in the $2d$ quantum system is analogue to a string in the $3d$ statistical problem and represent different sectors of the magnetisation. But this analogy allows us to go beyond our precedent result and *e.g.* study the scaling limit for a system of size $L_\perp \times L_\perp \times L_z$.

The first possible excitation is a single magnon state of energy

$$E(\mathbf{k}) = \epsilon(\mathbf{k}) - \epsilon(\mathbf{0}) \propto |\mathbf{k}|^2 \tag{III.69}$$

Its Boltzmann weight is $e^{-E(\mathbf{k})\cdot L_z}$ and since the smallest value of $|\mathbf{k}|$ is $\sim 1/L_\perp$, we need very anisotropic samples $L_z \gg L_\perp^2$ to suppress it. This explains why the probability distribution function (PDF) of the magnetisation is perfectly flat for a finite rectangular system.

However following a similar reasoning, we managed to generalise this argument for cubic systems and to explain why the PDF of M becomes rounded close to $M = \pm 1$ (see figure III.15). To do so, we assumed the absence of interactions between magnons, which allows an estimate of the energies

$$E_\eta \approx E_{\mathbf{q}_1} + ... + E_{\mathbf{q}_\eta} \tag{III.70}$$

where η is the number of magnons in the excitation. The important point is that within this approximation where we neglect magnon-magnon interaction, this energy only depends on the wavevectors of the magnons and their number η. Hence the energy spectrum is *almost* the same for all sectors, but with the crucial difference that a sector with n strings allows excitations with up to n magnons. Since $E_{\mathbf{q}} \approx \alpha\, k^2$ for small $\mathbf{k}$, the minimum excitation for η magnons is $E_\eta^{min} \approx \eta\ \alpha'/L_\perp^2$. The contribution for such excited states is then proportional to

$$\exp\left(-\alpha'\ \frac{\eta\, L_z}{L_\perp^2}\right) \tag{III.71}$$

For a cube in the thermodynamic limit ($L_\perp = L_z = L \gg 1/\alpha'$), multi-magnon excitations with $\eta \gg L$ become negligible according to equation (III.71). We can consider that **all sectors with a number of strings $n \gg L$ have access to the same energy spectrum and are then equiprobable.** This cut-off is similar to a Fermi level, except that it is not due to a particle number here but to the macroscopic size of the excitations leading to a macroscopic gap for some multi-magnon excitations. Since the magnetisation is $M = (N - 2n)/N$, where N is the number of spins in a (001) plane, the equiprobability is valid for

$$M \in \left[-1 + \frac{2}{\sqrt{N}}\ ;\ 1 - \frac{2}{\sqrt{N}}\right] \tag{III.72}$$

The domain of non-validity then disappears in the thermodynamic limit. This argument, even though it is approximate, is in qualitative agreement with figure III.15 and suggest **the possibility to observe such a transition in a spherical crystal** where all three directions have the same size.

Calculation of the correlation

Even if we might recover the multi-critical point of $\infty-$order for a cubic system in the thermodynamic limit, we must consider the anisotropic limit $L_z \gg L_\perp^2$ in order to calculate an analytical estimate of the two-points spatial correlation

$$\boxed{C(r_\perp, z) \propto \frac{1}{z}\ \exp\left(-\frac{r_\perp^2}{\zeta\, z}\right)} \tag{III.73}$$

where z and $r_\perp$ are respectively the distance along the [001] direction and in the (001) plane. ζ is a length characteristic of the microscopic details of the model. The inherent anisotropy of our problem provokes three distinct behaviours in the correlation:

- $r_\perp > 0$, $z \to 0$: $C \to 0$, there are no correlations between strings in the plane;
- $r_\perp = 0$, $z > 0$: $C \propto 1/z$ is the signature of the self-interaction of diffusive strings;
- $r_\perp > 0$, $z > 0$: the correlations decrease exponentially fast away from the [001] direction with a typical correlation length $\xi \sim \sqrt{z}$ characteristic of a $2d$ random walk.

It is intriguing to recover the same kind of correlation as for the Kasteleyn transition in diluted regime (close to the critical point, see [Jau08, Pow08]). This is because in the latter, the strings are far enough from each other to avoid contact and they behave as if they were alone (self-interaction), whereas at the KDP multi-critical point, the subtle equilibrium between energy cost and entropy gain makes the strings invisible to each other; on average the surrounding of each string is like a vacuum and self-interaction is the only relevant correlation.

The absence of correlations in the (001) plane is a direct consequence of our transfer matrix results III.4.c where we proved that the eigenvector corresponding to the maximal eigenvalue is $(1, 1, \ldots, 1)$; if all configurations within a given sector are equiprobable, then it means that the orientation of the spins is randomly distributed over the whole plane and the correlation (III.50) can be easily calculated. Let us define $N_\uparrow$ and $N_\downarrow$ respectively the number of *up* and *down* spins in a plane which are conserved for all layers in the system on the constrained manifold. We have $N = N_\uparrow + N_\downarrow$ and $M = (N_\uparrow - N_\downarrow)/N$. The correlation can then be directly computed on a (001) layer

$$\begin{aligned} C(\mathbf{r}) &= \left\langle \left\{ \left(\frac{N_\uparrow}{N}\frac{N_\uparrow - 1}{N-1} + \frac{N_\downarrow}{N}\frac{N_\downarrow - 1}{N-1} \right) - \left(2\frac{N_\uparrow\, N_\downarrow}{N\,(N-1)} \right) \right\} - M^2 \right\rangle \\ &= \left\langle M^2 \frac{N}{N-1} - \frac{1}{N-1} - M^2 \right\rangle = \left\langle \frac{M^2 - 1}{N-1} \right\rangle = -\frac{2/3}{N-1} \\ &\approx -\frac{1/3}{L_\perp^2} \end{aligned} \tag{III.74}$$

$C(\mathbf{r})$ is thus indeed independent of $\mathbf{r}$ and is equal to zero apart from a negative finite size contribution, because of a *cavity*-like term, in the sense that we shall not count the correlation of the spin with itself.

III.4.e Correlations

From our discussion in subsection III.4.b and III.4.d, we expect a competition between two contributions in the correlation:

- the scaling function $C(r) = g(r) - g_{\rm MF} = g_{\rm sc}(r) \propto \frac{1}{L}\, f_2\left(\frac{r}{L}\right)$ for a $3d$ cubic system;
- the self-interaction of strings of equation (III.73) in the limit $L_z \gg L_\perp^2$.

These behaviours can be tested using the Worm algorithm.

Mean Field critical behaviour

$C(r)$ is plotted in figure III.21 for different system sizes L; here we chose $r = r_\perp$ in the (001) plane. In the upper panel, as $C(r)$ is not zero, we clearly see that this function does not follow equation (III.73) for the self-interaction of strings, as expected since we are not in the limit $L_z \gg L_\perp^2$. Hence there must be another source of correlations and the scaling on the lower panel $C(r) \cdot L$ vs r/L seems to confirm the presence of critical correlations above the upper-critical dimension $g_{\rm sc}(r)$.

However the same scaling does not hold if we consider $r = z$ in the vertical direction. This proves that our mean field arguments need to be revised by taking into account the inherent anisotropy of the system. This can be done by defining two characteristic correlation lengths: $\xi_{//} \sim t^{-\nu_{//}}$ propagating along the $z-$axis and $\xi_\perp \sim t^{-\nu_\perp}$ in the orthogonal plane. Following [Bha91b], one would expect that $\nu_\perp = 1/2$ (characteristic of a $2d$ random walk) and $\nu_{//} = 1$ representing the self-interaction of strings for the Kasteleyn transition. In this context, the new hyper-scaling relation with $\gamma = 1$ and $\beta = 0$ gives

$$\gamma + 2\,\beta = (d-1)\nu_\perp + \nu_{//} \Rightarrow d_c = 1 \tag{III.75}$$

The upper-critical dimension is then reduced by one due to the anisotropy. As the system is however homogeneous in $d-1$ dimensions and with $\nu_\perp = 1/2$ *a priori*, this might explain why the scaling form of $g_{\rm sc}(r)$ is respected in the plane.

Self-interaction of strings

Now we shall turn our attention towards longer systems with $L_z \gg L_\perp^2$. In figure III.22 is plotted the correlation function $C(r_\perp, z)$: there is indeed no correlations when $z = 0$, except for a finite size *cavity* effect (see equation (III.74)) and we clearly see an exponential decay following equation (III.73) on the left panel whose y-axis is on a log scale. Additionally there is an effective "light cone" because the discreteness of the pyrochlore lattice hinders a string to propagate on an orthogonal distance $r_\perp$ bigger than a typical length scale $\ell(z) \sim z$, *i.e.* $C(r_\perp > \ell(z), z) = 0$.

Finally, one can check the evolution of the cavity term that should scale like $1/L_\perp^2$; this is confirmed in figure III.23.

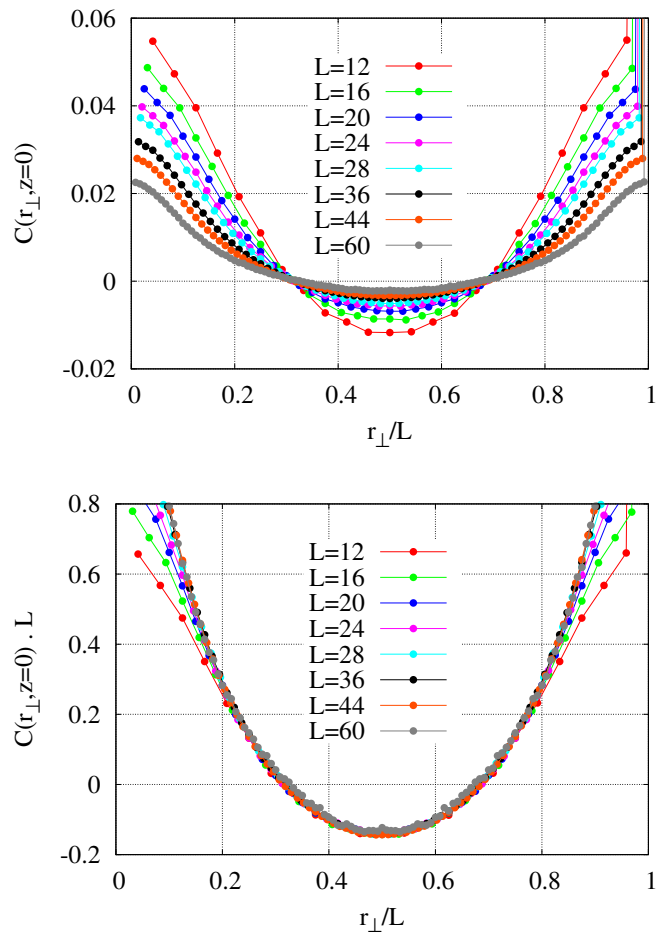

Figure III.21: **Mean Field critical correlations** for a cubic system of size L: we plot the correlation in the (001) plane as a function of $r_\perp/L$. *Top:* $C(r)$ is not zero which proves the existence of critical correlations. *Bottom:* the scaling of $C(r)$ agrees with the expected form $g_{\rm sc}(r)$.

We should add as a conclusion on this subsection on the correlations that dipolar-like correlations are still expected in the Coulomb phase for $T > T_c$.

This theoretical study of the KDP phase transition is now finished and we will use the last subsection to discuss the relevance of this phenomenon for experiments.

III.4.f Experiments

The experimental realisation of the KDP model in spin ice materials is not as straightforward as for the Kasteleyn transition where a simple magnetic field was necessary. As the required bond distortion only concerns the (001) layers, chemical disorder cannot be used. In fact the most standard realisation for this kind of distortion consists in a uniaxial pressure along the [001] axis, as moving the atoms closer or further apart will necessarily cause

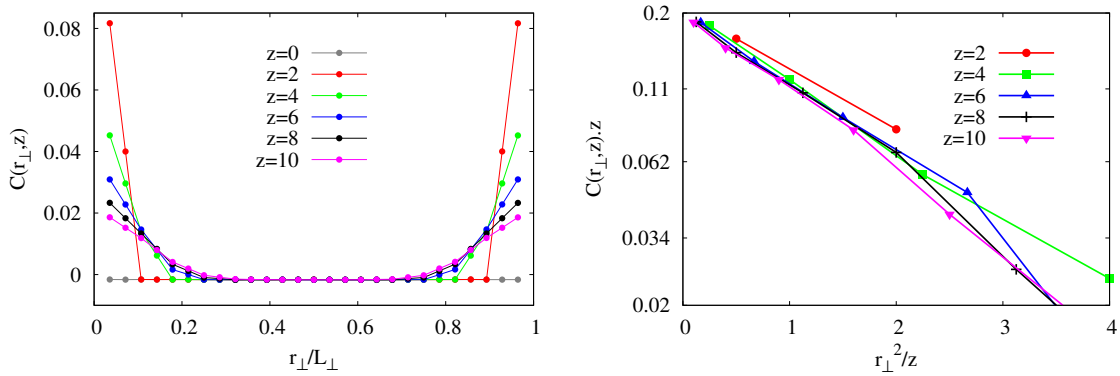

Figure III.22: **Anisotropic correlations:** The system size is $L_\perp = 14$ tetrahedra and $L_z = 196$. *Left:* Spatial correlation $C(r_\perp, z)$ vs $r_\perp/L_\perp$, the distance between two spins in the (001) plane. The different curves represent different values of $z = 0$ ($\times$), 2 ($\bullet$), 4 ($\blacksquare$), 6 ($\blacktriangle$), 8 (+), 10 ($\blacktriangledown$).The symmetry of the figure is due to periodic boundary conditions. We clearly see the two-stage process, with exponentially decaying correlations on short distances that become rigourously zero afterwards (in fact slightly negative due to finite size effects, see main text). *Right:* Zoom of the left part of the main panel to test the scaling of equation (III.73); $C \cdot z$ vs r^2/z on a log-lin scale. The result is in semi-quantitative agreement. The possible reasons of discrepancy can be the discreteness of the lattice that fails to reproduce the complexity of the continuous function (III.73) or the vertical size L_z that is not large enough (here $L_z = L_\perp^2$).

an anisotropic variation of the interactions (see figure III.24). But this raises an important question: by symmetry of the pyrochlore lattice, such pressure will affect the two fully saturated configurations along the [001] axis differently from the four others with magnetisation in the (001) plane, but will the former be *favoured or not* by applying pressure ?

This is indeed a legitimate question, as the origin of the effective nearest neighbour interaction is double (see equation (I.46))

$$J_{\text{eff}} = D_{nn} + J_{nn} = \frac{5D}{3} + \frac{J}{3} \tag{III.76}$$

Being of dipolar origin, the geometry of the pyrochlore lattice ensures a positive value of D for all possible spin ice compounds while J can vary greatly from one material to another. For Titanate-based compounds, the exchange coupling is antiferromagnetic and J is thus negative [dH00] whereas it is positive for $Ho_2Sn_2O_7$ [Kad02] and $Pr_2Sn_2O_7$ [Zho08a] (if this crystal proves to be a good realisation of the spin ice model in the future, see subsection I.3.f). However the nature of the transition requires a single crystal phase, which is not available for Stannate compounds, as a perfect $\mathcal{Z}_2$ symmetry is impossible for a powder sample, even locally. We must then deal with $D > 0$ and $J < 0$.

We will try to predict the evolution of J_{eff} with pressure, but even if computing the pressure dependence of D is feasible, it will turn out to be a very complex task for J. We

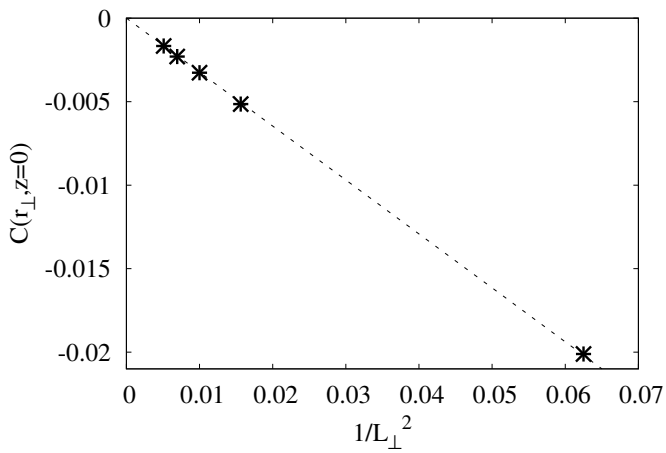

Figure III.23: **Finite size effects in the correlation:** $C(r_\perp, z = 0)$ (which is independent of $r_\perp$) as a function of $1/L_\perp^2$. The scaling of equation (III.74) is confirmed with a slope of -0.32.

shall first present our theoretical arguments and their limits, before analysing one of the only two papers on spin ice under pressure by Mito *& al.* [Mit07] that seems to confirm the relevance of uniaxial pressure.

Theoretical prediction

First of all we need to know the geometrical lattice distortion, *i.e.* if we compress along the [001] axis with an axial strain ϵ_{axial}, what will be the resulting transverse deformation ϵ_{trans} ? This is given by the Poisson ratio of the crystal

$$\nu \equiv -\frac{\epsilon_{trans}}{\epsilon_{axial}} \tag{III.77}$$

For most materials, this ratio is typically of order $0.2 - 0.5$ but ν does in fact highly depend on the experimental set-up. Following the method of [Mae00, Mit07], it is even possible to suppress the Poisson effect ($\nu = 0$) by setting the crystal in an epoxy resin that will make the transverse dilatation negligible ($\epsilon_{trans} \approx 0$).

If $L_z(P)$ is the size of the system in the [001] direction under pressure P, then we shall define the deformation parameter ϵ such that $L_z(P) = \rho\, L_z(P = 0)$ with $\rho = (1-\epsilon)$. Let us also define the anisotropic dipolar term D_x, D_y, D_z appearing in the definition of J_{eff} (III.76) corresponding respectively to the nearest neighbour bonds orthogonal to the x =[100], y =[010] and z =[001] axes. By symmetry we have $D_x = D_y$ and we want $D_x > D_z$ in order to fulfil the requirements of the KDP model with $\delta > 0$ (see Hamiltonian (III.2)). As described in figure III.24, we assume that the spins remain on the vertices of the pyrochlore lattice, pointing towards the centre of one of the two adjoining flattened tetrahedra. Following the expression of the dipolar interaction (I.44), this allows a tedious but otherwise quite easy calculation of the dipolar contribution δ_{dip}

in the bond distortion δ

$$D_z = D\,\frac{\rho^2+4}{\rho^2+2}, \quad D_x = D\,\frac{2\rho^2+3}{\rho^2+2}\sqrt{\frac{2}{1+\rho^2}}^{\,3} \tag{III.78}$$

$$\delta_{dip} = D_x - D_z \approx \frac{5D}{3}\,\frac{33}{30}\,\epsilon \sim D_{nn}\,\epsilon \tag{III.79}$$

obtained from a linear expansion valid for $\epsilon \lesssim 5\%$. δ_{dip} is thus positive as expected from a naive argument on a $1/r^3$ interaction and is directly proportional to the deformation ϵ with a factor of order unity.

On the other hand, the exchange coupling between spins is believed, within a good approximation, to decrease exponentially as a function of distance between spins [Zas77, Bra90], but a rigourous calculations of this dependence is nearly impossible for $4f$ atomic orbitals on the pyrochlore lattice. In a nutshell, we can say that both dipolar and exchange contributions get stronger for shorter distances, but the exponential antiferromagnetic exchange modification *seems* to overcome the algebraic dipolar ferromagnetic change which would then give rise to a *negative* value of δ. In this case a uniaxial pressure would result in the opposite effect that we are looking for the KDP transition, which would then require either a *bi-axial* pressure along the [100] and [010] axes, or a uniaxial *stretching* along the [001] direction; unfortunately such experiments are *a priori* non-realistic for a magnetic crystal. However we must be very cautious with this argument as we have made a very rough approximation for the distance dependence of the exchange coupling. Hopefully, the experimental paper by Mito *& al.* might give us a better hint about the influence of pressure.

Experimental analysis

As far as we know, there have only been two papers who studied spin ice under pressure. Mirebeau *&* Goncharenko studied $Ho_2Ti_2O_7$ but only in a *uniform* pressure and is thus not relevant to our problem. We should nonetheless note that this compound remains disordered down to 1.4 K and up to 6 GPa, as opposed to the potential quantum spin ice material $Tb_2Ti_2O_7$ that undergoes a remarkable partial Néel ordering at 2.1 K under uniform pressure [Mir02], whereas it remains a spin liquid down to 50 mK otherwise [Gar03].

In the second paper [Mit07], the authors measured the magnetisation of $Dy_2Ti_2O_7$ at 1.7 K in a magnetic field parallel to the applied pressure and for different directions [001], [110] and [111]. Their result is summarised in their figure 2 that we reproduced here for clarity. ΔM is negative and saturated for high field where all spins are *up*, because as we can see on the schema III.24, the pressure tends to tilt the spins in the (001) plane and thus makes their [001] component along the field smaller, giving $\Delta M < 0$. But the noteworthy particularity of the [001] axis is that ΔM becomes *positive* for small field; the configuration with all spins *up* is then favoured by the uniaxial pressure suggesting a degeneracy lift of the 2 *in* - 2 *out* ground state in favour of the *up/down* fully saturated configurations as stated by Mito *& al.* We should yet be cautious as this magnetisation shift might as well be explained by a modification of the demagnetisation effect due to a deformation of the sample. According to appendix B and using the same notations, we

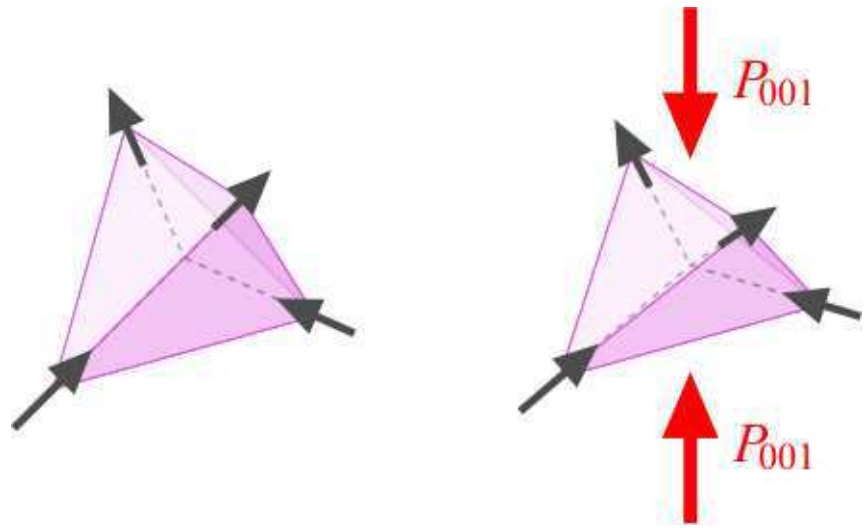

Figure III.24: **Uniaxial pressure:** Rare-earth ions in two successive (001) planes will be brought closer to each other, leading to a modification of their nearest neighbour interactions with respect to the bonds in the (001) plane. If we assume that the spins remain aligned along the (dashed) line joining the centres of neighbouring tetrahedra, then a compression along the $z-$axis will result in a diminution of the $z-$component of the magnetisation, and an increase of the $x-$ and $y-$component. Hence a measure of the saturated value of M in high magnetic field should directly give the extent of the geometrical compression.

have the following relation between internal and external magnetic field

$$H_{\text{ext}} \;=\; H_{\text{int}} \;+\; d\,M \tag{III.80}$$

And yet, since a reduction of the crystal size in the [001] axis will *increase* the demagnetisation factor N in this direction, it means that for a fixed value of H_{ext}, demagnetisation effect will tend to *diminish* the magnetisation M. As we do in fact measure an increase of M ($\Delta M > 0$ for small field), this means that this phenomenon of enhanced susceptibility $\Delta M/\Delta H_{\text{ext}}$ is even larger than observed, once the demagnetisation effects are subtracted.

Hence according to these experimental data and as opposed to our naive theoretical argument exposed above, a uniaxial pressure along the [001] axis does favour the *up/down* fully saturated configurations as required for the KDP model. An unambiguous confirmation would be to measure the magnetisation M parallel to an external field in the [100] or [010] orientations and for an orthogonal pressure axis [001]. We should then observe:

$$M(0, h_{001}) \;>\; M(P_{001}, h_{010}) = M(P_{001}, h_{100}) \tag{III.81}$$

for small fields, as the saturated value of the magnetisation in the plane orthogonal to the uniaxial compression is made larger (see figure III.24).

Similar behaviour has been recognised in $Ho_2Ti_2O_7$, but no details were given in the paper [Mit07].

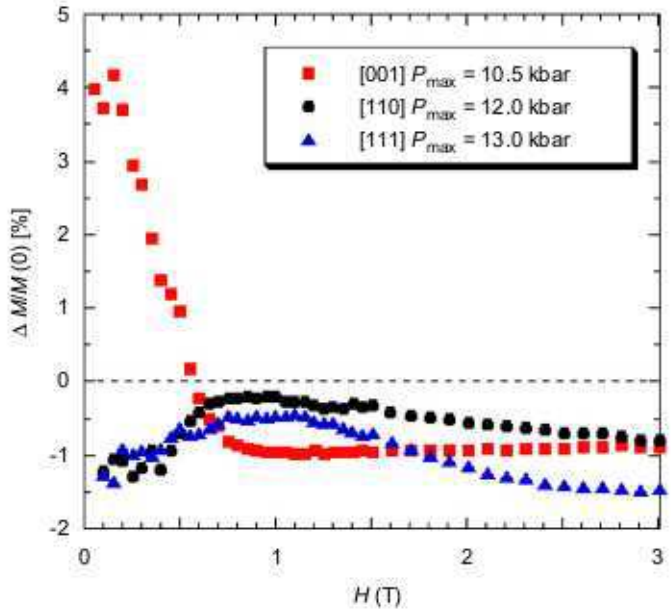

Figure III.25: **$Dy_2Ti_2O_7$ under uniaxial pressure:** Relative difference of the magnetisation $\Delta M(H) = (M(P_{max}, H) - M(0, H))/M(0, H)$ as a function of H, both P and H being applied in the same direction. The figure has been extracted from [Mit07].

Presence of defects

As opposed to the Kasteleyn transition, the presence of defects, necessary for equilibration (see next chapter), and of long range dipolar interactions will not make the transition disappear, but shall simply make it 2nd order instead of a multi-critical point of $\infty-$order. Hence because there is no symmetry breaking field, traces of the KDP transition can be measured even out of the topologically constrained manifold.

Unfortunately, we have to face here a problem that was absent for the Kasteleyn transition; it was easy to apply a high magnetic field with report to $J_{\text{eff}} \sim 1K$, but it is much more difficult to make δ large enough in order to translate the transition temperature in a regime where spin ice remains dynamical. For example for $Ho_2Ti_2O_7$, we have $J_{\text{eff}} = 1.8$ K and the system is frozen below $T_f \sim 0.7 - 0.8$ K. If δ can be made of the same order as T_f then the transition should be observed. Chemical pressure might also be an interesting way of investigation. Neutron scattering experiments might also be able to see the development of long range order in the scattering function, at least on microscopic length scale.

IV Constrained Monopoles Dynamics

IV.1 Presentation of the problem

IV.1.a Magnetic monopoles

As the preceding chapter has been essentially devoted to the constrained 2 *in* - 2 *out* manifold whose degeneracy is only slightly lifted by long range dipolar interactions (see subsection I.3.c), it was acceptable to consider only the nearest neighbour spin ice (NNSI) model. In order to give a simple and qualitative picture of this material, we shall at first continue to use this NNSI model; but since we are now going to be interested in magnetic relaxation measurements performed at temperature of the same order as the nearest neighbour effective interaction ($J_{\text{eff}} \sim 1$ K, see figure IV.3), we shall have to deal with the presence of local excitations out of the ground state and whose behaviour can only be quantitatively reproduced by the dipolar spin ice (DSI) or dumbbell models (see introduction I.3.c). We shall try to keep in mind these two aspects of spin ice, though the comprehension of its dynamics will turn out to be much more straightforward and elegant in the monopoles language. Let us now briefly summarise the main parallels we can make between these two models [Cas08].

Dipolar Spin Ice	**Dumbbell / Monopoles**
2 *in* - 2 *out* ground state	vacuum
3 *in* - 1 *out* defects (local excitations)	quasi-particles (monopoles)
dipolar interactions between magnetic dipoles	Coulomb interactions between magnetic monopoles
pyrochlore lattice	diamond lattice
canonical ensemble	grand canonical ensemble

Table IV.1: **Mapping from the dipolar spin ice to the dumbbell model**

As explained in the introduction I.3.c, this mapping is exact up to quadrupolar terms. To check this equivalence we have simulated a DSI system, starting on a random 2 *in* - 2 *out* configuration; by flipping spins, we can create and force the diffusion of a single pair of monopoles and then compute the energy of the system for each configuration; after averaging over a large number of initial microstates and paths of diffusion, we obtain the potential of interaction between two monopoles of opposite charges. For a distance $r = x\, r_{nn}$ where r_{nn} is the distance between nearest neighbour spins, the potential can be written [Cas08]

$$V(r) \;=\; -\frac{\mu_0}{4\pi}\frac{Q^2}{r} \;=\; -\frac{D_{\text{coul}}}{x}, \quad \text{where} \quad Q = \frac{2\mu}{r_d} \tag{IV.1}$$

where r_d is the distance between two vertices on the diamond lattice (see figure I.8) and the potential V is expressed as a function of x, giving

$$D_{\text{coul}} \;=\; \frac{\mu_0}{4\pi}\frac{4\,\mu^2}{\frac{3}{2}r_{nn}^2}\frac{1}{r_{nn}} \;=\; \frac{8}{3}\,D \approx 3.76 \text{ K} \tag{IV.2}$$

where $D \approx 1.41$ K is given in equation (I.45). Since $r_d = \sqrt{3/2}\, r_{nn}$, then the energy gained by the creation of a pair of monopoles with respect to the vacuum is $V_{min} = -3.07$ K. This potential V for the dumbbell model is compared with our numerical results for DSI in figure IV.1 with a very good agreement; the $1/x$ behaviour is clearly observed and the data perfectly respect the energy scale fixed by D_{coul}. The discrepancies come from the limit of accuracy of the dumbbell model of order $1/r^5$. The only fitting parameter is the energy reference of the DSI system that can translate the numerical data up or down. We should note that the same comparison has been made by [Cas08] in figure I.16 (we used the same units). However in the latter, they computed the energy of separation between monopoles for a single configuration, whereas we performed a statistical average here; this explains the small differences between our results.

The theoretical basis of these monopoles is thus clearly established. We should particularly stress that the Coulomb interaction is set by *magnetic* constants, hence it really does behave like a *magnetic* charge. Furthermore these monopoles correspond to divergences in the magnetic intensity $\mathbf{H}$, or magnetic moment $\mathbf{M}$, rather than in the magnetic induction: $\nabla \cdot \mathbf{B} = \nabla \cdot (\mathbf{H} + \mathbf{M}) = 0$; on all length scales above the atomic scale, a 3 *in* - 1 *out* defect appears to be a local sink in $\mathbf{M}$ and therefore a source of field lines in $\mathbf{H}$. Hence they are *not* Dirac monopoles [Jac99, Dir31], for the simple reason that their magnetic charge is not quantified but can be continuously varied by modifying the nearest neighbour distance between spins by applying external pressure [Cas08] and they do not require a modification of Maxwell's equations. However they are local excitations emerging from a topological ground state and they interact via an effective *magnetic* Coulomb law (see equation (IV.1) and figure IV.1). Furthermore we can assign to them a positive or negative charge when immersed in a magnetic field [Ryz05] that is conserved by creation and annihilation of monopoles. As the Coulomb potential is not confining in $3d$, these quasi-particles are also a remarkable instance of fractionalisation in high dimensions. They are therefore exciting classical analogues of Dirac monopoles and spin ice provides

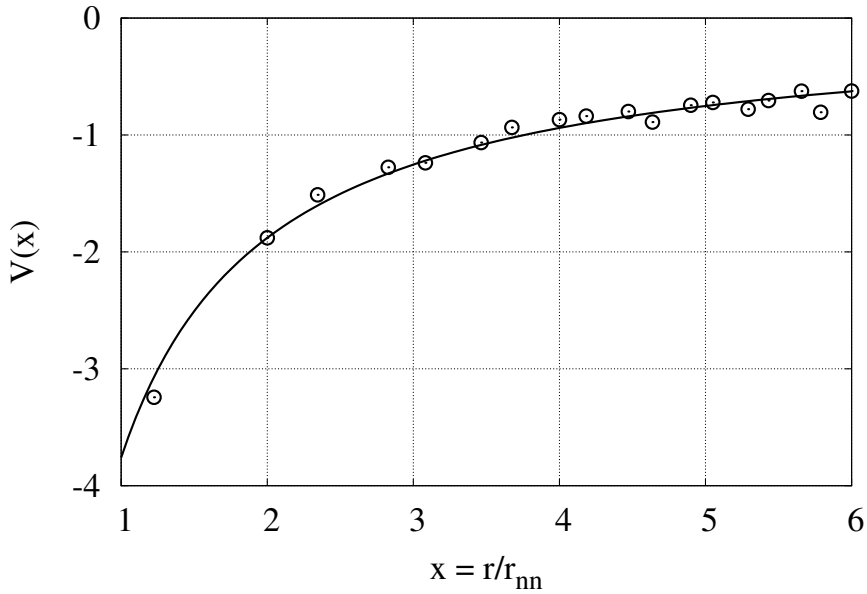

Figure IV.1: **Coulomb potential:** Effective interaction (in Kelvin) between a pair of monopoles in the dipolar spin ice model as a function of the distance between them in units of nearest neighbour distance between spins (open circles). The system size is $8 \times 8 \times 8$ unit cells, *i.e.* 8192 spins. The solid line is the Coulomb potential expected from the dumbbell model $V(x) = D_{\text{coul}}/x$. As we are on the diamond lattice, the smallest possible distance between monopoles is $x = r_d/r_{nn} = \sqrt{3/2}$.

the first $3d$ experimental realisation of deconfined magnetic monopoles.

Given the accessibility of these magnetic quasi-particles, the development of an experimental signature is of vital importance and interest. The "Stanford" superconducting coil experiment [Cas08, Cab82] could in principle detect the passage of a single magnetic quasi-particle, but this seems highly unlikely given that the charges have no mass and therefore have diffusive, rather than Newtonian dynamics. As spin ice has already been widely studied in the past 12 years, a more promising starting point is therefore to look for a signature of these monopoles in pre-existing experiments that have remained unexplained so far. For example Castelnovo & collaborators shed new light on the liquid-gas-like phase diagram observed in spin ice in a [111] field at low temperature [Sak03] that can be understood as a $2d$ condensation of magnetic monopoles where the field acts as a chemical potential. Here we shall present a more straightforward consequence of the presence of these quasi-particles whose dynamics are directly observable from magnetic relaxation measurements [Mat00, Ehl03, Sny04b].

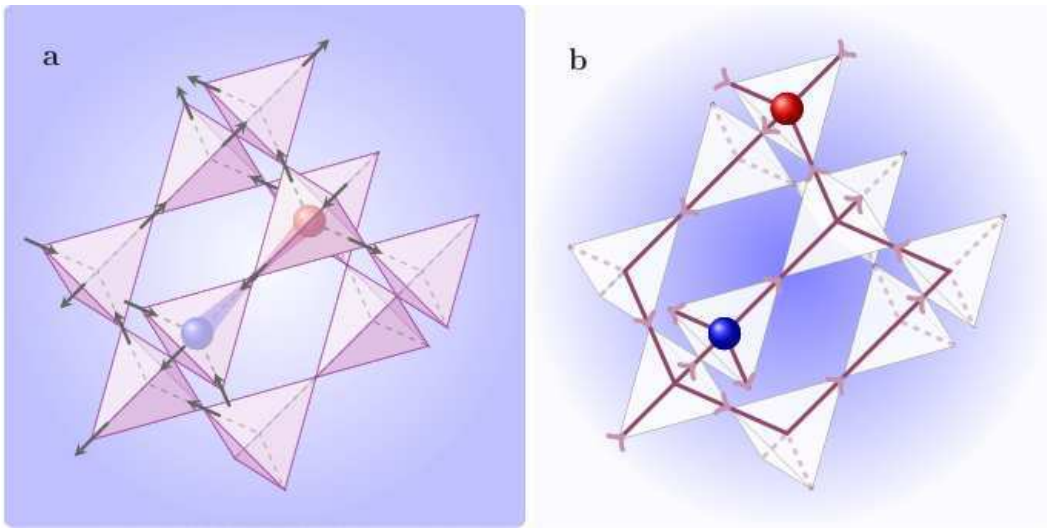

Figure IV.2: **Emergence of monopoles** a) The magnetic ions (Ho^{3+} or Dy^{3+}) lie on the sites of the pyrochlore lattice and are constrained to the bonds of the duel diamond lattice (dashed lines). Local topological excitations 3 *in* - 1 *out* or 3 *out* - 1 *in* correspond to magnetic monopoles with positive (blue sphere) or negative (red sphere) charges respectively. b) The diamond lattice provides the skeleton for the network of Dirac strings with the position of the monopoles restricted to the vertices. The orientation of the Dirac strings shows the direction of the local field lines in **H**.

IV.1.b Dynamics in spin ice

Let us give a brief reminder of the present understanding and open questions concerning the dynamics of spin ice (see introduction I.3.e for a more detailed presentation). We will not consider the high temperature regime ($\gtrsim 10$ K) that is dominated by a single-ion process [Ehl04] and well explained by an Arrhenius law with an energy scale of the order of the first crystal field levels $\sim 200 - 300$ K [Mat01, Sny01, Ehl03, Sut07, Lag07]; as fluctuations out of the easy-axis anisotropy become less and less negligible, we leave the spin ice regime and the study at high temperature is thus beyond the scope of this thesis.

On the other hand, no consensus has been made concerning the original low temperature regime. Even if we know it must be different from a spin glass phase [Mat01, Sny01], the intriguing quasi-temperature-independent plateau followed by a sharp freezing of the dynamics has led to different possible interpretations, based on quantum tunnelling, cluster dynamics due to increasingly strong correlations or the possible influence of lattice defects [Ehl03, Sny04a]. We shall see that quantum tunnelling is indeed inevitable, as explained in [Ehl03] and in the following section, but the evolution of the time relaxation with temperature (see figure IV.3) requires the consideration of magnetic monopoles.

Hence the goal of this chapter is double: to give a complete and coherent picture of the dynamics of spin ice at low temperature, and to provide a direct experimental signature

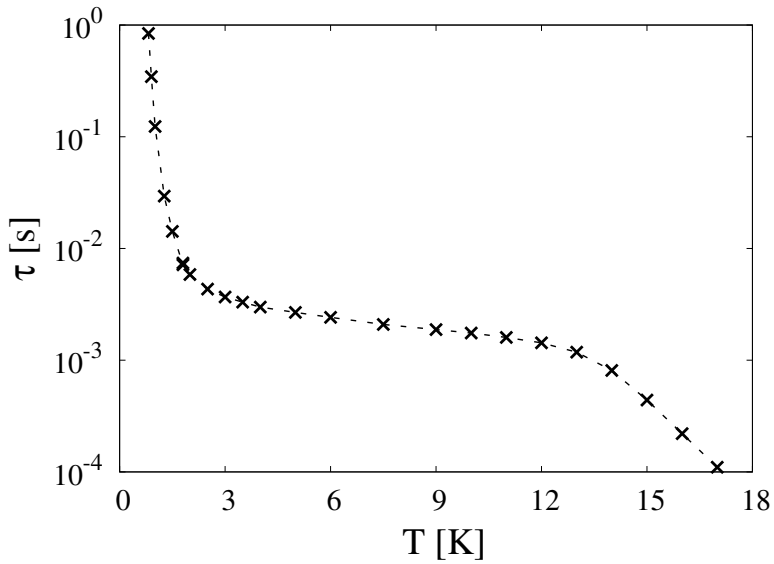

Figure IV.3: **Experimental relaxation time** τ for $Dy_2Ti_2O_7$ vs temperature T from Snyder *& al.* [Sny04a], courtesy of Peter Schiffer. The starting point of this work has been to shed new light on this result. Above 12 K the spins are not exactly Ising anymore. The quasi-plateau between 2 and 12 K is divided in two parts: the "high temperature" of the spin ice region above 6 K where one needs to consider double defects 4 *in* or 4 *out* and a large monopole density, and the "low temperature" regime below 6 K where our monopole model should hold. Below ~ 2 K, the system becomes frozen.

of monopole dynamics in the magnetic relaxation of this material.

IV.2 Deconfined quasi-particles

In the first paper explicitly dedicated to the dynamics of spin ice [Mat00], the authors fitted the relaxation time $\tau(T)$ with an Arrhenius law in the freezing region ($T \approx 1$ K) and obtained a characteristic energy barrier of $E_f = 19.6$ K and 27.5 K for $Ho_2Sn_2O_7$ and $Ho_2Ti_2O_7$ respectively. This is a rather surprising result as it does not match any energy scale involved in the spin ice model:

- ~ 200 K between the ground state doublet and the first excited crystal field levels;
- $\sim 4J_{\text{eff}} = 7.2$ K for $Ho_2Ti_2O_7$ and 4.4 K for $Dy_2Ti_2O_7$, due to single spin flips within the NNSI model;
- ~ 3 K for the limit of infinite separation between monopoles (see figure IV.1).

This freezing seems to be related to a single spin flip process, as it corresponds to the closest energy scale, but the difference with E_f is nonetheless too large to be the sole

contribution. In fact the possibility of a simple thermally activated process has been ruled out by the study of $Dy_2Ti_2O_7$ where the spin freezing is only qualitatively fitted by an Arrhenius law with an energy barrier of the order of 10 K [Mat01, Sny04b], as tested for the data of Snyder *& al.* (see green curve in the upper panel of figure IV.4); the Arrhenius scaling is quantitatively good below 2 K, but fails completely to reproduce the quasi-plateau region. The associated energy barrier is $E_f = 6.5$ K.

To the best of our knowledge, once a global picture of spin ice dynamics has emerged [Mat01, Ehl03], the behaviour of $\tau(T)$ has always been understood as a crossover between a quantum relaxation on the quasi-plateau and a non-spin glass freezing at very low temperature, the main question being what can explain this re-entrance into a strongly temperature-dependent dynamics ? Here we decided to follow a different approach and to interpret this problem as the superposition of two different contributions holding for the **whole** temperature window $0 - 10$ K; a quantum tunnelling process responsible for the "very high temperature" crossover at ~ 10 K and a thermally activated relaxation due to the creation and diffusion of monopoles interacting through long range Coulomb interactions. But before including these long range interactions in numerical simulations, we shall start by explaining the role of the quantum tunnelling and then give an insight into the underlying physics thanks to a phenomenological approach based on Arrhenius arguments.

IV.2.a Quantum tunnelling

From our point of view, the quantum process is not responsible for the temperature dependance of spin ice dynamics[1], at least in a first approximation. On the other hand, we think that this mechanism fixes the time scale of the quasi-plateau region, which can be very different from one material to another: $\tau_o \approx 10^{-8}$ s for $Ho_2Ti_2O_7$ [Cla09], whereas it is 10^{-3} s for $Dy_2Ti_2O_7$ [Sny04b].

To flip a spin, one need an energy of order J_{eff}, imposed by the interaction of the spin with its neighbours (this is the creation of a monopole), but because of the crystal field splitting, the system has to cross an energy barrier of order 200 K (single-ion anisotropy) for a spin to go from the state $|+15/2\rangle$ (say local *up* spin) to the state $|-15/2\rangle$ (say local *down spin*) (see table I.2). Obviously such energy is not accessible for $T \lesssim 10K$ and it can only occur thanks to quantum tunnelling between the two states of the ground state doublet, driven by an effective transverse field produced by the neighbouring spins, as proposed by Ehlers *& al.* [Ehl03]. It is this quantum tunnelling that will impose the inversion rate and thus the time scale of τ_o. The fact that τ_o is so large (up to milliseconds) is consistent with a quantum tunnelling picture as one might expect unconstrained microscopic time scales to be of order 10^{-12} s. This justifies *a priori* the use of Monte Carlo simulations with a local Metropolis argument.

According to the difference of the energy of the first excited level between $Dy_2Ti_2O_7$ ($\Delta \approx 380$ K) and $Ho_2Ti_2O_7$ ($\Delta \approx 240$ K) (see table I.2), this argument would explain the

[1]For example the energy barrier involved in the tunnelling could vary with temperature.

relative time scale difference between these two compounds; the 5 orders of magnitude being consistent with a quantum tunnelling process exponentially dependent in Δ. Unfortunately because of the complexity of the CEF of the rare-earth ions, it is not possible to estimate quantitatively the experimental inversion rate and the time scale τ_o will remain a fitting parameter in our theory.

Hence the point of view we will endeavour to clarify in this chapter is that spin ice dynamics are allowed thanks to quantum tunneling and thermally driven by creation of monopoles; the temperature dependance comes uniquely from the initial and final states due to interactions between spins, and *not* through the crossing of crystal-field energy barriers. This gives a temperature independent part to the dynamics which is the transition rate between Ising states.

IV.2.b Arrhenius argument

According to the energy of the 16 possible configurations of a tetrahedron on figure I.10, at low enough temperature, the system should mostly respect the ice-rules constraints from which should emerge topological defects created by pairs by a single spin flip for an energy cost $E = 4\,J_{\text{eff}}$. Following the idea that the quasi-plateau is in fact the *tail* of an exponential thermally activated behaviour, we have plotted on figure IV.4 different Arrhenius laws $\tau_0 \exp(E_p/T)$ where the energy barrier is varied. The time scale τ_0 is fixed by fitting to the experimental time at 3 K where the density of double defects (4 *in* and 4 *out*) is negligible and with $J_{\text{eff}} = 1.11$ K, the value estimated for $Dy_2Ti_2O_7$ [dH00].

The main result of this section is that the experimental data are poorly reproduced by an energy barrier $E_p = 4\,J_{\text{eff}}$, but are quantitatively well fitted with $E_p = 2\,J_{\text{eff}}$ over the region between 2.5 K and 5 K (see the lower panel of figure IV.4). This means that the lowest excitation responsible for the dynamics of spin ice materials is *not* the energy cost of a single spin flip, but only half of that *i.e.* the energy cost of a single topological defect; once a pair of defects is created, they can freely and separately propagate in the system and will be responsible for the magnetic relaxation. This test therefore provides very strong evidence for the **fractionalisation** of magnetic charge and the diffusion of deconfined monopoles[2] ! This outcome is particularly appealing as it explicitly requires the use of the quasi-particle language.

As shown on figure IV.4 the agreement becomes qualitative above 5 K. In order to prove this discrepancy is due to the presence of double defects, we shall construct a variant of the Arrhenius law that should include all relevant energy scales.

Multi-energy Arrhenius law

We shall use a mean field picture by assuming that the density of tetrahedra is simply given by their Boltzmann weights. In a concern to be concise, the different configurations 2 *in* - 2 *out*, 3 *in* - 1 *out* (or 3 *out* - 1 *in*) and 4 *in* (or 4 *out*) will be noted respectively

[2]Fractionalisation does not necessarily require *free* defects, a *non-confining* Coulomb potential is sufficient.

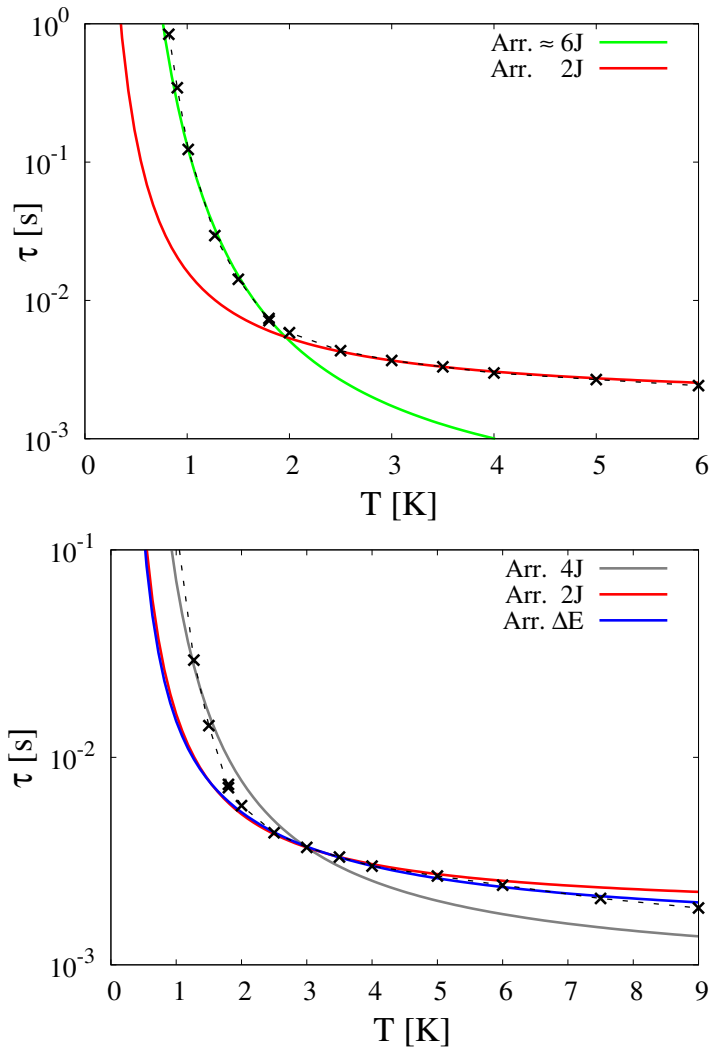

Figure IV.4: **Deconfined monopoles:** The experimental data of Snyder *& al.* [Sny04b] ($\times$ and dashed line) are compared with different Arrhenius functions. *Top:* The quasi-plateau region is in quantitative agreement with a thermally activated process with energy barrier $E_p = 2\,J_{\text{eff}}$ (red line) whereas the spin freezing is well reproduced with $E_p \approx 6\,J_{\text{eff}}$ (green line), but no unique function can fit the whole temperature window. *Bottom:* The characteristic excitation is the creation of a unique defect ($E_p = 2\,J_{\text{eff}}$, red line) rather than a single spin flip ($E_p = 4\,J_{\text{eff}}$, grey line). The fit is improved at higher temperature if we include the energy scales due to double defects in a modified Arrhenius law (blue line).

2, 3 and 4. Let us make a list of all the possible energies resulting from a single spin flip in table IV.2; as a spin always belongs to two tetrahedra, we must then take into account all possible evolutions of a pair of tetrahedra.

Initial	Final	δE	Probability
2|2	3|3	$+\,4\,J_{\text{eff}}$	1
2|3	3|2	0	3/4
	3|4	$+\,8\,J_{\text{eff}}$	1/4
2|4	3|3	$-\,4\,J_{\text{eff}}$	1
3|3	2|2	$-\,4\,J_{\text{eff}}$	9/16
	2|4	$+\,4\,J_{\text{eff}}$	6/16
	4|4	$+12\,J_{\text{eff}}$	1/16
3|4	4|3	0	1/4
	2|3	$-\,8\,J_{\text{eff}}$	3/4
4|4	3|3	$-12\,J_{\text{eff}}$	1

Table IV.2: **Energy scales resulting from a single spin flip:** Let us explain this table using the second row as an example. It means that if we flip a spin that initially belongs to a tetrahedron 2 *in* - 2 *out* and a tetrahedron 3 *in* - 1 *out*, then there is a probability of 3/4 simply to inverse the position of the defect (3|2) at no energy cost, and a probability of 1/4 to create an additional pair of defects (3|4) that cost an energy $\delta E = +8\,J_{\text{eff}}$. The probabilities are a statistical average, whether the spin under consideration is one of the three *in* spins of the 3 *in* - 1 *out* tetrahedron ($\delta E = 0$), or the fourth *out* spin ($\delta E = 8\,J_{\text{eff}}$).

One can here calculate the mean value of the energy barrier ΔE by including all moves that actually cost a positive energy, weighted by their probability and the Boltzmann factor of their initial configuration. We should note that there are two subtle points. The configurations (2|3) and (3|2) are different which gives a factor of 2 for their Boltzmann weight. More importantly, a single spin flip that actually creates a pair of defects will effectively only cost one half of δE, because of the fractionalisation of the excitations, but the process (3|3)→(2|4) will really cost $\delta E = +4\,J_{\text{eff}}$ as it simply moves a charge. ΔE is thus formally expressed as

$$\begin{aligned}\Delta E &= \frac{2\left(6\,e^{2\beta J_{\text{eff}}}\right)^2 + 4\left(2\,\frac{1}{4}\,6\,e^{2\beta J_{\text{eff}}}\,8\right) + 6\left(\frac{1}{16}\,8^2\right) + 4\left(\frac{6}{16}\,8^2\right)}{\left(6\,e^{2\beta J_{\text{eff}}}\right)^2 + \left(2\,\frac{1}{4}\,6\,e^{2\beta J_{\text{eff}}}\,8\right) + \left(\frac{1}{16}\,8^2\right) + \left(\frac{6}{16}\,8^2\right)}\,J_{\text{eff}} \\ &= 3\,\frac{6\,e^{4\beta J_{\text{eff}}} + 8\,e^{2\beta J_{\text{eff}}} + 10}{9\,e^{4\beta J_{\text{eff}}} + 6\,e^{2\beta J_{\text{eff}}} + 7}\,J_{\text{eff}} \xrightarrow[T\to 0]{} 2\,J_{\text{eff}}. \qquad \text{(IV.3)}\end{aligned}$$

We recover the energy of creation of a single defect in the low temperature limit. The resulting Arrhenius law $\tau_0\,\exp(\Delta E/T)$ is plotted on figure IV.4 (blue curve). It is almost

identical to the thermally activated process with $E_p = 2\,J_{\text{eff}}$ (red line) below 4 K, but differs at higher temperature and follows the experimental data up to ≈ 8 K; the differences above this limit are probably due to the exponentially decaying influence of the high temperature single-ion process.

In this section, we do not claim to have constructed a rigourous theory of spin ice dynamics, but we believe that this phenomenological approach is a very strong argument in favour of a magnetic relaxation assisted by thermally activated creation of deconfined quasi-particles and is an elegant manifestation of fractionalisation in this material.

However as shown on the upper panel of figure IV.4, any Arrhenius function ultimately fails, underestimating the time scale at very low temperature, which is compatible with our picture. On the quasi-plateau region the density of monopoles is high enough to hinder their diffusion on long distance and their creation is the only relevant energy scale, whereas as the temperature is lowered, their distribution becomes more and more scattered and long range Coulomb interactions then come into play.

Of course another possibility is the occurrence of a second process responsible for the Arrhenius law in the spin freezing region (green curve). But apart from the fact it is very difficult to find such a mechanism that could explain the variety of energy barriers for the different spin ice crystals (from 6.5 K to 27.5 K), it should also exactly disappear above 2 K and prevent the creation and diffusion of monopoles below 2 K, as the time relaxation should otherwise follow this Arrhenius law above 2 K (instead of the quasi-plateau region) and be dominated by the fractionalisation process below 2 K, making the overall relaxation mechanism much more efficient. We think this is very unlikely and this is why we shall implement the long range interactions in Monte Carlo simulations in the next section.

IV.3 Spin freezing

We have tested this idea by simulating both the dipolar spin ice model and a Coulomb gas of magnetic monopoles in the grand canonical ensemble, occupying the sites of the diamond lattice. In order to model the local dynamics of creation and diffusion of quasi-particles, we decided to use a Monte Carlo algorithm with single spin flip iterations. We shall *not* use the Worm algorithm here (see section II.3), even in addition to single spin flip, as its primary function is to overcome the sluggish dynamics of spin ice by forcing the system to equilibrate. We treated the long range interactions with the Ewald method presented in section II.4.

IV.3.a Dipolar spin ice

Simulations of the DSI model is relatively straightforward. We implemented both nearest neighbour and dipolar interactions, using the numerical values of J and D for $Dy_2Ti_2O_7$ given in table I.3. In order to extract a characteristic relaxation time τ, we computed the

auto-correlation function

$$C(t) \;=\; \frac{1}{N}\sum_i \mathbf{S}_i(0)\cdot\mathbf{S}_i(t), \tag{IV.4}$$

where N is the total number of spins and $\mathbf{S}_i(t)$ is the value of the unit vector representing the spin at the Monte Carlo time t. For the initial conditions we take a randomly distributed microstate, which we let evolve at high temperature $T = 10$ K until an equilibrium configuration is attained. This defines $t = 0$. $C(t)$ decays almost exponentially. The time is re-set to zero when $C(t)$ decays beyond 0.01 and the temperature T is lowered by δT. The process is repeated until we reach $T = 0.6$ K when numerical equilibration becomes diffciult. The resulting auto-correlation is averaged over many samples (between 50 and 100) in order to give a smoothly decaying function down to $C(T) = 0.1$. We have defined $\tau(T)$ such that $C(\tau) = C_o = 0.8$ and the time scale is then fixed at the value measured by Snyder *& al.* at 3 K, $\tau(T = 3\text{ K}) = 3.68$ ms [Sny04b]. Choosing other values for C_o makes small differences below ~ 1 K to the overall robust curve $\tau(T)$. We shall see that our approach becomes indeed only qualitative at very low temperature. We chose the reference temperature $T = 3$ K because double defects are then negligible (below 1%) which will be essential for comparisons with the dumbbell model. Before analysing the temperature dependance of τ in detail we first study the defect concentration in the DSI plotted on figure IV.5, which is noticeably smaller than the expected concentration for the NNSI model. One of the effects of the dipolar interactions is thus to hinder the creation of monopoles, which might be the reason for the brutal slowing down of the dynamics.

IV.3.b Magnetic monopoles and Dirac strings

The simulation of a Coulomb gas turns out to be more subtle than that of the spin system. First of all while a single spin flip Metropolis argument is simple to implement, here we must consider iterations including two sites of the diamond lattice, the possible outcome at time $t + 1$ being restricted by the local configuration at time t:

- if there are no quasi-particles on these two sites, then we shall consider the creation of a pair of opposite charges.
- if there is only one monopole, it can either move to the other site or stay where it is;
- if there are two opposite charges, they can annihilate;
- if there are two charges of the same sign, then nothing happens as we shall explain it below.

Chemical potential μ

Furthermore we need to introduce the chemical potential μ for simulations in the grand canonical ensemble. As we are interested in the low temperature regime ($\lesssim 3$ K) in order

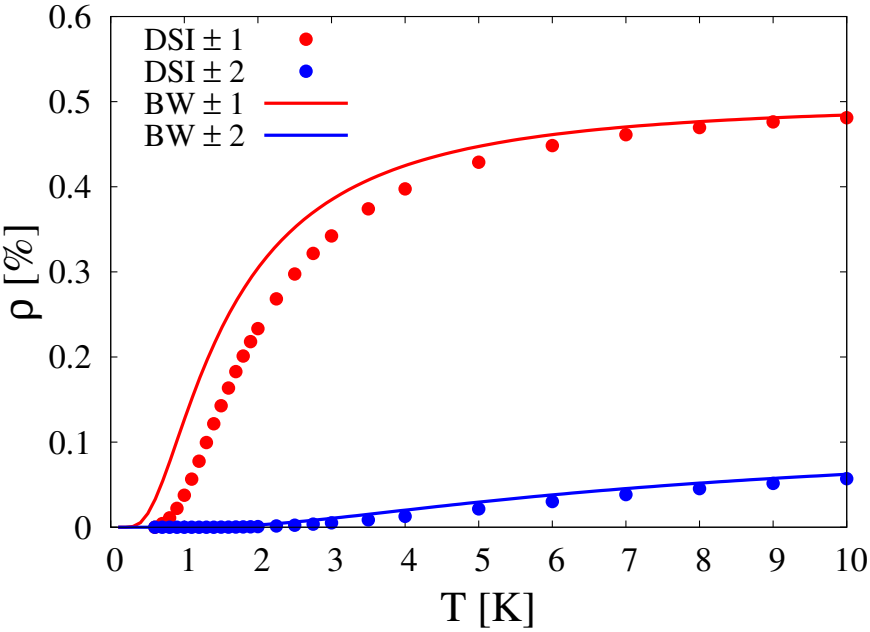

Figure IV.5: **Density of monopoles** for the dipolar spin ice model (•) and their expected Boltzmann weight for the nearest neighbour spin ice model (solid line) with the numerical values of $Dy_2Ti_2O_7$. In red (resp. blue) are plotted the concentration of 3 *in* - 1 *out* and 3 *out* - 1 *in* defects (resp. 4 *in* and 4 *out*), carrying a magnetic charge ± 1 (resp. ± 2). The system size is $N = 16000$ spins.

to reproduce the sharp spin freezing, we shall only consider the creation of 3 *in* - 1 *out* and 3 *out* - 1 *in* defects *i.e.* monopoles bearing a unit charge Q. This will spare us the introduction of a second chemical potential responsible for the presence of double defects. Our results are thus not expected to hold for temperatures much larger than 5 or 6 K. In a first series of simulations we have estimated μ numerically by calculating the difference between the Coulomb energy gained by creating a single pair of neighbouring magnetic monopoles $\Delta U_{\text{mono}} < 0$ in a vacuum and that required to produce a unique pair of topological defects out of the 2 *in* - 2 *out* manifold in the dipolar spin ice model $\Delta U_{\text{def}} > 0$, giving a configurationally averaged estimate $\mu_1 \equiv \Delta U_{\text{def}} - \Delta U_{\text{mono}} = 8.92$ K. In a second series of simulations, $\mu_2(T)$ was taken as the value required to reproduce the same defect concentration as in a simulation of dipolar spin ice at temperature T plotted on figure IV.5. Here $\mu_2(T)$ varied by 3% only, with the same mean value as in the first series, showing that our procedure is consistent. The chemical potential used is thus *not* a free parameter.

We should dwell on this chemical potential, as the very fact it exists is another validation of the dumbbell model and turns out to be the main explanation for the very low temperature freezing. μ_1 has been defined for a unique pair of quasi-particles, which is seldom the case for spin ice materials at finite temperature. It is hence a valid question to check that the chemical potential $\mu(T) \equiv \Delta U_{\text{def}}(T) - \Delta U_{\text{mono}}(T)$ remains close to μ_1

on average. To do so, we have simulated the DSI model (with $N = 16000$ spins) using the same Metropolis argument as presented in the precedent subsection, *in parallel* with a Coulomb gas, *i.e.* for each single spin flip the corresponding monopole configuration on the diamond lattice is updated accordingly, making it possible for every Monte Carlo step to compare the energy of the spin configuration with its mirror in the dumbbell model. Hence after equilibration at a given temperature T and for each accepted creation or annihilation of a pair of defects, we compute the energy required by this Monte Carlo move in the DSI model $\Delta U_{\text{def}} > 0$ and the energy gained in the corresponding Coulomb gas system $\Delta U_{\text{mono}} < 0$, the difference giving rise to the chemical potential μ for this specific move. By averaging these values over the Monte Carlo time and for different initial configurations, one finds the temperature evolution of these energies as well as their standard deviation, plotted in figure IV.6. Note that since we are interested in the creation/annihilation of monopoles, we have artificially prevented the apparition of double defects in the system for all temperatures.

We believe that the whole physics of spin ice at low temperature is included in this figure. First of all even if the standard deviation can be very large for ΔU_{def} and ΔU_{mono} (up to $\pm 40\%$), these quantities turn out to be *highly correlated* since their difference giving rise to μ is very precisely defined ($\pm 4\%$ at most). Hence not only does the energy separation between two monopoles follow a magnetic Coulomb potential (see figure IV.1), but the energy of creation/annihilation is also consistent with a Coulomb gas in the grand canonical ensemble ! As we have plotted the absolute value of ΔU_{mono}, the chemical potential is simply the sum of the two curves (red and blue) on average; large energy cost ΔU_{def} (top of the red bars) correspond to small energy gain ΔU_{mono} (bottom of the blue bars) and *vice-versa*.

As the temperature decreases, the large values of ΔU_{def} are less and less accepted by the Metropolis argument which gives rise to a diminution of both standard deviations (blue and red), naturally accompanied by a slightly decrease (resp. increase) of the averaged energy cost $\langle \Delta U_{\text{def}} \rangle$ (resp. $\langle |\Delta U_{\text{mono}}| \rangle$) down to 2 or 3 K. Apart from the fact that there is a quasi-continuous range of energy values to create monopoles instead of a unique one for the NNSI model, this is the same argument as for the phenomenological approach of the preceding section IV.2.b. We should also note that the mean value $\langle \Delta U_{\text{def}} \rangle$ is close to the energy cost of a single spin flip in the NNSI model $E = 4\, J_{\text{eff}} = 4.44$ K. The dynamics of the DSI model thus seems to be a thermally activated process with a statistically averaged value of the energy barrier.

Now let us take advantage of the Coulomb gas picture to gain a more fundamental understanding of the low temperature properties of spin ice. From the standard deviation of ΔU_{mono} (blue curve), one sees that almost all accepted creations of quasi-particle bring an energy gain larger than the energy of deconfinement of a pair of monopoles in a vacuum $|V_{min}| = 3.07$ K (lower dashed line, see equation (IV.1)). This means that the newly created pair is more stable than in a vacuum. This can only be true thanks to *attractive* interactions of the quasi-particles with their neighbours; if each monopole is on average closer to quasi-particles of opposite charge, then the creation is favoured, otherwise it is exponentially suppressed by the Metropolis argument. This is an analogue

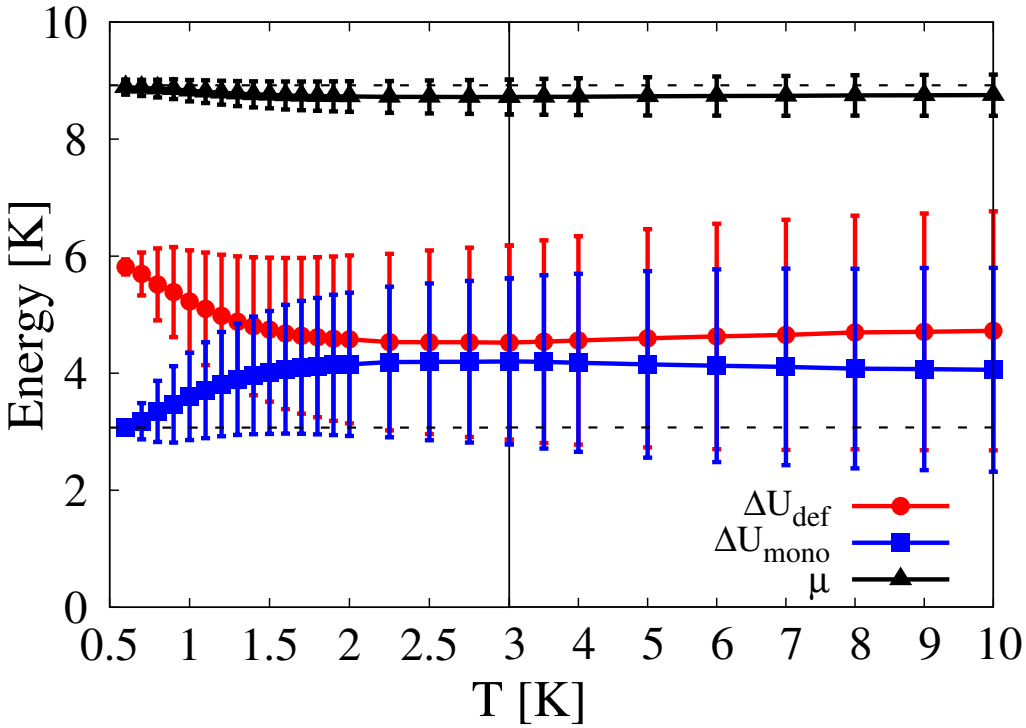

Figure IV.6: **Creation/annihilation of a pair of quasi-particles:** Energy required in the dipolar spin ice model (ΔU_{def} , red •) or gained for a Coulomb gas ($|\Delta U_{mono}|$, blue ■) and the resulting chemical potential $\mu(T)$ (▲) as a function of temperature. The vertical bars are not error bars but the standard deviation of these quantities. $\mu(T)$ tends to the limit $\mu_1 = 8.92$ K (dashed line) at very low temperature. The lower dashed line is the analytical prediction of the energy gained by creating a pair of monopoles in a vacuum $|V_{min}| = 3.07$ K (see equation (IV.1)). The temperature scale below 3 K is enlarged for a better display.

of a *Debye cloud* in an electrolyte solution. However the density of magnetic monopoles decreases with the temperature (see figure IV.5) and this stabilisation becomes weaker and weaker. Apparently this occurs below ~ 2.5 K when the largest values of $|\Delta U_{\text{mono}}|$ disappear brutally; on the other side of the mirror, this results in the surprising *increase* of the mean value of the energy cost $\langle \Delta U_{\text{def}} \rangle$ (red line) with decreasing temperature. The brutal non-Arrhenius spin freezing is thus an ***avalanche effect***: less monopoles hinder the Debye screening which reduces the number of creations of quasi-particles, which leads to less monopoles, *etc.* If this slowing down is sharp *but* continuous, it is because the system remains thermally activated; as long as the material remains "hot" enough to allow the creation of a pair of monopoles out of the vacuum,*i.e.* a single spin flip of energy $\Delta U_{\text{def}} = \mu_1 - |V_{min}| \approx 5.8$ K, the system will remain dynamic through the creation and diffusion of monopoles. Our simulations hit this limit for $T \approx 0.6$ K and we thus expect equilibration in experiments to become dramatically difficult below

this temperature; this is exactly what Snyder *& al.* observed at 0.65 K for $Dy_2Ti_2O_7$ in FC-ZFC measurements [Sny04b].

We shall recall here that all this physics of magnetic monopoles has naturally emerged from simulations on the dipolar spin ice model.

Dirac strings

One last point to consider before making a quantitative study of monopole dynamics is the inclusion of the constrained topology in the Coulomb gas. The monopoles hop between nearest neighbour sites via the Metropolis Monte Carlo algorithm, giving diffusive dynamics, but with a further local constraint: in the spin model a 3 *in* - 1 *out* topological defect can move at low energy cost by flipping one of the three in spins, the direction of the out spin being barred by an energy barrier of $8\,J_{\text{eff}}$ that would result in a double defect whose density is negligible for the temperature range of interest. An isolated monopole can therefore hop to 3 out of 4 of its nearest neighbour sites only, dictated by an oriented network of constrained trajectories similar to the ensemble of classical *Dirac string* [Cas08] of overturned dipoles [Jac99]. The positively charged monopoles move in one sense along the network while the negative charges move in the opposite direction (see figure IV.2.b). The network is dynamically re-arranged through the evolution of the monopole configuration. The vacuum for monopoles in spin ice thus has an internal structure; the Dirac strings which, in the absence of monopoles, satisfy the ice rules at each vertex. Again, one should note that the strings defined by Dirac do in fact differ from the ones presented in figure IV.2; in his original work, two monopoles of opposite charges should be connected by a *single* and *unobservable* chain of dipoles or solenoid [Jac99]. The analogy is nonetheless appealing, especially since these Dirac strings are the very reason of the existence of the monopoles. Local excitations are more the rule than the exception in magnetic materials, but here separating them usually costs an energy linear in their distance, whereas the underlying Dirac strings structure in spin ice provides a network of pre-existing paths for the diffusion of monopoles at finite energy cost once they are created [Cas08].

This structure is manifest in the dynamics and influences the resulting time scales. In fact the characteristic time scale that we compare with experiment comes from the evolution of the network of Dirac strings rather than from the monopoles themselves. The problem of the dumbbell model for comparison with spin ice compounds is that it cannot take into account its own vacuum filled by tetrahedra respecting the ice-rules even if they are dominant (see figure IV.5). This is why we must restore the contribution of the vacuum, in order to quantify the relaxation of the whole system, by using the Dirac strings as an image of the underlying spin structure. In other words magnetic experiments measure spins, not monopoles[3]. We locally define the string network by an integer $\sigma = \pm 1$ giving the orientation of the Dirac string along each bond of the diamond

[3]maybe with the notable exception of recent μSR experiments that have *directly* measured magnetic charge transport in $Dy_2Ti_2O_7$ [Bra09]

lattice, and define the auto-correlation function

$$C(t) \;=\; \frac{1}{N}\sum_i \sigma_i(0)\sigma_i(t). \tag{IV.5}$$

Following the same method as introduced for the DSI model (see below equation (IV.4)), one can extract the relaxation time τ from $C(t)$. To be sure that the Dirac strings network corresponds to the monopole configuration, we consider an initial ordered microstate with no monopoles that we let equilibrate at high temperature $T = 10$ K. The resulting time τ is also scaled with respect to the experimental data at 3 K.

IV.3.c Comparison to experiments

Relaxation time

As expected from our analysis of figure IV.6, the characteristic time scale of the simulations shown on figure IV.7 reproduce the sharp spin freezing observed experimentally [Jau09b].

i Since the preliminary works by Gingras and collaborators [dH00, Bra01a, Gin01, Fuk02, Mel04] and Isakov *& al.* [Isa05], the DSI model is known for being the most accurate representation of spin ice crystals[4]. Hence the matching between the grey squares ■ (DSI) and the experimental black crosses × on figure IV.7 is of course an additional confirmation of this model, but more importantly is a successful test of the Metropolis dynamics used in our simulations. There is indeed no reason to consider the Metropolis time as the real experimental time *in general*, but this is justified here by the presence of an inversion rate due to quantum tunneling (see subsection IV.2.a). Knowing that, we can now use the same dynamics to simulate a Coulomb gas of quasi-particles, as described in the previous subsection IV.3.b).

ii We believe that the net improvement with respect to the Arrhenius behaviour (red line) and the quantitative comparison between the different numerical and experimental data is a clear but nonetheless remarkable demonstration of the constrained dynamics of magnetic monopoles in spin ice. Both pictures from the DSI and dumbbell model are correct, but the second one allows a pleasantly simple understanding of the underlying physics and proves the presence of deconfined point like magnetic charges in the sample. Allowing the variation of $\mu(T)$ for the Coulomb gas provides a further evolution towards the experimental data, compared with that for fixed μ_1, showing the importance of the monopoles density in the dynamics.

Even if the fit is quantitatively good down to ~ 1.5 K, differences remain at this level of comparison below this temperature with a (slightly) better result for the DSI model, *a priori* due to quadrupolar corrections absent in the dumbbell model. To go further would

[4]Even if further exchange coupling beyond nearest neighbours happens to be of importance for a perfect comparison with neutron scattering data [Yav08].

require an even more detailed modelling of spin ice [Yav08] as well as complementary experimental measurements. In a nutshell, the dynamics of spin ice is thus dictated by:

- a thermally activated creation of deconfined magnetic monopoles;
- Dirac strings constraints that impose the direction of the monopole diffusion along a continuously evolving network filling the vacuum;
- an attractive Coulomb interaction that hinders but does not prevent the propagation of quasi-particles, as confirmed by a remarkable recent paper by Fennell *& al.* who measured the exponential divergence of the Dirac string length at low temperature [Fen09];
- a Debye screening of the Coulomb potential provoking an avalanche effect that accelerates the disappearance of the monopoles below ~ 2 K, responsible for the observed spin freezing. This effect is the main contribution in the slowing down of the dynamics.

As predicted by [Mat00, Sny01], the processes involved here are very different from a spin glass transition, essentially because of the deconfinement of the quasi-particles that can thus diffuse in the entire material once they are created.

Magnetic field

As first observed by [Sny01], a magnetic field tends to slightly increase the freezing temperature of spin ice materials, in opposition to standard spin glass behaviour. On the top panels of figure IV.8, one can see the real part of the AC susceptibility $\chi'(T)$. For $Dy_2Ti_2O_7$ (left), the double peak shape is characteristic of the two processes (above and below 12 K) that occurs in this material. We see that a magnetic field strongly suppresses the low temperature process. The same result holds for $Ho_2Ti_2O_7$ (right panel) with the additional effect that the high temperature mechanism only appears in χ' when the low temperature process is sufficiently slowed down by the magnetic field. Finally on the bottom panel one can directly ascertain the diminution of the frequency f, and thus the increase of $\tau = 1/f$ as a function of the magnetic field.

In light of the monopole dynamics we have established here, the suppression of this low temperature mechanism becomes understandable. In presence of a field, the monopoles are not deconfined anymore because the Dirac string joining a pair of quasi-particles and made of flipped dipoles cost a Zeeman energy that grows linearly with the separation between the two monopoles, which cannot anymore "freely" propagate in the crystal. The energy scale should thus be larger than the energy of creation of a single monopole and explains the slowing down of the dynamics, as discussed in more details in the next section.

Dilution

As displayed in figure IV.9, dilution with a non-magnetic ion has an effect exactly inverse to that of the magnetic field and enhances the real part of the AC susceptibility. In

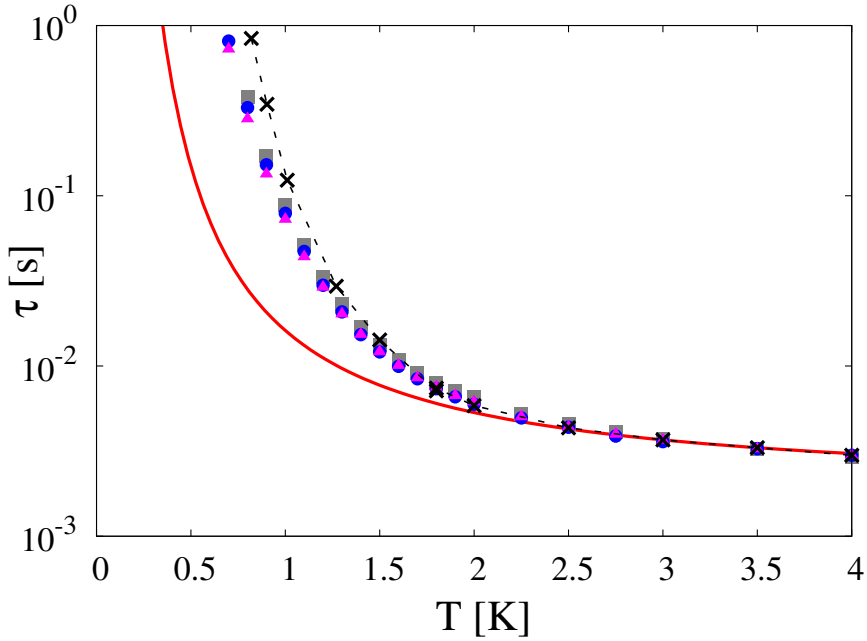

Figure IV.7: **Spin freezing in $Dy_2Ti_2O_7$:** The experimental data (×) are from Snyder *& al.* [Sny04b]. The Arrhenius law (red line) represents the free diffusion of topological defects in the nearest neighbour model. The relaxation time scale of the Dirac string network for the Coulomb gas has been obtained for fixed chemical potential (▲) and with μ varying slowly to match the defect concentration in dipolar spin ice (•), whereas the dipolar spin ice relaxation time is given by ■.

the monopole language, lattice defects behaves like fixed quasi-particles with a charge $Q/2 = \mu/r_d$ resulting from two spins *in* and one *out* and *vice-versa*. Additionally to the fact that creating a monopole next to a lattice defect usually only costs $2\,J_{\text{eff}}$, these half charges act as a permanent source of Debye screening, even at very low temperature when thermally activated monopoles become rare. However this argument is only valid for relatively small dilution (here up to $x = 0.4$), because larger dilution will first hinder the propagation of monopoles which cannot diffuse if most of the Dirac strings are interrupted by lattice defects; and ultimately, as x gets closer to 2, we shall simply end up with a random dipolar magnet without any sign of the original spin ice model. Snyder *& al.* do indeed find a slowing down of the dynamics for dilution higher than $x = 0.4$ [Sny04a].

Open questions

We believe that this study shows strong evidence of a low temperature dynamical process assisted by magnetic monopoles, especially as this theory is in quantitative agreement with the magnetic relaxation time measured in $Dy_2Ti_2O_7$ and is qualitatively coherent with many other observations. Of course a satisfying understanding of the influence of a magnetic field or of dilution would require a much more detailed analysis, maybe based on

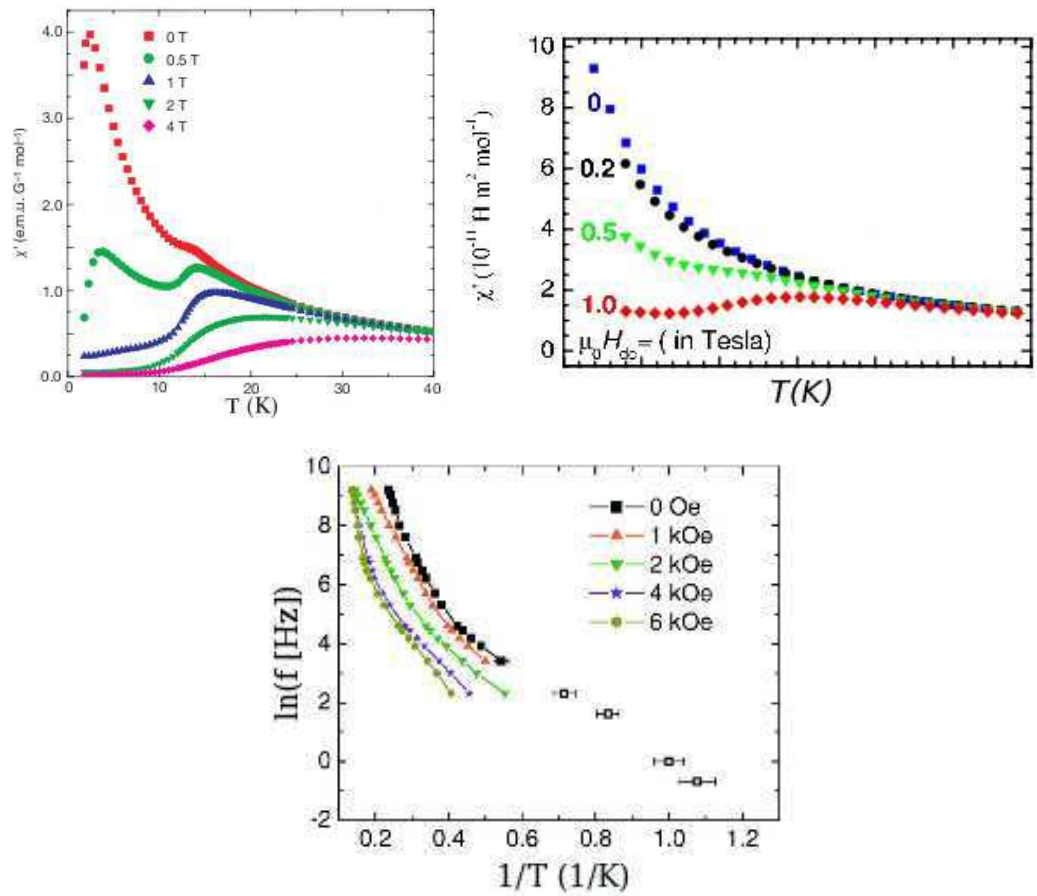

Figure IV.8: **Influence of a magnetic field on the dynamics:** *Top Left:* Real part of the AC susceptibility of $Dy_2Ti_2O_7$ vs temperature T for several different fields at 100 Hz [Sny01]. *Top Right:* Real part AC susceptibility results for $Ho_2Ti_2O_7$ measured with a field of 1 T applied along [111] [Ehl03]. *Bottom:* Frequency $f = 1/\tau$ of the dynamics of $Dy_2Ti_2O_7$ for different fields [Sny04b].

further simulations, but we think that the strength of spin ice materials and especially of the dumbbell model [Cas08] is to allow pleasantly simple and elegant, but yet surprisingly accurate explanations of non-trivial experimental observations.

There are though two points we did not address here. First of all, we do not have an explanation for the different time scales measured for $Dy_2Ti_2O_7$ by [Sny04b] and [Lag07]; they did observe the same shape of the relaxation time, but while the former found the quasi-plateau at ~ 5 ms, the latter measures it at 0.5 μs. This is undoubtedly a consequence of the use of two different experimental techniques with very different experimental time window; AC susceptibility for the former, μSR for the second, but this remains an open question.

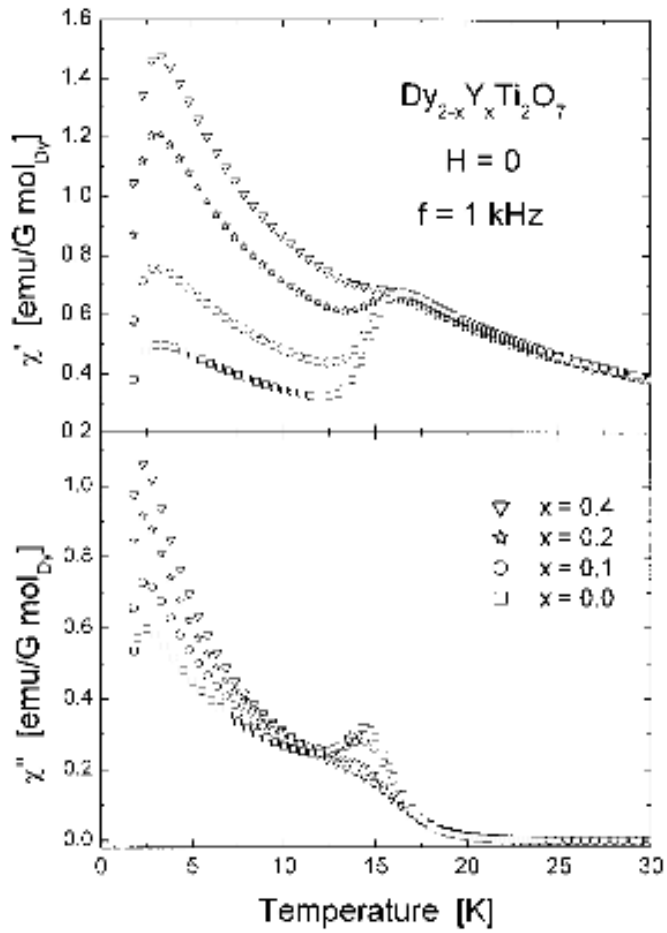

Figure IV.9: **Influence of dilution on the dynamics:** Temperature dependence of the real and imaginary parts of the AC magnetic susceptibility χ' and χ'' of $Dy_2Ti_2O_7$ at 1kHz and in the absence of a DC magnetic field [Sny02].

The other issue we have not discussed here is the relaxation time measured by Orendac *& al.* at extremely low temperature $T \sim 350$ mK using a magnetocaloric technique [Ore07]. We expect spin ice to fall out-of-equilibrium at such temperature, which is indeed observed by these authors, as the magnetocaloric effect takes advantage of this out-of-equilibrium feature to extract the relaxation time. However the time scales they measured are one or two orders of magnitude lower than those we would expect from our simulations. Again, being based on heat pulse rather than on a sinusoidal external magnetic field, this method is very different from AC susceptibility and may require the consideration of spin-lattice coupling, but their result is intriguing, especially because as they can fit their data either with a Raman $1/T^9$ or an Arrhenius process with an energy scale of 3.6 K.

Before closing this chapter on the dynamics of monopoles, we shall consider in the

next section their response to a [001] magnetic field, in a attempt to observe a magnetic current.

IV.4 Monopoles in a field

Applying such a [001] field to a system for closed circuit geometry (periodic boundaries), one might expect the development of a monopole current in the steady state [Ryz05], as for a standard electronic circuit in an electric field. This is not the case, at least for the *nearest neighbour model*, where we find that a transient current decays rapidly to zero (see figure IV.10). The passage of a positive charge in the direction of the field re-organises the network of strings, leaving a wake behind it that can be followed either by a negative charge, or by a positive one moving against the field, with the result that the current stops. This is a dynamic rather than static effect and is not related to confinement of monopole pairs by the background magnetisation. We have simulated systems with periodic boundary conditions (PBC) and with open boundaries on the extremities of the $z-$axis. The flux of particles appears to be the same for a model with PBC (black curve) and for a local measure in the bulk ($z = L_z/2$) of an open system (red curve). However, even if the current remains transient and disappears exponentially, it differs when the flux is measured at the surface of the open system (blue curve). As the response to a step function of the magnetic field is not homogeneous, this suggests the development of charge separation in an open system.

This is indeed the case despite the fact that monopole numbers are not conserved at open boundaries. In figure IV.11 we show the profile of 3 *in* - 1 *out* defect density across a sample of size $L_z = 30$ spins, with open boundaries, for varying fields. As we know from our work on the Kasteleyn transition III.2, a [001] field will favour a 2 *in* - 2 *out* configuration and will thus hinder the creation of topological defects as observed in the figure. However the noticeable point is that there is a clear build up of defects over a band of 4-5 lattice spacings. As the ratio T/h and the monopole density go to zero the band narrows as one expects for a fully saturated system. In the absence of topological defects the magnetization is conserved from one layer to another, so that a charge density profile manifests itself as a magnetization profile. For a real crystal whose surface is not as "clean" as our numerical simulation and where Coulomb interactions should come into play, this density profile will certainly be quantitatively modified but we expect this result to be qualitatively robust; the data here suggest charge build up in a layer several nanometres thick, making it in principle a measurable effect. The experimental set-up remains nonetheless an open question: after discussing with Pierre Dalmas de Réotier and Yann Chapuis, it appeared for example that μSR may not be able to measure effects so close to the surface.

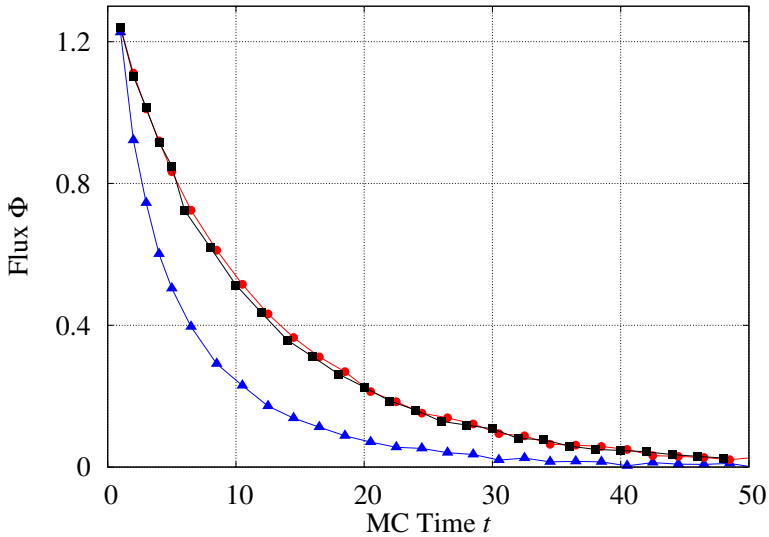

Figure IV.10: **Transient monopole current:** A magnetic field h is applied at $t = 0$ along the z-axis ([001] direction). We display the transient flux of positive charges, Φ, passing through a plane perpendicular to the field, as a function of Metropolis time t. The simulations are obtained using the nearest neighbour spin ice model with periodic boundary conditions (■) and open boundaries, with current measured either at the surface (▲) or in the bulk (●).

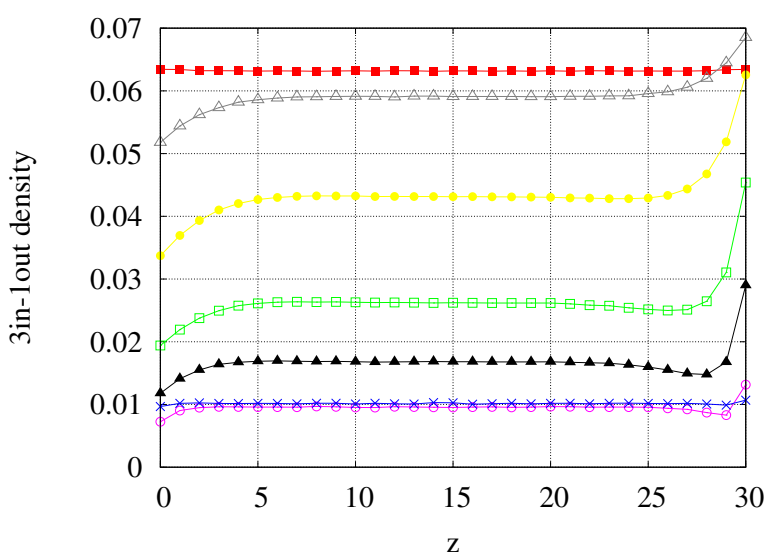

Figure IV.11: **Monopole density profile:** Density of 3 *in* - 1 *out* defects in the (001) planes at position z for $T = 1\,K$ and for different magnetic field $h = 0$, 0.5, 1.0, 1.5, 2.0, 2.5, 3.0, 4.0 (in units of $k_B T/\mu\mu_0$). Increasing h correspond to a decreasing value of the bulk density, $h = 4$ being the straight blue line.

V Zero Field Susceptibility in $Ho_2Ti_2O_7$

V.1 An appealing experimental result

This project has been initiated by neutron scattering experiments performed by Mark Harris who measured the susceptibility of a Holmium Titanate crystal for different scattering vectors $\mathbf{q}$ in Fourier space at the ILL on the IN14 instrument. As these are unpublished data, I would like to express my gratitude to him for allowing me to use them in this manuscript.

Figure V.1 shows $\chi(\mathbf{q}, T)$ for $\mathbf{q} = [0, 0, 0.9]$ on a log-log plot. It is this very result that drew our interest as it does not follow a Curie law (see equation (I.29), red curve on the figure), even at relatively high temperature[1] but is *apparently* quantitatively fitted by a power law $1/T^\gamma$ with $\gamma \approx 1.15$ (green curve), as if the system were going towards a critical point at very low temperature $T = 0^+$ with an unusual critical exponent γ.

However we know that spin ice remains statically disordered down to the lowest accessible temperatures. In fact, let us consider the expression of the bulk susceptibility in the canonical ensemble with N spins

$$\begin{aligned}
\chi &= \frac{1}{NT} \sum_{i,j} \left(\langle \mathbf{S}_i \cdot \mathbf{S}_j \rangle - \langle \mathbf{S}_i \rangle \langle \mathbf{S}_j \rangle \right) \\
&= \frac{1}{T} \left(\frac{1}{N} \sum_i \langle \mathbf{S}_i^2 \rangle + \frac{1}{N} N \sum_{i \neq 0} \langle \mathbf{S}_i \cdot \mathbf{S}_0 \rangle \right) \\
&= \frac{1}{T} \left(1 + \sum_{i \neq 0} \langle \mathbf{S}_i \cdot \mathbf{S}_0 \rangle \right) \qquad \text{(V.1)}
\end{aligned}$$

where $\langle \mathbf{S}_i \rangle = 0$, $\langle \mathbf{S}_i^2 \rangle = 1$, $\forall i$. For a paramagnet without correlations we recover the Curie law $1/T$, but since the ice-rules make spin ice correlations algebraic, the peculiar behaviour of the susceptibility observed in $Ho_2Ti_2O_7$, even if not for $\mathbf{q} = 0$ as in the above equation (V.1), may be a direct signature of spin ice frustration ! As we have previously developed a functional technique on the Husimi tree that has proven to be quite efficient

[1] We recall that $J_{\text{eff}} = 1.8$ K for $Ho_2Ti_2O_7$

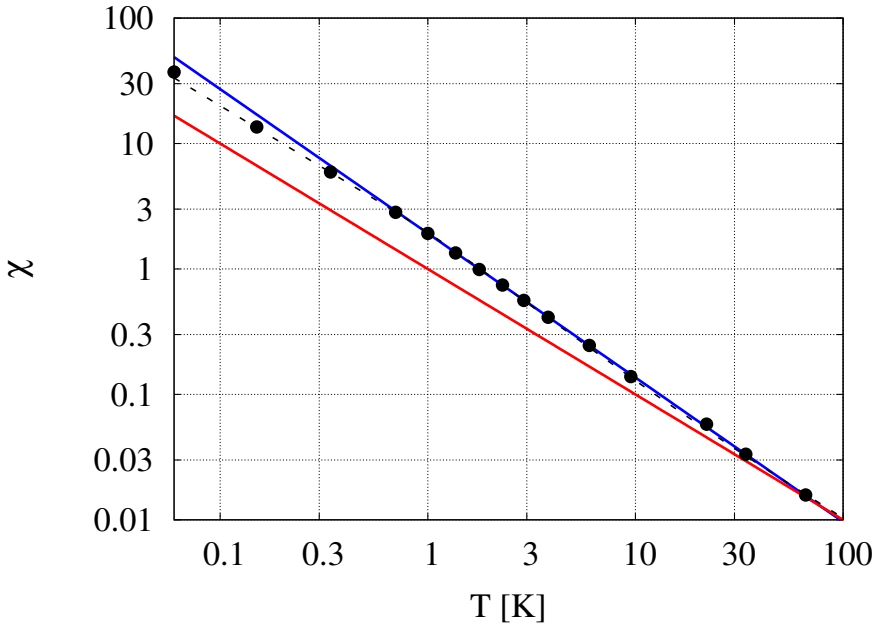

Figure V.1: **Experimental susceptibility** measured by neutron scattering for the scattering vector $\mathbf{q} = [0, 0, 0.9]$ (•) as a function of the temperature T on a log-log scale (*unpublished data* obtained by Mark Harris), compared with different fitting curves: a Curie law (red), a power law $1/T^\gamma$ with $\gamma \approx 1.15$ (blue) and the result from the Husimi tree (dashed). The susceptibility scale is not defined for the experimental data; we thus fixed this scale by a pre-factor in order to fit to the theory. This is our only fitting parameter as the temperature scale has been fixed by $J_{\text{eff}} = 1.8$ K (see table I.3). For convenience, we did not include the factor of 1/3 due to the scalar product between spins that are not parallel.

in fitting experimental data (see figure III.9), our first attempt will be to calculate the bulk susceptibility analytically.

V.2 Husimi tree

Analytical results

As in chapter III, we shall start our calculations by equations (II.68) and (II.69) providing the general expression of the magnetisation in a field h and with bond distortion set to zero $\delta = 0$. We cannot use the results of section III.2 as they have been obtained on the constrained manifold whereas we want now an expression valid for all temperatures, *i.e.* including all terms in βJ. Unfortunately, it is impossible to obtain a general result in presence of a field *and* of topological defects, but since the definition of the susceptibility

is

$$\chi \equiv \left(\frac{\partial M}{\partial h}\right)_{h=0}, \tag{V.2}$$

we can consider an infinitesimal field and perform a 1st order expansion in h. However we still need to find the root of a polynomial in Y of degree 4 (equation (II.68)), but a further simplification is possible. In absence of a field we expect the magnetisation to be zero $M = 0$ which is equivalent to $Y = 1$. Hence a small field h will give $Y = 1 - \epsilon$ with an infinitesimal but positive value of ϵ. After linearisation of equation (II.68), we obtain the following relation between h and ϵ.

$$\epsilon \;=\; \beta h \, \frac{4 \,+\, 3\, e^{2\beta J} \,+\, e^{-6\beta J}}{2 \,+\, e^{2\beta J} \,+\, e^{-6\beta J}} \tag{V.3}$$

From equation (II.69), the magnetisation M can be easily expressed in order $\mathcal{O}(\epsilon)$.

$$M \;=\; 2\epsilon \, \frac{1 + e^{2\beta J}}{4 \,+\, 3\, e^{2\beta J} \,+\, e^{-6\beta J}} \tag{V.4}$$

giving the susceptibility

$$\boxed{\chi \equiv \left(\frac{\partial M}{\partial h}\right)_{h=0} \;=\; 2\beta \, \frac{1 + e^{2\beta J}}{2 \,+\, e^{2\beta J} \,+\, e^{-6\beta J}}} \tag{V.5}$$

If we assume that taking the limit of small h *before* the derivation is correct, then the above result is exact on the Husimi tree. The asymptotic limits of $\chi(T)$ extracted are particularly interesting

$$\boxed{\chi(T \to \infty) \sim 1/T \qquad \chi(T \to 0) \sim 2/T} \tag{V.6}$$

At high temperature we recover the standard Curie law, whereas at very low temperature, when we reach the 2 *in* - 2 *out* manifold, we obtain a **collective Curie law**[2], the latter being twice as big as the former.

To the best of our knowledge, Yoshida *& al.* have been the only one who studied the susceptibility theoretically using the cactus approximation [Yos02]; the philosophy of this method is very close to the Husimi tree, but the authors did not provide an analytical expression of χ, nor did they compare it with experimental data or noted the presence of a crossover. The coefficient of 2 in the collective Curie law has been predicted by Ryzhkin from a microscopic model of charges in a field [Ryz05].

One can also obtain this pre-factor exactly on the Husimi tree by considering the correlations between n^{th} neighbours on the 2 *in* - 2 *out* manifold. This approach is of course redundant with equation (V.5), but we shall present it here in order to discuss

[2]because we are in a collective paramagnet phase.

the relevance of the Husimi tree with regards to the pyrochlore lattice. Our goal is to calculate $\sum_i \langle \mathbf{S}_i \cdot \mathbf{S}_0 \rangle$ from equation (V.1), that can be re-written

$$\sum_{i \neq 0} \langle \mathbf{S}_i \cdot \mathbf{S}_0 \rangle = \sum_{n=1}^{+\infty} \sum_{i \in n^{\text{th}} NN} \langle \mathbf{S}_i \cdot \mathbf{S}_0 \rangle \equiv \sum_{n=1}^{+\infty} g_n \tag{V.7}$$

where g_n is defined through the last sum $\sum_{i \in n^{\text{th}} NN}$ that runs over all n^{th} nearest neighbours with respect to a central spin indexed 0. One can show recursively that $g_n = 2/3^n$. As the exact demonstration happens to be quite long and tedious, we shall rather give a less rigourous but nonetheless accurate proof:

i Let us consider a central spin surrounded by 6 nearest neighbours in 2 tetrahedra. Once this spin is fixed, there are 3 possible configurations left for each tetrahedron that respect the ice-rules: for one of the configuration, all 3 other spins per tetrahedron are aligned with the central spin, whereas the 2 other configurations have one spin aligned and two spins anti-aligned with the central spin. Hence for the former case, on average[3], $\langle \mathbf{S}_i \cdot \mathbf{S}_0 \rangle_{1 \text{ config.}} = (1+1+1)/3 = 1$, whereas for the latter two configurations $\langle \mathbf{S}_i \cdot \mathbf{S}_0 \rangle_{1 \text{ config.}} = (1-1-1)/3 = -1/3$.

ii One can now take the mean value for all three configurations

$$\langle \mathbf{S}_i \cdot \mathbf{S}_0 \rangle_{\text{all config.}} = \frac{1}{3}\left(1 - \frac{1}{3} - \frac{1}{3}\right) = \frac{1}{9} \tag{V.8}$$

which means that on average, the correlations between a spin and one of its nearest neighbour is 1/9

iii Since there are 6 nearest neighbours, we get

$$\sum_{i \in NN} \langle \mathbf{S}_i \cdot \mathbf{S}_0 \rangle_{\text{all config.}} = 6 \cdot \frac{1}{9} = \frac{2}{3} = g_1 \tag{V.9}$$

iv There are $6 \cdot 3^{n-1} = 2 \cdot 3^n$ n^{th} nearest neighbours and the correlation between the central spin and one of them is $(1/9)^n$, which gives $g_n = 2/3^n$.

Hence the total susceptibility for the Husimi tree is

$$\chi = \frac{1}{T}\left(1 + \sum_{n=1}^{+\infty} \frac{2}{3^n}\right) = \frac{2}{T} \tag{V.10}$$

[3] Again we do not include the (1/3) scalar product for convenience.

Analysis of the experiment

The expression of the susceptibility (V.5) is compared with the experimental result on figures V.1 and V.2. The fit is quantitatively good[4] with *no* fitting parameter for the temperature and an overall pre-factor for the susceptibility scale. In figure V.2 one can see how the susceptibility evolves from one asymptotic limit to the other (between the two dashed lines).

This means that according to the Husimi tree picture, the unusual behaviour of χ with temperature is in fact due to a **crossover** from the paramagnetic phase to the spin ice regime without defect ! The best argument in favour of this crossover is on figure V.2, where we note that the power law $T^{-\gamma}$ fails to reproduce the very low temperature experimental data, which are on the other hand well fitted by a plateau for χT, characteristic of the collective Curie law. It is remarkable that a *collective* paramagnet such as spin ice can display a modified Curie law. We would like to stress the experimental success to have measured the susceptibility down to such low temperatures; our comparison with the Husimi tree shows that the system was indeed equilibrated at 0.15 K !

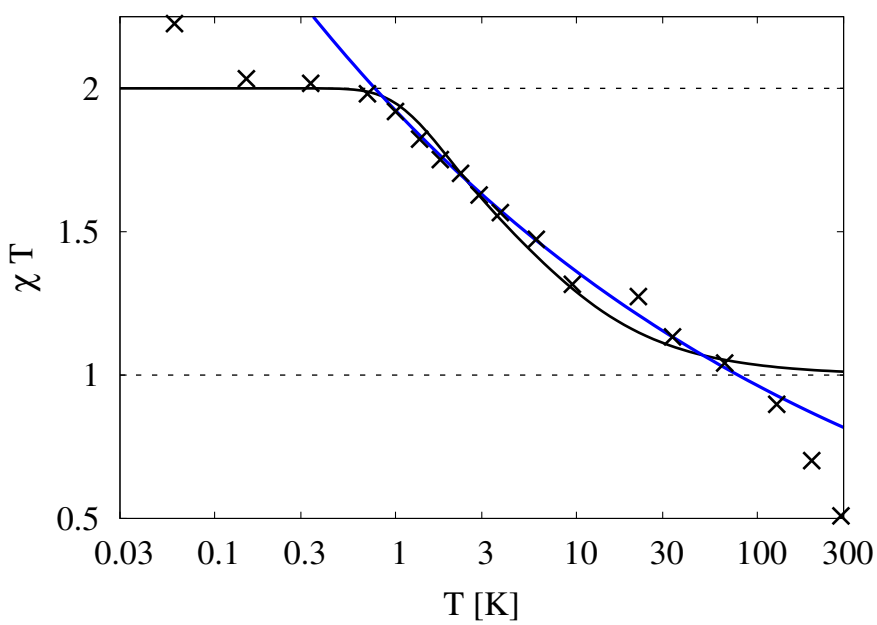

Figure V.2: **Susceptibility crossover:** susceptibility times temperature (χT) vs temperature T on a log-lin scale. We have plotted the experimental data (•), the Husimi tree result (dashed line) and the power law fit $\chi \propto T^{-\gamma}$. The Curie law $1/T$ and the collective Curie law $2/T$ are the horizontal dashed lines. The fit is not good at high temperature because according to [Cla09], the spins lose their Ising nature above ~ 30 K for $Ho_2Ti_2O_7$ and our model does not hold anymore.

[4]It is even excellent on a logarithmic plot, which is *a piori* the natural scale for an observable varying over more than 3 orders of magnitude.

Although based on a lattice of infinite dimensions, the Husimi tree provides here a very good fit to experimental data and brings to light the signature of the crossover from a standard to a collective paramagnet, hidden in the unusual temperature dependance of the susceptibility. However, even if this study does answer our original question, it also opens new ones that can be summarised as follows: "Why does it work so well ?" This is a legitimate question, because there are different levels of approximations going on.

For example the Husimi tree is very close to the pyrochlore lattice because it captures most of its microscopic details, except for closed loops (hexagons and higher order). In equation (V.10), the first terms $g_1 = 2/3$ and $g_2 = 2/9$ are rigourously the same, discrepancies only occurring for some of the further neighbours; hence there may be corrections to the $2/T$ collective Curie law for the $3d$ material, but this must be a very close estimation as comparison with Monte Carlo simulations on the $3d$ pyrochlore lattice are excellent (see figure V.4 below).

Furthermore since part of the data are at very high temperature for $Ho_2Ti_2O_7$ ($J_{\text{eff}} = 1.8$ K), the concentration of defects is far from being negligible and we should need to include dipolar interactions, but the NNSI model already turns out to be quantitatively good. Last but not least, we have fitted a *local* measurement of the scattering function in Fourier space for $\mathbf{q} = [0, 0, 0.9]$ with an analytic expression of the *bulk* susceptibility. Hence further study *a priori* requires the explicit consideration of the non-uniform scattering function $S(\mathbf{q}, T)$. Unfortunately this is impossible with the Husimi tree because of its infinite dimension geometry. We shall thus pursue this analysis with Monte Carlo simulations.

V.3 Q-dependance of the susceptibility

Our goal here is to compute the scattering function $S(\mathbf{q}, T)$ as a function of temperature and for different characteristic points in reciprocal space. We use the NNSI model in order to be able to compare our results directly with the Husimi tree. By definition, this function is the Fourier transform of the thermally averaged two-spin correlation function, giving $\chi(\mathbf{q}, T) \equiv S(\mathbf{q}, T)/NT$, and is expressed as follows

$$S(\mathbf{q}, T) \equiv \left\langle \left| \sum_{i=1}^{N} \mathbf{S}_{i\perp} \, e^{i\mathbf{q}\cdot\mathbf{r}_i} \right|^2 \right\rangle \tag{V.11}$$

where N is the number of spins whose positions are given by $\mathbf{r}_i$. $\mathbf{S}_{i\perp}$ is the component of the spin orthogonal to the scattering vector $\mathbf{q}$. The thermal average $\langle \dots \rangle$ is performed on statistically independent samples equilibrated at a temperature T. The finite value of T makes the single spin flip (SSF) Metropolis algorithm essential in order to create/annihilate topological defects. The Worm algorithm has also been used in addition to SSF for some of the simulations, allowing a more efficient decorrelation of the system and equilibration to lower temperatures.

We should warn the reader that this section is still ☢*work in progress*☢ and the conclusion is thus only partial, but it nonetheless reveals some intriguing aspects of spin ice

that we plan to clarify in a (hopefully) near future.

Contribution of $\mathbf{S}_{i\perp}$

In order to justify the following comparison between the Husimi tree and simulations, we should stress that by taking the orthogonal component of the spin $\mathbf{S}_{i\perp}$, we lose 1/3 of the magnetic susceptibility. To show this, we define a new set of axes with z' parallel to $\mathbf{q}$ and (x', y') form the scattering plane. The scattering function can be trivially expressed in this new basis

$$S(\mathbf{q},T) = \left\langle \left(\sum_{i=1}^{N} S_{i\,x'} \cos(\mathbf{q}\cdot\mathbf{r}_i)\right)^2 + \left(\sum_{i=1}^{N} S_{i\,x'} \sin(\mathbf{q}\cdot\mathbf{r}_i)\right)^2 + \left(\sum_{i=1}^{N} S_{i\,y'} \cos(\mathbf{q}\cdot\mathbf{r}_i)\right)^2 + \left(\sum_{i=1}^{N} S_{i\,y'} \sin(\mathbf{q}\cdot\mathbf{r}_i)\right)^2 \right\rangle$$

In the paramagnetic phase, the crossed terms disappear $\langle S_{i\,x'}\, S_{j\,x'}\rangle = \delta_{ij}\, S^2_{i\,x'}$ and we get

$$S(\mathbf{q}, T\to\infty) = \sum_{i=1}^{N} \left(S^2_{i\,x'} + S^2_{i,y'}\right) = \frac{1}{2}\sum_{\alpha=1}^{N/2}\sum_{\kappa=1}^{4} \left[1 - (\mathbf{S}_{\alpha\,\kappa}\cdot\mathbf{q})^2\right]$$

where the sums run over the $N/2$ tetrahedra α and the 4 sublattices κ. $\mathbf{q}$ is normalised here. Using the vectorial expression of the spins (I.38), we can directly show that for *any* scattering vector $\mathbf{q}$

$$S(\mathbf{q}, T\to\infty) = \frac{N}{4}\left[4 - \frac{4}{3}\right] = \frac{2N}{3} \Rightarrow \chi(\mathbf{q}, T\to\infty) \sim \frac{2}{3T} \tag{V.12}$$

instead of the standard $1/T$ Curie law because we have lost the contribution of the component along $\mathbf{q}$. We should outline that this result is not as trivial as it seems; equation (V.12) is valid for all vectors in the reciprocal space because of the specific geometry of the pyrochlore lattice with local Ising spins. For example if all spins were parallel, this would highly depend on the orientation of $\mathbf{q}$. For spin ice, the scattering function is thus uniform in the paramagnetic phase, assuming we can reach this phase before the spins lose their Ising nature and thermally fluctuate out of their local easy-axis.

In order to compare Monte Carlo outcomes with equation (V.5), we shall then use a pre-factor of 2/3.

Scattering function

We used the Worm algorithm together with SSF to compute the scattering function in the $[hh\ell]$ plane at $T = 1$ K. The result is very similar to what we can find in the literature, except that our simulations do not include the magnetic form factor and thus do not weaken for large $|\mathbf{q}|$, as observed in [Bra01b, Fen04, Fen09].

In particular we clearly observe the *pinch points* at [0,0,2], [1,1,1] and [2,2,2] (see appendix C). We shall now look at the temperature dependance of some specific points along the [0,0,ℓ], $[h,h,0]$ and $[h,h,h]$ axes.

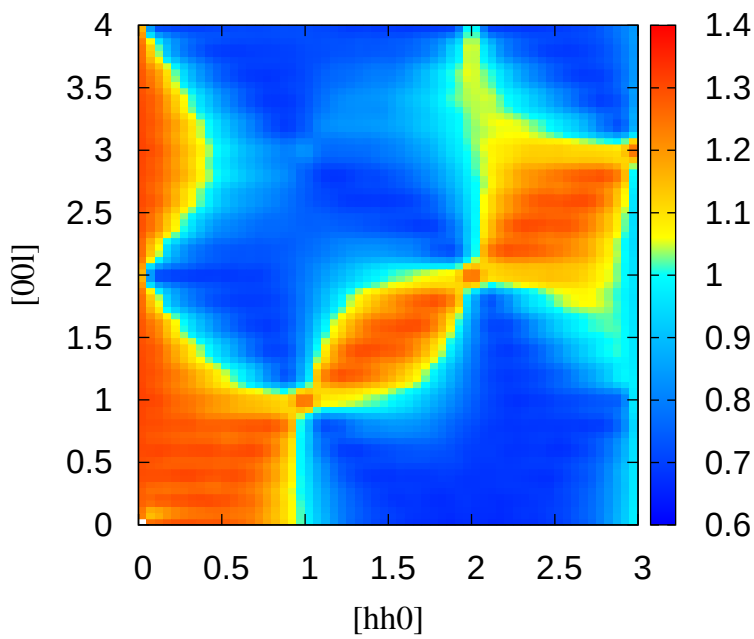

Figure V.3: **Scattering function** of the nearest neighbour spin ice model at $T = 1$ K for a system of 4000 spins, simulating $Ho_2Ti_2O_7$ with $J_{\text{eff}} = 1.8$ K

Susceptibility $\chi(\mathbf{q}, T)$

Figure V.4 shows the crossover between the paramagnetic phase and the topological spin ice regime for different vectors $\mathbf{q}$. As we have used the SSF algorithm only, the system does not manage to equilibrate at low temperature. In a concern of clarity we did not plot all our simulations; in a nutshell we can say that we obtain the same results for [0,0,ℓ] ($\ell = 0.831, 1, 2, 2.3$) and $[h,h,h]$ ($h = 0.5, 1, 1.5, 2$), but *not* for [1,1,0] and [2,2,0]. The symmetry between the axes [0,0,ℓ] and $[h,h,h]$ and the difference with $[h,h,0]$ are understandable from figure V.3, even if we do not have an explanation for the specific behaviour of the latter case, but the remarkable points are that

- Monte Carlo simulations for [0,0,ℓ] and $[h,h,h]$ reproduces perfectly the Husimi tree and the experiments at $\mathbf{q}_{\text{exp}} = [0, 0, 0.9]$, which means that $\mathbf{q}_{\text{exp}}$ in spin ice is well described by the NNSI model and we do not need the implementation of long range interactions;

- For the NNSI model, the axes passing through the pinch points conserves the same value of $S(\mathbf{q})$ all along. This is an important fact as neutron scattering experiments display the same behaviour *except at the pinch point* [Har07]. Measurements performed at [0,0,0.9], [0,0,1.05] and [0,0,2.95] gives the same value of the scattering function and thus follow the Husimi tree calculation, whereas the susceptibility at the pinch point [0,0,2] is a standard $1/T$ Curie law !

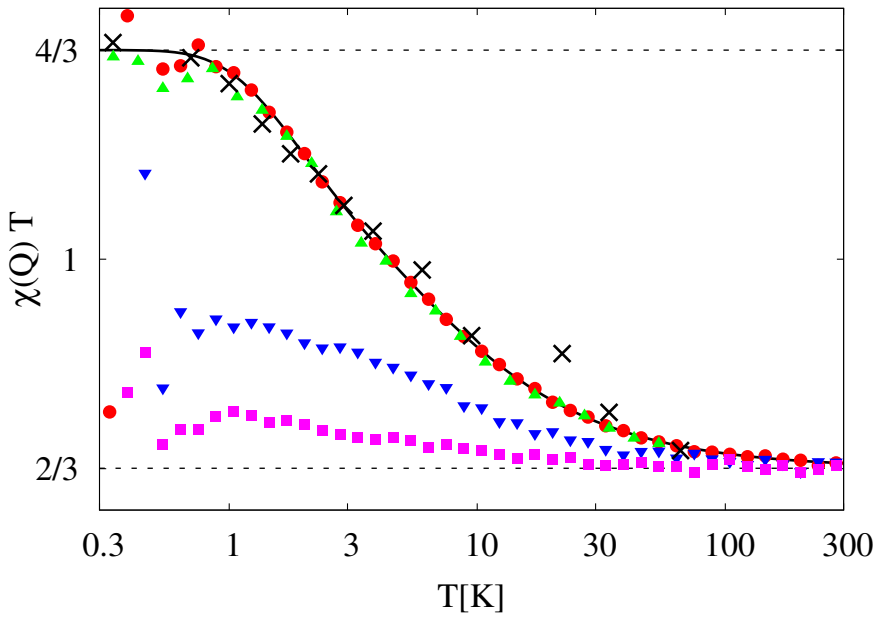

Figure V.4: **Susceptibility** $\chi(\mathbf{q}, \mathbf{T})$**:** Experimental data for $\mathbf{q} = [0, 0, 0.9]$ ($\times$), Husimi tree for for $\mathbf{q} = 0$ scaled by 2/3, Monte Carlo simulations for $\mathbf{q} = [0, 0, 1]$ (●), $[1, 1, 1]$ (▲), $[1, 1, 0]$ (▼) and $[2, 2, 0]$ (■). The Curie law $1/T$ and the collective Curie law $2/T$ are the horizontal dashed lines.

Neutron scattering experiments on spin ice materials thus display a very rich family of phenomena. Here we gave prominence to the crossover between a standard and a *collective* paramagnetic phase, both of them being asymptotically characterised by a susceptibility $\chi \propto 1/T$ but differentiated by a factor 2, giving rise to what we called a *collective* Curie law, with the underlying consequence that spin ice can behave exactly like the nearest neighbour model.

A $\mathbf{q}-$dependent study of the susceptibility, both theoretical and experimental, revealed a more complex picture where the crossover can partially or completely disappear for some values of $\mathbf{q}$. More work needs to be done to understand these points, that will inevitably take advantage of the recent paper by Tom Fennell *& al.* who used polarised neutron scattering to validate the projective equivalence(see susection I.3.c) between the NNSI and DSI model and observed for the first time a stunning pinch point in zero field in spin ice [Fen09].

VI Conclusion

In this thesis, we have endeavoured to present a wide range of the properties and unique characteristics of spin ice materials, considering both dynamical and equilibrium aspects, taking advantage of the specificities of the nearest neighbour, dipolar and dumbbell model.

We have first investigated the influence of a [001] magnetic field h on the 2 *in* - 2 *out* manifold with nearest neighbour interactions [Jau08, Jau09a]. The divergence free condition prevents the creation of local topological defects and forces the system to relax through extensive string excitations spanning the entire sample along the [001] axis, dividing the phase space into sectors defined by a given number of strings or equivalently a given value of the magnetisation.

The competition between the Zeeman energy cost and the entropic gain due to closed loops of finite size responsible for the fluctuations of the strings within a sector determines the entire physics of the problem, reminiscent of the Kasteleyn transition observed in some dimer models [Kas63, Bha83, Moe03a], but for the first time predicted in a $3d$ magnetic system. At low temperature and in the thermodynamic limit, string relaxation is extensively suppressed as the corresponding Gibbs free energy cost is linear in system size, but above a well-defined transition temperature T_{K}, strings become suddenly entropically favoured. The transition is continuous because of entropic string repulsion. We studied this problem analytically (on the Husimi tree) and numerically (with a rejection-free Worm algorithm), both methods agreeing perfectly *without* any fitting parameter, except for logarithmic corrections due to fluctuations at the upper-critical dimension $d_c = 3$. A mapping onto a (2+1) dimensional quantum phase transition enables calculations of the correlations, displaying a crossover from dipolar correlations in $1/r^3$ in the Coulomb phase to self-correlations in $1/r$ for diluted concentration of strings at T_{K}^{+}. In order to compare our theory with experiments, we have included thermally activated topological defects; the transition becomes rounded as string excitations of finite length, terminated by two defects, are possible. The two sets of experimental magnetisation curves are in quantitative agreement with the theory, up to a fitting parameter in the temperature or magnetic field.

The next step in this project would be for example to include dipolar interactions between spins to test the robustness of the Kasteleyn transition with long range interactions and for a better fit to experiments.

The influence of the magnetic field was to lift the extensive degeneracy of spin ice in favour of a *unique* ground state. We want to outline here it is quite remarkable to obtain a phase transition in presence of a symmetry-breaking field, as confirmed by the fact it disappears as soon as we release the topological constraints ! In that sense, it looks promising to find another way to lift the degeneracy while keeping the global $\mathbb{Z}_2$ symmetry; this can be done using bond distortion δ, by weakening all NN interactions in the (001) planes, hence favouring the two fully saturated microstates in the [001] direction.

If we apply both perturbations on the 2 *in* - 2 *out* manifold, the transition remains a Kasteleyn one, but the slope of the magnetisation at T_{K}^{+} becomes steeper as the ratio h/δ is decreased, *i.e.* the string relaxation process is more efficient. In the limit $h/\delta \to 0$, the slope becomes infinite and the magnetisation looks discontinuous; this is a $3d$ version of the KDP transition which was believed to be 1st order [Sla41, Lie67a, Nag69]. However all different methods we have used (Husimi tree, Worm algorithm, transfer matrix, mapping onto a (2+1) quantum critical point) show the equiprobability of all sectors in the thermodynamic limit[1], exactly at the transition; the PDF of the magnetisation is flat, a signature of a *multi-critical point of* $\infty-$*order* which is expected to look at first sight like a 1st order transition, but bears all characteristics of a critical point (no hysteresis, no double peaks in the PDF of the energy) [Ben77]. Furthermore, as we are *above* the upper-critical dimension, we have discovered that the main contribution to the susceptibility does not come from local fluctuations through finite size scaling, but from the homogeneous fluctuations of a mean field system. In the limit $L_z \gg L_\perp^2$, all configurations within a given sector are equiprobable, which means that the strings do not interact with each other and are only correlated with themselves in the [001] direction.

According to experimental results from [Mit07], such a bond distortion seems to be feasible in spin ice under uniaxial [001] pressure, even if the presence of defects and maybe also of dipolar interactions may turn this transition continuous.

On the bounce of the remarkable paper by Castelnovo *& al.* [Cas08], we decided to study the intriguing behaviour of the magnetic relaxation time [Sny04a] for the purpose of finding a potential dynamical signature of magnetic monopoles in spin ice. We have shown that below ~ 10 K, the relaxation time τ can be explained by the superposition of two contributions: a quantum tunnelling mechanism that allows single spin flips without requiring an energy cost of the order of the first excited energy level (~ 200 K), and a thermally assisted process responsible for the creation and proliferation of *deconfined* magnetic monopoles; the quasi-plateau region is well-fitted by an Arrhenius law [Jau09b]. At lower temperature, below ~ 3 K, a quantitative understanding of the spin freezing requires the implementation of long range interactions; for this range of temperature, the density of monopoles is too low to provide an efficient Debye screening of the magnetic Coulomb interactions, which hinders the creation of new monopoles, and thus decreases even more their density. This spin freezing is thus due to an *avalanche effect* provoked by Coulomb interactions between magnetic monopoles. The next step will surely be to study in more details the static and dynamic properties of this Coulombic system, both in the

[1]The result is **exact** when $L_z \gg L_\perp$ and we have strong evidence it also holds for a cube $L_z = L_\perp \gg 1$

context of SI experiments and more generally as this represents a fascinating theoretical system.

In the last chapter (§ V), we have presented the susceptibility of $Ho_2Ti_2O_7$ which clearly displays a crossover between a standard Curie law $1/T$ in the paramagnetic phase, and a *collective* Curie law $2/T$ in the Coulomb phase at very low temperature. Experimental data agree with both an analytical expression extracted from the Husimi tree and Monte Carlo simulations. This study opens many questions concerning the temperature dependance of the scattering function $S(\mathbf{q}, T)$, suggesting the presence of points $\mathbf{q}$ in the reciprocal space where the NNSI model might be quantitatively correct. The recent paper [Fen09] will most certainly give some hints for future developments.

As a summary, we would like to outline the remarkable properties that makes spin ice unique among magnetic materials. First of all, because of the classical nature of the Ising spins and of the projective equivalence [Isa05, Fen09] the NNSI usually gives semi-quantitative, and sometimes even very good agreement with experiments and enables surprisingly accurate analytical expressions. On top of that, the dumbbell model allows simple arguments to provide a fundamental and detailed picture of spin ice including long range interactions, through deconfined monopoles feeling an effective Coulomb potential in the grand canonical ensemble; once a pair of defect is created, it cannot "suddenly" disappear, but needs to be annihilated by hitting another monopole of opposite charge. We should also not forget the existence of several spin ice compounds that all share similar properties, two of them ($Dy_2Ti_2O_7$ and $Ho_2Ti_2O_7$) being available in single crystals which is primordial for angle dependance experiments.

Concerning spin ice candidates, I am especially interested in $Pr_2Sn_2O_7$ which displays a thermally activated relaxation process over a wide range of temperature with an energy scale of the order of the effective nearest neighbour interactions [Zho08b]. More importantly, this material remains dynamic down very low temperature [Zho08b]; $\tau_{\mathrm{Pr}} \sim 10^{-11}$ s at 200 mK whereas $\tau_{\mathrm{Dy}} \sim 10^{0}$ s at 800 mK. This absence of spin freezing is particularly intriguing: is it due to a modification of the dipolar moments for Pr ($\mu = 2.6\mu_B$) compared to Dy or Ho ($\mu = 10.6\mu_B$) ? Or is it a consequence of the relatively small energy gap between the ground state and the first excited state, that may include quantum fluctuations $\gtrsim$ 100 K ? If $Pr_2Sn_2O_7$ turns out to be a spin ice material, then one will need to understand its zero-point entropy that disagrees with Pauling's estimate, but its dynamics may shed a new light on spin ice and open new experimental possibilities.

A Generalisation of Pauling's argument

Pauling constructed a simple but nonetheless efficient estimate of the entropy of ice at zero temperature [Pau35] that only differs from the most accurate reference by an error of 1.5 % [Nag66].

His argument, applied to spin ice, was the following; among the 16 possible configurations of a single tetrahedron, 6 of them form the ground state; hence among the 2^N microstates of the N spins, there is only approximately a ratio of $(6/16)^{N/2}$ that respect the ice-rules (where $N/2$ is the number of tetrahedra); the total number of ground state configurations is then

$$\Omega \,=\, 2^N \left(\frac{6}{16}\right)^{N/2} = \left(\frac{3}{2}\right)^{N/2} \tag{A.1}$$

giving Pauling's zero-point entropy

$$S_{\text{Pauling}} \,=\, N\,\frac{1}{2}\ln\left(\frac{3}{2}\right) \tag{A.2}$$

This argument turns out to be exact on the Husimi tree, because it neglects the self-interaction of tetrahedra due to small closed loops in the pyrochlore lattice. In fact it is possible to make a phenomenological generalisation at finite temperature and for more complex models, as for example with bond distortion. Our goal will be to reproduce the analytical expression of the entropy III.35.

Let us define X such that for each tetrahedron, there is a ratio of $(X/16)$ of the total number of configurations which is accessible. X is not anymore an integer *a priori* and is strongly temperature- and model-dependent. Included in equation (A.1), this gives

$$\Omega(X) \,=\, 2^N \left(\frac{X}{16}\right)^{N/2} = \left(\frac{X}{4}\right)^{N/2} \Rightarrow S(X) \,=\, N\,\frac{1}{2}\ln\left(\frac{X}{4}\right) \tag{A.3}$$

There is no rigourous way to compute X, but we can define it phenomenologically such as the "averaged" number of configurations available per tetrahedron. Let us note p_i and g_i respectively the Boltzmann probability and the degeneracy of a configuration i. This

enables the definition of an entropy per tetrahedron that can be expressed as a function of X as follows

$$S_{\text{tet}} \equiv \ln X \equiv -\sum_i g_i\, p_i\, \ln\, p_i \tag{A.4}$$

A rapid test immediately gives Pauling's entropy (*i.e.* $X = 6$) with $g_i = 6$ and $p_i = 1/6$ at zero temperature. Now if we consider the model with bond distortion (see figure II.1), there are four energy scales:

- 2 *in* - 2 *out* (all spins *up* or *down*): $p_{2\uparrow} = p_{2\downarrow} = \exp\left[2\beta(J+\delta)\right]/z$ and $g_{2\uparrow} = g_{2\downarrow} = 1$;
- 2 *in* - 2 *out* (others): $p_{2\,o} = \exp\left[2\beta(J-\delta)\right]/z$ and $g_{2\,o} = 4$;
- 3 *in* - 1 *out* and 3 *out* - 1 *in*: $p_3 = 1/z$ and $g_3 = 8$;
- 4 *in* and 4 *out*: $p_4 = \exp\left[-\beta(6J-2\delta)\right]/z$ and $g_4 = 2$.

where z is the partition function for a single tetrahedron

$$z \;=\; 8 \;+\; 4\, e^{2\beta(J-\delta)} \;+\; 2\, e^{2\beta(J+\delta)} \;+\; 2\, e^{-\beta(6J-2\delta)} \tag{A.5}$$

Once injected in equation (A.4), we obtain

$$S_{\text{tet}} \;=\; \ln z \;-\; \frac{2\beta}{z}\left[2(J+\delta)\, e^{2\beta(J+\delta)} \;+\; 4(J-\delta)\, e^{2\beta(J-\delta)} \;-\; (6J-2\delta)\, e^{-\beta(6J-2\delta)}\right] \tag{A.6}$$

The corresponding value of X gives the same value of the entropy $S(X)$ than the one obtained from a direct calculation on the Husimi tree III.35, where we recall that $N_t = N/2$.

In the limit $J \to +\infty$, we should only take into account the 2 *in* - 2 *out* microstates and the entropy is then expressed in equation (III.37). The remaining Boltzmann probabilities become

$$p_{2\uparrow} = p_{2\downarrow} = \frac{e^{4\beta\delta}}{4 + 2\, e^{4\beta\delta}}, \qquad p_{2\,o} = \frac{1}{4 + 2\, e^{4\beta\delta}}. \tag{A.7}$$

At the transition $T_c = 4\delta/\ln 2$, the density of tetrahedra configurations is

$$n_{2\uparrow} \;=\; g_{2\uparrow}\, p_{2\uparrow} \;=\; n_{2\downarrow} \;=\; 25\%, \qquad n_{2\,o} \;=\; g_{2\,o}\, p_{2\,o} \;=\; 50\% \tag{A.8}$$

which gives

$$S_{\text{tet}} = -2 \cdot \frac{1}{4} \ln \frac{1}{4} \;-\; 4 \cdot \frac{1}{8} \ln \frac{1}{8} \Rightarrow X \;=\; 4\sqrt{2} \tag{A.9}$$

and we recover $S = (1/4)\, \ln 2$ of equation (III.37).

B Demagnetisation Effect

Definititon

The notion of demagnetisation is quite subtle and requires a precise definition of the variables we use. Let be $(\mathbf{B}_{\text{int}}, \mathbf{B}_{\text{ext}})$ and $(\mathbf{H}_{\text{int}}, \mathbf{H}_{\text{ext}})$ respectively the internal and external magnetic fields and magnetic strengths[1] . If we consider a magnetic material with magnetic permeability μ_r surrounded by a vacuum, then we can write the following relations

$$\mathbf{B}_{\text{ext}} \,=\, \mu_0\, \mathbf{H}_{\text{ext}}, \qquad \mathbf{B}_{\text{int}} \,=\, \mu_0 \mu_r\, \mathbf{H}_{\text{int}} \,=\, \mu_0 (\mathbf{H}_{\text{int}} + \mathbf{M}) \tag{B.1}$$

where $\mathbf{M}$ is the magnetisation of the compound and its unit is A.m^{-1}. The spins $\mathbf{S}_i$ in the system feels the magnetic strength $-\mu_0\, \mathbf{H}_{\text{int}} \cdot \mathbf{S}_i$ rather than the magnetic field $\mathbf{B}_{\text{int}}$. It will prove to be convenient to define the effective internal magnetic field $\mathbf{B}^*_{\text{int}} \equiv \mu_0\, \mathbf{H}_{\text{int}}$.

Demagnetisation field

When an external magnetic field $\mathbf{B}_{\text{ext}}$ is applied on a magnetic material, the spins of the latter tend to align with $\mathbf{H}_{\text{ext}}$ creating an overall finite macroscopic magnetisation $\mathbf{M}$. However this magnetisation will also give rise to an effective magnetic strength following

$$\mathbf{H}_{\text{int}} \,=\, \mathbf{H}_{\text{ext}} \,-\, d\, \mathbf{M} \tag{B.2}$$

where d is the demagnetisaiton factor and solely depends on the shape of the sample and the field orientation; there is usually one factor defined for each symmetry axis (*e.g.* 1 for a sphere, 2 for an ellipsoide). As the influence of the magnetisation is opposed to the external magnetic strength, it is called the demagnetisation field. From equation (B.1), one immediately gets

$$\mathbf{B}^*_{\text{int}} \,=\, \mathbf{B}_{\text{ext}} \,-\, \mu_0 d\, \mathbf{M} \tag{B.3}$$

The demagnetisation effect can thus be neglected for experiments or simulations with zero magnetisation. This is why we did not consider it when we analysed the magnetic relaxation time in zero field (§ IV), but we had to subtract its contribution in magnetisation curves (see subsections III.2.e and III.4.f). For a discussion of the demagnetisation effect in the context of the Ewald summation in spin ice, we refer the reader to Appendix C of [Mel04].

[1] There are many alternative names for both B and H and we chose these ones for clarity.

Application to spin ice experiments [Fen05]

Our goal is to apply the above expression B.3 to figure III.9 for the experimental measurements by Fennell *& al.* on a spherical sample ($d = 1/3$) and in a [001] magnetic field. In the case of $Ho_2Ti_2O_7$, we have 16 atoms in a unit cell of size 10.1 Å allowing a rewriting of equation (B.3)

$$\mathbf{B}^*_{\text{int}} = \mathbf{B}_{\text{ext}} - \mu_0 d\, \rho_{\text{ion}} \mathbf{M}_{\text{ion}} \mu_B \tag{B.4}$$

where $\mathbf{M}_{ion}$ is in units of the Bohr magneton μ_B and $\rho_{ion} = 15.5\, 10^{27}\, m^{-3}$ is the density of rare-earth ions. The [001] direction of the field does not favorise any sublattice which gives the same value of the saturation for all spins

$$(\mathbf{M}_{\text{ion}})_{\text{sat}} = \frac{g_J\, J}{\sqrt{3}} = \frac{10.6}{\sqrt{3}} = 6.11 \tag{B.5}$$

From the right panel of figure III.9, one can now extract the linear dependance of $\mathbf{M}_{\text{ion}}$ with respect to the external magnetic field $\mathbf{B}_{\text{ext}}$ (for small fields): $\mathbf{M}_{\text{ion}} = 10.3\, \mathbf{B}_{\text{ext}}$. Using the numerical values of $\mu_B = 9.27\, 10^{-24}$ J.T^{-1} and $\mu_0 = 4\pi\, 10^{-7}$ J.A^{-2}.m^{-1}, we finally obtain the relation:

$$\mathbf{B}^*_{\text{int}} = 0.38\, \mathbf{B}_{\text{ext}} \tag{B.6}$$

Comparison with theory

According to our Hamiltonian III.2, the theoretical Boltzmann factor of the Zeeman energy is $\exp(-h\, \sigma'_i/T)$ whereas its experimental value is $\exp(-\mathbf{B}^*_{int} \cdot \mathbf{S}_i/(k_B\, T))$. It leads to the direct relation:

$$h = \frac{g_J\, J\, \mu_B}{\sqrt{3} k_B} \mathbf{B}^*_{\text{int}} = 4.1\, \mathbf{B}^*_{\text{int}} \tag{B.7}$$

giving from equation (B.6)

$$h = 1.56\, \mathbf{B}_{\text{ext}} \tag{B.8}$$

Hence when we compare our results with the experimental data as a function of $\mathbf{B}_{\text{ext}}$, we should simply divide our theoretical field h by this factor of 1.56. But in fact, the best fit is obtained by the factor:

$$\left(\frac{h}{\mathbf{B}_{\text{ext}}}\right)_{bestfit} \approx 0.98 \tag{B.9}$$

The ratio of the expected theoretical value over the best fit is then $h_{\text{theo}}/h_{\text{exp}} \approx 1.56/0.98 \approx 1.6$.

I am thankful to John Chalker and Steven Bramwell for enlightening discussions on this matter, the rest of my understanding coming from my reference books from the Agrégation [Rou97, Kit96] as well as [LÓ7]. I am *not* thankful to CGS and SI units.

C Neutron Scattering & Pinch Points

Why neutron scattering ?

Neutrons present several advantages for investigating features of condensed matter. Their incident energy can be adapted to correspond to the energy scale one is interested in, and since it does not carry an electric charge, it can penetrate deeply into the target and thus comes closer to the nucleus of the atom. But its most relevant property for magnetic materials is its magnetic moment that can interact with the spins of the electrons in crystals [Squ96].

It is this latter characteristic that makes neutrons a valuable tool for spin ice, as the scattering function $S(\mathbf{q})$ measured by neutron scattering is an experimental representation of the Fourier-transformed correlation function between spins, theoretically given by

$$S(\mathbf{q}) = \left| \sum_{i=1}^{N} \mathbf{S}_{i\perp} \, e^{i\mathbf{q}\cdot\mathbf{r}_i} \right|^2 \tag{C.1}$$

where N is the number of spins whose positions are given by $\mathbf{r}_i$ and $\mathbf{S}_{i\perp}$ is the component of the spin orthogonal to the scattering vector $\mathbf{q}$. Neutron scattering can thus immediately reveal magnetic ordering, or for spin ice, the establishment of dipolar correlations imposed by the ice-rules.

Experimental observation of pinch points

As explained in subsection I.3.c, the divergence free condition leads to intriguing anisotropic algebraic correlations. Youngblood & Axe studied them in the $2d$ 6-vertex model and showed the emergence of a clear signature of the ice-rules in the scattering function, predicted to appear as *pinch points* [You81], where the scattering function is locally singular in one direction and diffuse in the two others, whereas $S(\mathbf{q})$ is singular (resp. diffuse) in all three directions at a critical point (resp. in a paramagnetic phase) [Fen07]; this is a direct consequence of the anisotropic form of the dipolar correlations.

Even if such pinch points have been observed in the ferroelectric compound KD_2PO_4 [Ska70], their manifestation in magnetic materials remained unsettled until two years ago when they were clearly detected in $Ho_2Ti_2O_7$ in a [111] field [Fen07], after the theoretical prediction made by Moessner & Sondhi [Moe03a]. Further progress has been made very recently using polarised neutron scattering, a technique that gives the opportunity to

measure the different contributions of the scattering function separately [Fen09]; the authors of this paper showed that one of these two contributions behaves like NNSI to an excellent approximation, with the expected apparition of a pinch point in zero field ! At finite temperature, when the ice-rules are not enforced, the width of this pinch point that should be infinitesimal becomes small but finite [You81]; this is a distinct signature of local monopole like excitations in spin ice [Fen09].

One last point we should outline here, is that $Ho_2Ti_2O_7$ has been extensively studied using neutron scattering, but $Dy_2Ti_2O_7$ has been much less investigated, as several isotopes of Dy display a strong neutron absorption, making the scattering very week. On the other hand $Ho_2Ti_2O_7$ is an ideal compound for neutrons.

Pinch points in 2d: the divergence free constraint

We shall here construct a continuous model of spin ice, capturing the essential details necessary for the emergence of pinch points. The simplest phenomenological Gibbs free energy with a magnetic strength $\mathbf{H}$ and dipolar interactions is

$$G \,=\, \frac{1}{2}\kappa\, M^2 \,-\, \mathbf{M}\cdot\mathbf{H} \tag{C.2}$$

where the first term hinders the saturated magnetisation. In Fourier space, we have

$$G(\mathbf{q}) \,=\, \sum_{\mathbf{q}} \frac{1}{2}\kappa\, M^2(\mathbf{q}) \,-\, \mathbf{M}(\mathbf{q})\cdot\mathbf{H}(\mathbf{q}), \tag{C.3}$$

while the ice-rules impose the divergence free condition

$$\nabla\cdot\mathbf{M}(\mathbf{r}) = 0 \qquad \Leftrightarrow \qquad \mathbf{q}\cdot\mathbf{M}(\mathbf{q}); \tag{C.4}$$

$$\Leftrightarrow \qquad q_x\, M_x \,+\, q_y\, M_y = 0 \tag{C.5}$$

Injecting equation (C.5) into C.3 gives rise to an energy that only depends on M_x if H is chosen parallel to the $x-$axis.

$$G(\mathbf{q}) \,=\, \sum_{\mathbf{q}} \frac{1}{2}\kappa \left(1 + \frac{q_x^2}{q_y^2}\right) M_x^2(\mathbf{q}) \,-\, M_x(\mathbf{q})\;\; H(\mathbf{q}), \tag{C.6}$$

By minimising this energy with respect to M_x, one gets

$$S_{xx}(\mathbf{q}) \,=\, \kappa\frac{q_y^2}{q_x^2+q_y^2}, \quad S_{xy}(\mathbf{q}) \,=\, -\kappa\frac{q_y q_x}{q_x^2+q_y^2}, \tag{C.7}$$

This result can be generalised for higher dimension [You81], but this $2d$ calculation already provides a good idea of the anisotropic behaviour whether we approach the pinch point from $q_x \to 0$ or $q_y \to 0$.

This appendix has highly benefited from discussions with Tom Fennell & Steven Bramwell and notes from the latter.

Bibliography

[AB08] Marco Aurelio Alves Barbosa and Vera Bohomoletz Henriques. Frustration and anomalous behavior in the Bell-Lavis model of liquid water. *Physical Review E*, **77** (5) 051204 (2008).

[And50] P. W. Anderson. Antiferromagnetism - theory of superexchange interaction. *Physical Review*, **79** (2) 350–356 (1950).

[And56] P. W. Anderson. Ordering and antiferromagnetism in ferrites. *Physical Review*, **102** (4) 1008–1013 (1956).

[And73] P. W. Anderson. Resonating valence bonds - new kind of insulator. *Materials Research Bulletin*, **8** (2) 153–160 (1973).

[And87] P. W. Anderson. The resonating valence bond state in La_2CuO_4 and superconductivity. *Science*, **235** 1196–1198 (1987).

[Aok04] H. Aoki, T. Sakakibara, K. Matsuhira and Z. Hiroi. Magnetocaloric effect study on the pyrochlore spin ice compound $Dy_2Ti_2O_7$ in a [111] magnetic field. *Journal of the Physical Society of Japan*, **73** (10) 2851–2856 (2004).

[Arc97] P. Archambault, S. T. Bramwell and P. C. W. Holdsworth. Magnetic fluctuations in a finite two-dimensional XY model. *Journal of Physics A-Mathematical and General*, **30** (24) 8363–8378 (1997).

[Bai88] M. N. Baibich, J. M. Broto, A. Fert, F. N. Vandau, F. Petroff, P. Eitenne, G. Creuzet, A. Friederich and J. Chazelas. Giant magnetoresistance of (001)Fe/(001)Cr magnetic superlattices. *Physical Review Letters*, **61** (21) 2472–2475 (1988).

[Bar57] J. Bardeen, L. N. Cooper and J. R. Schrieffer. Theory of superconductivity. *Physical Review*, **108** (5) 1175–1204 (1957).

[Bar98] G. T. Barkema and M. E. J. Newman. Monte Carlo simulation of ice models. *Physical Review E*, **57** (1) 1155–1166 (1998).

[Bax07] R. J. Baxter. *Exactly solved models in statistical mechanics*. Dover Publications (2007).

[Bec30] R. Becker. Zur Theorie der Magnitisierungskurve. *Zeitschrift Für Physik*, **62** 253–269 (1930).

[Bed86] J. G. Bednorz and K. A. Muller. Possible High-Tc superconductivity In The Ba-La-Cu-O system. *Zeitschrift Für Physik B-Condensed Matter*, **64** (2) 189–193 (1986).

[Ben77] L. Benguigui. Critical-point of infinite type. *Physical Review B*, **16** (3) 1266–1269 (1977).

[Ber33] J. D. Bernal and R. H. Fowler. A theory of water and ionic solution, with particular reference to hydrogen and hydroxyl ions. *Journal of Chemical Physics*, **1** (8) 515–548 (1933).

[Ber70] V. L. Berezinskii. Destruction of long-range order in one-dimensional and 2-dimensional systems possessing a continuous symmetry group .i. classical systems. *Zhurnal Eksperimentalnoi i Teoreticheskoi Fiziki*, **59** 907–920 (1970).

[Ber07] M. Berhanu, R. Monchaux, S. Fauve, N. Mordant, F. Petrelis, A. Chiffaudel, F. Daviaud, B. Dubrulle, L. Marie, F. Ravelet, M. Bourgoin, P. Odier, J.-F. Pinton and R. Volk. Magnetic field reversals in an experimental turbulent dynamo. *Europhysics Letters*, **77** (5) 59001 (2007).

[Bet35] H. A. Bethe. Statistical Theory of Superlattices. *Proceedings of the Royal Society of London A*, **150** 552–575 (1935).

[Bha83] S. M. Bhattacharjee, J. F. Nagle, D. A. Huse and M. E. Fisher. Critical-behavior of a 3-dimensional dimer model. *Journal of Statistical Physics*, **32** (2) 361–374 (1983).

[Bha91a] S. M. Bhattacharjee. Vertex model in d-dimensions - an exact result. *Europhysics Letters*, **15** (8) 815–820 (1991).

[Bha91b] S. M. Bhattacharjee and J. J. Rajasekaran. Absence of anomalous dimension in vertex models - semidilute solution of directed polymers. *Physical Review A*, **44** (10) 6202–6212 (1991).

[Bin89] G. Binasch, P. Grunberg, F. Saurenbach and W. Zinn. Enhanced magnetoresistance in layered magnetic-structures with antiferromagnetic interlayer exchange. *Physical Review B*, **39** (7) 4828–4830 (1989).

[Bin97] K. Binder and D. W. Heermann. *Monte Carlo Simulation in Statistical Physics*. Springer, Berlin (1997).

[Blo69] H. W. J. Blote, R. F. Wielinga and W. J. Huiskamp. Heat-capacity measurements on rare-earth double oxides $R_2M_2O_7$. *Physica*, **43** (4) 549 (1969).

[Bra90] S. T. Bramwell. Temperature-dependence of the isotropic exchange constant. *Journal of Physics-Condensed Matter*, **2** (36) 7527–7536 (1990).

[Bra93] S. T. Bramwell and P. C. W. Holdsworth. Magnetization and universal subcritical behavior in 2-dimensional XY magnets. *Journal of Physics-Condensed Matter*, **5** (4) L53–L59 (1993).

[Bra98] S. T. Bramwell and M. J. Harris. Frustration in Ising-type spin models on the pyrochlore lattice. *Journal of Physics-Condensed Matter*, **10** (14) L215–L220 (1998).

[Bra01a] S. T. Bramwell and M. J. P. Gingras. Spin ice state in frustrated magnetic pyrochlore materials. *Science*, **294** 1495–1501 (2001).

[Bra01b] S. T. Bramwell, M. J. Harris, B. C. den Hertog, M. J. P. Gingras, J. S. Gardner, D. F. McMorrow, A. R. Wildes, A. L. Cornelius, J. D. M. Champion, R. G. Melko and T. Fennell. Spin correlations in $Ho_2Ti_2O_7$: A dipolar spin ice system. *Physical Review Letters*, **87** (4) 047205 (2001).

[Bra09] S. T. Bramwell, S. R. Giblin, S. Calder, R. Aldus, D. Prabhakaran and T. Fennell. Measurement of the charge and current of magnetic monopoles in spin ice. *Nature*, **461** (7266) 956–959 (2009).

[Bre69] D. J. Breed, Gilijams K. and A. R. Miedema. Magnetic properties of K_2CoF_4 and Rb_2CoF_4 - 2-dimensional Ising antiferromagnets. *Physica*, **45** (2) 205 (1969).

[Bro90] C. Broholm, G. Aeppli, G. P. Espinosa and A. S. Cooper. Antiferromagnetic fluctuations and short-range order in a Kagome lattice. *Physical Review Letters*, **65** (25) 3173–3176 (1990).

[Cab82] B. Cabrera. First results from a superconductive detector for moving magnetic monopoles. *Physical Review Letters*, **48** 1378–1381 (1982).

[Can72] V. Cannella and J. A. Mydosh. Magnetic ordering in gold-iron alloys. *Physical Review B*, **6** (11) 4220 (1972).

[Can01] B. Canals and D. A. Garanin. Spin-liquid phase in the pyrochlore antiferromagnet. *Canadian Journal of Physics*, **79** (11-12) 1323–1331 (2001).

[Car02] J. Cardy. *Scaling and Renormalization in Statistical Physics*. Cambridge University Press (2002).

[Cas07] Claudio Castelnovo and Claudio Chamon. Topological order and topological entropy in classical systems. *Physical Review B*, **76** (17) 174416 (2007).

[Cas08] C. Castelnovo, R. Moessner and S. L. Sondhi. Magnetic monopoles in spin ice. *Nature*, **451** 42–45 (2008).

[Cas09] C. Castelnovo. private communication (2009).

[Cha92] J. T. Chalker, P. C. W. Holdsworth and E. F. Shender. Hidden order in a frustrated system - properties of the heisenberg Kagome antiferromagnet. *Physical Review Letters*, **68** (6) 855–858 (1992).

[Cha94] P. Chandra and B. Doucot. Spin liquids on the husimi cactus. *Journal of Physics A-Mathematical and General*, **27** (5) 1541–1556 (1994).

[Cha02] J. D. M. Champion, S. T. Bramwell, P. C. W. Holdsworth and M. J. Harris. Competition between exchange and anisotropy in a pyrochlore ferromagnet. *Europhysics Letters*, **57** (1) 93–99 (2002).

[Che74] M. S. Chen, L. Onsager, J. Bonner and J. Nagle. Hopping of ions in ice. *Journal of Chemical Physics*, **60** (2) 405–419 (1974).

[Cla09] J. P. Clancy, J. P. C. Ruff, S. R. Dunsiger, Y. Zhao, H. A. Dabkowska, J. S. Gardner, Y. Qiu, J. R. D. Copley, T. Jenkins and B. D. Gaulin. Revisiting static and dynamic spin-ice correlations in $Ho_2Ti_2O_7$ with neutron scattering. *Physical Review B*, **79** (1) 014408 (2009).

[Col97] M. F. Collins and O. A. Petrenko. Triangular antiferromagnets. *Canadian Journal of Physics*, **75** (9) 605–655 (1997).

[Dai95] P. Dai, B. C. Chakoumakos, G. F. Sun, K. W. Wong, Y. XIN and D. F. Lu. Synthesis and neutron powder diffraction study of the superconductor $HgBa_2Ca_2Cu_3O_{8+\delta}$ by Tl substitution. *Physica C*, **243** (3-4) 201–206 (1995).

[dH99] B. C. den Hertog, M. J. P. Gingras, S. T. Bramwell and M. J. Harris. Comment on "Ising Pyrochlore Magnets: Low Temperature Properties, "Ice Rules" and Beyond" by R. Siddharthan et al. *condmat*: 9912.220 (1999).

[dH00] B. C. den Hertog and M. J. P. Gingras. Dipolar interactions and origin of spin ice in Ising pyrochlore magnets. *Physical Review Letters*, **84** (15) 3430–3433 (2000).

[Die04] H. T. Diep, editor. *Frustrated Spin Systems*. World Scientific Publishing, Singapore (2004).

[Dir31] P. A. M. Dirac. Quantised singularities in the electromagnetic field. *Proceedings of the Royal Society of London A*, **133** 60–72 (1931).

[dL80a] S. W. de Leeuw, J. W. Perram and E. R. Smith. Simulation of electrostatic systems in periodic boundary-conditions .1. lattice sums and dielectric-constants. *Proceedings of the Royal Society of London A*, **373** (1752) 27–56 (1980).

[dL80b] S. W. de Leeuw, J. W. Perram and E. R. Smith. Simulation of electrostatic systems in periodic boundary-conditions 2. equivalence of boundary-conditions. *Proceedings of the Royal Society of London A*, **373** (1752) 57–66 (1980).

[dL83] S. W. de Leeuw, J. W. Perram and E. R. Smith. Simulation of electrostatic systems in periodic boundary-conditions .3. further theory and applications. *Proceedings of the Royal Society of London A*, **388** (1794) 177–193 (1983).

[Edw75] S. F. Edwards and P. W. Anderson. Theory of spin glasses. *Journal of Physics F-Metal Physics*, **5** (5) 965–974 (1975).

[Ehl03] G. Ehlers, A. L. Cornelius, M. Orendac, M. Kajnakova, T. Fennell, S. T. Bramwell and J. S. Gardner. Dynamical crossover in 'hot' spin ice. *Journal of Physics-Condensed Matter*, **15** (2) L9–L15 (2003).

[Ehl04] G. Ehlers, A. L. Cornelius, T. Fennell, M. Koza, S. T. Bramwell and J. S. Gardner. Evidence for two distinct spin relaxation mechanisms in 'hot' spin ice $Ho_2Ti_2O_7$. *Journal of Physics-Condensed Matter*, **16** (11) S635–S642 (2004).

[Elo95] M. O. Elout and W. J. A. Maaskant. A first-order phase-transition in a 3-dimensional vertex model. *Journal of Statistical Physics*, **80** (3-4) 919–927 (1995).

[Ewa21] P. P. Ewald. Die Berechnung optischer und elektrostatischer Gitterpotentiale. *Annalen der Physik*, **369** (3) 253–287 (1921).

[Fen04] T. Fennell, O. A. Petrenko, B. Fak, S. T. Bramwell, M. Enjalran, T. Yavors'kii, M. J. P. Gingras, R. G. Melko and G. Balakrishnan. Neutron scattering investigation of the spin ice state in $Dy_2Ti_2O_7$. *Physical Review B*, **70** (13) 134408 (2004).

[Fen05] T. Fennell, O. A. Petrenko, B. Fak, J. S. Gardner, S. T. Bramwell and B. Ouladdiaf. Neutron scattering studies of the spin ices $Ho_2Ti_2O_7$ and $Dy_2Ti_2O_7$ in applied magnetic field. *Physical Review B*, **72** (22) 224411 (2005).

[Fen07] T. Fennell, S. T. Bramwell, D. F. McMorrow, P. Manuel and A. R. Wildes. Pinch points and Kasteleyn transitions in kagome ice. *Nature Physics*, **3** (8) 566–572 (2007).

[Fen09] T. Fennell, P. P. Deen, A. R. Wildes, K. Schmalzl, D. Prabhakaran, A. T. Boothroyd, R. J. Aldus, D. F. McMorrow and S. T. Bramwell. Magnetic Coulomb Phase in the Spin Ice $Ho_2Ti_2O_7$. *Science*, **326** (5951) 415–417 (2009).

[Fer86] G. Ferey, R. Depape, M. Leblanc and J. Pannetier. Ordered magnetic frustration .8. crystal and magnetic-structures of the pyrochlore form of FeF_3 between 2.5 K and 25 K from powder neutron-diffraction - comparison with the other varieties of FeF_3. *Revue De Chimie Minerale*, **23** (4-5) 474–484 (1986).

[Fis88] D. S. Fisher and P. C. Hohenberg. Dilute bose-gas in 2 dimensions. *Physical Review B*, **37** (10) 4936–4943 (1988).

[Fow40] R. H. Fowler and E. A. Guggenheim. Statistical Thermodynamics of Super-Lattices. *Proceedings of the Royal Society of London A*, **174** (957) 189–206 (1940).

[Fre02] D. Frenkel and B. Smit. *Understanding Molecular Simulations*. Academic Press Elsevier Science (2002).

[Fuk02] H. Fukazawa, R. G. Melko, R. Higashinaka, Y. Maeno and M. J. P. Gingras. Magnetic anisotropy of the spin-ice compound $Dy_2Ti_2O_7$. *Physical Review B*, **65** (5) 054410 (2002).

[Gar99] J. S. Gardner, S. R. Dunsiger, B. D. Gaulin, M. J. P. Gingras, J. E. Greedan, R. F. Kiefl, M. D. Lumsden, W. A. MacFarlane, N. P. Raju, J. E. Sonier, I. Swainson and Z. Tun. Cooperative paramagnetism in the geometrically frustrated pyrochlore antiferromagnet $Tb_2Ti_2O_7$. *Physical Review Letters*, **82** (5) 1012–1015 (1999).

[Gar03] J. S. Gardner, A. Keren, G. Ehlers, C. Stock, E. Segal, J. M. Roper, B. Fak, M. B. Stone, P. R. Hammar, D. H. Reich and B. D. Gaulin. Dynamic frustrated magnetism in $Tb_2Ti_2O_7$ at 50 mK. *Physical Review B*, **68** (18) 180401 (2003).

[Gar10] J. S. Gardner, M. J. P. Gingras and J. E. Greedan. Magnetic pyrochlore oxides. to be published in Reviews of Modern Physics (2010).

[Gia36] W. F. Giauque and J. W. Stout. The entropy of water and the third law of thermodynamics - The heat capacity of ice from 15 to 273 degrees K. *Journal of the American Chemical Society*, **58** 1144–1150 (1936).

[Gin00] M. J. P. Gingras, B. C. den Hertog, M. Faucher, J. S. Gardner, S. R. Dunsiger, L. J. Chang, B. D. Gaulin, N. P. Raju and J. E. Greedan. Thermodynamic and single-ion properties of Tb^{3+} within the collective paramagnetic-spin liquid state of the frustrated pyrochlore antiferromagnet $Tb_2Ti_2O_7$. *Physical Review B*, **62** (10) 6496–6511 (2000).

[Gin01] M. J. P. Gingras and B. C. den Hertog. Origin of spin-ice behavior in Ising pyrochlore magnets with long-range dipole interactions: an insight from mean-field theory. *Canadian Journal of Physics*, **79** (11-12) 1339–1351 (2001).

[Gla69] M. L. Glasser. Evaluation of partition functions for some 2-dimensional ferroelectric models. *Physical Review*, **184** (2) 539 (1969).

[Gol92] Nigel Goldenfeld. *Lectures on Phase Transitions and the Renormalization Group*, volume 85 of *Frontiers in Physics*. Perseus Books, Massachusetts (1992).

[Gre01] J. E. Greedan. Geometrically frustrated magnetic materials. *Journal of Materials Chemistry*, **11** (1) 37–53 (2001).

[Guj84] P. D. Gujrati. Ordering field, order parameter, and self-avoiding walks. *Physical Review Letters*, **53** (26) 2453–2456 (1984).

[Guj95] P. D. Gujrati. Bethe or Bethe-like lattice calculations are more reliable than conventional mean-field calculations. *Physical Review Letters*, **74** (5) 809–812 (1995).

[Har53] F. Harary and G. E. Uhlenbeck. On the number of husimi trees .1. *Proceedings of the National Academy of Sciences of the United States of America*, **39** (4) 315–322 (1953).

[Har97] M. J. Harris, S. T. Bramwell, D. F. McMorrow, T. Zeiske and K. W. Godfrey. Geometrical frustration in the ferromagnetic pyrochlore $Ho_2Ti_2O_7$. *Physical Review Letters*, **79** (13) 2554–2557 (1997).

[Har98] M. J. Harris, S. T. Bramwell, P. C. W. Holdsworth and J. D. M. Champion. Liquid-gas critical behavior in a frustrated pyrochlore ferromagnet. *Physical Review Letters*, **81** (20) 4496–4499 (1998).

[Har07] M. J. Harris. private communication (2007).

[Hen05] C. L. Henley. Power-law spin correlations in pyrochlore antiferromagnets. *Physical Review B*, **71** (1) 014424 (2005).

[Her04] M. Hermele, M. P. A. Fisher and L. Balents. Pyrochlore photons: The U(1) spin liquid in a S=1/2 three-dimensional frustrated magnet. *Physical Review B*, **69** (6) 064404 (2004).

[Hig03a] R. Higashinaka, H. Fukazawa and Y. Maeno. Anisotropic release of the residual zero-point entropy in the spin ice compound $Dy_2Ti_2O_7$: Kagome ice behavior. *Physical Review B*, **68** (1) 014415 (2003).

[Hig03b] R. Higashinaka, H. Fukazawa and Y. Maeno. Specific heat of single crystal of spin ice compound $Dy_2Ti_2O_7$. *Physica B-Condensed Matter*, **329** 1040–1041 (2003).

[Hig04a] R. Higashinaka, H. Fukazawa, K. Deguchi and Y. Maeno. A Kagome ice state in the spin ice compound $Dy_2Ti_2O_7$. *Journal of Physics-Condensed Matter*, **16** (11) S679–S683 (2004).

[Hig04b] R. Higashinaka, H. Fukazawa, K. Deguchi and Y. Maeno. Low temperature specific heat of $Dy_2Ti_2O_7$ in the kagome ice state. *Journal of the Physical Society of Japan*, **73** (10) 2845–2850 (2004).

[Hig05] R. Higashinaka and Y. Maeno. Field-induced transition on a triangular plane in the spin-ice compound $Dy_2Ti_2O_7$. *Physical Review Letters*, **95** (23) 237208 (2005).

[Hir03] Z. Hiroi, K. Matsuhira and M. Ogata. Ferromagnetic Ising spin chains emerging from the spin ice under magnetic field. *Journal of the Physical Society of Japan*, **72** (12) 3045–3048 (2003).

[Hou50] R. M. F. Houtappel. Order-disorder in hexagonal lattices. *Physica*, **16** (5) 425–455 (1950).

[Hus50] K. Husimi. Note on mayers theory of cluster integrals. *Journal of Chemical Physics*, **18** (5) 682–684 (1950).

[Hus03] D. A. Huse, W. Krauth, R. Moessner and S. L. Sondhi. Coulomb and liquid dimer models in three dimensions. *Physical Review Letters*, **91** (16) 167004 (2003).

[Isa04a] S. V. Isakov, K. Gregor, R. Moessner and S. L. Sondhi. Dipolar spin correlations in classical pyrochlore magnets. *Physical Review Letters*, **93** (16) 167204 (2004).

[Isa04b] S. V. Isakov, K. S. Raman, R. Moessner and S. L. Sondhi. Magnetization curve of spin ice in a [111] magnetic field. *Physical Review B*, **70** (10) 104418 (2004).

[Isa05] S. V. Isakov, R. Moessner and S. L. Sondhi. Why spin ice obeys the ice rules. *Physical Review Letters*, **95** (21) 217201 (2005).

[Isi25] E. Ising. Beitrag zur Theorie des Ferromagnetismus. *Zeitschrift Für Physik*, **31** 253–258 (1925).

[Jac99] J. D. Jackson. *Classical Electrodynamics*. Wiley, New-York (1999).

[Jau08] L. D. C. Jaubert, J. T. Chalker, P. C. W. Holdsworth and R. Moessner. Three-dimensional kasteleyn transition: Spin ice in a [100] field. *Physical Review Letters*, **100** (6) 067207 (2008).

[Jau09a] L. D. C. Jaubert, J. T. Chalker, P. C. W. Holdsworth and R. Moessner. The Kasteleyn transition in three dimensions: Spin ice in a [100] field. *Journal of Physics: Conference Series*, **145** 012024 (2009).

[Jau09b] L. D. C. Jaubert and P. C. W. Holdsworth. Signature of magnetic monopole and Dirac string dynamics in spin ice. *Nature Physics*, **5** (4) 258–261 (2009).

[Kad02] H. Kadowaki, Y. Ishii, K. Matsuhira and Y. Hinatsu. Neutron scattering study of dipolar spin ice $Ho_2Sn_2O_7$: Frustrated pyrochlore magnet. *Physical Review B*, **65** (14) 144421 (2002).

[Kas63] P. W. Kasteleyn. Dimer statistics and phase transitions. *Journal of Mathematical Physics*, **4** (2) 287 (1963).

[Kaw86] C. Kawabata and A. R. Bishop. A monte-carlo study of the two-dimensional Heisenberg-model with easy-plane symmetry. *Solid State Communications*, **60** (2) 167–171 (1986).

[Kik51] R. Kikuchi. A theory of cooperative phenomena. *Physical Review*, **81** (6) 988–1003 (1951).

[Kit96] C. Kittel. *Introduction to Solid State Physics*. John Wiley & Sons, Inc., 7 edition (1996).

[Kos73] J. M. Kosterlitz and D. J. Thouless. Ordering, metastability and phase-transitions in 2 dimensional systems. *Journal of Physics C-Solid State Physics*, **6** (7) 1181–1203 (1973).

[Kra34] H. A. Kramers. The interaction between the magnetogenic atoms in a paramagnetic crystal. *Physica*, **1** 182–192 (1934).

[Kra96] W. Krauth. Introduction To Monte Carlo Algorithms. *condmat*: 9612.186 (1996).

[Kra06] W. Krauth. *Statistical Mechanics: Algorithms and Computations*. Master Series. Oxford University Press, New-York (2006).

[L9̈6] H. Lütkepohl. *Handbook of Matrices*. Wiley (1996).

[L9́7] L.-P. Lévy. *Magnétisme et supraconductivité*. Inter Editions / CNRS Editions, Paris (1997).

[Lac10] C. Lacroix, P. Mendels and F. Mila, editors. *Highly Frustrated Magnetism*. Springer Verlag (2010).

[Lag07] J. Lago, S. J. Blundell and C. Baines. μSR investigation of spin dynamics in the spin-ice material $Dy_2Ti_2O_7$. *Journal of Physics-Condensed Matter*, **19** (32) 326210 (2007).

[Lau08] C. Laumann, A. Scardicchio and S. L. Sondhi. Cavity method for quantum spin glasses on the Bethe lattice. *Physical Review B*, **78** (13) 134424 (2008).

[LB02] M. Le Bellac. *Des phénomènes critiques aux champs de jauges*. EDP Sciences / CNRS Éditions, Paris, 3rd edition (2002).

[Lee02] S. H. Lee, C. Broholm, W. Ratcliff, G. Gasparovic, Q. Huang, T. H. Kim and S. W. Cheong. Emergent excitations in a geometrically frustrated magnet. *Nature*, **418** 856–858 (2002).

[Lie67a] E. H. Lieb. Exact solution of 2-dimensional slater KDP model of a ferroelectric. *Physical Review Letters*, **19** (3) 108 (1967).

[Lie67b] E. H. Lieb. Exact solution of F model of an antiferroelectric. *Physical Review Letters*, **18** (24) 1046 (1967).

[Lie67c] E. H. Lieb. Exact solution of problem of entropy of 2-dimensional ice. *Physical Review Letters*, **18** (17) 692 (1967).

[Lie67d] E. H. Lieb. Residual entropy of square ice. *Physical Review*, **162** (1) 162 (1967).

[Lie86] R. Liebmann. *Statistical Mechanics of Periodic Frustrated Spin Systems*. Springer, Berlin (1986).

[Mae00] M. Maesato, Y. Kaga, R. Kondo and S. Kagoshima. Uniaxial strain method for soft crystals: Application to the control of the electronic properties of organic conductors. *Review of Scientific Instruments*, **71** (1) 176–181 (2000).

[Mat00] K. Matsuhira, Y. Hinatsu, K. Tenya and T. Sakakibara. Low temperature magnetic properties of frustrated pyrochlore ferromagnets $Ho_2Sn_2O_7$ and $Ho_2Ti_2O_7$. *Journal of Physics-Condensed Matter*, **12** (40) L649–L656 (2000).

[Mat01] K. Matsuhira, Y. Hinatsu and T. Sakakibara. Novel dynamical magnetic properties in the spin ice compound $Dy_2Ti_2O_7$. *Journal of Physics-Condensed Matter*, **13** (31) L737–L746 (2001).

[Mat02a] K. Matsuhira, Y. Hinatsu, K. Tenya, H. Amitsuka and T. Sakakibara. Low-temperature magnetic properties of pyrochlore stannates. *Journal of the Physical Society of Japan*, **71** (6) 1576–1582 (2002).

[Mat02b] K. Matsuhira, Z. Hiroi, T. Tayama, S. Takagi and T. Sakakibara. A new macroscopically degenerate ground state in the spin ice compound $Dy_2Ti_2O_7$ under a magnetic field. *Journal of Physics-Condensed Matter*, **14** (29) L559–L565 (2002).

[Mat04] K. Matsuhira, C. Sekine, C. Paulsen and Y. Hinatsu. Low-temperature magnetic properties of the geometrically frustrated pyrochlore $Pr_2Sn_2O_7$. *Journal of Magnetism and Magnetic Materials*, **272** E981–E982 (2004).

[Mel96] R. Melin, J. C. A. d'Auriac, P. Chandra and B. Doucot. Glassy behaviour in the ferromagnetic Ising model on a Cayley tree. *Journal of Physics A-Mathematical and General*, **29** (18) 5773–5804 (1996).

[Mel01a] R. G. Melko. Low Temperature Physics of Dipolar Spin Ice: A Monte Carlo Study. Master's thesis, University of Waterloo (2001).

[Mel01b] R. G. Melko, B. C. den Hertog and M. J. P. Gingras. Long-range order at low temperatures in dipolar spin ice. *Physical Review Letters*, **87** (6) 067203 (2001).

[Mel04] R. G. Melko and M. J. P. Gingras. Monte Carlo studies of the dipolar spin ice model. *Journal of Physics-Condensed Matter*, **16** (43) R1277–R1319 (2004).

[Mer66] N. D. Mermin and H. Wagner. Absence of ferromagnetism or antiferromagnetism in 1- or 2-dimensional isotropic Heisenberg models. *Physical Review Letters*, **17** (22) 1133 (1966).

[Met53] N. Metropolis, A. W. Rosenbluth, M. N. Rosenbluth, A. H. Teller and E. Teller. Equation of state calculations by fast computing machines. *Journal of Chemical Physics*, **21** (6) 1087–1092 (1953).

[Min88] H. Minc. *Non-negative matrices*. Wiley (1988).

[Mir02] I. Mirebeau, I. N. Goncharenko, P. Cadavez-Pares, S. T. Bramwell, M. J. P. Gingras and J. S. Gardner. Pressure-induced crystallization of a spin liquid. *Nature*, **420** 54–57 (2002).

[Mit07] M. Mito, S. Kuwabara, K. Matsuhira, H. Deguchi, S. Takagi and Z. Hiroi. Uniaxial pressure effects on spin-ice compound $Dy_2Ti_2O_7$. *Journal of Magnetism and Magnetic Materials*, **310** (2) E432–E434 (2007).

[Moe98a] R. Moessner. Relief and generation of frustration in pyrochlore magnets by single-ion anisotropy. *Physical Review B*, **57** (10) R5587–R5589 (1998).

[Moe98b] R. Moessner and J. T. Chalker. Low-temperature properties of classical geometrically frustrated antiferromagnets. *Physical Review B*, **58** (18) 12049–12062 (1998).

[Moe01] R. Moessner. Magnets with strong geometric frustration. *Canadian Journal of Physics*, **79** (11-12) 1283–1294 (2001).

[Moe03a] R. Moessner and S. L. Sondhi. Theory of the [111] magnetization plateau in spin ice. *Physical Review B*, **68** (6) 064411 (2003).

[Moe03b] R. Moessner and S. L. Sondhi. Three-dimensional resonating-valence-bond liquids and their excitations. *Physical Review B*, **68** (18) 184512 (2003).

[Moe06] R. Moessner and A. R. Ramirez. Geometrical frustration. *Physics Today*, **59** (2) 24–29 (2006).

[Moe09] R. Moessner. Unconventional magnets in external magnetic fields. *Journal of Physics: Conference Series*, **145** 012001 (2009).

[Mol07] H. R. Molavian, M. J. P. Gingras and B. Canals. Dynamically induced frustration as a route to a quantum spin ice state in $Tb_2Ti_2O_7$ via virtual crystal field excitations and quantum many-body effects. *Physical Review Letters*, **98** (15) 157204 (2007).

[Mon98] J. L. Monroe. Frustrated Ising systems on Husimi trees. *Physica A-Statistical Mechanics and Its Applications*, **256** (1-2) 217–228 (1998).

[Mor76] T. Morita. Lattice model for a polymer-chain in dilute-solution. *Journal of Physics A-Mathematical and General*, **9** (1) 169–177 (1976).

[Nag66] J. F. Nagle. Lattice statistics of hydrogen bonded crystals .i. residual entropy of ice. *Journal of Mathematical Physics*, **7** (8) 1484 (1966).

[Nag69] J. F. Nagle. Proof of first order phase transition in slater KDP model. *Communications In Mathematical Physics*, **13** (1) 62 (1969).

[Nag73a] J. F. Nagle. Lipid bilayer phase-transition - density-measurements and theory. *Proceedings of the National Academy of Sciences of the United States of America*, **70** (12) 3443–3444 (1973).

[Nag73b] J. F. Nagle. Theory of biomembrane phase-transitions. *Journal of Chemical Physics*, **58** (1) 252–264 (1973).

[Obr88] X. Obradors, A. Labarta, A. Isalgue, J. Tejada, J. Rodriguez and M. Pernet. Magnetic frustration and lattice dimensionality in $SrCr_8Ga_4O_19$. *Solid State Communications*, **65** (3) 189–192 (1988).

[Onn11] H. K. Onnes. Further experiments with liquid helium D - On the change of the electrical resistance of pure metals at very low temperatures, etc V The disappearance of the resistance of mercury. *Proceedings of the Koninklijke Akademie van Wetenschappen te Amsterdam*, **14** 113–115 (1911).

[Ons44] L. Onsager. Crystal statistics. I. A two-dimensional model with an order-disorder transition. *Physical Review*, **65** (3-4) 117–149 (1944).

[Ore07] M. Orendac, J. Hanko, E. Cizmar, A. Orendacova, M. Shirai and S. T. Bramwell. Magnetocaloric study of spin relaxation in dipolar spin ice $Dy_2Ti_2O_7$. *Physical Review B*, **75** (10) 104425 (2007).

[Pau35] L. Pauling. The structure and entropy of ice and of other crystals with some randomness of atomic arrangement. *Journal of the American Chemical Society*, **57** 2680–2684 (1935).

[Pet03] O. A. Petrenko, M. R. Lees and G. Balakrishnan. Magnetization process in the spin-ice compound $Ho_2Ti_2O_7$. *Physical Review B*, **68** (1) 012406 (2003).

[Pli06] M. Plischke and B. Bergerson. *Equilibrium Statistical Physics*. World Scientific, Singapore, 3rd edition (2006).

[Pow08] S. Powell and J. T. Chalker. Classical to quantum mappings for geometrically frustrated systems: Spin-ice in a [100] field. *Physical Review B*, **78** (2) 024422 (2008).

[Pre03] M. Pretti. A note on cactus trees: Variational vs. recursive approach. *Journal of Statistical Physics*, **111** (3-4) 993–1015 (2003).

[Ram90] A. P. Ramirez, G. P. Espinosa and A. S. Cooper. Strong frustration and dilution-enhanced order in a quasi-2d spin-glass. *Physical Review Letters*, **64** (17) 2070–2073 (1990).

[Ram94] A. P. Ramirez. Strongly geometrically frustrated magnets. *Annual Review of Materials Science*, **24** 453–480 (1994).

[Ram99] A. P. Ramirez, A. Hayashi, R. J. Cava, R. Siddharthan and B. S. Shastry. Zero-point entropy in 'spin ice'. *Nature*, **399** 333–335 (1999).

[Ros00] S. Rosenkranz, A. P. Ramirez, A. Hayashi, R. J. Cava, R. Siddharthan and B. S. Shastry. Crystal-field interaction in the pyrochlore magnet $Ho_2Ti_2O_7$. *Journal of Applied Physics*, **87** (9) 5914–5916 (2000).

[Rou97] Paul Roux. *Électromagnétisme*. Physique Sup & Spé. Ellipses (1997).

[Ruf05] J. P. C. Ruff, R. G. Melko and M. J. P. Gingras. Finite-temperature transitions in dipolar spin ice in a large magnetic field. *Physical Review Letters*, **95** (9) 097202 (2005).

[Ryz05] I. A. Ryzhkin. Magnetic relaxation in rare-earth oxide pyrochlores. *Journal of Experimental and Theoretical Physics*, **101** (3) 481–486 (2005).

[Sai05] M. Saito, R. Higashinaka and Y. Maeno. Magnetodielectric response of the spin-ice $Dy_2Ti_2O_7$. *Physical Review B*, **72** (14) 144422 (2005).

[Sak03] T. Sakakibara, T. Tayama, Z. Hiroi, K. Matsuhira and S. Takagi. Observation of a liquid-gas-type transition in the pyrochlore spin ice compound $Dy_2Ti_2O_7$ in a magnetic field. *Physical Review Letters*, **90** (20) 207205 (2003).

[San06] A. W. Sandvik and R. Moessner. Correlations and confinement in nonplanar two-dimensional dimer models. *Physical Review B*, **73** (14) 144504 (2006).

[Sat06] H. Sato, K. Matsuhira, T. Tayama, Z. Hiroi, S. Takagi and T. Sakakibara. Ferromagnetic ordering on the triangular lattice in the pyrochlore spin-ice compound $Dy_2Ti_2O_7$. *Journal of Physics-Condensed Matter*, **18** (22) L297–L303 (2006).

[Sch96] P. Schiffer, A. P. Ramirez, K. N. Franklin and S. W. Cheong. Interaction-induced spin coplanarity in a Kagome magnet: $SrCr_{9p}Ga_{12-9p}O_19$. *Physical Review Letters*, **77** (10) 2085–2088 (1996).

[Sid99] R. Siddharthan, B. S. Shastry, A. P. Ramirez, A. Hayashi, R. J. Cava and S. Rosenkranz. Ising pyrochlore magnets: Low-temperature properties, "ice rules", and beyond. *Physical Review Letters*, **83** (9) 1854–1857 (1999).

[Sid01] R. Siddharthan, B. S. Shastry and A. P. Ramirez. Spin ordering and partial ordering in holmium titanate and related systems. *Physical Review B*, **63** (18) 184412 (2001).

[Sil64] H. B. Silsbee, E. A. Uehling and V. H. Schmidt. Deuteron intrabond motion + ferroelectricity in KD_2PO_4. *Physical Review A*, **133** (1A) A165 (1964).

[Ska70] J. Skalyo, B. C. Frazer and G. Shirane. Ferroelectric mode motion in KD_2PO_4. *Physical Review B*, **1** 278–286 (1970).

[Sla41] J. C. Slater. Theory of the transition in KH_2PO_4. *Journal of Chemical Physics*, **9** (1) 16–33 (1941).

[Sny01] J. Snyder, J. S. Slusky, R. J. Cava and P. Schiffer. How 'spin ice' freezes. *Nature*, **413** 48–51 (2001).

[Sny02] J. Snyder, J. S. Slusky, R. J. Cava and P. Schiffer. Dirty spin ice: The effect of dilution on spin freezing in $Dy_2Ti_2O_7$. *Physical Review B*, **66** (6) 064432 (2002).

[Sny04a] J. Snyder, B. G. Ueland, A. Mizel, J. S. Slusky, H. Karunadasa, R. J. Cava and P. Schiffer. Quantum and thermal spin relaxation in the diluted spin ice $Dy_{2-x}M_xTi_2O_7$ (M=Lu,Y). *Physical Review B*, **70** (18) 184431 (2004).

[Sny04b] J. Snyder, B. G. Ueland, J. S. Slusky, H. Karunadasa, R. J. Cava and P. Schiffer. Low-temperature spin freezing in the $Dy_2Ti_2O_7$ spin ice. *Physical Review B*, **69** (6) 064414 (2004).

[Squ96] G. L. Squires. *Introduction to the theory of thermal neutron scattering*. Dover Publications, Mineola, New-York (1996).

[Sta71] H. E. Stanley. *Introduction to Phase transitions and Critical Phenomena*. Oxford University Press (1971).

[Sut67] B. Sutherland. Exact solution of a 2-dimensional model for hydrogen-bonded crystals. *Physical Review Letters*, **19** (3) 103–104 (1967).

[Sut07] John P. Sutter, Satoshi Tsutsui, Ryuji Higashinaka, Yoshiteru Maeno, Olaf Leupold and Alfred Q. R. Baron. Relaxation in the spin ice $Dy_2Ti_2O_7$ studied using nuclear forward scattering. *Physical Review B*, **75** (14) 140402 (2007).

[Tab06] Y. Tabata, H. Kadowaki, K. Matsuhira, Z. Hiroi, N. Aso, E. Ressouche and B. Fak. Kagome ice state in the dipolar spin ice $Dy_2Ti_2O_7$. *Physical Review Letters*, **97** (25) 257205 (2006).

[Tak48] Y. Takagi. Theory of the transition in KH_2PO_4 .2. *Journal of the Physical Society of Japan*, **3** (3) 273–274 (1948).

[Tes54] J. R. Tessman. Magnetic anisotropy at 0-degrees-K. *Physical Review*, **96** (5) 1192–1195 (1954).

[Tou77] G. Toulouse. Theory of frustration effect in spin-glasses .1. *Communications on Physics*, **2** (4) 115–119 (1977).

[Tsu82] D. C. Tsui, H. L. Stormer and A. C. Gossard. Two-dimensional magnetotransport in the extreme quantum limit. *Physical Review Letters*, **48** (22) 1559–1562 (1982).

[Uem94] Y. J. Uemura, A. Keren, K. Kojima, L. P. Le, G. M. Luke, W. D. Wu, Y. Ajiro, T. Asano, Y. Kuriyama, M. Mekata, H. Kikuchi and K. Kakurai. Spin fluctuations in frustrated Kagome lattice system $SrCr_8Ga_4O_19$ studied by muon spin relaxation. *Physical Review Letters*, **73** (24) 3306–3309 (1994).

[Vil77] J. Villain. Spin glass with nonrandom interactions. *Journal of Physics C-Solid State Physics*, **10** (10) 1717–1734 (1977).

[Vil79] J. Villain. Insulating spin-glasses. *Zeitschrift Für Physik B-Condensed Matter*, **33** (1) 31–42 (1979).

[Vil80] J. Villain, R. Bidaux, J. P. Carton and R. Conte. Order as an effect of disorder. *Journal de Physique*, **41** (11) 1263–1272 (1980).

[Vol91] A. R. Volkel, G. M. Wysin, A. R. Bishop and F. G. Mertens. Dynamic correlations in the classical 2-dimensional antiferromagnetic Heisenberg-model with easy-plane symmetry. *Physical Review B*, **44** (18) 10066–10078 (1991).

[Wad98] K. Wada and Y. Ogawa. Application of the cluster variation method to anisotropic polarization fluctuations in KD_2PO_4-type crystals above and below the transition temperature. *Journal of the Physical Society of Japan*, **67** (1) 112–118 (1998).

[Wan50] G. H. Wannier. Antiferromagnetism - the triangular Ising net. *Physical Review*, **79** (2) 357–364 (1950).

[Wan01] Z. W. Wang and C. Holm. Estimate of the cutoff errors in the Ewald summation for dipolar systems. *Journal of Chemical Physics*, **115** (14) 6351–6359 (2001).

[Wat99] G. I. Watson. Symmetry relations for the six-vertex model. *Journal of Statistical Physics*, **94** (5-6) 1045–1054 (1999).

[Wen95] X. G. Wen. Topological orders and edge excitations in fractional quantum Hall states. *Advances In Physics*, **44** (5) 405–473 (1995).

[Wen04] X. G. Wen. *Quantum Field Theory of Many-Body Systems*. Oxford University Press (2004).

[Wil02] A. S. Wills, R. Ballou and C. Lacroix. Model of localized highly frustrated ferromagnetism: The kagome spin ice. *Physical Review B*, **66** (14) 144407 (2002).

[Wu68] F. Y. Wu. Remarks on modified potassium dihydrogen phosphate model of a ferroelectric. *Physical Review*, **168** (2) 539 (1968).

[Yan66] C. N. Yang and C. P. Yang. 1-dimensional chain of anisotropic spin-spin interactions .3. applications. *Physical Review*, **151** (1) 258 (1966).

[Yav08] T. Yavors'kii, T. Fennell, M. J. P. Gingras and S. T. Bramwell. $Dy_2Ti_2O_7$ spin ice: A test case for emergent clusters in a frustrated magnet. *Physical Review Letters*, **101** (3) 037204 (2008).

[Yos02] S. Yoshida, K. Nemoto and K. Wada. Application of the cluster variation method to spin ice systems on the pyrochlore lattice. *Journal of the Physical Society of Japan*, **71** (3) 948–954 (2002).

[Yos04] S. Yoshida, K. Nemoto and K. Wada. Ordered phase of dipolar spin ice under [110] magnetic field. *Journal of the Physical Society of Japan*, **73** (7) 1619–1622 (2004).

[You81] R. W. Youngblood and J. D. Axe. Polarization fluctuations in ferroelectric models. *Physical Review B*, **23** (1) 232–238 (1981).

[Zas77] C. E. Zaspel and J. E. Drumheller. Temperature-dependence of exchange interaction and applications to electron-paramagnetic resonance. *Physical Review B*, **16** (5) 1771–1780 (1977).

[Zho08a] H. D. Zhou, C. R. Wiebe, L. Balicas, Y. J. Yo, Y. Qiu, J. R. D. Copley and J. S. Gardner. Intrinsic spin-disordered ground state of the Ising garnet $Ho_3Ga_5O_{12}$. *Physical Review B*, **78** (14) 140406 (2008).

[Zho08b] H. D. Zhou, C. R. Wiebe, J. A. Janik, L. Balicas, Y. J. Yo, Y. Qiu, J. R. D. Copley and J. S. Gardner. Dynamic Spin Ice: $Pr_2Sn_2O_7$. *Physical Review Letters*, **101** (22) 227204 (2008).